A Selection of published/presented papers

Volume II (1)
(1983-1986)

Papers 1-33

S Lee

A SELECTION OF PUBLISHED PAPERS VOL II

(1983 - 1990)

S. LEE

Plasma Research Laboratory
Department of Physics
Universiti Malaya
Kuala Lumpur

A Selection of Published Papers (1983 - 1990) by S. Lee

1 "An energy consistent snow-plough model for pinch design"
J. Phys. D: Applied Phys. 16, 2463 (1983)
S. Lee

2 "Radius ratio of argon pinches"
Australian J. Physics 35, 891 (1983)
S. Lee

3 "Streak photography and focus pinch models"
Bull. Phys. M'sia 4, 189 (1983)
T.Y. Tou and S. Lee

4 "The effect of specific heat ratio on argon pinch configuration"
Bull. Phys. M'sia 4, 1 (1983)
S. Lee

5 "Strong MHD compressions in a coupled circuit"
Bull. Phys. M'sia 4, 57 (1983)
S. Lee, A.C. Chew, C.S. Wong, T.Y. Tou, Y.S. Chen, K.E. Ling, S.L. Lo, C.H. Tan, S.H. Yap and E.H. Yeo

6 "A new theory for the fast compressional pinch"
Invited paper, Spring College on Radiation in Plasma Trieste, Italy, May 1983, published in "Radiation in Plasmas" p. 967-977, World Scientific Publishing Co. (1984)
S. Lee

7 "Plasma focus model yielding trajectory and structure"
Spring College on Radiation in Plasma, Trieste, Italy, May 1983, published in "Radiation in Plasmas", p. 978-987 World Scientific Publishing Co. (1984)
S. Lee

8 "Neutron and X-rays diagnostics of pulsed plasma sources"
Procs. Second Int. Symp. Radiation Phys. Penang, p. 233-240 (1983)
C.S. Wong, S. Lee, S.P. Moo and Y.H. Chen

9 "Regional centres for research transfer within South-East Asian countries"
Invited paper presented at the International Conf. 1984 ICTP, Trieste, Italy, to be published in Procs.
S. Lee

10 "A current-stepping technique to enhance pinch compression"
J. Phys. D: Appl. Phys. 17, 733 (1984)
S. Lee

11 "Preliminary measurements in a linear pinch plasma"
J. Fiz. Mal. 5, 149 (1984)
S.M. Low, B.C. Tan and S. Lee

12 "A generalised slug model for the pinch"
J. Fiz. Mal. 5, 153 (1984)
Jalil Ali, S. Lee, T.Y. Tou and Y.C. Yong

13 "A universal solar-powered electronic pulser with varied applications - from control to communication lasers"
J. Fiz. Mal. 5, 97 (1984)
S. Lee

14 "Energy balance theory applied to radiation-driven compressions"
J. Fiz. Mal. 5, 53 (1984)
S. Lee

15 "Vacuum spark as a reproducible X-ray source"
Rev. Sci. Instru. 55(7), 1125 (1984)
C.S. Wong and S. Lee

16 "Voltage and current computation of an inductive plasma focus model"
Sing. J. Physics 1, 75 (1984)
S. Lee, C.S. Wong, A.C. Chew, T.Y. Tou and Jalil Ali

17 "The dynamic pinch problem: A new concept and new computations"
Sing. J. Phys. 1, 103 (1984)
Also in Procs. of First Asia-Pacific Phys. Conf., World Scientific Publishing Co. (1984), Vol. 1, 676
S. Lee

18 "Experimental inference of a physical model for the vacuum spark"
Procs. Asia-Pacific Phys. Conf., p. 685, Singapore (1984)
C.S. Wong and S. Lee

19 "Pinch dynamics of the plasma focus"
Published in laser and plasma technology, World Scientific Publishing Co. (1985), Part III, Paper XIV, p. 627-680
Procs. of the First Tropical College
T.Y. Tou and S. Lee

20 "Dynamics of REB-sputtered copper plasma jets"
J. Fiz. Mal. 6, 23 (1985)
S. Lee, Harith Ahmad, T.Y. Tou, K.H. Kwek and C.S. Wong

21 "Simple method of pulsed plasma discharge current analysis"
J. Appl. Phys. 57, 11, 5102 (1985)
C.S. Wong and S. Lee

22 "Parametric study of the nitrogen laser circuit"
J. Fiz. Mal. 6, 165 (1985)
S. Lee, A.V. Gholap, A.J. Smith, K.H. Kwek, A.C. Chew, T.Y. Tou and S. Sapru

23 "Energetic plasma-injected particles for sputtering applications"
Jakarta Conference, September 9-12, 1985
Harith Ahmad and S. Lee

24 "Toroidal plasmoids in an electromagnetic shock tube"
Singapore J. Physics 3, 75 (1986)
S. Lee, M. Eissa, A.V. Gholap, K.H. Kwek, S. Mulyodrono, S. Sapru, A.J. Smith, Suryadi, T.Y. Tou, W. Usada, C.S. Wong, and Mohamad Zakaullah

25 "Initiating Physics Research in Developing Countries"
Asia-Pacific Physics News, Vol. 1, May 1986
S. Lee

26 "Plasma Research at the University of Malaya"
Invited review paper delivered at Second Tropical College on Applied Physics, March 1986, Kuala Lumpur,
Procs. "Laser and Plasma Technology", Ed. S. Lee et.al
World Scientific (1988)
S. Lee

27 "Analysis of voltage and current measurements in a DPF"
Paper read at the Second Tropical College on Applied Physics, Malaysia, April 1986 (to appear in Procs.)
T.Y. Tou and S. Lee

28 "Circuit effects on the operation of a plasma focus"
Paper read at the Second Tropical College on Applied Physics, Malaysia, April 1986 (to appear in Procs)
M.A. Eissa, M. Zakaullah and S. Lee

29 "A simple high current switch"
Paper read at the Second Tropical College on Applied Physics, Malaysia, April 1986 (to appear in Procs.)
A.J. Smith, Suryadi, Jasbir Singh and S. Lee

30 "Numerical design of the UNU/ICTP Plasma Focus"
Paper read at the Second Tropical College on Applied Physics, Malaysia, April 1986 (to appear in Procs.)
K.H. Kwek, T.Y. Tou and S. Lee

31 "Determining nitrogen laser channel parameters"
J. Fiz. Mal., 7, 125 (1986)
K.H. Kwek, A.J. Smith, T.Y. Tou, A.V. Gholap and S. Lee

32 "Design and operation of a hard-pumped ruby laser system"
Malaysian J. Sci. 8: (1986)
Harith Ahmad and S. Lee

33 "Preliminary results of the UNU/ICTP Plasma Focus"
J. Fiz. Mal. 7, 1 (1986)
S. Lee et.al.

34 "Application of plasma neutrons for half-life measurements"
Singapore J. Phys. 4, 131 (1987)
S.P. Moo and S. Lee

35 "Measurement of nitrogen laser channel current, inductance and resistance"
IEEE J. Quantum Electronics QE-23, 283 (1987)
A.J. Smith, K.H. Kwek, T.Y. Tou, A.V. Gholap and S. Lee

36 "Recent results from Rotamak Experiments at Flinders University"
Paper read at the 8th U.S. Compact Toroid Symposium, University of Maryland, June 1987
H. Kirolous, A. Knight, D. Brotherton-Ratcliffe, Wu Cheng, S. Lee and I.R. Jones

37 "A small plasma focus device for neutron, X-ray and electron beam studies"
Paper read at the Spring College on Plasma Physics, ICTP, Trieste, June 1987, (in Procs.)
T.Y. Tou, K.H. Kwek, Y.C. Yong and S. Lee

38 "A TEA nitrogen laser for optical diagnostic for a plasma focus"
Paper read at the Spring College on Plasma Physics, ICTP, Trieste, June 1987 (in Procs.)
K.H. Kwek, T.Y. Tou, and S. Lee

39 "The design, construction and performance studies of a Linear Z-pinch for current-stepping experiments"
Paper read at the Spring College on Plasma Physics, ICTP, Trieste, June 1987 (in Procs.)
S.H. Saw, C.S. Wong and S. Lee

40 "Streak laser shadowgraphy of the plasma focus"
Paper read at the Asian Physics Symposium, Kuala Lumpur, Malaysia, October 1987 (to appear in Procs.)
T.Y. Tou, E.H. Yee, B.C. Tan and S. Lee

41 "Observation of temperature variations in a plasma focus from soft X-ray measurements"
Paper read at the Asian Physics Symposium, Kuala Lumpur, Malaysia, October 1987 (to appear in Procs.)
T.Y. Tou, and S. Lee

42 "Pulsed plasma X-ray sources for applications in lithography and microscopy"
Paper read at the Asian Physics Symposium, Kuala Lumpur, Malaysia, October 1987 (to appear in Procs.)
C.S. Wong, S.P. Moo, S.H. Saw and S. Lee

43 "Sharing of fusion-related technology among developing countries"
Invited paper read at the Energy Independence Conference at Rio de Janeiro, August 1987; also to appear in revised version in Majalah Fizik
Proc. Fusion Energy and Plasma Physics, 754 (1988) World Scientific (Ed. : P.H. Sakanaka)
S. Lee

44 "Physics and perspectives of small plasma devices"
Asia-Pacific Physics News, Vol 3, June/July 1988
S. Lee

45 "A simple facility for the teaching of plasma dynamics and plasma nuclear fusion"
American J. Phys. 56, 62 (1988)
S. Lee et. al.

46. "Third World Nuclear Fusion Programmes and South-South Collaboration in Plasma Technology"
Invited paper delivered at Third Tropical College on Applied Physics, June 1988, Kuala Lumpur,
Procs. "Laser and Plasma Technology" Ed. C.S. Wong et.al., World Scientific (1990)
S. Lee and M.H.A. Hassan

47 "Half-life Measurements Using Plasma Neutrons"
1988, Proc. 3rd Tropical College on Appl. Phys. Kuala Lumpur
S.P. Moo, C.K. Chakrabarty and S. Lee

48 "High Resolution Plasma Visualisation by Subnanosecond Optical Techniques"
J. Phys. Mal., 9, 36 - 40 (1988)
K.H. Kwek, T.Y. Tou and S. Lee

49 "A Preionised Nitrogen Laser as a Diagnostic Light Source for Fast Pulse Experiments"
IEEE Trans. Instrumentation & Measurements IM-38, 1 103-107 (1989)
K.H. Kwek, T.Y. Tou and S. Lee

50 "Multi-slit streak photography for plasma dynamics studies"
Review Sci. Instru., 59, 11 2370-2374 (1989)
T.Y. Tou and S. Lee

51 "Density ratios in compressions driven by radiation pressure"
Laser and Particle Beams, 6, 597-606 (1988)
S. Lee

52 "A Numerical Study of the Effect of Y on the Shock Speed for Atomic and Molecular Hydrogen"
J. Fiz. Mal., 9, 93 (1988)
S.H. Saw, S. Lee and C.S. Wong

53 "Technology of a Small Plasma Focus"
Invited lecture at the Spring College on Plasma Physics - Trieste, Italy, May-June 1989
Proc. Small Plasma Physics Experiments II pp. 114-169 (1990)
World Scientific (Edited by S. Lee and P.H. Sakanaka)
S. Lee

54 "A Current-Stepping Technique to Enhance Pinch Compression - An Experimental Study"
Small Plasma Physics Experiments (II) pp. 289-295 (1990)
S.H. Saw, S. Lee and C.S. Wong

55 "Non-Pertubing Plasma Focus Measurements in the Run Down Phase"
IEEE Trans. Plasma Science 17, 311-315 (1989)
T.Y. Tou, S. Lee and K.H. Kwek

56 "Current sheath structures of the Plasma Focus in the Run-down Phase"
IEEE Trans. Plasma Science 18, p. 826-830 (1990)
K.H. Kwek, T.Y. Tou and S. Lee

57 "Half-life Measurements of ^{116}In Using Plasma Focus Neutrons"
J. Fiz. Mal., 10, 57 (1989)
S.P. Moo, C.K. Chakrabarty and S. Lee

58 "Sequenced Nitrogen Lasers"
J. Appl. Phys. 65, 4133-4137 (1989)
S. Lee, K.H. Kwek, Jalil Ali, M.V.H.V. Prabhakar, Y.S.Shishodia and A.G. Warmate

59 "Fusion Programmes in Malaysia"
Invited lecture at the Symposium on South-North Collaboration - June 1989 Trieste, Italy, June 1989
S. Lee

60 "Observations of Compact Torus FRC in single-phase Operation of a Transistorised Rotamak"
J. Fiz. Mal., 10, 61 (1989)
S. Lee, S.Y. Xu, G. Cotrell and I.R. Jones

61 "Pulse Technology, Laser Development and Technology Resource Network"
Invited Plenary Paper at Second Regional Symposium on Optoelectronics, 27th-28th Nov 1989, Jakarta, Indonesia (also delivered as invited paper at First National Symp. on Laser Technology, UTM, Skudai, Malaysia in Oct 1989
S. Lee

62 "Diagnostics of the Plasma Focus"
Invited Paper at the Beijing College on Plasma Physics: Diagnostics, Oct 29 - Nov 1989, Beijing, P.R. China
Proc. pg. 5-19 (Edited by S.T. Tsai and Y.A. Li) 1989
S. Lee

63 "A Compact Low Voltage Flash X-ray Tube"
Japan J. Appl. Phys. 28, 1264 (1989)
C.S. Wong, S. Lee, C.X. Ong and O.H. Chin

64 "Shadowgraphy of Laser Induced Sparks"
J. Fiz. Mal., 11, 24 (1990)
S.S. Kumar, S. Lee, H.B. Ahmad and C.Y. Jing

65 "A Simple Shadowgraphy system and some results"
Jurnal Fizik Malaysia, 11, 1, (1990)
S. Lee et. al.

66 "Plasma Focus Dynamics - Its Role in An AAAPT Training Programme"
Invited Paper-Association Plasma Studies of China Third Summer School - University of Tsingdao, Tsingdao, P.R. China 15-22 August 1990; Procs. Ed. by Tsai Shih-Tung and Li Yin-An pg. 53 (1990), also presented as invited paper at Quaid-I-Azam University, Islamabad, Pakistan during Basic Course on Plasma Physics Oct. 29th., 1990
S. Lee

67 "Training Programmes for Research Transfer-Experience and Results"
Invited Paper Int. Conf. on Physics & Physicists for Development - Univ. of Twente, Netherlands 11-12th Sept. 1990
S. Lee

68 "Effect of Targets on Plasma Focus Dynamics"
IEEE Trans Plasma Science, Dec 1990 (scheduled)
S. Lee et. al.

69 "Laser Induced Plasmas and Fusion"
Guest Lectures - Second South East Asian Laser School, Yogyakarta, Indonesia (7 - 18th, Jan. 1991)
S. Lee

70 "An Investigation of the Ion Beam of a Plasma Focus Using a Metal Obstacle and a Deuterated Target"
IEEE Trans. on Plasma Science (accepted)
S.P. Moo, C.K. Chakrabarty and S. Lee

J. Phys. D: Appl. Phys., 16 (1983) 2463–2469. Printed in Great Britain

An energy-consistent snow-plough model for pinch design

S Lee

Plasma Research Laboratory, Physics Department, University of Malaya, Kuala Lumpur 22-11, Malaysia

Received 18 May 1983

Abstract. A general theory is developed in which a snow-plough model is coupled to a circuit equation with two scaling parameters for the computation of pinch trajectory and pinch current covering the complete range of pinch operation. The integration of the pinch trajectory is properly terminated by the application of a new energy balance theory. This model thus gives the trajectory, the current and the quasi-equilibrium pinch radius ratio r_p/r_0 for the genral pinch device. The simplicity and flexibility of this physically realistic model make it an excellent aid for the consideration of pinch design.

1. Introduction

An extensive review of the dense Z-pinch has been made by Haines (1982) in which various classes of pinches are discussed. In the present paper we deal with electromagnetically driven pinches in a cylindrical imploding geometry. The trajectory and final radius of such a pinch has been described by Potter (1978) using a slug model but applied only to the case of a constant-current pinch.

More recently an energy balance theory has been formulated to give an energy-consistent estimate of the radius ratio r_p/r_0 of an electromagnetically compressed pinch at quasi-equilibrium. This theory is applicable to pinches of varying length driven by varying currents (Lee 1981, 1983). In this theory, the work done by the magnetic piston is assumed to be converted, without loss, into the enthalpy of the pinched plasma. This conversion yields an expression for the plasma temperature T at the quasi-equilibrium radius r_p of

$$T = \frac{\mu}{4\pi^2 \rho r_p^2 l_p} \frac{M}{R_0} \frac{\gamma - 1}{\gamma} \frac{1}{\zeta} \int_{r_p}^{r_0} \frac{lI^2 \, dr}{r} \tag{1}$$

where μ is permeability, M is the molecular weight of the ambient gas, R_0 is the universal gas constant and γ, ρ, l_p and ζ are respectively the specific heat ratio, the density, the length and the departure coefficient of the plasma compressed to radius r_p. The length of the column is written as l at the corresponding radial position r of the magnetic piston driven by current I.

If r_p is the position of the magnetic piston at quasi-equilibrium then at this radius there is also balance between the kinetic and the magnetic pressures. This gives us

independently another expression for the quasi-equilibrium temperature:

$$T = \frac{\mu I_p^2}{8\pi^2 \rho r_p^2} \frac{M}{R_0} \frac{1}{\zeta}. \tag{2}$$

Combining equations (1) and (2) gives

$$I_p^2 = \frac{2(\gamma - 1)}{\gamma l_p} \int_{r_p}^{r_0} \frac{I^2 l \, dr}{r}. \tag{3}$$

In general if I and l are known functions of r, then the integral of equation (3) may be evaluated and this equation may then be solved for the radius ratio. The simplest example with a constant current, constant length pinch has already been discussed (Lee 1983) and has the solution:

$$(r_p/r_0) = \exp[-\gamma/2(\gamma - 1)]. \tag{4}$$

For the general situation of a constant length pinch powered by a capacitor bank it is well-known that the early trajectory is adequately described by a snow-plough equation. The snow-plough equation, however, does not provide a physical termination to the pinch trajectory and the integration of the equation leads to a zero radius for the magnetic piston. This has serious consequences on the use of the circuit-coupled snow-plough equation for design purposes since a zero radius introduces an infinite inductance into the circuit equation.

In this paper we use the snow-plough equation coupled to a circuit equation to compute the trajectory of the pinch. At each step of the numerical integration we check for the energy balance as expressed by equation (3) so that the integration may be correctly stopped at the point at which further compression is energetically not possible. The energy efficiency of the system as an example may then be correctly discussed.

2. Theory

The pinch system is shown schematically in figure 1. When the switch is closed, the capacitor voltage, initially V_0, is applied across the pinch electrodes. The gas breaks down and the current starts flowing axisymmetrically in a thin sheath of radius r_0. The current sheath, acting as a magnetic piston with field B_θ, then implodes inwards sweeping all the gas encountered into itself. This is the snow-plough model. The equation of motion (Glasstone and Lovberg 1960) of the imploding plasma sheet driven by the

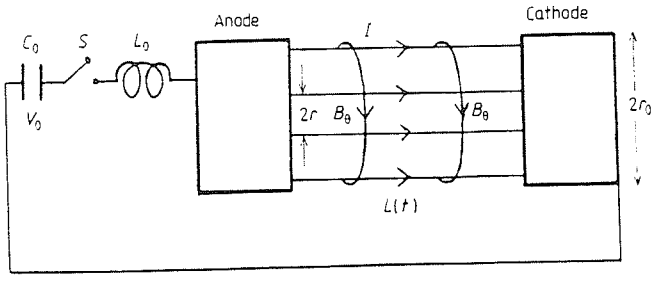

Figure 1. Schematic drawing showing pinch dynamics and pinch circuit (Note: The pinch return current path is at a radial position of r_0; this is not shown in the drawing).

magnetic piston is:

$$\frac{\mathrm{d}}{\mathrm{d}t}\left(\pi\rho_0(r_0^2 - r^2)\frac{\mathrm{d}r}{\mathrm{d}t}\right) = -\frac{\mu I^2}{4\pi r}. \tag{5}$$

From figure 1 we may write the circuit equation as:

$$\frac{\mathrm{d}}{\mathrm{d}t}[(L + L_0)I] = V_0 - \frac{\int I\,\mathrm{d}t}{C_0} \tag{6}$$

where C_0 is the capacitance of the capacitor bank, L_0 is the fixed stray inductance of the circuit, and where the inductance of the current sheet at r with its coaxial return path at radial position r_0 may be written as

$$L = (\mu l/2\pi)(\ln r_0/r)$$

where l is the length of the pinch.

Thus the radial position r of the pinch may be coupled by its inductance into the circuit equation (6), which may then be written as:

$$\left(\frac{\mu l}{2\pi}\ln(r_0/r) + L_0\right)\frac{\mathrm{d}I}{\mathrm{d}t} - \frac{\mu l}{2\pi}I\frac{(\mathrm{d}r/\mathrm{d}t)}{r} = V_0 - \frac{\int I\,\mathrm{d}t}{C_0}. \tag{7}$$

Equations (5) and (7) may be integrated simultaneously to obtain the trajectory r and the current I as functions of t. Equation (3) is used to determine the limit of the integration.

The equations are normalised in the usual manner as follows:

$$\kappa = r/r_0 \qquad \tau = t/t_c \qquad \iota = I/I_0$$

where

$$t_c = (L_0C_0)^{1/2} \qquad I_0 = V_0/(L_0/C_0)^{1/2}.$$

The normalised equations are:

Motion:
$$\frac{\mathrm{d}^2\kappa}{\mathrm{d}\tau^2} = \frac{-\alpha^2\iota^2/\kappa + 2\kappa(\mathrm{d}\kappa/\mathrm{d}\tau)^2}{(1 - \kappa^2)} \tag{8}$$

Circuit:
$$\frac{\mathrm{d}\iota}{\mathrm{d}\tau} = \frac{1 - \int\iota\,\mathrm{d}\tau + \beta\iota(\mathrm{d}\kappa/\mathrm{d}\tau)/\kappa}{(1 - \beta\ln\kappa)} \tag{9}$$

where $\alpha = t_c/t_p$ and the characteristic pinch time t_p is found from the normalisation to be:

$$t_p = \left(\frac{4\pi^2\rho_0 r_0^4}{\mu I_0^2}\right)^{1/2}.$$

Here α is a scaling parameter which may be used to set the ratio of the characteristic capacitor discharge time to characteristic pinch time to suit the system under consideration. The other scaling parameter is $\beta = (\mu l/2\pi)/L_0$ which is the ratio of the characteristic pinch inductance to the external inductance.

The energy balance equation may also be written in normalised form as:

Energy balance:
$$\iota_p^2 = \frac{2(\gamma - 1)}{\gamma}\int_{\kappa_p}^{1}\frac{\iota^2\,\mathrm{d}k}{\kappa} \tag{10}$$

where we have taken l as constant.

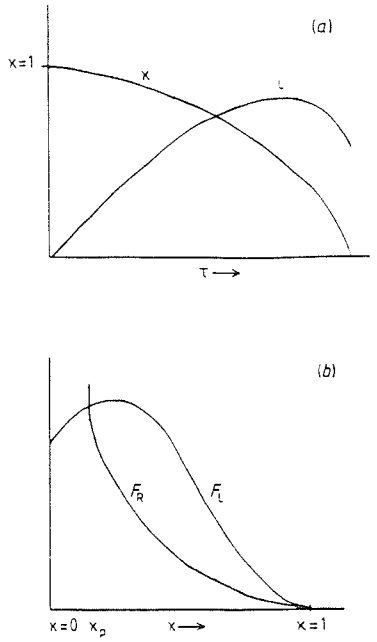

Figure 2. (*a*) General forms of snow-plough trajectory and circuit current as functions of time. (*b*) General forms of the functions F_L and F_R as derived from figure (2*a*).

In order to solve equation (10) simultaneously with equations (8) and (9) by a step-by-step integration it is necessary to analyse the form of equation (10). We first note that the snow-plough trajectory and current have the general form as shown in figure 2(*a*). Thus the two functions representing the left-hand-side (denoted by F_L) and the right-hand-side (denoted by F_R) respectively of equation (10) have the general forms as shown in figure 2(*b*). We consider these general forms. From the point $\kappa = 1$, as κ decreases the function F_L is greater than the function F_R until a cross-over point. The cross-over point must occur, since from its general form the function F_R tends to infinity as κ tends to zero whilst the function F_L remains finite. Thus the point where the two curves intersect is the energy balance limit giving the quasi-equilibrium radius ratio, κ_p, of the pinch.

For design purposes it should be useful to compute an energy matching ratio (EMR) defined here as the ratio of the plasma enthalpy at the minimum radius to the energy initially stored in C_0. Thus

$$\text{EMR} = \int_{r_p}^{r_0} \frac{\mu^2 I^2}{4\pi^2 r^2 (2\mu)} 2\pi r l \, \mathrm{d}r / (\tfrac{1}{2} C_0 V_0^2)$$

which may be written as

$$\text{EMR} = \beta \int_{\kappa_p}^{1} \frac{\iota^2 \, \mathrm{d}\kappa}{k}. \tag{11}$$

We note that EMR is just $\beta\gamma/[2(\gamma - 1)]$ times the function F_R.

3. Computation procedure

The initial conditions are

$$\tau = 0 \qquad \kappa = 1 \qquad \frac{d\kappa}{d\tau} = 0 \qquad \frac{d^2\kappa}{d\tau^2} = \text{undefined from equation (8)}$$

$$\int \iota \, d\tau = 0 \qquad \iota = 0 \qquad \frac{d\iota}{d\tau} = 1.$$

The initial value of $d^2\kappa/d\tau^2$, although undefined from equation (8), yet has a physically definite value considering the behaviour of equation (8) starting from finite values of τ towards a value of τ tending towards zero. As a practical solution an initial value of $d^2\kappa/d\tau^2$ may be estimated and the integration of the equations (8) and (9) may then be attempted on a step-by-step basis with τ being incremented by steps of 0.001. Using a linear approximation method it was found that an initial value of $d^2\kappa/d\tau^2 = -0.02$ enables fairly rapid convergence to a smooth solution. The accuracy of the solution was also checked by varying the starting value of $d^2\kappa/d\tau^2$ and also the step size and checking that the starting value and the step size (when sufficiently small) did not affect the solution at finite values of τ.

To check on the energy balance represented by equation (10), at each step the value of ι^2 was computed and also the quantity designated as ENSUM, where

$$\text{ENSUM}_{\text{new}} = \text{ENSUM}_{\text{old}} + [2(\gamma - 1)/\gamma](\kappa_{\text{new}} - \kappa_{\text{old}})/\kappa_{\text{new}}.$$

The quantity κ_{new} is the last computed value of κ and the quantity $(\kappa_{\text{new}} - \kappa_{\text{old}})$ is the last computed step of κ. This quantity $\text{ENSUM}_{\text{new}}$ thus represents the function F_R at every point τ. At each step the quantity $\text{ENSUM}_{\text{new}}$ was compared with the quantity ι^2 and when $\text{ENSUM}_{\text{new}} \geqslant \iota^2$ the intercept point as shown in figure 2(*b*) has been reached and the pinch limit was found. The value of

$$\text{EMR} = \text{ENSUM}_{\text{new}}\beta\gamma/[2(\gamma - 1)]$$

was also computed at the pinch limit.

4. Results and pinch design consideration

It was found that for a given value of α, say $\alpha = 1$, the EMR increases towards 1 for $\beta \rightarrow \infty$. For a practical pinch, however, β is of the order of 1. For example, for a pinch of length 10 cm connected to a fast capacitor bank with $L_0 = 10$ nH, the value of β is 2. Thus for the purpose of pinch design one should examine β in the range of 0.1 to 10, computing the values of EMR as α is varied. The resulting family of curves is shown in figure 3.

From figure 3 for a chosen value of β we can then obtain the α parameter for which the EMR is a maximum. For example for $\beta = 1$ a good value of α for operation from the point of view of energy efficiency would be $\alpha = 0.7$. In figure 4 several examples of the trajectories are shown. The case of $\alpha = 1$, $\beta = 0.01$ (with $L_0 \gg L$) has a pinch current that is almost sinusoidal. The case of $\alpha = 100$, $\beta = 0.01$ is for a pinch operating in the early part of a sinusoidal current, corresponding to the well-known case of $I = I_0 \omega t$. In both these cases, the EMR is very small. The other case shown is for $\alpha = 0.7$, $\beta = 1$ and

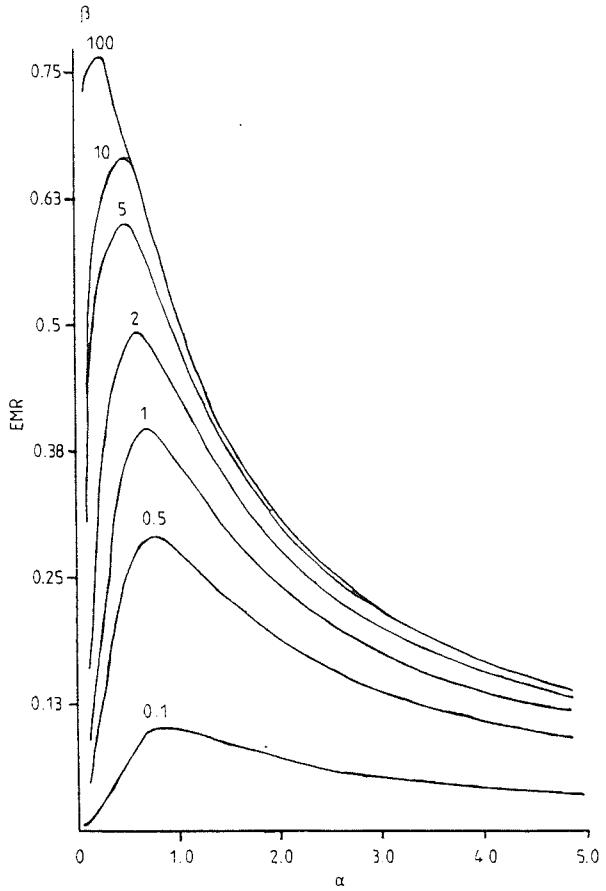

Figure 3. Computed values of the EMR versus α for various values of β.

this is a typical pinch with good energy matching, with an EMR of almost 40%. For this case a peak current of 73% of I_0 is reached and the final radius ratio is 0.39. In terms of the production of a high density plasma this radius ratio is disappointing. However, a consideration of equation (10) and figure 2(*b*) raises the exciting possibility of current shaping to increase pinch compression.

5. Conclusion

A general theory has been discussed in which a snow-plough model is coupled to a circuit equation for the computation of pinch trajectory and pinch current. The pinch trajectory is correctly terminated at the quasi-equilibrium pinch radius r_p by an energy balance equation, so that this theory gives the trajectory as well as the final pinch radius ratio. Two scaling parameters are incorporated in the equations. The first, α, scales the ratio of the capacitor characteristic time to the pinch characteristic time. The second, β, scales the ratio of the pinch characteristic inductance to the fixed circuit inductance. These two scaling parameters allow the theory to cover the complete range of pinch operation.

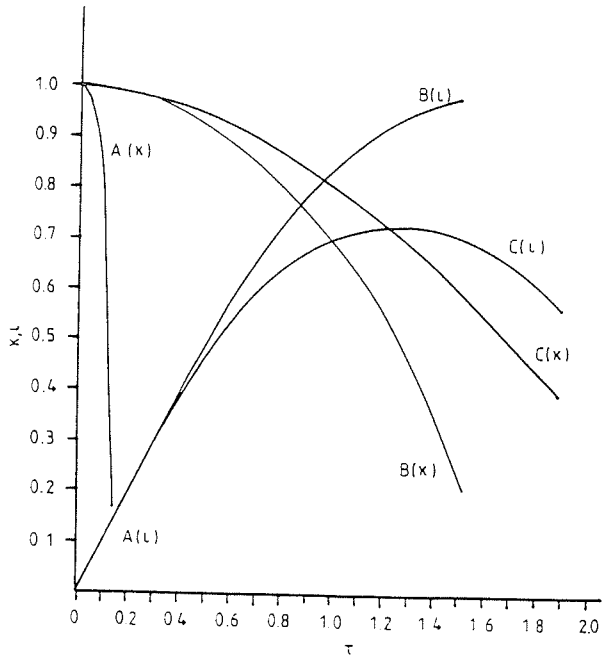

Figure 4. Computation of κ and ι as functions of τ for three sets of scaling parameters: (A) $\alpha = 100$, $\beta = 0.01$ (linear current); (B) $\alpha = 1$, $\beta = 0.01$ (sinusoidal current); and (C) $\alpha = 0.7$, $\beta = 1$ (typical example with good energy coupling).

Acknowledgment

The help of several members of the Plasma Research Group of the University of Malaya in parts of the computation is acknowledged.

References

Glasstone S and Lovberg R H 1960 *Controlled Thermonuclear Reactions* (New York: Van Nostrand) p 231
Haines M G 1982 *Phys. Scr.* **T2/2** 380
Lee S 1981 *Bul. Fizik Malaysia* **2** 240
—— 1983 *Plasma Phys.* **25** 571
Potter D 1978 *Nucl. Fusion* **18** 813

Aust. J. Phys., 1983, 36, 891–5

Radius Ratios of Argon Pinches

S. Lee

Plasma Research Laboratory, Physics Department,
University of Malaya, Kuala Lumpur 22–11, Malaysia.

Abstract

According to a new theory based on energy balance, the radius ratio r_p/r_0 of a constant-current plasma pinch depends only on the value of the effective specific heat ratio γ of the pinched plasma. In this paper the value of γ for argon is computed as a function of temperature. From these values the constant-current pinch ratios are computed. The results show argon pinch ratios of about 0·08 from (2–4) × 10^6 K, rising to 0·18 at 1·1 × 10^7 K and to 0·27 at 10^8 K. There is good agreement between this theory and an Imperial College measurement of $r_p/r_0 \sim 0{\cdot}17$ for a constant-current argon pinch at an estimated temperature of 1 keV.

1. Introduction

It has been observed (Yong and Lee 1977) that an argon plasma focus undergoes more severe electromechanical effects than a pure deuterium plasma focus. An increase in compression has also been observed (Baldock *et al.* 1982) in the linear Z-pinch operated in argon when compared with one operated in hydrogen. It is proposed here that this effect can be explained solely on the basis of the difference in effective specific heat ratio γ of the argon plasma when compared with the γ of the deuterium or hydrogen plasma.

This proposal is a natural consequence of the recent energy balance theory by Lee (1981, 1983). Based on a fundamental consideration of energy and pressure balance, the pinch ratio r_p/r_0 for the case of a constant-current constant-length pinch is found to be

$$r_p/r_0 = \exp\{-\gamma/2(\gamma-1)\}, \qquad (1)$$

where γ is the effective specific heat ratio of the hot plasma in quasi-equilibrium. For a high temperature hydrogen pinch $\gamma = \frac{5}{3}$ and this constant-current pinch ratio is 0·29, according to equation (1). This agrees, within experimental error, with the published result (Haines 1981) of Imperial College of a pinch ratio of approximately $\frac{1}{3}$ measured on a constant-current hydrogen pinch.

An extension of this theory to the deuterium plasma focus, taken as a pinch of constant current but of variable length (Lee 1983), gives a pinch radius ratio of 0·14 compared with an experimental value of 0·13.

Recently a pinch ratio of approximately $\frac{1}{6}$ has been reported (Baldock *et al.* 1982) for a constant-current argon pinch at an estimated temperature of 1 keV. This

0004-9506/83/060891S02.00

greater compression appears consistent with equation (1) since it is known that γ for argon drops to below 1·20 during its freely ionizing temperature range. As the temperature is increased above 4×10^6 K, argon becomes fully ionized and γ then rises towards $\frac{5}{3}$. It is the purpose of this paper to compute the value of γ as a function of temperature and hence to compute the value of r_p/r_0 for an argon pinch as a function of temperature.

2. Theory

The value of γ may be defined in terms of the enthalpy per unit mass h as

$$h = \frac{\gamma}{\gamma-1}\frac{R_0}{M}T\zeta, \tag{2}$$

where the departure coefficient is

$$\zeta = 1 + \sum_{r=1}^{r=n} r\alpha_r. \tag{3}$$

Here R_0 is the universal gas constant, M the molecular (or atomic) weight, T the temperature and α_r the fraction of the plasma which is ionized to the rth ionized state. The enthalpy of a plasma such as argon may also be written in terms of its ionization and excitation energies as

$$h = \tfrac{5}{2}(R_0/M)T\zeta + m^{-1}\sum_{r=1}^{r=n}\alpha_r I_r + m^{-1}\sum_{r=0}^{r=n}\alpha_r \bar{E}_r. \tag{4}$$

Here I_r is the total energy required to raise one ion from its unionized state to its rth ionized state and $\bar{E}_r$ is the average excitation energy per rth ionized ion. The ionization potentials are known quantities whilst the excitation energies are temperature dependent and are computed from the tabulated values of atomic and ionic energy levels and the statistical weights of these levels (Moore 1949), once a suitably converging summation scheme is adopted. The mass of the atom or ion is here denoted as m.

From equations (2) and (4) we may compute the value of γ by writing

$$\frac{\gamma}{\gamma-1} = \tfrac{5}{2} + \left(m^{-1}\sum_{r=1}^{r=n}\alpha_r I_r + m^{-1}\sum_{r=0}^{r=n}\alpha_r \bar{E}_r\right)\Big/(R_0/M)T\zeta, \tag{5}$$

where the α_r may be computed for any given temperature by the use of Saha's equations. We note that equation (5) gives $\gamma = \frac{5}{3}$ for two cases:

(*a*) when the excitation and ionization modes are negligible at low T;

(*b*) when the temperature is high enough for the plasma to be fully ionized, the numerator of the second term in equation (5) reaches its maximum value. If T is increased further this second term in equation (5) becomes correspondingly smaller and becomes negligible when compared with the first term at a sufficiently high temperature so that $\gamma\rightarrow\frac{5}{3}$. For argon, as will be seen, the value of γ is 1·569 at 4×10^7 K.

3. Computation Procedure

In several argon computations (Lee 1969) for relatively low temperatures the values of γ have been computed by a full procedure involving the evaluation of the

α_r and the $\bar{E}_r$ up to 5×10^4 K at which point $\alpha_4 \approx 1$. In a more recent full computation (Yong and Lee 1977), on the trajectory of an argon plasma focus, the values of the ionization fractions have been determined up to full ionization with $\alpha_{18} = 1$ being achieved at 4×10^6 K.

We discuss here a simple procedure for estimating the values of γ from the available curves of the α. To adopt this procedure we note that as the curve for a particular ionization fraction, α_s say, rises to its maximum value of $\alpha_s \leqslant 1$, at that point the second term of equation (5) is dominated by the ionization energy. At this point, if we assume that $\alpha_s \approx 1$, then we have

$$\sum_{r=1}^{r=n} \alpha_r I_r + \sum_{r=0}^{r=n} \alpha_r \bar{E}_r \approx I_s. \tag{6}$$

Hence, estimates of the values of γ may be readily made at 17 points of temperature, each point at successively higher temperatures corresponding to the maximum values of α_1 to α_{17}, by use of the approximate formula

$$\frac{\gamma}{\gamma-1} \approx \tfrac{5}{2} + \frac{I_s/m}{(R_0/M)T(1+s\alpha_s)}. \tag{7}$$

Here we emphasize that the approximation (7) is used only at the successive temperature corresponding to the maximum of each of the α versus T curves.

As T is raised further and α_{18} approaches 1, the approximation (7) becomes exact and remains exact for all higher temperatures of T. Thus for all values of T higher than that temperature at which $\alpha_{18} = 1$ we have

$$\frac{\gamma}{\gamma-1} = \tfrac{5}{2} + \frac{I_{18}/m}{19(R_0/M)T}. \tag{8}$$

Table 1. Data for computation of γ

s	T (K)	$\zeta \sim 1+s\alpha_s$	I_s (eV)	s	T (K)	$\zeta \sim 1+s\alpha_s$	I_s (eV)
1	$1{\cdot}5\times10^4$	2	15·8	10	$3{\cdot}4\times10^5$	11	1479
2	$2{\cdot}3\times10^4$	3	43·4	11	$3{\cdot}8\times10^5$	12	2009
3	$3{\cdot}3\times10^4$	4	84·3	12	$4{\cdot}6\times10^5$	13	2669
4	$5{\cdot}0\times10^4$	5	144	13	$5{\cdot}5\times10^5$	14	3394
5	$6{\cdot}3\times10^4$	6	219	14	$6{\cdot}0\times10^5$	15	4209
6	$8{\cdot}5\times10^4$	7	310	15	$6{\cdot}5\times10^5$	16	5159
7	$9{\cdot}5\times10^4$	8	434·4	16	$1{\cdot}8\times10^6$	17	6189
8	$2{\cdot}1\times10^5$	9	577·9	17	$2{\cdot}7\times10^6$	18	10889
9	$3{\cdot}0\times10^5$	10	999	18	$4{\cdot}0\times10^6$	19	15989

4. Results

For the computation of γ by the above simplified procedure, we used the data of Yong and Lee (1977) in Table 1. These data were used with equations (7) and (8) to compute the values of γ as a function of T. The result is shown in Fig. 1 (curve A). It is seen that the value of γ has fallen to below 1·14 by 15000 K and remains at about 1·12 up to about 10^5 K when $\alpha_7 \approx 1$. Thus in this range of temperature (which has been called the freely ionizing range) the effective degree of freedom f of the

plasma is approximately 17, since we may write $\gamma = (2+f)/f$. The next ionization involves a closed shell and thus between $1{\cdot}2$ and 2×10^5 K the plasma behaves energetically as a fully ionized gas so that over this range of temperature γ rises smoothly from $1{\cdot}12$ to $1{\cdot}20$. Then from 2 to $6{\cdot}5\times10^5$ K the value of γ again drops towards $1{\cdot}14$ as the ionization effects gain further dominance over the plasma enthalpy. From $6{\cdot}5\times10^5$ to $1{\cdot}8\times10^6$ K there is a further smooth rise of γ from $1{\cdot}14$ to $1{\cdot}26$, as over this range the plasma again behaves energetically as a fully ionized gas because of the closed-shell effect. Between $1{\cdot}8$ and 4×10^6 K the value of γ drops to $1{\cdot}24$; and above 4×10^6 K, with the gas fully ionized, there is a smooth and gradual increase of γ towards its eventual value of $\frac{5}{3} = 1{\cdot}667$. By 4×10^7 K its value has already increased to $1{\cdot}569$.

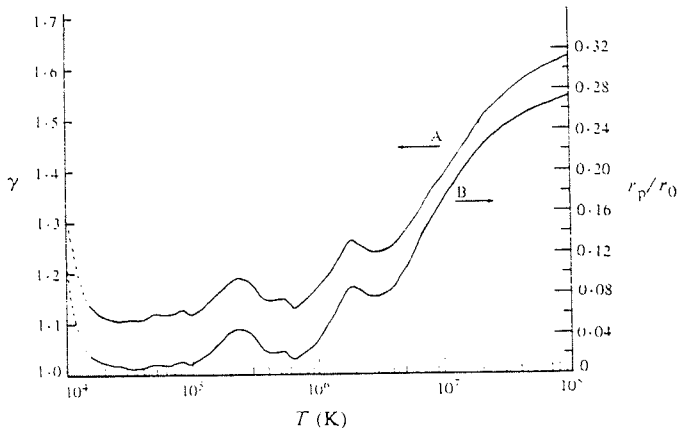

Fig. 1. Effective specific heat ratio γ (curve A), and constant-current pinch radius ratio r_p/r_0 (curve B) of argon as functions of temperature.

Curve B of Fig. 1 shows the effect of the variation of γ with temperature on the radius ratio of argon pinches. The two limits of the pinch ratios are noted from equation (1). For $\gamma = 1$, corresponding to a gas with $f = \infty$, the pinch radius ratio is 0; and, for $\gamma = \frac{5}{3}$, corresponding to an ideal gas with $f = 3$, the radius ratio is $0{\cdot}287$.

As a function of temperature, the argon pinch ratio drops to as low as $0{\cdot}006$ and remains around this value from 2×10^4 to 10^5 K, this being the freely ionizing range. Between 10^5 and 2×10^5 K, exhibiting fully ionized behaviour, the pinch ratio rises to $0{\cdot}04$, then falls again in the next freely ionizing range from 3 to $6{\cdot}5\times10^5$ K at which temperature α_{15} reaches a maximum. From $7{\cdot}0\times10^5$ to $1{\cdot}8\times10^6$ K the pinch ratio rises again to $0{\cdot}085$ in closed-shell behaviour with $\alpha_{16} \approx 1$ over this large range of temperature. Between 2 and 4×10^6 K the pinch ratio drops slightly to around $0{\cdot}08$ before rising towards the limit of $0{\cdot}29$ in the final fully ionized phase. This final rise starts at 4×10^6 K. The pinch ratio has increased to a value of $0{\cdot}17$ at 10^7 K, $0{\cdot}25$ at 4×10^7 K and $0{\cdot}27$ at 10^8 K.

Thus we note that for a constant-current argon pinch in the temperature range from 2 to 4×10^6 K, the pinch compression is more severe than in a hydrogen (or deuterium) pinch, with a pinch ratio of $0{\cdot}08$ compared with the hydrogen pinch

ratio of 0·29. This difference in pinch ratios is still significant at 10^7 K with 0·17 for the argon pinch compared with 0·29 for the hydrogen pinch. At 10^8 K the difference has become insignificant.

5. Comparison with Experiment

As mentioned in the Introduction, the plasma focus in argon produces spectacularly more severe electromechanical effects than in a deuterium focus. This is indicated by the enhanced severity in current dip and voltage spike. This effect is consistent with a greater compression in argon.

Since the focus temperature is known to be in the region from 0·5 to 0·7 keV (Lee 1982), the compression in the argon focus, in terms of the pinch ratio, could be two to three times more severe than in the hydrogen focus according to our results as shown by curve B in Fig. 1. Thus for the plasma focus there is qualitative agreement between the above computation and experimental observations.

Finally we consider the Imperial College observation of a constant-current pinch ratio in argon of $\frac{1}{6} \approx 0{\cdot}17$ (Baldock *et al.* 1982) at an estimated temperature of ≈ 1 keV. This result compares with our computed value of 0·18 for argon at the corresponding temperature of $1{\cdot}16 \times 10^7$ K.

It would appear from this theory that if a high compression pinch is desired at a high temperature, say between 10^7 and 10^8 K, it would be advantageous to use krypton or xenon as, for these two gases, in this range of temperature the ionization is still not complete and the resultant low γ values would ensure correspondingly small pinch ratios. This effect could be important in the development of intense soft X-ray sources from pinch-type devices.

6. Conclusions

In this paper we have used a simplified method to compute the values of the specific heat ratio of argon as a function of temperature. From the energy balance theory we then computed the argon pinch ratio r_p/r_0 (which is γ-dependent) as a function of temperature. The results indicate agreement between our theory and a measurement of the argon pinch ratio made at Imperial College.

References

Baldock, P. F. M., *et al.* (1982). 'High Density High Temperature Plasma Production in Fast Z-pinch'. Ninth Ann. Conf. on Plasma Physics, Oxford.

Haines, M. G. (1981). *Phil. Trans. R. Soc. London* A **300**, 649.

Lee, S. (1969). Ph.D. Thesis, Australian National University.

Lee, S. (1981). *Bul. Fizik Malaysia* **2**, 240.

Lee, S. (1982). 'Fusion Energy–1981', IAEA-SMR-82, p. 288 (IAEA: Vienna).

Lee, S. (1983). *Plasma Phys.* **25**, 571.

Moore, C. E. (1949). 'Atomic Energy Levels', U.S. Bureau of Standards Cir. No. 467.

Yong, Y. C., and Lee, S. (1977). 'Multiple Ionization in an Argon Plasma Focus', Proc. Physics Symp. 1977, Kuala Lumpur, p. 149 (Univ. of Malaya: Kuala Lumpur).

Manuscript received 26 May, accepted 24 June 1983

Bull. Phys. M'sia 4, 189 (1983)

STREAK PHOTOGRAPHY AND FOCUS PINCH MODELS

T.Y. TOU and S. LEE FIPM
Plasma Research Laboratory
Physics Department
University of Malaya, Kuala Lumpur.

Abstract

A parameter of great importance in the understanding of the plasma focus is the pinch radius ratio, that is, the ratio of the final compressed radius to the initial radius. Only in 1982 has the pinch radius ratio been predicted self-consistently by generalised slug model and energy balance theory. Energy balance theory predicts that the pinch radius ratio depends only on the specific heat ratio, γ. We compute the values of γ for various temperatures in argon and hence calculate the corresponding pinch radius ratio. There is good agreement between the theoretical predictions and the streak photograph measurements on both the deuterium and argon focus.

Introduction

Despite the considerable advances in plasma focus technology, particularly in diagnostics, there has been very little reliable measurement on the dynamic pinch phase of the focus. These measurements have become important recently in the light of new theoretical modelling in which the key feature of the focus has been identified as an axial elongation of the column during the radial pinch phase, this elongation being found to be almost solely responsible for the reduced radius ratio of the focus when compared to the pinch. There is now no question about the role of this elongation which has been clearly identified in recent shadowgraphs[1].

Other questions regarding focus dynamics include whether the focus pinch agrees with the generalised slug model[2], which predicts that the piston driving the plasma slug-layer comes to a stop as the shock front hits the axis. Earlier ideas of the focus pinch suggests that a reflected shock wave from the axis will interact with the piston resulting in oscillations in the pinch column.

In these present experiments, streak photographs have been carefully taken and interpreted to show the pinch dynamics. Features in the photograph have been compared to the expected features from the generalised slug model. Radius ratios have been measured from these streak photographs and compared to predictions based on an energy balance model.

The Generalised Slug Model

A simple 1–D physical model, the generalised slug model[2], was adopted to describe the radial pinch dynamics of the plasma focus.

The slug model[3] assumes an infinite conductivity in the plasma and hence the current flows through a thin layer at the magnetic piston position. The imploding piston which sweeps up the collision-dominated plasma is preceded by a strong shock of small thickness. The plasma between the piston and the shock front is assumed to have uniform pressure in space though this pressure will change with time. During the pinch dynamics, the shock front is allowed to separate from the piston by an adiabatic rule. Hence, one would envisage an increasing plasma slug thickness as the piston collapses radially. When the shock front hits the axis, the magnetic piston comes to rest.

A comprehensive computation has been done on the deuterium focus[2] using the generalised slug model in which the circuit was coupled and the axial elongation of the plasma column was included in a self-consistent manner. The computation yielded the trajectories of the piston, shock front and the increasing thickness of the slug. The computation was terminated when the shock front hits the axis (see Fig. 1).

The Energy Balance Theory

In the pinch phase of the plasma focus, as the current sheath sweeps around the end of the centre electrode, the initial length of the plasma column is zero. As the piston implodes radially, the length of the plasma column ℓ increases and it is found empirically[4] to be :

$$\ell = \ell_p \left(\frac{r_o - r}{r_o - r_p} \right) \tag{1}$$

where r_o is the initial radius, r_p is the final pinch radius and ℓ_p is the length of the final compressed plasma column.

Assume that the total work done by the magnetic piston goes into the plasma without loss[5]. When the plasma temperature is high enough so that the kinetic pressure equals the magnetic pressure, the piston comes to rest at the quasi-equilibrium radius r_p, leading to an expression[6] :

$$I_p^2 = \frac{2(\gamma - 1)}{\gamma \ell_p} \int_{r_p}^{r_o} I^2 \ell \frac{dr}{r} \tag{2}$$

where I_p is the current flowing at the time the quasi-equilibrium is first established and γ is the specific heat ratio.

During the pinch phase, the current I deviates by only 5% and for simplicity a constant I is assumed. Then by substituting equation (1) into equation (2), thus allowing equation (2) to be integrated, an expression is obtained :

$$ln(1/\kappa_p) = (1-\kappa_p)(1 + \frac{\gamma}{2(\gamma-1)}) \quad (3)$$

where $\kappa_p = r_p / r_o$. Hence, the pinch radius ratio depends only on the value of γ.

Specific Heat Ratio computation for Argon

An approximate calculation on specific heat ratio for argon was done very recently[7,8]. Consider the plasma enthalpy per unit mass :

$$h = \frac{\gamma}{\gamma-1}\frac{R_o T Z}{M} \quad (4)$$

and from the atomic physics point of view :

$$h = \frac{5}{2}\frac{R_o T Z}{M} + \frac{1}{m}\left(\sum_{i=1}^{i=n} \alpha_i I_i + \sum_{i=0}^{i=n} \alpha_i \bar{E}_i\right) \quad (5)$$

where α_i is the i^{th} degree of ionization, R_o the universal gas constant, I_i the total ionization potential from its unionized state, $\bar{E}_i$ the average excitation energy of i^{th} ionization stage, T the temperature, Z the departure coefficient, m the mass of a particle and M is the molecular weight. From equations (4) and (5), an expression for γ may be written as

$$\gamma = 1.0 + \frac{1.0}{1.5 + F1/F2} \quad (6)$$

where $$F1 = \frac{1}{m}\left(\sum_{i=1}^{i=n} \alpha_i I_i + \sum_{i=0}^{i=n} \alpha_i \bar{E}_i\right) \text{ and}$$

$$F2 = \frac{R_o T Z}{M}$$

Assuming Local Thermodynamic Equilibrium in the argon plasma focus[9], the degrees of ionization α_i (i = 1, 2, ..., 18) can be found using Saha equations at any given temperature. The values I_i and $\bar{E}_i$ are computed at each temperature so that γ can be calculated using equation (6). Figure 2 shows the results of the computation with γ, Z and κ_p as functions of temperature in the region of 1×10^6 °K to 1×10^7 °K, where κ_p is computed using equation (3).

Experimental Set Up

Figure 3a is a schematic representation of the experimental set up for the streak photography in the plasma focus. It is important to synchronise the operation of the streak camera and the start of the pinch phase of the plasma focus. To start with, an SCR pulse (labelled 1) is sent to trigger a Krytron high-voltage pulse generator[10]. A low output pulse (labelled 2) from this generator then triggers the oscilloscope which, besides recording the voltage and current signals, is also used as a delay unit for triggering the streak camera (labelled 4 & 5). About 1.65μs after the oscilloscope is triggered, the capacitor bank is switched by the high voltage pulses from this generator

(labelled 3). The oscilloscope delays the operation of the streak camera for a further 2–3 μs which is typically the time required for the current sheath to move down the axial acceleration region to the start of the radial implosion phase.

The streak camera focusses through a narrow slit at about 3mm off the surface of the centre electrode (see Fig. 3b). So the camera is restricted to record only the images that appear through the slit. Consider that during the pinch phase, the plasma collapses radially from the co-ordinates (r_1, t_1) to (r_2, t_2) and to (r_3, t_3), where r and t are radial position and time respectively. The plasma images at these co-ordinates are electronically recorded on the polariod film with plasma radial position r on the vertical axis, and time t on the horizontal axis (see Fig. 3c).

Experimental Observations

In these experiments, streak photographs are taken for the deuterium and argon focus. Figure 4a shows the deuterium pinch dynamics at 5.5 *torr*, 12 kV capacitor bank voltage. The collapse trajectories of the piston κ_p and shock front κ_s are observed. The slug thickness and shock speed increase as the piston implodes radially. As the shock front implodes onto the axis, a pinch radius ratio of 0.18 is measured from the streak photograph. This compares to 0.17 obtained by the generalised slug model. The further motion of the piston from this point is not predicted by the generalised slug model. An estimated value of 0.12 for the final pinch radius ratio is compared to 0.14 predicted by equation (3) with $\gamma = 5/3$. A value of 0.13 was obtained by shadowgraphy[1].

For the case of the argon plasma focus, a relatively weak-focussing shot at 1 *torr*, 20 kV is presented in Fig. 4b. We note that when the shock front hits the axis a pinch radius ratio of 0.12 is obtained. The piston moves further inwards until a final radius ratio of $k_p = 0.07$ is observed.

To compare this with the theory as predicted by equation (3), we need to know the value of γ of the plasma column. This is estimated in the following way. The final shock speed as the shock front hits the axis is estimated from the streak photograph (Fig. 4b) as 3×10^5 ms^{-1}. From strong shock theory and the data of Figure 2, this speed corresponds to a temperature of 3×10^6 °K. For this temperature and again using the data of Figure 2 we estimate a value of $\gamma = 1.34$ for the observed plasma column. Then using the energy balance theory of equation (3), we obtain an expected value of $\kappa_p = 0.06$.

Conclusion

The streak photographs indicate that several features of the slug model are observed. Firstly, the plasma layer thickness increases as it moves radially inwards. Secondly, the radius ratio of the deuterium focus as the shock hits the axis is measured as 0.18, in agreement with the slug model value of 0.17. The piston is also observed to slow down rapidly as the shock goes on axis.

However, the slug model requires the piston to stop as the shock hits the axis. An examination of the slug model (which does not incorporate any loss mechanism) for energy balance by applying equation (2) at its quasi-equilibrium point shows that

the generalised slug model is not energy-consistent, and that energy consistency requires a further inward motion of the piston. Thus the end-point of the generalised slug model needs to be corrected by energy balance consideration. In deuterium the final radius ratio κ_p = 0.12 (measured) compares with a value of κ_p = 0.14 (energy balance theory).

The streak photograph measurement of argon confirms the same comparative features. A final value of κ_p = 0.07 (measured) may be compared with a value of κ_p = 0.06 (energy balance theory).

It appears that the generalised slug model with an energy balance correction for κ_p is able to describe the main features of the pinch phase of the plasma focus for both deuterium and argon.

REFERENCES

1. S. Lee, Y.H. Chin, Bul. Fiz. Mal. 2, 105 (1981)
2. S. Lee, Bul. Fiz. Mal. *3*, 197 (1982)
3. D.E. Potter, Nucl. Fusion *18*, 813 (1978)
4. S. Lee, Bul. Fiz. Mal. *2*, 240 (1981)
5. S. Lee, Plasma Phys. *25*, 571 (1983)
6. S. Lee, J. Appl. Phys. *54*, 3603 (1983)
7. S. Lee, Bul. Fiz. Mal. *4*, 1 (1983)
8. S. Lee, Australian J. Phys. (to be published in Dec. 1983 issue).
9. Y.C. Yong, 'Multiple Ionizations in Argon Plasma Focus'. M.Sc. thesis, UM, Kuala Lumpur (1978)
10. S.P. Thong and S. Lee, Malaysian J. Sc. 2(B), 157 (1973).

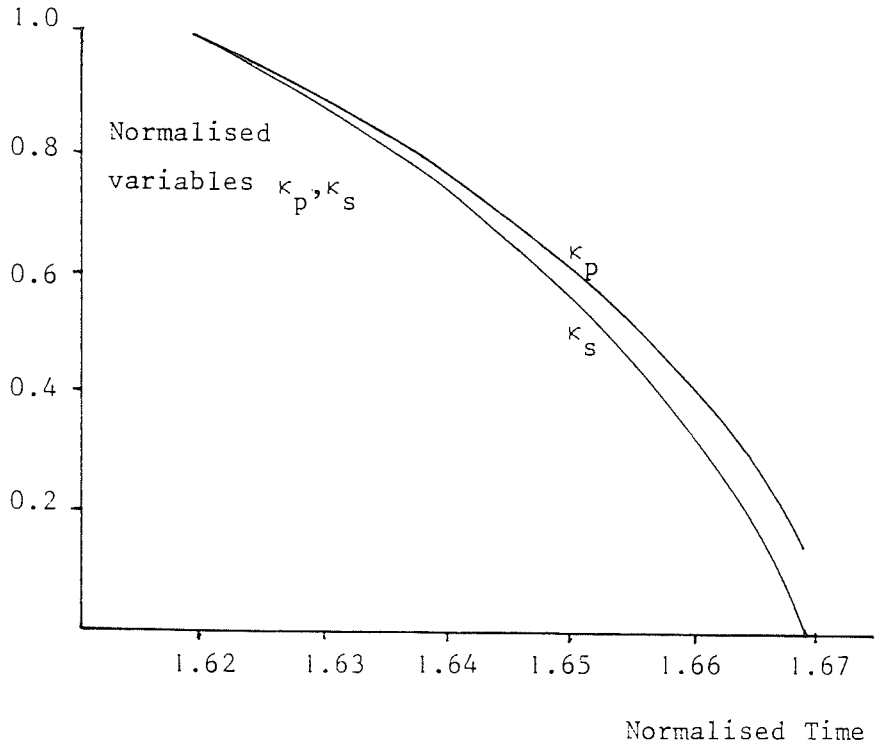

Figure 1. Trajectories of the magnetic piston (κ_p) and the shock front (κ_s) according to the generalised slug model.

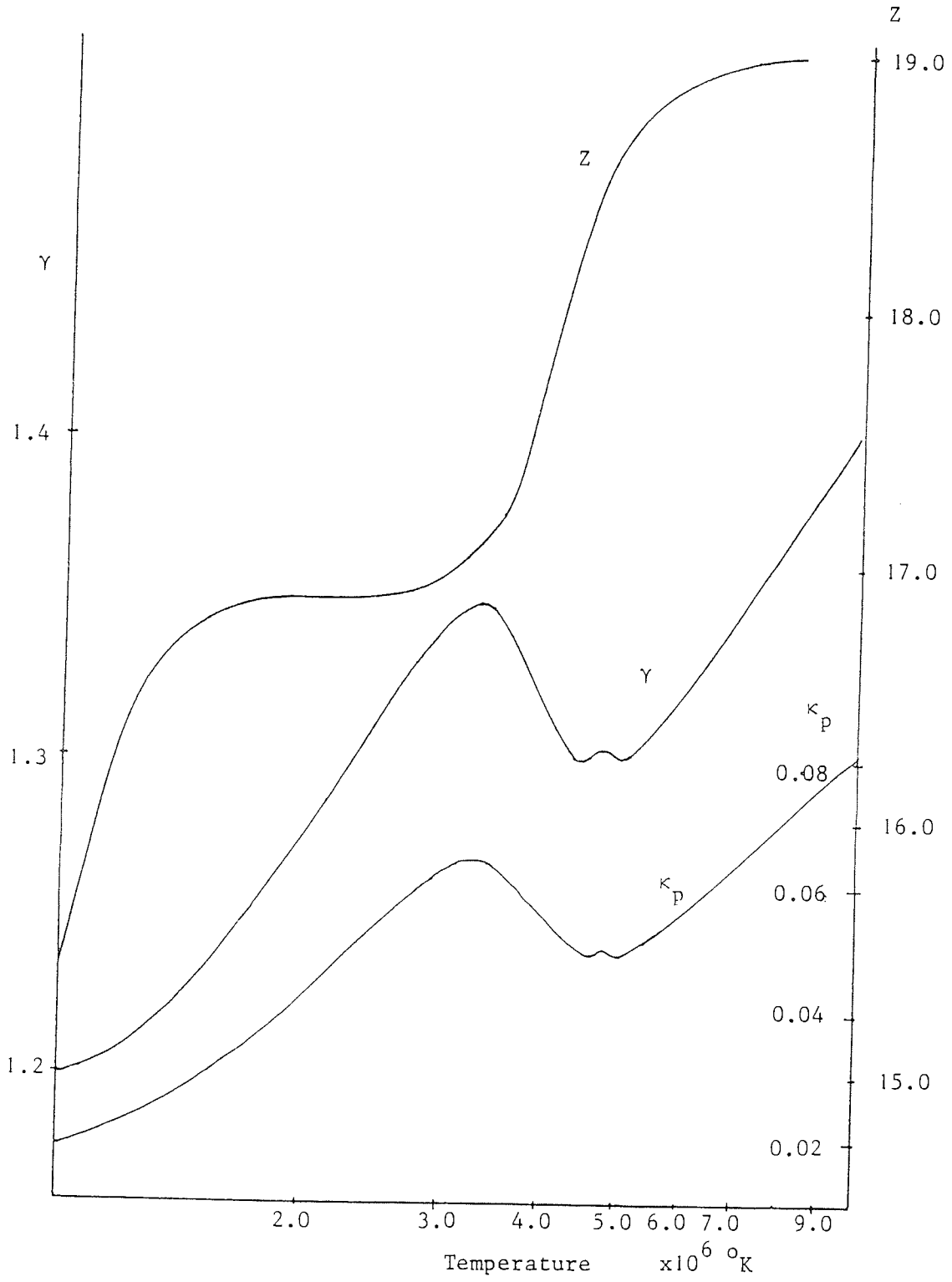

Figure 2. Solutions of Z, γ and κ_p as functions of temperature.

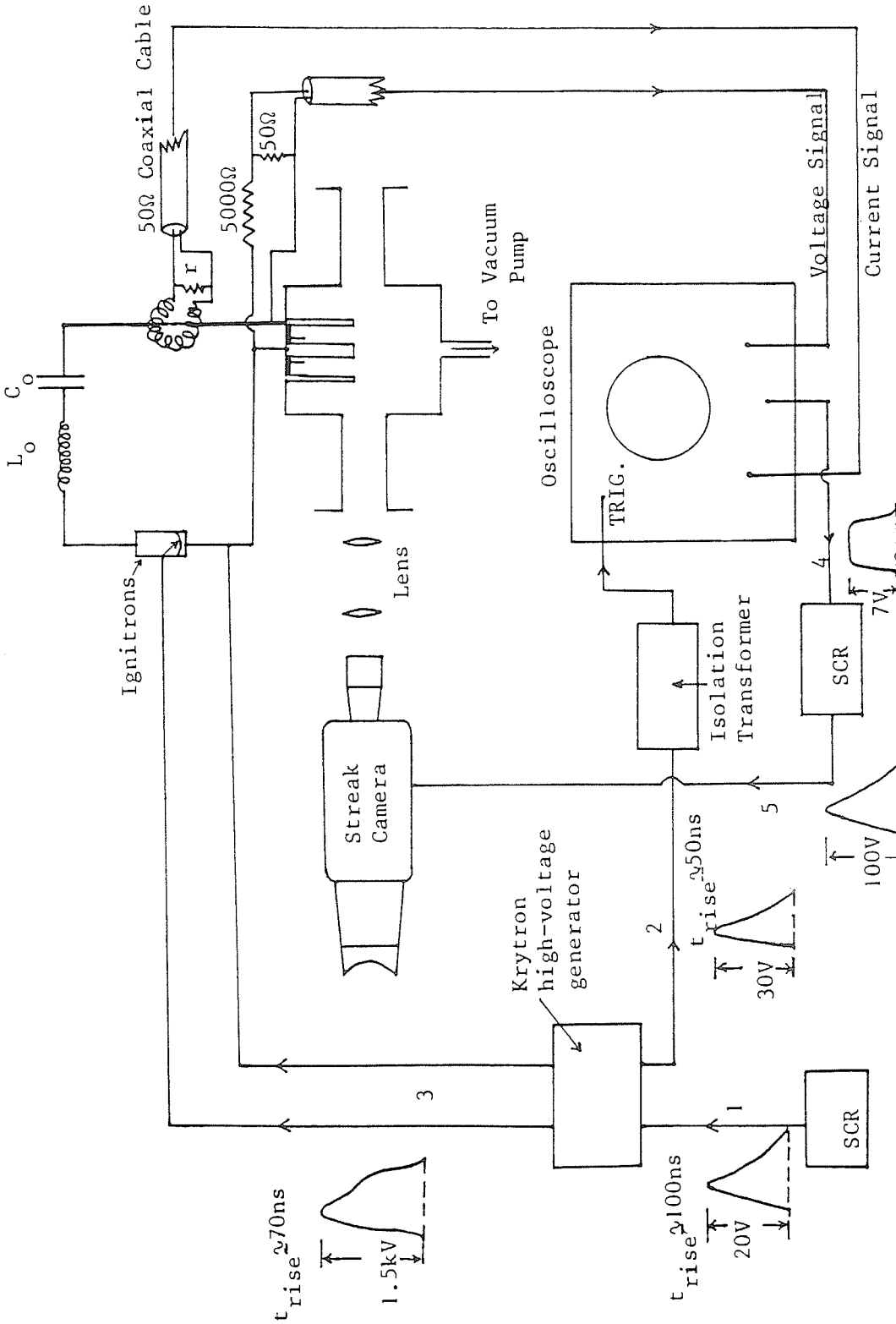

Fig. 3a Schematic representation of the arrangement for the streak photography of the plasma focus.

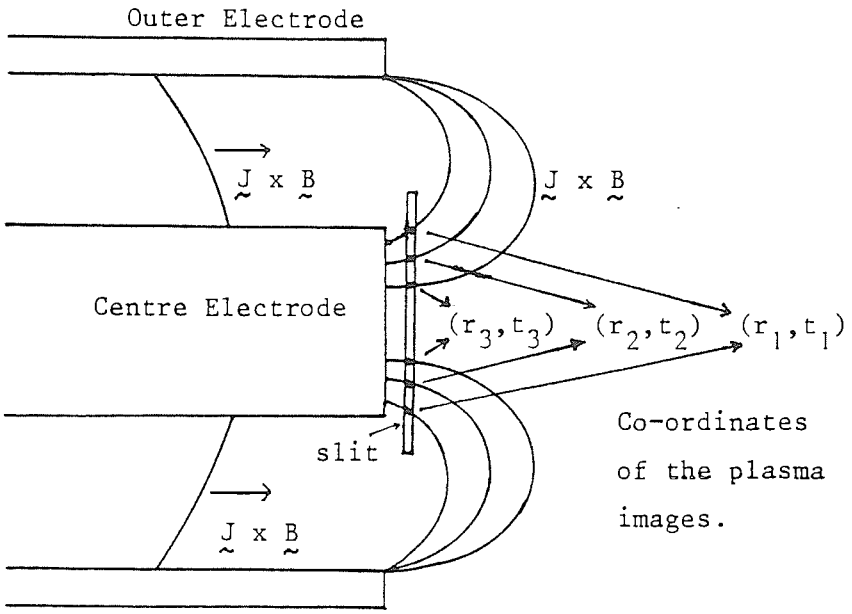

Fig. 3b Position of the narrow slit.

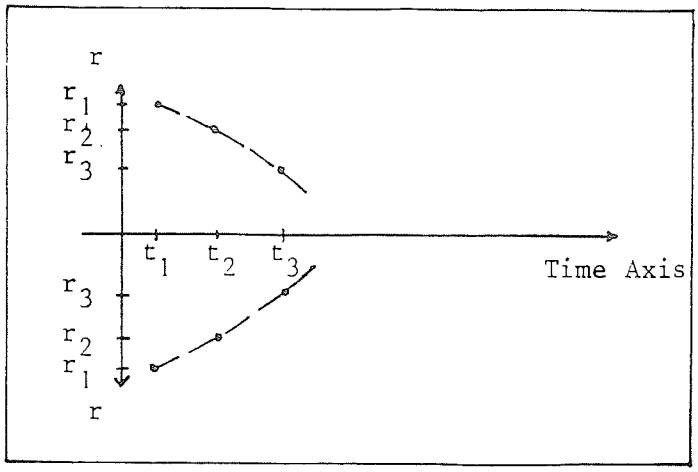

Fig. 3c Plasma images being recorded on the polariod film.

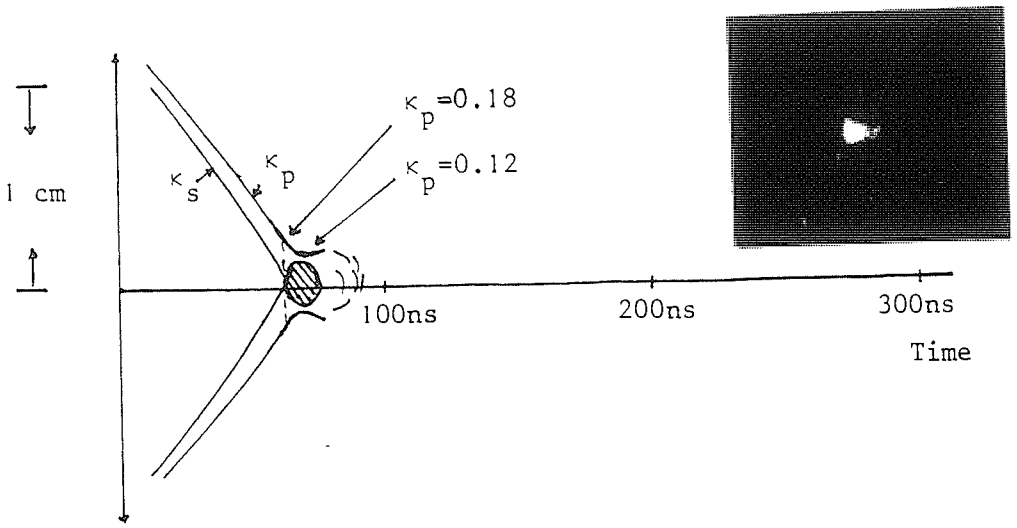

Fig. 4a Streak photograph of a deuterium focus pinch at 5.5torr, 12 kV.

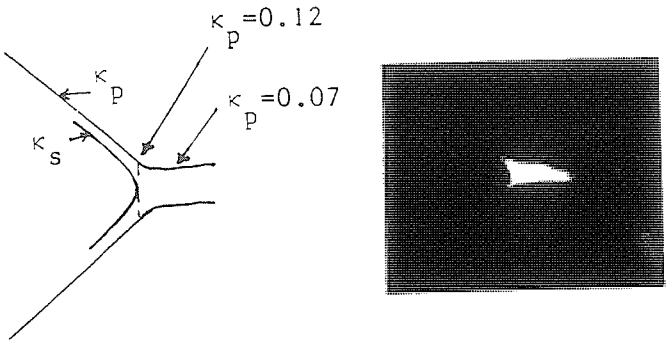

Fig. 4b Streak photograph of a argon focus pinch at 1 torr, 20 kV.

Bull. Phys. M'sia 4, 1, (1983)

THE EFFECT OF SPECIFIC HEAT RATIO ON ARGON PINCH CONFIGURATION

S. LEE, FIPM
Plasma Research Laboratory
Physics Department
University of Malaya, Kuala Lumpur

Abstract

A simple energy balance theory by Lee indicates that plasma pinch radius ratios (r_p/r_o) are dependent only on the specific heat ratio γ of the pinched plasma. We extend the theory to argon and estimate the values of γ as a function of temperature, using, for simplicity, a method which avoids the computation of excitation energies. From these values of γ, the pinch ratios are computed as a function of temperature. The result shows pinch ratios around 0.08 from $2 - 4 \times 10^6$ K; 0.18 at 1 keV and rising to 0.27 at 10^8 K. There is good agreement between this theory and an Imperial College measurement of $r_p/r_o \sim 0.17$ at 1 keV in argon.

Introduction

The quasi-equilibrium geometry of Z-pinches has been of considerable interest in the study of high temperature dense plasmas. Recently Lee[1,2] has shown that a simple analysis based on a fundamental consideration of energy and pressure balance suffices to yield a pinch ratio, for the case of a constant current, constant length pinch, of

$$\frac{r_p}{r_o} = exp \frac{-\gamma}{2(\gamma - 1)} \qquad (1)$$

where γ is the specific ratio of the hot plasma in quasi-equilibrium. For a high temperature hydrogen pinch $\gamma = \frac{5}{3}$ and this constant current pinch ratio turns out to be 0.29. This agrees, within experimental error, with published results [7, 8] of Imperial College of a pinch ratio $r_p/r_o \sim 1/3$ measured on a constant current hydrogen pinch, the Mark I.

An extension of this result to the plasma focus taken as a pinch of constant current but variable length[2] gives a pinch radius ratio of 0.14 compared to experimental results of 0.13 reported by the Malaysian Group[3]. These values may also be compared with a value of 0.16 computed from a self-consistent MHD theory[9] with inherent energy balance which allows for a self-consistent length variation (which turned out to be non-linear) and a circuit-coupled current.

There have been suggestions that in argon more intense pinch compressions are observed, both in pinches[8] as well as in the plasma focus[6]. Indeed a pinch ratio of 1/6 has been reported for a constant current argon pinch[8] at an estimated temperature of 1 keV. On the basis of pinch theory represented by Eqn. (1) this appears consistent since it is well known that the effective specific heat ratio for argon drops towards 1.14 during its freely-ionising[5] temperature range.

However since argon becomes completely ionised in the range of temperatures above 4 x 10^6 K, it may be shown that the value of γ will hen rise towards 5/3. Thus on the basis of Eqn. (1) alone one could expect the pinch ratios of argon to be $\sim$ 1/50 in its freely ionizing range of temperature and that the pinch ratios will increase from 1/50 towards 0.29 again as the value of γ rises from 1.14 towards 5/3.

Because of the traditional complex approach to the problem there has been little quantitative data presented in the literature of either pinch ratios or values of γ for high temperature plasmas such as in argon. In this paper we use a simple method to estimate the values of γ for argon over a range of temperatures such as might be encountered in high temperature pinches, hollow pinches or the plasma focus.

Theory

The value of γ may be defined in terms of the enthalpy per unit mass h as:

$$h = \frac{\gamma}{\gamma - 1} \frac{R_0}{M} T\zeta \qquad \ldots. (2)$$

where the departure coefficient

$$\zeta = 1 + \sum_{r=1}^{r=n} r\,\alpha_r \qquad \ldots. (3)$$

Here $R_\circ$ is the universal gas constant and M the molecular (or atomic) weight, T the temperature and α_r the fraction of the plasma which is ionized to the rth-ionized state. The enthalpy of a plasma such as argon may also be written in terms of its ionization and excitation energies as:

$$h = \frac{5}{2}\frac{R_\circ}{M} T\zeta + \frac{1}{m}\sum_{r=1}^{r=n} \alpha_r I_r + \frac{1}{m}\sum_{r=0}^{r=n} \alpha_r \bar{E}_r \qquad \ldots.(4)$$

Here I_r is the total energy required to raise one ion from its un-ionized state to its rth-ionized state and $\bar{E}_r$ is the average excitation energy per rth-ionized ion. The ionization potentials are known quantities whilst the excitation energies are temperature dependent and can be computed from the tabulated values of atomic and ionic energy levels and the statistical weights of these levels[4], once a suitably converging summation scheme is adopted[5]. The mass of the atom or ion is here denoted as m.

From equations (2) and (4) we may compute the value of γ by writing:

$$\frac{\gamma}{\gamma - 1} = \frac{5}{2} + \frac{\frac{1}{m}\sum_{r=1}^{r=n} \alpha_r I_r + \frac{1}{m}\sum_{r=0}^{r=n} \alpha_r \bar{E}_r}{\frac{R_\circ}{M} T\zeta}$$

where the $\alpha_r's$ may be computed, for any given temperature, by the use of Saha's equations[6].

This equation gives $\gamma/(\gamma - 1) = 5/2$ or $\gamma = 5/3$ for two cases:

(a) when the excitation and ionization modes are negligible at low T,

(b) when the temperature is high enough for the plasma to be fully ionized the numerator of the second term in equation (5) reaches its maximum value. If T is increased further, this second term in equation (5) becomes correspondingly smaller and becomes negligible when compared with the first term at sufficiently high temperature so that $\gamma \to 5/3$. For argon, as will be seen the value of γ is 1.569 for $T = 4 \times 10^7$ K.

Computation procedure

In several argon computations[5] at relatively low temperatures the values of γ have been computed by a full computation involving the evaluation of the $\alpha_r's$ and the excitation energies $E_r's$ up to $T \sim 5 \times 10^4$ °K at which point $\alpha_4 \sim 1$. In a more recent full computation[6] on the trajectory of an argon plasma focus the value of α_r have been determined up to full ionization with $\alpha_{18} = 1$ being achieved at 4×10^6 K. In that computation however the value of γ was determined only up to $T \sim 2 \times 10^5$ K.

An estimate of the values of γ to cover the whole range of temperatures of interest may be made by noting that as the curve for a particular ionization fraction, α_s say, rises to its maximum vallue of $\alpha_s \cong 1$, at that point the second term of equation (5) is dominated by the ionization energy. That is

$$\sum_{r=1}^{r=n} \alpha_r I_r + \sum_{r=0}^{r=n} \alpha_r \bar{E}_r \cong I_s \qquad \ldots (6)$$

Hence estimates of the value of γ may be easily made at 17 points of temperatures, each point at successively higher temperatures corresponding to the maximum values of α_1 to α_{17}, by the use of the approximate formula:

$$\frac{\gamma}{\gamma - 1} \cong \frac{5}{2} + \frac{I_s/m}{\frac{R_\circ}{M} T(1 + s\alpha_s)} \qquad \ldots (7)$$

Here we emphasize that the approximation of equation (7) is used only at the successive temperature corresponding to the maximum of the α_r curves i.e. for each $\alpha_s \sim 1$.

As T is raised further and α_{18} approaches 1, the approximation of (7) becomes exact and remains exact for all higher temperatures of T; thus

$$\frac{\gamma}{\gamma - 1} = \frac{5}{2} + \frac{I_{18}/m}{19(\frac{R_\circ}{M}) T} \qquad \ldots (8)$$

Results

For our computation of γ we use the data[6] as tabulated in Table 1. We then use equations (7) and (8) and compute the value of γ as a function of temperature. The result is shown in Fig. 1 (a).

It is seen that the value of γ has fallen to below 1.14 by 15,000 K and remains about 1.12 up to about 10^5 K when $\alpha_7 \sim 1$. Thus in this range of temperature (which

has been called the freely ionizing range)[5] the effective degree of freedom, f, in the plasma is $f \cong 17$ (from $\gamma = [2+f]/f$). The next ionization involves a closed shell and, between 1.2×10^5 K to 2×10^5 K, the plasma behaves energetically as a fully ionized gas. Over this range of temperature γ rises smoothly from 1.12 to 1.20. From 2×10^5 K to 6.5×10^5 K the value of γ again drops towards 1.14 as the ionization effects gain further dominance over the plasma enthalpy. From 6.5×10^5 K to 1.8×10^6 K there is a further smooth rise of γ from 1.14 to 1.26 as over this range the plasma again behaves energetically as a fully ionized gas because of the closed shell effect. Between 1.8×10^6 to 4×10^6 K the value of γ drops to about 1.24, and above 4×10^6 K there is a smooth increase of γ towards its eventual value of 5/3 or 1.667. By 4×10^7 K the value of γ is 1.569.

In Fig. 1 (b) we show the effect of the variation of γ with temperature on the radius ratios of argon pinches. The two limits of the pinch ratios are noted from equation (1). For $\gamma = 1$ corresponding to a gas with $f = \infty$, the pinch ratio $r_p/r_o = 0$ and for $\gamma = 5/3$ corresponding to an ideal gas with $f = 3$, $r_p/r_o = 0.287$.

For argon pinches, the pinch ratio drop to as low as 0.006 and remains around this value in the range of temperatures from 2×10^4 to 10^5 K, the freely ionizing range. From 10^5 to 2×10^5, exhibiting fully ionized behaviour, the pinch ratio rises to 0.04, then falls again in the next freely ionizing range from 3×10^5 to 6.5×10^5 K at which temperature α_{15} reaches a maximum. From 7.0×10^5 to 1.8×10^6 K the pinch ratio rises again to 0.085 in closed-shell behaviour with $\alpha_{16} \sim 1$ over this large range of temperature. Between $2 \times 10^6 - 4 \times 10^6$ the pinch ratio drops slightly to around 0.08 before rising towards 0.29 in the final fully ionized phase. This final rise starts at 4×10^6. The pinch ratio reaches 0.17 at 10^7 K, 0.25 at 4×10^7 K and 0.27 at 10^8 K.

Thus for constant-current argon pinches in the temperature range of $2-4 \times 10^6$ K, the compression is more severe than in a hydrogen (or deuterium) pinch; with a pinch ratio of 0.08 compared to hydrogen pinch ratio of 0.28. This difference is still significant at 10^7 K with 0.17 for the argon pinch compared to 0.28 for the hydrogen pinch. At 10^8 K, the difference becomes small.

Comparison with Experiment

It has been observed in plasma focus experiments that in argon the focus produced spectacularly more severe electromechanical effects (than in a deuterium focus) as indicated by the enhanced severity in current dips and voltage spikes[6]. This effect is consistent with a greater compression.

Since the focus temperature in the UMDPFI is known to be in the region of 0.5 – 0.7 keV, the compression in the argon focus in terms of pinch ratios, could be 2 to 3 times more severe than the hydrogen focus. Thus there is qualitative agreement between the above computation and experimental observations in the UMDPFI. It is envisaged that more experimental measurements on the argon focus will provide quantitative confirmation of this γ effect.

It has been reported[7] that in a constant-current, constant-length pinch operated at the Imperial College a pinch ratio of $\frac{1}{3} \sim 0.33$ has been consistently observed in hydrogen

whilst a pinch ratio of $\frac{1}{6} \sim 0.17$ has likewise been observed in argon[8] at an estimated temperature of 1 keV. These results compare with our theoretical values of 0.29 for hydrogen and 0.18 for argon at the corresponding temperature of 1.14×10^7K (1 keV).

It would appear from this computation that if a high compression pinch is desired at a high temperature, say between $10^7 - 10^8$K, it would be advantageous to use krypton or even xenon as, for these 2 gases, at this range of temperature the ionization is still not complete and the resulting low γ values would ensure correspondingly small pinch ratios. The predictions of this theory could be important in the development of intense soft x-ray sources from pinch-type devices.

Conclusion

In this paper we have used an approximate method to estimate the value of γ for argon as a function of temperature. From the energy balance theory we then compute the argon pinch ratio (which is γ-dependent) as a function of temperature. The results indicate a remarkable agreement between our theory and a measurement of argon pinch ratio made at the Imperial College. We intend to extend this theory to the plasma focus work in our UMDPFI facility.

References

1. S. Lee, Bul. Fiz, Malaysia *2*, 240 (1981).
2. S. Lee "Energy Balance and the Radius of Electromagnetically Pinched Plasma Columns" – accepted for publication in Plasma Physics.
3. S. Lee "The Application of Energy Balance to Compute Plasma Pinch Ratios" – accepted for publication in J. App. Phys.
4. C. E. Moore "Atomic Energy Levels" U. S. Bureau of Standards Cir. 467, 1949.
5. S. Lee "Transverse Ionizing Shock Waves in a Planar Electromagnetic Shock Tube" – Ph.D. Thesis, A.N.U. 1969.
6. Y. C. Yong and S. Lee "Multiple Ionization in an Argon Plasma Focus" – Procs. Symp. Phys. (UM) 149 (1977).
7. M. G. Haines Phil. Trans. R. Soc. Lond. A300, 649 (1981).
8. P. F. M. Baldock, A. E. Dangor, M. B. Favre Dominguez, D. Grimsley, J. D. Hares, E. Kahan, S. Lee, "High density, high temperature plasma production in fast *Z*-pinch" Ninth Ann. Conf. Plasma Phys. Oxford (1982).
9. S. Lee Bul. Fiz, Malaysia *3*, (1982).

Table 1: Data for computation of γ

s	$T(K)$	$\zeta \sim 1 + s\alpha_s$ (approx.)	I_s (eV)
1	1.5×10^4	2	15.8 ($\sim 2.5 \times 10^{-18}$ J)
2	2.3×10^4	3	43.4
3	3.3×10^4	4	84.3
4	5.0×10^4	5	144
5	6.3×10^4	6	219
6	8.5×10^4	7	310
7	9.5×10^4	8	434.4
8	2.1×10^5	9	577.9
9	3.0×10^5	10	999
10	3.4×10^5	11	1479
11	3.8×10^5	12	2009
12	4.6×10^5	13	2669
13	5.5×10^5	14	3394
14	6.0×10^5	15	4209
15	6.5×10^5	16	5159
16	1.8×10^6	17	6189
17	2.7×10^6	18	10889
18	4.0×10^6	19	15989

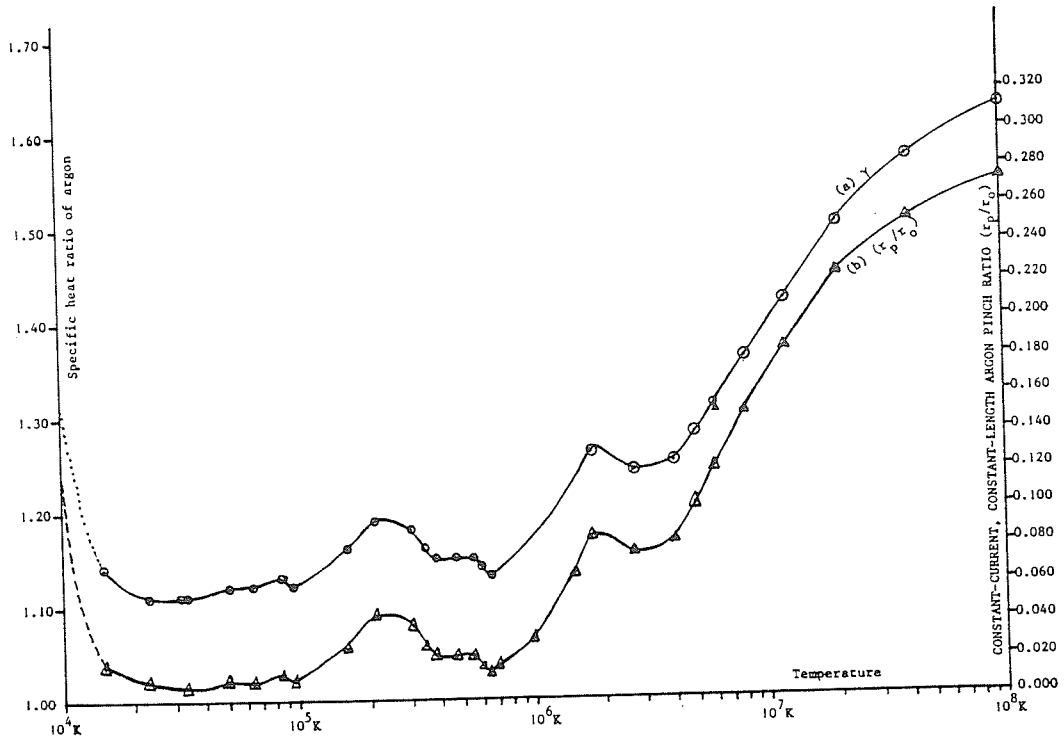

Fig. 1 (a) Specific heat ratio and
(b) Pinch ratio of argon as functions of temperature

Bull. Phys. M'sia 4, 57 (1983)

STRONG MHD COMPRESSIONS IN A COUPLED CIRCUIT

S. LEE, FIPM, A. C. CHEW, MIPM, C. S. WONG, MIPM, T. Y. TOU,
Y. S. CHAN, S. L. LO, K. E. LING, C. H. TAN, S. H. YAP, E. H. YEO
Plasma Research Laboratory
Physics Department
University of Malaya
Kuala Lumpur 22–11
Malaysia

ABSTRACT

The general solution of the trajectory of fast MHD compressions is presented with a circuit-coupled current. A snow-plow model is used with a realistic quasi-equilibrium end-point as provided by the energy balance of Lee. The results show that at a typical operating parameter of $\beta = 1$, maximum efficiency is achieved at $\alpha = 0.7$ with a plasma energy of 30% of the capacitor storage.

INTRODUCTION

The classical snow-plow model is considered here for the strong magnetohydrodynamic (MHD) compression. In this model a magnetic piston is used to radially compress a column of plasma at high temperatures (Fig. 1).

A thin cylindrical current sheath forms as the discharge across the gas occurs. This sheath produces a magnetic field (B_θ) which interacts with the current and produces a foce acting radially inwards. The gas that the current sheath encounters is swept up in the sheath, assumed thin. Thus in the classical model, the sheath collapses to the axis and a zero-radius plasma[1] is formed. This is not a physical situation[1]. Physically, the pinch must compress to a minimum radius at which point quasi-equilibrium conditions are achieved.

Lee[2-5] has formulated an energy balance theory which, by equating the work done by the magnetic piston to the plasma enthalpy, defines the quasi-equilibrium pinch radius by the following equation:

$$I_p^2 = \frac{2(\gamma - 1)}{\gamma \ell_p} \int_{r_p}^{r_o} I^2 \ell \frac{dr}{r} \qquad \ldots\ldots (1)$$

where I_p is the current flowing at the time the pinch reaches quasi-equilibrium and ℓ_p is the length of the pinch at quasi-equilibrium. Using this model Lee has predicted the radius ratio r_p/r_o for several cases: (1) 0.29 for the case of a constant current, constant length pinch[2] with $\gamma = 5/3$; (2) 0.17 for the case of a constant length pinch with $\gamma = 5/3$

driven by a current of form $I = I_o\ \omega t$; and 0.21 for a typical sinusoidal driving current[4]; (3) 0.14 for the pinch phase of a $\gamma = 5/3$ plasma focus[3] and (4) 0.18 for the case of a constant current constant length pinch in argon[5] at a temperature at 1 keV. For all these cases, agreement with experimentally observed radius ratios has been noted.

In this paper we consider the case of a general circuit-coupled current, and its effect on the radius ratio of strong MHD compressions. We couple a circuit equation to the snow-plow equation thus obtaining simultaneously the radius and current as functions of time. In the numerical integration, equation (1) is used to determine the radius at which quasi-equilinrium is achieved. Thus the method gives the trajectory as well as the radius ratio.[4]

THEORY

Referring to Fig. 1, the current comes from a large capacitor bank. This current sets up an azimuthal magnetic field B_θ outside the current sheath. Interaction between B_θ and the current density J, provides the inwardly imploding force which pushes the current sheath radially inwards sweeping up all the gas encountered. We can write the equation of motion of the moving plasma sheath as:

$$\frac{d}{dt}\left\{\pi \rho_o\ (r_o^2 - r^2)\ \ell \frac{dr}{dt}\right\} = -\frac{B_\theta^2}{2\mu}\ 2\pi r \ell$$

Rearranging, we get:

$$\frac{d}{dt}\left\{\left(1 - \frac{r^2}{r_o}\right)\ \frac{dr}{dt}\right\} = -\frac{\mu I^2}{4\pi^2 \rho_o r_o^2 r} \qquad \ldots\ldots (2)$$

since for this geometry $B_\theta = \dfrac{\mu I}{2\pi r}$

From this equation, it is possible to compute the trajectory of the pinch if the current is a known function of time. The limit of the trajectory is governed by the energy balance of equation (1).

The current supplied by the capacitor bank when passing through the plasma is affected by the behaviour of the plasma. The inductance of the plasma changes as the radius of the plasma changes. The circuit in Fig. 2 is a schematic sketch of the coupling.

For the condition of the strong MHD pinch compression the pinch resistance may be assumed to be negligible.

The equation of the circuit is :

$$\frac{d}{dt}\left\{ (L_o + L)\, I \right\} = V_o - \frac{\int I dt}{C_o} \qquad \ldots\ldots (3)$$

where $L = \frac{\mu \ell}{2\pi} ln \left(\frac{r_o}{r}\right)$ is the pinch inductance at radus r.

Thus

$$\frac{dL}{dt} = - \frac{\mu \ell}{2\pi} \frac{dr}{dt} / r$$

and the circuit equation may be written as :

$$\left\{ L_o + \frac{\mu \ell}{2\pi} ln \left(\frac{r_o}{r}\right) \right\} \frac{dI}{dt} - \left\{ I \frac{\mu \ell}{2\pi} \frac{dr}{dt} \right\} / r = V_o - \frac{\int I\, dt}{C} \qquad \ldots\ldots (4)$$

Equations (2) and (4) form a close set of coupled equations which may be integrated for r and I. The limit of the integration is set by equation (1).

NORMALISATION

The equations (2), (4) and (1) are normalised by writing

$$\kappa = r/r_o , \qquad \tau = t/t_c , \qquad \iota = I/I_o$$

where r_o is the initial radius of the column,

t_c is the capacitor characteristics time $(L_o C_o)^{\frac{1}{2}}$

and I_o is defined by $I_o = V_o / (L_o / C_o)^{\frac{1}{2}}$

With this normalisation the three equations defining the system become :

Motion: $$\frac{d}{d\tau} \left\{ (1 - \kappa^2) \frac{d\kappa}{d\tau} \right\} = - \frac{\alpha^2 \iota^2}{\kappa} \qquad \ldots\ldots (5)$$

Circuit: $$(1 - \beta\, In\, \kappa) \frac{d\iota}{d\tau} - \frac{\beta \iota}{\kappa} \frac{d\kappa}{d\tau} = 1 - \int \iota\, d\tau \qquad \ldots\ldots (6)$$

Energy Balance Limit: $$\iota_p^2 = \frac{2(\gamma - 1)}{\gamma} \int_{\kappa_p}^{1} \frac{\iota^2\, d\kappa}{\kappa} \qquad \ldots\ldots (7)$$

In these equations two scaling parameters have been introduced which enable the system to be scaled to all possible circuit conditions. The scaling parameters are:

$$\alpha = t_c / t_p$$

where $t_p = (4\pi r_o^4 \rho_o / \mu I_o^2)^{\frac{1}{2}}$

and $\beta = \left(\frac{\mu \ell}{2\pi}\right) / L_o$

where $\frac{\mu \ell}{2\pi}$ is here considered as a characteristic inductance of the compression.

COMPUTATION PROCEDURE

The two basics equations of the system are rewritten as :

Motion:
$$\left(\frac{d^2\kappa}{d\tau^2}\right) = \frac{-\frac{\alpha^2 \iota^2}{\kappa} + 2\kappa \left(\frac{d\kappa}{d\tau}\right)^2}{(1 - \kappa^2)} \qquad \text{..... (8)}$$

Circuit:
$$\left(\frac{d\iota}{d\tau}\right) = \frac{(1 - \int \iota d\tau) + \beta \iota \frac{d\kappa}{d\tau} / \kappa}{(1 - ln\kappa)} \qquad \text{..... (9)}$$

Initial Conditions:

To begin the integration we write for the zeroth step :

$$\tau = 0, \left(\frac{d^2\kappa}{d\tau^2}\right) = -0.02 \text{ (an estimate}^6\text{)}, \quad \frac{d\kappa}{d\tau} = 0,$$

$$\kappa = 1, \left(\frac{d\iota}{d\tau}\right) = 1, \quad \iota = 0, \quad \int \iota d\tau = 0.$$

To solve equations (8) and (9) by linear approximation, we increase the time by $\Delta\tau$ and write for the (n+1) th step:

$$\left(\frac{d\kappa}{d\tau}\right)_{n+1} = \left(\frac{d\kappa}{d\tau}\right)_n + \left(\frac{d^2\kappa}{d\tau^2}\right)_n \Delta\tau$$

$$(\iota)_{n+1} = (\iota)_n + \left(\frac{d\iota}{d\tau}\right)_n \Delta\tau \qquad \text{..... (10)}$$

$$(\kappa)_{n+1} = (\kappa)_n + \left(\frac{d\kappa}{d\tau}\right)_n \Delta\tau$$

$$\left(\int \iota\, d\tau\right)_{n+1} = \left(\int \iota\, d\tau\right)_n + (\iota)_n \Delta\tau$$

except for the first step where for the purpose of initialization, we put

$$(\kappa)_1 = (\kappa)_0 + \left(\frac{d\kappa}{d\tau}\right)_1 \Delta\tau$$

The result of this procedure has been checked with the Runge-Kutta method and found to be of sufficient accuracy, so long as sufficient number of steps are taken.

PARAMETRIC VARIATION

To determine the limit of the trajectory, we implement the energy balance equation (7). We define a quantity ISQ = ι^2, and a quantity for the (n + 1) th step :

$$(\text{ENSUM})_{n+1} = (\text{ENSUM})_n + \frac{2(\gamma-1)\,\text{ISQ}}{\gamma}\left(\kappa_{n+1} - \kappa_n\right) \quad \ldots\ldots (11)$$

At each step[7] we compare ISQ with $(\text{ENSUM})_{n+1}$ and where $\text{ISQ} \leqq (\text{ENSUM})_{n+1}$ the condition as described by energy balance equation (7) has been reached and the integration is stopped. The raduis ratio κ at that point is the quasi-equilibrium radius ratio κ_p.

We may define an energy matching ratio[7] (EMR) as :

$$\text{EMR} = \beta\,(\text{ENSUM})\left\{\gamma/2(\gamma-1)\right\} \quad \ldots\ldots (12)$$

which is a measure of the ratio of plasma enthalpy at quasi-equilibrium to the capacitor energy $\frac{1}{2} C_o V_o^2$. We would like to maximise the value of EMR within reasonable limits of α and β. Since in a practical situation β is fixed by constraints of electrical components and engineering, we set a value of β with a value of α, and obtain a trajectory by numerical integration as described above and its corresponding EMR. We may then vary α; at each value of α we integrate for the corresponding trajectory and the EMR. We thus obtain a curve of EMR versus α at a fixed value of β. We then change the value of β and obtain another curve. In this way we obtain a family of curves as shown in Fig (3).

RESULTS

Although large values of β enable the value of EMR to increase to values closer to 1, typical operations of MHD compression has $\beta \sim 1$. For this value of β we note that the maximum EMR is at $\alpha \simeq 0.7$. This case is plotted in Fig (4).

CONCLUSION

The general solution of the trajectory of fast MHD compressions and the corresponding driving current as functions of time have been presented. A snow-plow model has been used with a realistic quasi-equilibrium end-point as provided by the new method of energy balance. It is noted that for the typical operation of $\beta = 1$ the maximum value of EMR = 0.39 is achieved at $\alpha = 0.7$. At this operating point the current reaches about 73% of its short-circuit value and the quasi-equilibrium radius is $r_p/r_o \simeq 0.39$ for the ideal gas case of $\gamma = 5/3$. This radius ratio is disappointingly large and we expect from a consideration of equation (1) that some attempt should be made to reduce this ratio by current shaping[7].

REFERENCES

1. Glasstone S. and Lovberg R. H. (1960) "Controlled Thermonuclear reactions" Chap. 7. (D. Van Nostrand Company Inc.)
2. S. Lee Bul Fiz Malaysia 2, 240 (1981).
3. S. Lee "Energy Balance and The Radius of Electromagnetically Pinched Plasma Column" – accepted for publication in Plasma Physics (1983).
4. S. Lee "The Application of Energy Balance to Compute Plasma Pinch Ratios" – accepted for publication in J. Applied Physics (1983).
5. S. Lee Bul. Fiz. Malaysia 4, 1 (1983).
6. S. Lee Bul. Fiz. Malaysia 3, 197 (1982).
7. S. Lee "A Finite-Radius Snow-plow Model for the Design of Pinch Devices" – to be published.

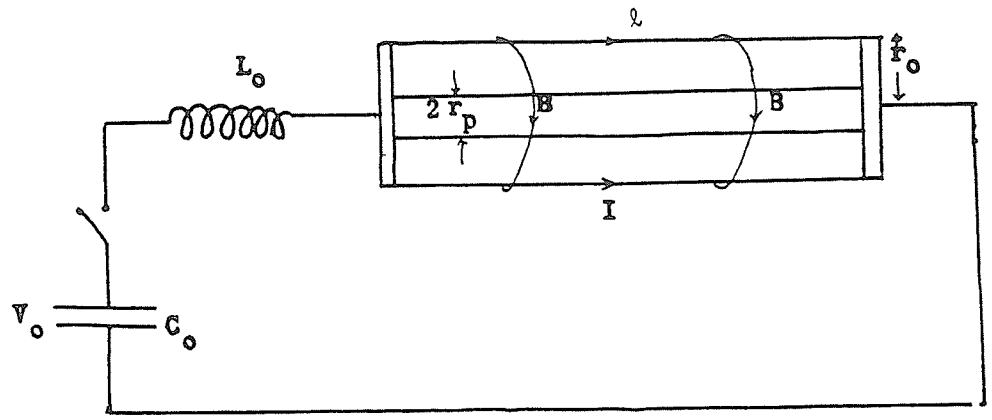

Fig. 1

The snow-plow Model for a strong MHD Pinch Compression.

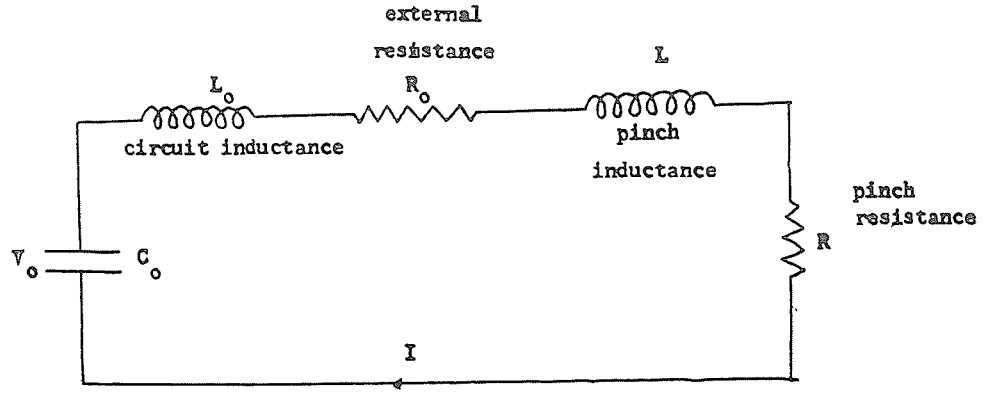

Fig. 2

Circuit of the MHD Compression.

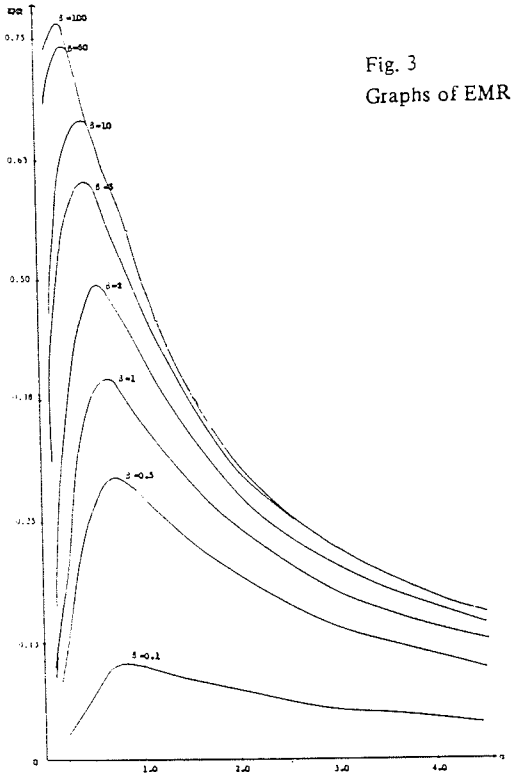

Fig. 3
Graphs of EMR versus Alpha (α) with Beta (β) constant.

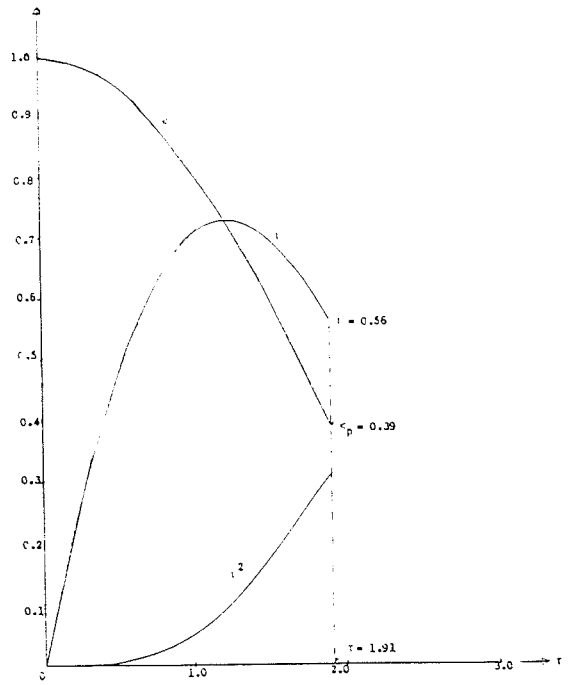

Fig. 4
Variation of κ, ι, ι^2, with time parameter (τ) of a typical MHD compression for β = 1, α = 0.7.

A NEW THEORY FOR THE FAST COMPRESSIONAL PINCH

S. Lee

Plasma Research Laboratory, University of Malaya
Kuala Lumpur, Malaysia

ABSTRACT

A new theory is reviewed which by using the general principles of energy and momentum balance enables the radius ratio r_m/r_o of the quasi-equilibrium column of pinch devices to be computed. Because the theory is simple and general it has been used successfully to calculate the radius ratio for a wide variety of pinches ranging from the constant length pinch to the variable length pinch (Plasma focus) and from pinches with fixed specific heat ratio γ to an argon pinch with γ varying with temperature and also to pinches with circuit-coupled currents. Results are compared with published experiments.

Introduction

There has been renewed interest in the development of the dense plasma pinch as an intense soft x-ray source and as a fusion reactor. Two promising approaches have been reviewed by Haines[1]. The first of these is the fast compressional pinch[2] whilst the second is the axis initiated gas-embedded pinch[3]. There has recently been considerable theoretical effort[1] on the axis initiated gas-embedded pinch. However although new advances in power technology has revived interest in the fast compressional pinch with apparent new regimes of stability the theoretical approach is far from satisfactory, even in very basic aspects.

For example the classical treatment of the pinch[4] is by 2 separate approaches:

1. A snow-plow equation of motion which by relating the driving magnetic force to the rate of change of momentum in the 'snow-plowed' layer enables the computation of the trajectory of the thin layer as it implodes.

2. The consideration of the quasi-static column by the Bennett approach which gives the structure of the column.

The snow-plow model gives a satisfactory trajectory in the early part of the pinch collapse but because of its structureless nature

Radiation in Plasmas Ed. B.Mc Namara,
World Scientific Publishing Co. (1984)

the pinch compresses to zero radius according to the snow-plow equation. This is of course physically impossible. On the other hand the Bennett approach gives the structure of the column without any reference to the dynamic phase. Both these methods are not capable even of computing the quasi-equilibrium radius r_m of the pinch column.

The introduction of a kinetic retarding pressure term into the snow-plow equation[5] enables r_m to be computed. But since the snow-plow equation essentially applies to a thin structureless layer, it is inconsistent with the introduction of a kinetic force term which is structure-dependent. In 1978, Potter[6] showed through an MHD computation using a slug structure that the radius ratio r_m/r_o is dependent only on the specific heat ratio γ of the pinched plasma. However because his theory is essentially model-dependent he obtained definite result only for 1 specific case - that of a constant-current, constant length pinch.

Lee[7,8] has recently published a simple general method which shows that the radius ratio r_m/r_o is in fact uniquely determined independent of model when one considers energy and pressure balance in the compressing pinch column. Because this new theory is fundamental and simple the radius ratio may be computed for many situations, including plasma pinches with variable current, variable length and variable γ. We review this theory and some of its applications in the following sections.

Theory

Consider the following general model for the pinch. On initiation the current I flows axisymmetrically in a thin sheath of radius r_o as shown in Fig. 1. The current acts as a magnetic piston, with field B_ϑ, and implodes inwards collecting all the gas encountered in a thickening sheath. This sheath collapses into a column when the front-running shock wave has imploded onto the axis. The magnetic piston continues moving inwards until the temperature of the column becomes high enough to eventually stop the piston motion. At that point we have a quasi-static column at pinch radius r_m.

The piston exerts a magnetic pressure $P_B = B_\vartheta^2/2\mu$ where $B_\vartheta = \mu I/2\pi r$ at any radius r. The work done by the piston in moving from position

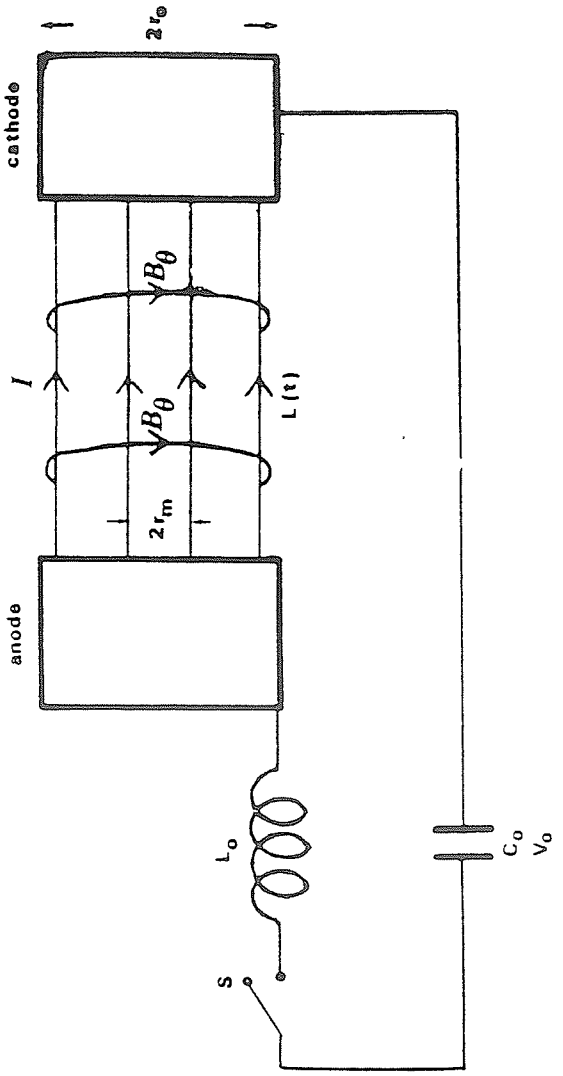

Fig.1. Schematic drawing showing pinch dynamics and pinch circuit (note: the pinch return current path is at radial position of r_0; this is not shown in the drawing).

r_o to r_m is :

$$W = \frac{1}{\rho_m \pi r_m^2 \ell_m} \int_{r_m}^{r_o} \frac{\mu^2 I^2}{4\pi^2 r^2 (2\mu)} 2\pi r \ell dr \tag{1}$$

per unit mass of the final plasma column. Here in general I and pinch length ℓ are functions of r (or time t) and ρ_m, r_m, ℓ_m are the density, radius and length of the quasi-equilibrium pinch.

The enthalpy per unit mass of the quasi-equilibrium plasma may be written as

$$h = \frac{P}{\rho_m} \frac{\gamma}{\gamma-1} = \frac{R_o}{M} T_m D \frac{\gamma}{\gamma-1} \tag{2}$$

here $P = (R_o/M)\, T_m D\, P_m$ is the plasma pressure and T_m, D and γ are the temperature, the departure coefficient and the specific heat ratio of the pinched plasma respectively; with R_o and M being the universal gas constant and the molecular weight of the ambient gas respectively.

Assume that W is completely converted into h with no losses and we obtain the plasma temperature at r_m as:

$$T_m = \frac{\mu}{4\pi^2 \rho_m r_m^2 \ell_m} \frac{M}{R_o D} \frac{\gamma-1}{\gamma} \int_{r_m}^{r_o} \frac{I^2 \ell dr}{r} \tag{3}$$

Now, in the state of quasi-equilibrium we may write independently the pressure balance $P_B = P$ giving us :

$$T_m = \frac{\mu I_m^2}{8\pi^2 \rho_m r_m^2} \frac{M}{R_o D} \tag{4}$$

where I_m is the current flowing at the time r_m is reached. Combining (3) and (4) we have the equation :

$$I_m^2 = \frac{2(\gamma-1)}{\gamma \ell_m} \int_{r_m}^{r_o} \frac{I^2 \ell dr}{r} \tag{5}$$

In general the integral in (5) which we call the energy integral may be evaluated only if I and ℓ are known functions of r. Several cases have been discussed and compared with published experimental results:

Case 1. Pinch with I = constant, ℓ = constant

For this case [7] equation (5) immediately gives :

$$(r_m/r_o) = \exp\left\{\frac{-\gamma}{2(\gamma-1)}\right\} \quad . \tag{6}$$

Notice that the pinch ratio is a function only of γ. For $\gamma = 5/3$ equ(6) predicts $r_m/r_o = 0.29$,

Case 2. Pinch with I = constant, $\ell = \{\ell_m/(r_o-r_m)\}(r_o - r)$

This case applies to the plasma focus, which in its pinch phase has an approximately constant current whilst its length increases, empirically [8] , as r decreases. Substituting I and ℓ into the energy integral of equ. (5) gives :

$$\ell n(r_m/r_o) = \left(\frac{r_m}{r_o} - 1\right) \left\{1 + \frac{\gamma}{2(\gamma-1)}\right\} \tag{7}$$

which gives a pinch ratio for the plasma focus of $r_m/r_o = 0.14$ for the case of $\gamma = 5/3$.

Case 3. Pinch with I = constant, ℓ = constant, γ varying with temperatures; an argon pinch

The specific heat ratio of the plasma has been defined with reference to the enthalpy per unit mass in equ.(2). The enthalpy per unit mass of an argon plasma may also be computed from the formula

$$h = \frac{5}{2}\frac{R_o}{M} TD + \frac{1}{m}\sum_{r=1}^{r=n} \alpha_r I_r + \frac{1}{m}\sum_{r=0}^{r=n} \alpha_r \bar{E}_r \quad . \tag{8}$$

Here I_r is the total energy required to raise one ion from its un-ionized state to its rth-ionized state and $\bar{E}r$ is the average excitation energy per rth-ionized ion; α_r is the ionization fraction of the rth-ionized state and m is the mass of the ion. The Saha equations may be used to compute the α_r's and the $\bar{E}_r$'s may be computed from either known or estimated energy levels. Once h is computed as a function of T from equ (8), the effective specific heat ratio γ may be computed as a function of T from equ (2).

The result[9] is shown in Fig. 2 and we note that the pinch ratio r_m/r_o goes from a low value of 0.01 at 10^5K through two minor peaks with values of 0.04 and 0.08 at 2.5×10^5K and 2×10^6K respectively, before rising finally towards the ideal gas value of 0.29 at high temperatures. At 1.16×10^7K (1 keV) we note from Fig. 2 that the value of r_m/r_o is 0.18.

Case 4 Pinch with ℓ = constant, I = circuit-coupled

To solve this general case we have used a snow-plow equation of motion[4] coupled to a circuit equation.
equation of motion:

$$\frac{d}{dt}\{\pi\rho_o(r_o^2-r^2)\frac{dr}{dt}\} = -\frac{\mu I^2}{4\pi r} \qquad -(9)$$

circuit equation:

$$\frac{d}{dt}\{(L_o+L)I\} = V_o - \frac{\int I dt}{C_o} \qquad -(10)$$

where ρ_o is the ambient density, V_o the initial voltage on the capacitor of capacitance C_o, and L_o is the fixed circuit inductance. Here L is the time varying inductance of the plasma and we may write

$$L = \frac{\mu}{2\pi}(\ell n\frac{r_o}{r})\ell \qquad -(11)$$

where ℓ is the length of the pinch ; coaxial return at r_o is assumed.

We write equations (9), (10) and (5) in normalized form and eliminate L from equation (10) by means of equation (11). Then we have:
Equation of motion:

$$\frac{d^2\kappa}{d\tau^2} = \frac{-\alpha^2 i^2/\kappa + 2\kappa(\frac{d\kappa}{d\tau})^2}{(1-\kappa^2)} \qquad -(12)$$

Circuit equation:

$$\frac{di}{d\tau} = \frac{1 - \int i d\tau + \beta i \frac{d\kappa}{d\tau}/\kappa}{(1-\beta\ell n\kappa)} \qquad -(13)$$

energy balance equation for quasi-equilibrium radius:

$$i_m^2 = \frac{2(\gamma-1)}{\gamma}\int_\kappa^1 \frac{i^2 d\kappa}{\kappa} \qquad -(14)$$

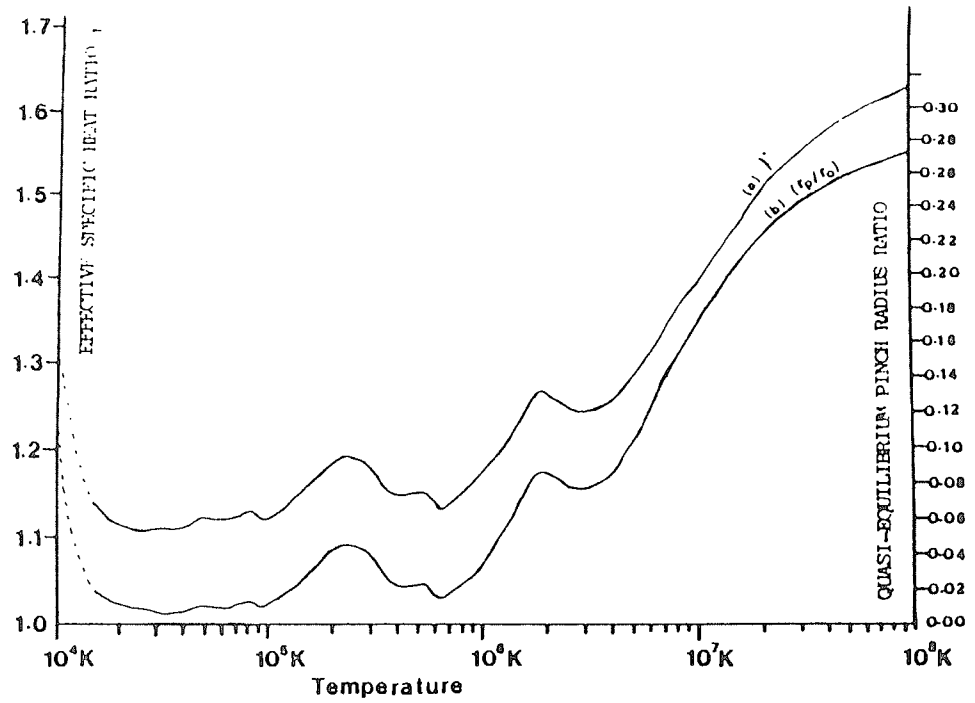

Fig.2 (a) Specific heat ratio
(b) Constant-current pinch radius ratio of argon as functions of temperature

where $\kappa = r/r_o$ $\tau = t/t_c$, $\iota = I/I_o$

$t_c = (L_o C_o)^{\frac{1}{2}}$ and $I_o = V_o/(L_o/C_o)^{\frac{1}{2}}$

with the scaling factors $\alpha = t_c/t_p$ and $\beta = (\mu\ell/2\pi)/L_o$

where t_p the characteristic pinch time turns out to be

$$t_p = \{4\pi^2 \rho_o r_o^4 / \mu I_o^2\}^{\frac{1}{4}} .$$

To integrate equations (12) and (13) simultaneously we set appropriate values of α and β and write the initial conditions as :

$$\tau = 0, \quad \kappa = 1, \quad \iota = 0, \quad d\kappa/d\tau = 0, \quad \int \iota \, d\tau = 0$$
$$d\iota/d\tau = 1, d^2\kappa/d\tau^2 = -0.02 \text{ (an estimate)}^{11)}.$$

We then integrate step-by-step using a linear approximation method. To ensure a meaningful end-point for the trajectory, at each step we compare the values of ι^2 and $\{2(\gamma-1)/\gamma\}\{\int_{\kappa}^{1} \iota^2 d\kappa/\kappa\}$. The quasi-equilibrium radius κ_m is reached when these quantities are equal indicating the attainment of equation (14).

The scaling factors α and β allow a choice of the ratio of the capacitor discharge time to the pinch characteristic time and the ratio of the pinch characteristic inductance to the fixed circuit inductance. For example for $\alpha = 1$, $\beta = 0.01$ we have[10] a near sinusoidal discharge; (i.e. $I = I_o \sin \omega t$) with $r_m/r_o = 0.21$; for $\alpha = 100$, $\beta = 0.01$ we have a pinch occuring early in a sinusoidal discharge (i.e. $I = I_o \omega t$) with $r_m/r_o = 0.17$; and a parametric variation shows that at $\alpha = 0.7, \beta = 1$, good energy efficiency is achieved with 30% of capacitor energy transfered to the plasma column at r_m but with a rather large ratio of $r_m/r_o = 0.39$. The trajectory and current for several cases are shown in Fig. 3.

Energy-consistent trajectory with structure

It can be shown that primarily the snow-plow model is not energy-consistent because of its assumed zero-thickness structure. An energy-consistent model may be constructed by linking the shock front velocity to the magnetic piston pressure and then allowing the piston to separate from the shock front by the correct and careful

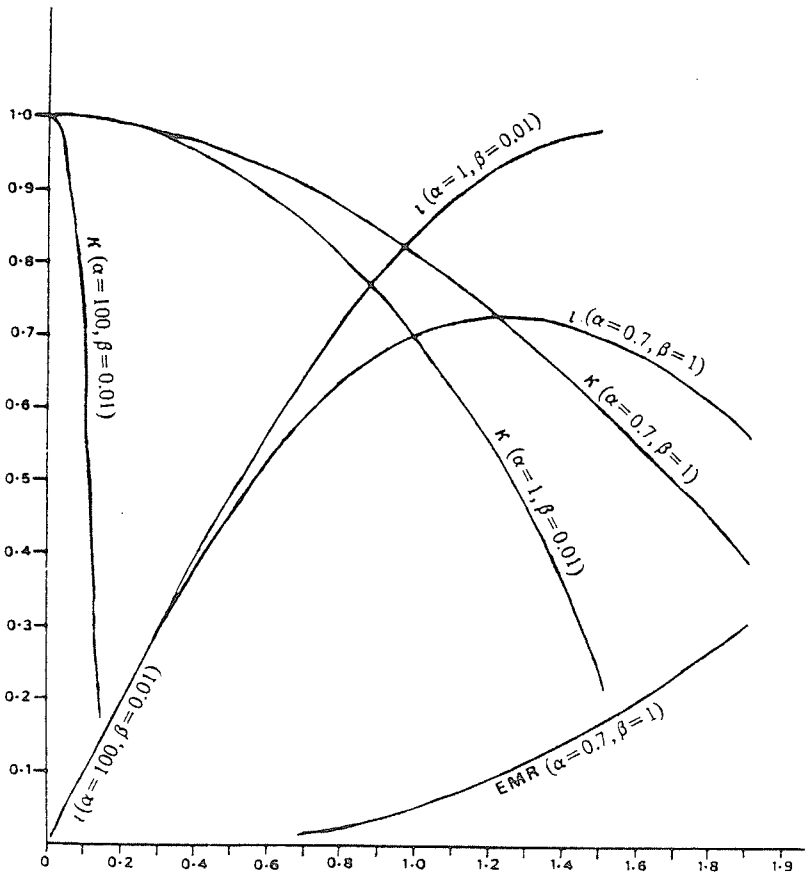

Fig.3. Computation of α and ι as functions of τ for three sets of scaling parameters: i) $\alpha = 100, \beta = 0.01$ (linear current) ii) $\alpha = 1, \beta = 0.01$ (sinusoidal current) and iii) $\alpha = 0.07$, $\beta = 1$ (typical example with good energy coupling).

application of the adiabatic expansion rule as advocated by Potter[6] We are in the process of developing this model[11] for the general case of a pinch with variable I, ℓ and γ.

Comparison with Experiment

In the following table we summarise our main theoretical results and show a comparison with published experimental results:

Case	Energy balance theory	Energy consistent trajectory with structure	Experimental
1. I=constant, ℓ=constant, γ=5/3	0.29	0.31	1/3~0.33*
2. I=constant ℓ=empirical (for plasma focus), γ= 5/3	0.14		0.13+
3. I=constant, ℓ=constant, γ= γ(T), argon	0.18 (at 1keV)		1/6~0.17** (at ~1 keV)
4a. $I=I_o \omega t$ ℓ=constant, γ=5/3	0.17		
4b. $I=I_o \sin \omega t$ (α=1) ℓ=constant, γ=5/3	0.21		0.23++
4c. I=coupled (α=0.7, β=1), γ= 5/3 ℓ=constant	0.39		
5. I=coupled, ℓ=coupled (plasma focus), γ= 5/3		0.16	0.13+

Table 1. Summary of pinch ratios r_m/r_o

* Imperial College[1,2] + University of Malaya DPF1[5,7,8]

** Imperial College[2] Culham[12]

Conclusion

The results show good agreement between the new energy balance theory and experimental results over a fairly wide range of conditions ranging from a constant-length pinch to a variable length pinch (plasma focus) and from $\gamma=5/3$ hydrogen and deuterium plasmas to a variable γ argon plasma. The simplicity of the theory will enable it to be applied to many other cases, for example: 1. doped plasma – deuterium doped with small percentage of argon 2. low γ plasmas at extended high temperatures; use of xenon could extend the low γ range of operation to higher temperatures than argon; this could be of importance for the development of high intensity soft x-ray sources and 3. an examination of equ. (5) shows exciting possibilities for the use of current-shaping to enhance pinch compression.

References

1. M.G.Haines "The Physics of the Dense Z-Pinch in Theory and in Experiment with Application to a Fusion Reactor" 1982 Int.Conf. on Plasma Physics, Goteborg (1982).
2. P.F.M. Baldock, A.E. Dangor, M.B. Favre Dominguez, D.Grimsley, J.D. Hares, E.Kahan, S.Lee "High Density High Temperature Plasma Production in Fast Z-Pinches" - Ninth Ann.Conf. on Plasma Physics Oxford (1982).
3. A.E. Dangor, M.B. Favre Dominguez, E.Kahan, S.Lee "Observation of Radial Equilibrium and Transition to a Helix of a Gas-embedded Z-Pinch" - submitted to Phys. Rev A.
4. S.Glasstone and R.H. Lovberg "Controlled Thermonuclear Reactions" (Van Nostrand, New York).
5. S.Lee "Fusion Energy-1981" (IAEA-SMR-82) 288(1982).
6. D.E. Potter, Nucl.Fusion 18 , 813 (1978).
7. S.Lee, Bul.Fizik Malaysia 2,240 (1981).
8. S.Lee "Energy Balance and the Radius of Electromagnetically Pinched Columns" - Plasma Physics (in press).
9. S.Lee, Bul.Fizik Malaysia 4,1 (1983).
10. S.Lee, "The Application of Energy Balance to Compute Plasma Pinch Ratios" J.Applied Phys. (in press).
11. S.Lee, Bul.Fizik Malaysia 3, 197 (1982).
12. H.A.B. Bodin, A.A. Newton and N.J. Peacock, Nucl.Fusion 1, 54 (1960).

PLASMA FOCUS MODEL YIELDING TRAJECTORY AND STRUCTURE

S.Lee

Plasma Research Laboratory, Physics Department,
University of Malaya, Kuala Lumpur, Malaysia.

ABSTRACT

Potter has used a slug model to obtain the trajectory and structure of the constant current, constant length pinch. This paper extends the model to the plasma focus which in its pinch phase has an increasing length and decreasing current. The model we develop relates the radial shock speed to the magnetic pressure, the focus axial shock speed to the radial shock speed and the radial piston speed to the radial shock speed by the careful application of the adiabatic law. The current is computed self-consistently through a plasma-linked circuit equation. The integration of the model starts with the axial acceleration phase, continues into the radial pinch phase and ends when the radial shock front reaches the axis at which time the radial piston is at the position of the quasi-equilibrium radius.

INTRODUCTION

The plasma focus is now well established as a device by which a hot, dense plasma may be produced with consequent generation of fusion neutrons. The key technical and experimental features of this device are now well documented so that a simple functional device may be built without resorting to sophisticated technology. The situation concerning the theoretical treatment of the device is however quite different. The axial acceleration region poses no problem, but there has been no simple method of computing even the dynamics of the radial pinching phase. Potter[1] has set up a two-dimensional code which gives a detailed description of the axial acceleration phase as well as the radial pinching phase. However the code is complex and its accuracy during the axial acceleration phase had to be checked against the predictions of a simple one-dimensional snow-plow model. The radial implosion phase could not be checked against a simple physical model because none existed which could give even a physically acceptable quasi-equilibrium radius.

Simple physical models have been constructed for the plasma focus based on the snow-plow equation. As is well known this model when applied to a radial compression gives a zero-radius column. Attempts have been made to overcome this by devising a retarding kinetic pressure term. Other attempts use criteria for the minimum radius such as the Larmor radius[2]. However Lee[3,4] has shown that these methods are not energy-consistent and therefore should be replaced by an energy-balance model

"Radiation in Plasmas" Ed. B. McNamara
World Scientific Publishing Co. (1984)

which provides the correct end-point for the implosion trajectory, thus giving the correct quasi-equilibrium radius. Combining the conventional snow-plow model with an energy-balance criterion enables a complete energy-consistent trajectory to be obtained[5].

The snow-plow model however is essentially a structureless model. Potter[6] has suggested a slug model which he has applied to the specific case of a constant current, constant length pinch to obtain a collapsing layer with structure. We extend this slug model to the radial compression phase of the plasma focus, allowing the length of the pinching column and the plasma current to vary self-consistently.

THEORY

We divide the focus into two phases, the axial acceleration phase and the radial pinch phase. The geometry for the two phases is shown schematically in Figure 1.

Axial Phase

For the axial acceleration phase a simple one-dimensional snow-plow model coupled to a circuit equation is adequate to describe the relationship between the plasma trajectory and the driving current. In this model all the mass encountered by the current sheet in its motion from z=0 to position z has been swept up, and at time t all this mass $\rho_o \pi(b^2-a^2)z$ is gathered at the position z leaving a vacuum between z and z=0. Ahead of z the gas is undisturbed. The driving force is obtained by integrating the magnetic force between the radial boundaries b and a, and when this force is equated to the rate of change of momentum at the current sheet we have the following snow-plow equation of motion:

$$\frac{d}{dt}\{\pi\rho_o(b^2-a^2)z\frac{dz}{dt}\} = \frac{I^2}{4\pi}\ell n(b/a) \qquad (1)$$

The circuit equation is:

$$\frac{d}{dt}\{(L_o+L)I\} = V_o - \frac{1}{C_o}\int Idt \qquad (2)$$

Writing the inductance of the coaxial current path between z=0 to z as

$$L = \frac{\mu}{2\pi}\ell n(b/a)z \qquad (3)$$

we may re-write the circuit equation as:

$$\{ L_o + \frac{\mu}{2\pi}(\ell n\ b/a)z \}\frac{dI}{dt} + \frac{\mu}{2\pi}(\ell n\ b/a)I\frac{dz}{dt}$$

$$= V_o - \frac{1}{C_o}\int I dt \qquad (4)$$

The following normalization procedure is adopted:

$\zeta = z/z_o$, $\tau = t/t_c$, $\imath = I/I_o$ where

$t_c = (L_o C_o)^{\frac{1}{2}}$ and $I_o = V_o/(L_o/C_o)^{\frac{1}{2}}$

are the characteristic time and current of the discharge circuit under short-circuit condition.

The normalized equations may be written as:

Motion $$\frac{d^2\zeta}{d^2\tau} = \{\alpha^2 \imath^2 - (\frac{d\zeta}{d\tau})^2 \} / \zeta \qquad (5)$$

Circuit $$\frac{d\imath}{d\tau} = (1 - \int \imath d\tau - \beta\imath\frac{d\zeta}{d\tau}) / (1+\beta\zeta) \qquad (6)$$

where $\alpha = t_c/t_a$ is a scaling parameter and t_a is the characteristic axial run-down time defined by the normalization of the equations as:

$$t_a = \{ \frac{4\pi^2(b^2-a^2)\rho_o z_o^2}{\mu(\ell n\ b/a)\ I_o^2} \}^{\frac{1}{2}} \qquad (7)$$

The second scaling parameter is $\beta = \{(\mu/2\pi)(\ell n\ b/a)z_o\}/L_o$. For a set of values of α and β chosen to suit a particular experiment equations (5) and (6) may be integrated numerically using the following starting conditions:

$$\tau = 0, \quad \zeta = 0, \quad \frac{d\zeta}{d\tau} = 0, \quad \frac{d^2\zeta}{d\tau^2} = \text{trial value};$$

$$\imath = 0, \quad \frac{d\imath}{d\tau} = 1$$

Although the value of $\frac{d^2\zeta}{d\tau^2}$ is determined by equation (5) for all times $\tau > 0$, its value at $\tau = 0$ is not so defined; so that to start the integration a trial value ~ 1 may be used whilst a check is made that the trial value results in sufficient numerical stability and rapid convergence to a smooth solution. The integration is continued until the value of ζ reaches 1; at which point the integration of this phase is

terminated and the integration of the radial phase started.

Radial Compression Phase

Figure 1b shows the geometry of the compressing column. At a given time t the magnetic piston has moved to the position r_p from 'a' driving a shock front ahead of it at position r_s. All the gas encountered by the shock front in its journey from 'a' to r_s is now contained between r_s and r_p. This forms a 'slug' of plasma. Because of the diverging streamlines through the region bounded by r_s and r_p conditions through the slug are in general functions of r and may not be considered to be uniform from one value of r to another at any given time t. However because the shock-front is assumed to be thin the planar shock-jump equations hold across the shock front.

In the radial phase the magnetic piston is known to be highly supersonic and therefore the sound speed in the slug is large compared to the particle speed. Under these conditions we may make the assumption that the one quantity that may be taken as uniform across the slug is the pressure P. Thus this pressure P may be related by the shock-jump equations to the shock speed $v_s = \frac{dr_s}{dt}$ as:

$$P = \frac{2}{\gamma+1} \rho_o v_s^2 \tag{8}$$

Further, at the magnetic piston we may equate the pressure P to the magnetic pressure P_B so that:

$$P = P_B \tag{9}$$

where

$$P_B = \frac{\mu I^2}{8\pi^2 r_p^2} \tag{10}$$

Thus from equations (8) to (10) we have:

$$v_s = \frac{dr_s}{dt} = -\left\{\frac{\mu(\gamma+1)}{\rho_o}\right\}^{\frac{1}{2}} \times \frac{I}{4\pi r_p} \tag{11}$$

where the negative sign indicates radial inward motion.

Also since the pressure is assumed uniform throughout the slug we may write the speed of the free axial front of the focus column as:

$$\frac{dz_f}{dt} = -\frac{dr_s}{dt} \tag{12}$$

The circuit equation for the system in the pinch phase may be written in the same manner as in equ.(2); but we note that now:

$$L = \frac{\mu}{2\pi} (\ell n\ b/a) z_o + \frac{\mu}{2\pi} (\ell n\ b/r_p) z_f \tag{13}$$

where both z_f and r_p vary. Thus the circuit equation may be written as:

$$\{L_o + \frac{\mu}{2\pi} (\ell n\ b/a) z_o + \frac{\mu}{2\pi} (\ell n\ b/r_p) z_f\} \frac{dI}{dt} + I \frac{\mu}{2\pi} (\ell n\ b/r_p) \frac{dz_f}{dt}$$
$$- I \frac{\mu}{2\pi} \frac{z_f}{r_p} \frac{dr_p}{dt} = V_o - \frac{\int I dt}{C_o} \tag{14}$$

Equations (11), (12) and (14) are insufficient to define the problem since there are four variables r_s, r_p, z_f and I to be determined as functions of time. The fourth equation may be obtained by applying the adiabatic expansion law to a fixed mass of gas in the slug at any given instant. For this we write:

$$PV^{\gamma} = \text{constant} \tag{15}$$

or
$$\frac{\gamma dV}{V} + \frac{dP}{P} = 0 \tag{16}$$

where γ is the effective specific heat ratio of the plasma and the volume of the slug is:

$$V = \pi(r_p^2 - r_s^2) z_f \tag{17}$$

To eliminate V from equ.(16) we need to differentiate equ.(17) to obtain dV as a function of dr_p, dr_s and dz_f. To do this we need to consider very carefully so that the differential quantities dr_p, dr_s and dz_f are applied to a fixed mass of gas. For example when the piston moves by dr_p no new mass of gas is introduced into the corresponding new volume V+dV. However when the shock front moves from r_s to r_s+dr_s it admits into the new volume V+dV a new mass of gas. This new mass of gas is compressed by a ratio $(\gamma+1)/(\gamma-1)$ and will occupy part of the increase in volume, so that the actual increase in volume available to the original mass of gas in volume V does not correspond to the increment dr_s but to an effective (reduced) increment $dr_s x 2/(\gamma+1)$. This also applies to the increment dz_f.

Thus to apply the adiabatic law of equ.(16) to the slug we need to write the differential of equ.(17) in the following form:

$$dV=2\pi(r_p dr_p-\frac{2}{\gamma+1}r_s dr_s)z_f+(r_p^2-r_s^2)\frac{2\pi}{\gamma+1}dz_f \tag{18}$$

giving us:

$$\frac{dV}{V}=\frac{2(r_p dr_p-\frac{2}{\gamma+1}r_s dr_s)z_f+(r_p^2-r_s^2)\frac{2}{\gamma+1}dz_f}{z_f(r_p^2-r_s^2)} \tag{19}$$

We may also eliminate dP/P from equ.(16) by writing from equ.(8) and equ.(11):

$$\frac{dP}{P}=\frac{2dv_s}{v_s}=2\left(\frac{dI}{I}-\frac{dr_p}{r_p}\right) \tag{20}$$

Substituting equations (19) and (20) into equation (16) and re-arranging we obtain the adiabatic law in the following form:

$$\frac{dr_p}{dt}=\frac{\frac{2}{\gamma+1}\frac{r_s}{r_p}\frac{dr_s}{dt}-\frac{r_p}{\gamma I}\left(1-\frac{r_s^2}{r_p^2}\right)\frac{dI}{dt}-\frac{1}{\gamma+1}\frac{r_p}{z_f}\left(1-\frac{r_s^2}{r_p^2}\right)\frac{dz_f}{dt}}{(\gamma-1)/\gamma+(1/\gamma)\,r_s^2/r_p^2} \tag{21}$$

The four equations (11),(12),(14) and (21) form a close set of equations which may be integrated for r_s, r_p, z_f and I. For this phase the following normalization procedure is adopted:

$\tau=t/t_c$, $\iota=I/I_o$ as in the axial phase but with

$\kappa_p=r_p/a$, $\kappa_s=r_s/a$ and $\zeta_f=z_f/a$.

This gives us, after re-arrangement, the set of equations representing the generalized slug model in normalized form as folows:

Radial shock
$$\frac{d\kappa_s}{d\tau}=-\alpha\alpha_1\iota/\kappa_p \tag{22}$$

Axial shock
$$\frac{d\zeta_f}{d\tau}=-\frac{d\kappa_s}{d\tau} \tag{23}$$

Radial piston
$$\frac{d\kappa_p}{d\tau}=\frac{\frac{2}{\gamma+1}\frac{\kappa_s}{\kappa_p}\frac{d\kappa_s}{d\tau}-\frac{\kappa_p}{\gamma\iota}\left(1-\frac{\kappa_s^2}{\kappa_p^2}\right)\frac{d\iota}{d\tau}-\frac{1}{\gamma+1}\frac{\kappa_p}{\zeta_f}\left(1-\frac{\kappa_s^2}{\kappa_p^2}\right)\frac{d\zeta_f}{d\tau}}{(\gamma-1)/\gamma+(1/\gamma)\,(\kappa_s^2/\kappa_p^2)} \tag{24}$$

Current
$$\frac{d\iota}{d\tau}=\frac{1-\int\iota d\tau+\frac{\beta_1}{F}(\ln\kappa_p/c)\iota\frac{d\zeta_f}{d\tau}+\iota\frac{\beta_1}{F}\frac{\zeta_f}{\kappa_p}\frac{d\kappa_p}{d\tau}}{\{1+\beta-(\beta_1/F)(\ln\kappa_p/c)\zeta_f\}} \tag{25}$$

where $c=b/a$ and $F=z_o/a$. The new scaling parameters introduced for the pinch phase are:

$$\alpha_1 = \{(\gamma+1)(c^2-1)\}^{\frac{1}{2}} F/(2\,\ell nc) \quad \text{and} \quad \beta_1 = \beta/\ell nc \ .$$

Thus whereas the scaling factors α and β enable the axial phase to be scaled for ratios of capacitor to axial run-down times and axial phase inductance to external inductance, the scaling factors $\alpha\alpha_1$ and β_1 allow the radial phase to be scaled for ratios of capacitor to radial pinch times and for characteristic pinch to external inductances.

The radial phase starts after the axial phase reaches $\tau=\tau_a$ at which time: $\zeta=1$, $\imath=\imath_a$, $\kappa_s=1$, $\kappa_p=1$, and $\zeta_f=0$.

The radial phase ends when $\kappa_s=0$ at which time the shock front has reached the axis and the position of κ_p represents κ_m the radius of the quasi-equilibrium column for the pinch phase of the plasma focus.

INTEGRATION

The integration of equations (5) and (6) and subsequently equations (22) to (25) has been performed using a simple linear approximation method which was checked against a Runge-Kutta method and found to be of sufficient accuracy when 1000 time-steps were taken in each phase. The program runs well in the BASIC language on a Sinclair Spectrum 48K micro-computer but in fact has been run on several other micro-computers[7].

RESULTS AND DISCUSSION

A typical set of results is shown in Figures 2a and 2b. Fig. 2a shows the trajectory ζ versus τ in the axial phase and the current wave-form $\imath$ versus τ for both phases. It is seen that already in the axial phase the current has flattened out and reaches a peak value of $0.6I_o$ at around $\tau=1.2$. The slight but clearly noticeable dip in the current just past $\tau=1.6$ correspond to the radial collapse phase. The trajectories of this phase κ_p and κ_s versus τ are shown in Fig.2b on expanded time-scale. For the condition of: $\alpha=1.5$, $\beta=1.0$, $F=6.4$, $\gamma=5/3$ and $c=3.4$ it was found that the quasi-equilibrium radius ratio of the plasma focus pinch is 0.16.

This model presents a relatively simple way for computing the plasma focus trajectory with an energy-consistent quasi-equilibrium

radius ratio. The simplicity and low computing requirements of the model makes it very useful for design and optimization studies. The coupling mechanism between the plasma and the magnetic field has been assumed to be purely electromagnetic and this limits the accuracy of the model towards the end of the trajectory as the quasi-equilibrium column is being formed. This is because towards the end of the pinch phase the electron Hall parameter attains values greater than unity and the plasma may become anomalously resistive. This effect, not included in the present dynamic model probably plays a dominant role in the experimentally observed complex structure and dynamics of the actual plasma focus in its phases subsequent to the pinch phase we have discussed in this paper.

REFERENCES

1) D.E.Potter, Phys. Fluids 14, 1911 (1971)
2) P.G.Elgroth, Phys. Fluids 25, 2408 (1982)
3) S.Lee, Bul.Fizik Malaysia 2, 240 (1981)
4) S.Lee, "Energy Balance and the radius of electromagnetically pinched plasma columns"- Plasma Physics (in press)
5) S.Lee, " Finite-radius snow-plow model for the design of pinch devices"- in preparation
6) D.E.Potter, Nucl. Fusion 18, 813 (1978)
7) S.Lee, Bul.Fizik Malaysia 3, 197 (1982)

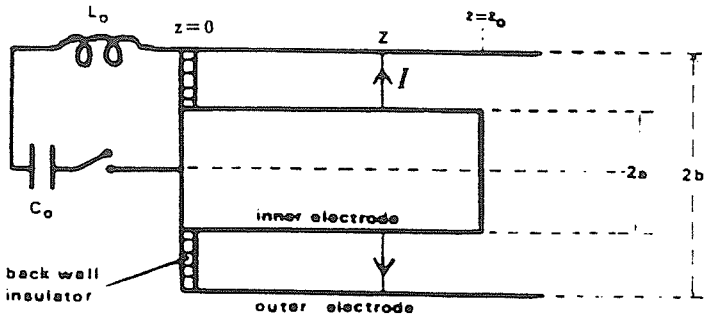

Fig. 1a. Phase 1: axial acceleration phase using a snow-plow model

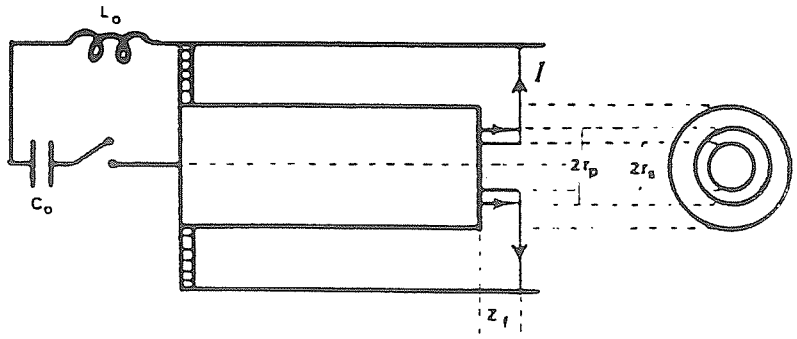

Fig. 1b. Phase 2: radial compression phase using a generalized slug model

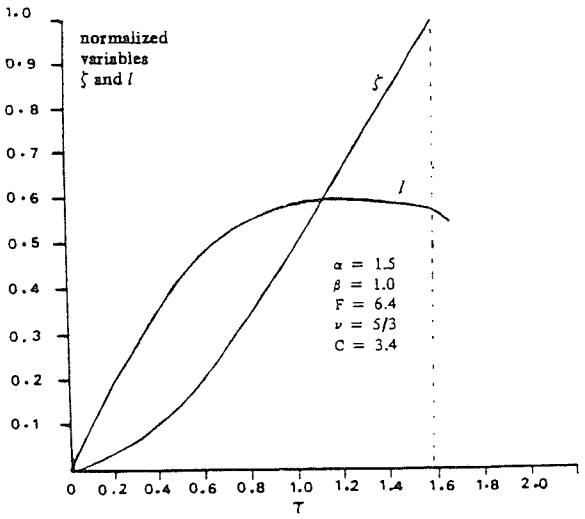

Fig. 2a: Solutions of ζ and l as functions of τ

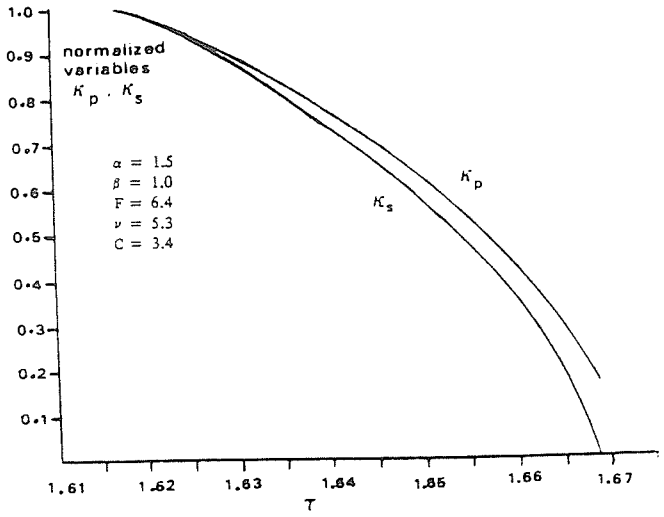

Fig. 2b: Solutions of ζ and l as functions of τ

Proc. 2nd Int. Symp. Radn. Phys. 1983

NEUTRON AND X-RAY DIAGNOSTICS OF PULSED PLASMA SOURCES

C.S. Wong, S. Lee, S.P. Moo and Y.H. Chen
Plasma Physics Laboratory
Physics Department
University of Malaya

ABSTRACT

The emission of neutrons and x-rays from pulsed plasma sources such as the dense plasma focus and the vacuum spark devices are characterised by high intensity, short duration and large shot-to-shot variation. These properties of the plasma demand that the detectors used must have fast response and wide dynamic range. In this paper, several detection systems used to diagnose the neutron and x-ray emitted from the plasma focus and the vacuum spark devices are described. Some of the results obtained are also presented.

I. INTRODUCTION

Many pulsed plasmas which are produced in the laboratory are intense sources of radiations such as neutron, microwave, x-ray as well as electron and ion beams. Two examples of such plasma sources are those produced in the dense plasma focus and the vacuum spark. In fact, radiation processes are so significant during the evolution of these plasmas that many of their properties can be deduced by studying the radiations emitted from them.

The dense plasma focus has been studied extensively since its invention by Filippov et al[1] and Mather[2]. Today, many of the phenomena observed in this device are understood and explained. The neutron production mechanism has recently been shown to be very complex[3,4] and research interest in this area persists due to the great potential in using the focus device as a pulsed neutron source for neutronic study of fusion reactor design[5]. In recent years, the possibility of utilising the energetic ion beams produced in the plasma focus to breed fissile fuel has also been considered[6].

The vacuum spark, on the other hand, is an intense source of pulsed x-ray which has been utilised extensively in spectroscopic studies of highly stripped ions such as Fe-XXVI and Ni-XXVII[7,8]. Its x-ray spectrum has been found to resemble those of solar flares[9,10] thus making it possible for scientists to simulate the solar flare spectrum in the laboratory. In view of the extremely hot and dense plasma conditions of the vacuum spark, attempts have also been made recently to develop it as a neutron producing device[11,12].

In this paper, we describe briefly the neutron and x-ray diagnostic techniques of the dense plasma focus (UMDPF1) and the vacuum spark (UMDPF2) devices in the Plasma Physics Laboratory, Physics Department, University of Malaya[13]. Some of the results obtained will also be presented.

II. Neutron measurements of the dense plasma focus

In order to obtain a better understanding of the plasma heating mechanism of the plasma focus, both the absolute yield and energy of the neutrons produced must be measured. The absolute neutron yield can be measured by the delayed counting technique of the indium foil activation detector whose set-up is shown in Fig. 1. The reactions of interest are

(a) $^{115}In + n \rightarrow {}^{116}In \rightarrow {}^{116}Sn + \beta^- (\tau_{\frac{1}{2}} = 14\ s)$

and (b) $^{115}In + n \rightarrow {}^{116m}In \rightarrow {}^{116}Sn + \beta^- (\tau_{\frac{1}{2}} = 54\ min)$

with reaction cross-sections of 42 and 157 barns respectively for thermal n. However, due to the comparatively long half-life of the second reaction, it will be more convenient to count the 14 second delay[14]. This can be done by choosing a counting time which is long enough to count more than 90% of the activity of the 14 second decay while the 54 min component has hardly decayed. We have chosen the counting time to be 40 seconds at which the contribution due to the fast decay component is 88% of the total counts obtained.

Ideally, the detector should be calibrated against a pulsed source of similar duration and energy spectrum. However, since such a pulsed source is not available, an alternative constant source of ^{228}Th-Be with strength of about 2×10^5 neutrons/second was used. The yield of the pulsed source that can produce the equivalent amount of radio-

activity in indium as a constant source of strength S activating for a time of t_a is given by

$$\frac{S}{\lambda}(1 - e^{-\lambda t_a})$$

where λ is the decay constant of the induced radionuclide. The calibration factor F of the detector is

$$F = \frac{S}{\lambda}(1 - e^{-\lambda t_a})\frac{1}{C} \text{ neutrons per count.}$$

where C is the total number of counts recorded in 40 seconds. The calibration factor at a distance of 8 cm from the source is determined to be $(1.5 \pm 0.1) \times 10^4$ neutrons/count for the present detection system. This means that in order to achieve a minimum of 10% statistical counting error in our measurement, the neutron yield of our focus must be at least 10^6 neutrons per burst. With the unoptimised version of the focus tube used in our laboratory, the yield has been measured to be consistently within the range of 10^7 to 10^8 neutrons/burst. However, after optimisation[15], the yield has been increased to 10^9.

The angular distribution of the neutron emission from our focus has also been measured by using a pair of indium-foil activation detectors with the focus operated at 1 torr which is in a low-pressure regime. The angular distribution is anisotropic with the measurement in the forward axial direction almost double that in the direction perpendicular to the axis of the tube as shown in Fig. 2. In fact, by using the shadow bar method[15], neutrons have been detected at locations as far as 15 cm from the truncated end of the focus tube along the axis, although the focused plasma is situated at about 1 cm from the anode and having a length of only about 1 cm. This strongly suggests the possibility of beam-target type of neutron production mechanism. This is further confirmed by measuring the energy of the neutrons in both forward and backward directions. In this case, two sets of fast scintillator-photomultiplier detection systems at a distance of 10 m apart have been used. A typical set of signals recorded by these detectors is shown in Fig. 3. By measuring the neutron time-of-flight from near to far detector, its energy can be deduced. It is found the neutron energy thus measured in the forward and backward directions differ significantly. In the forward direction, the neutron energy is

measured to be 2.6 MeV whereas in the backward direction, its value is only 2.2 MeV[16]. Since the mean energy of the D-D fusion neutron is typically 2.45 MeV, these results suggest that the fusioning deuterons are moving in the forward direction with mean energy of about 250 keV.

III. X-ray measurements of the vacuum spark

The plasma produced in the vacuum spark is known to be an intense source of x-ray and hence x-ray diagnostic may provide an easy means of investigating its conditions during its very hot and dense phase. The intensity of the x-ray has been found to be so intense that its image can be recorded on a pinhole camera with 20 μm Al, 0.005 cm mylar and 20 cm air between the source and the film. The pinhole is 300 μm in diameter and Polaroid 667 type of film is used. The image of the vacuum spark x-ray source shows a complex structure as shown in Fig. 4. It consists of a cloud of plasma situated within the space in between the electrodes with several localised bright spots. These spots are circular and sharp-edged indicating that they are actually the image of the pinhole projected by x-ray sources which are smaller than the size of the pinhole. The size of each of these spots can be estimated by considering the umbra of their projection and they are found to be typically about 100 μm in diameter.

The temporal development of the vacuum spark plasma has been studied by employing two x-ray PIN diodes with risetime of the order of 2 ns. The x-ray detection pass-band of these diodes can be varied by adjusting their absorption foils so as to exclude line radiation. An example of the x-ray pulse obtained is displayed in Fig. 5. By using two such detectors and using aluminium foils of various thicknesses, the electron temperature of the plasma can be estimated by the absorption technique[17] in which the experimental x-ray transmission ratio of the two detectors with different foil thickness is compared with theoretical value as shown in Fig. 6. The electron temperature is estimated to be within the range of 3 to 10 keV by this comparison.

Since the charge sensitivity of the PIN diode in the x-ray region is known[18], the power of x-ray emission from the vacuum spark plasma can be deduced from the x-ray pulse-height recorded. Assuming the emission to be isotropic, the x-ray emission rate from our vacuum spark is calculated to be of the order of a few megawatt.

V. CONCLUSION

We have seen from the above discussion that the plasma produced in the dense plasma focus and the vacuum spark are indeed intense sources of radiation. Even in a 12 kJ focus, 10^9 neutrons per burst and peak neutron emission rate in excess of 10^{16} neutrons per second are consistently measured. This strong burst of neutrons has been measured by indium foil activation detectors. On the other hand, the vacuum spark is found to be an intense point source of x-ray with an emission power of several megawatts.

ACKNOWLEDGEMENTS

We are grateful to Prof. C. Grey Morgan for his encouragement and help particularly in the handling of high power laser technology. We also wish to acknowledge Prof. B.C. Tan and other members of the Plasma Physics Group of the Physics Department, University of Malaya for their continuing support.

The capacitor bank and the pulsed ruby laser used for the vacuum spark device are gifts from the Alexander von Humboldt Foundation of the Republic of West Germany. One of us (C.S. Wong) has been supported by the University of Malaya to attend the 'Second Internationsl Symposium on Radiation Physics' held in Penang.

VI REFERENCES

1. N.V. Filippov, T.I. Fillipova and V.N. Vinagradov, Nucl. Fusion Suppl., Pt. 2, p577 (1962).
2. J.W., Mather, Phy. Fluids, Suppl. 1, p528 (1964).
3. M.G. Haines, Phil. Trans. R. Soc. Lond., A300, 649-663 (1981).
4. K. Steinmetz, K. Huebner, J.P. Rager and B.V. Robouch, Nucl. Fusion, 22(1), 25 (1982).
5. P. Cloth, H. Conrads, H.R. Ihle, C. Gourlan, Ch. Maisonnier and B.V. Robouch, Paper presented in Int. Conf. on Radiation Test Facilities for the CTR surface and materials program, July 1975.
6. Kazunnari Ikuta, Research Report (IPPJ-541), Institute of Plasma Physics, Nagoya University, Japan (1981).
7. T.N. Lie and R.C. Eltan, Phys. Rev. A., 3(3), 865 (1971).
8. B.S. Fraenkel and J.L. Schwov, Phys. Lett., 40A(1), 83 (1972).
9. T.N. Lee, Astrophy. J., 190, 467 (1974).
10. E. Ya. Gol'ts. I.A. Zhinik, E. Ya. Kononov, S.L. Mandel'shtam and

Yn. V. Sidel'nikov, Sov. Phys. Dokl., 20(1), 49 (1975).

11. S. Lee and H. Conrads, Phys. Lett., 57A(3), 233 (1976).
12. C.S. Wong and S. Lee, Paper presented in the Symposium on Plasma Research Theory and Experiment, ICTP, Trieste, Italy (1981). Proc. to be published.
13. C.S. Wong, Bull. Phys. Msia, 1(4) 161 (1980). Proc. International Conf. on Physics and Technology in the Eighties, Kuala Lumpur.
14. C.S. Wong, M.Sc. Thesis, Universiti Malaya (1978).
15. Y.H. Chen, Ph.D. Thesis, Universiti Malaya (1978).
16. S. Lee and Y.H. Chen, Mal. J. Sci., 3B, 159 (1975).
17. F.C. Jahoda, E.M. Little, W.F. Quinn, G.A. Sawyer and T.F. Stratton, Phys. Rev., 119(3) 843 (1960).
18. D.M. Corallo, D.M. Creek and G.M. Murray, J. Phys. E: Sci. Instrum., 13, 623 (1980).

DISCUSSION

Iyengar: What is the minimum neutron flux you can measure with your indium detector?

Wong: As you can see the calibration factor of the detector is about 1.5×10^4 neutrons per count. So if we need a minimum statistical accuracy of 10%, the threshold we set is 10^6 neutrons per burst.

Iyengar: I understand that now there are some chemicals which include indium with which we can go down much further to about 10^3 neutrons per burst.

Wong: Yes, in fact we have tried another detector, the medium 6 class scintillation detector but that requires faster electronics. Also because our neutron flux is in the region of 10^8 to 10^9 neutrons per burst, we would rather prefer to use the present detector because this is more reliable in the higher flux region.

Iyengar: What is the power of the condenser banks in the plasma focus?

Wong: The energy input is 12 kilo joules.

Iyengar: You mentioned that you measured the energy distribution in a forward direction and a backward direction and you established that it is due to the ions moving in the forward direction. Thus you can't talk of a temperature in a plasma focus. It is really not a thermal nuclear reaction.

Wong: No, it is not a thermal nuclear reaction. In fact, at the moment, the common belief is that the neutron production mechanism is more of the target type rather than the thermal type.

Iyengar: Yes, but there is also a theory which shows that there are filamentary regions in which these neutrons are produced.

Wong: Yes, there are some studies in this respect which state that when they observe the filaments they found that the neutron yields are higher. We have no such experience.

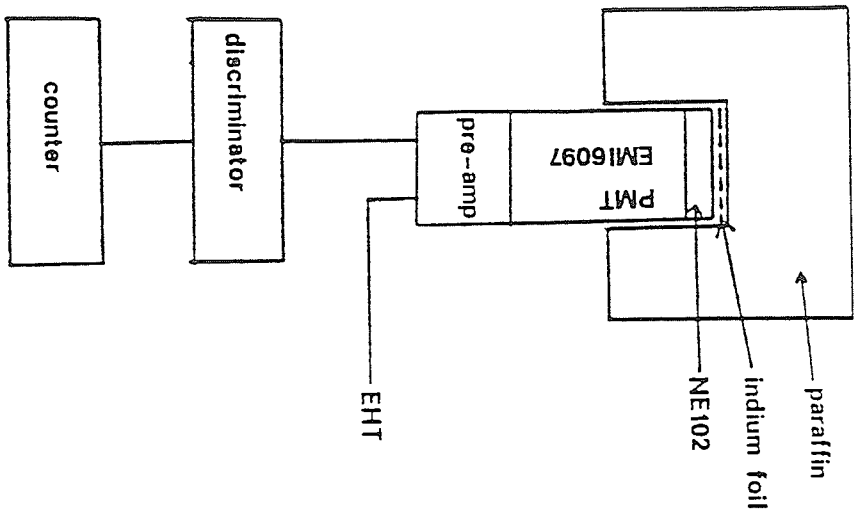

Fig.1: Neutron detector set-up

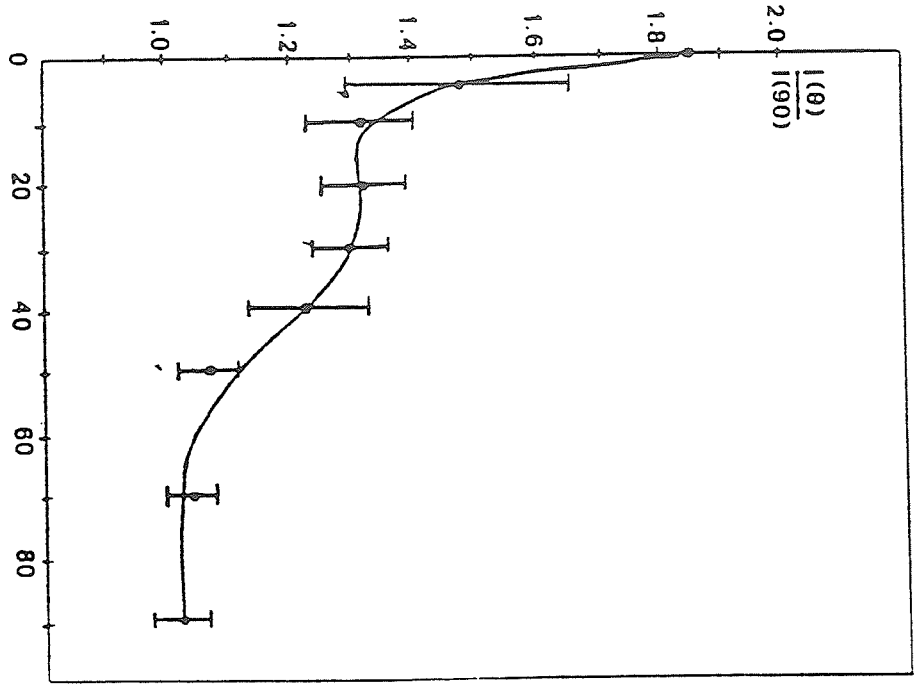

Fig.2: Neutron angular distribution of plasma focus

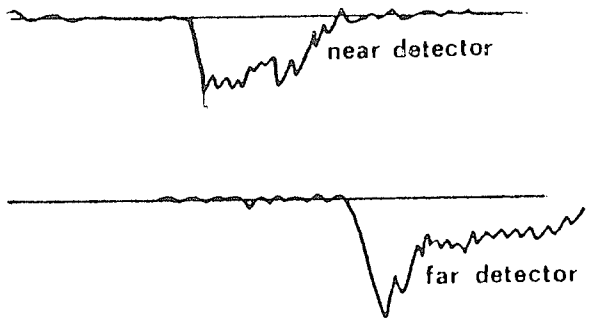

Fig.3: Neutron time-of-flight signals

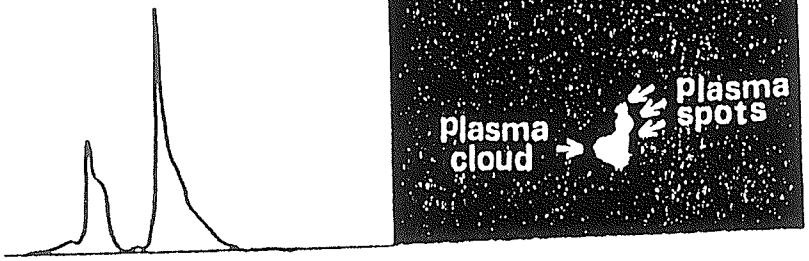

Fig.5: X-ray pulses

Fig.4: X-ray pinhole images

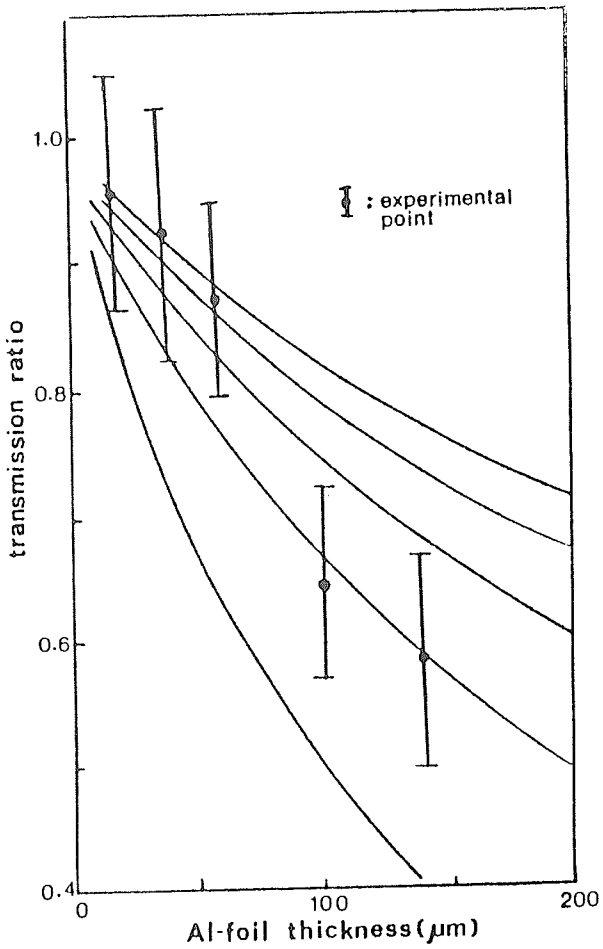

Fig.6: X-ray transmission curves

REGIONAL CENTRES FOR RESEARCH TRANSFER WITHIN SOUTH-EAST ASIAN COUNTRIES

S. Lee

Physics Department, University of Malaya
Kuala Lumpur 22-11, Malaysia

Abstract

A plan is proposed to identify successful self-developed research groups in South-East Asia to be designated as Regional Centre for Research Transfer in their respective areas of physics research specialty. A Regional Centre for Research Transfer will take the initiative to prepare a comprehensive program to transfer its research capability, including all technical infrastructure and expertise to a recipient group with a commitment to develop a sustained research effort in the area offered. The transfer is via a 3-6 months training program conducted at the Regional Centre. The plan is very cost effective since no capital cost is involved except for a small amount needed for specialised components needed by the recipient group in constructing its facility. Several such centres in South-East Asia will have a considerable impact on the development of physics research in the region.

Invited Lecture presented at
International Conference on Physics for Development
at International Centre for Theoretical Physics
Trieste, Italy, 8-12 October, 1984.

Introduction

One of the general aims of this Conference, I understand, is to inform the physics communities about potential sources of assistance for the development of physics research in the Third World. A conclusion of the First Tropical College on Applied Physics held early this year and attended by participants mainly from South-East Asian countries is that mutual assistance among institutions in South-East Asia could form the basic ingredient in an effective and low-cost plan for the development of physics research in the region. This talk will deal with a plan for specific action for initiative and cooperation in the development of physics research among third world countries.

Physics research always takes place against the background of physics education and problems of the two should not be discussed in isolation one from the other. The problems in physics education in several South East Asian countries, among others, have been extensively discussed at the 1981 Khon Kaen Conference on Methods of Teaching Physics. That Conference showed that on the whole a satisfactory level of organisation in physics school and undergraduate education exists in countries like Thailand, the Philippines, Malaysia and Indonesia, among others. Curriculum organisation and reform, laboratory aids, teaching methods, books and man-power requirements are among the problems being successfully faced and gradually improved upon by most of the South-East Asian countries.

Against this background of a relatively progressive scene of physics education may be viewed the much more laborious progress being made in physics research in the following physics areas: solid state physics, nuclear/radiation physics, high energy physics, electronics, biophysics, atmospheric physics, geophysics, laser physics, material science, non-destructive testing, plasma physics, optics, crystallography, instrumentation, non-conventional energy and areas in theoretical, computational and mathematical physics and in experimental and applied physics. In each of these subject areas progress is very slow when averaged over the whole geographical region; but in several of the subject areas institutions may be identified where satisfactory progress has been made and continuing effort is being sustained on the basis of individual groups. These groups form the key to the present plan.

Problems in Physics Research

Major problems have been identified by various authors at national, regional and international conferences and publications. The crux of the problem may be stated thus: How to develop high level man-power and initiative in physics research? - against a background of lack of research tradition and atmosphere; with little equipment, funding and technical support; where bureaucracy has not provided priorities and incentives and where physicists are isolated and lack numerical 'critical mass'.

Traditionally South-East Asian countries have their highest level of physics man-power trained overseas in advanced countries: the U.K., the U.S.A., Germany, France, Australia, Canada, for example. At postgraduate level typical training consists of a research programme drawn up to fit the student into the ongoing work at the host institution. The student learns how to carry out the research program using the equipment and technical resources available at the host institution. On completing his Master or Doctorate the student returns to his home institute where he now faces the problem of having to create the environment, including technical resources, needed to carry on any worthwhile research.

Various proposals have been formulated to alleviate these problems:- from proposals to choose 'relevant' topics for postgraduate training, so that presumably more official funding then becomes available, to networks of regional centres and travelling scientists schemes. The most remarkable success in these efforts to encourage third world physicists is the ICTP itself, set up to alleviate the isolation of scientists from developing countries; and succeeding marvellously - especially for theoretical physicists and mathematicians. Success to the same degree has probably not been achieved for experimental physicists. The experimental physicist benefits enormously from the contacts, stimulating atmosphere and fresh ideas of the ICTP, but unlike the theoretical physicists is unable to continue working with just ideas back in his home institute. He needs equipment and technical support.

What the fresh, young enthusiastic Ph.D. in experimental physics needs is the opportunity and the ability to transfer from somewhere a self-contained infrastructure of technology for a specific research area: choice of a feasible and worthwhile facility, design and construction concepts, the control, power and measuring techniques, modelling,

optimisation and computational principles and techniques, all adaptable to the resources of his home institute. The technology has to be simplified so that he can firstly become the technical expert, and then train his technicians on the job. The technology has to have been evolved or have been modified to be at once effective and suitable for implementation in the atmosphere of the developing country. The technology has to have a basic structure that is self-contained, self-sustainable and low cost. Having chosen and learned the technology, the young physicist should then build this facility hinself to gain the vital self-confidence and to have the technical expertise to adapt the facility as his research horizons expand. How may we help the young physicist do this, in a reasonable period of time and at reasonable cost?

There are in existence in South-East Asia research groups which have built up, over the last one or two decades, a self-contained environment for research incorporating all the technical and physics elements required for a sustained research effort. Some of these groups have the capacity and willingness to take the initiative in research initiation and transfer.

Regional Centres for Research Transfer

The proposal is this. Use the facilities and resources of an existing group in a developing country to prepare a program to transfer its total research technology to another group in the region having an interest and commitment in the subject area offered. We shall for the moment discuss programmes that have a strong experimental basis. Designate the group as a Centre for Research Transfer.

Identification of a Regional Centre for Research Transfer

The Centre shall have:-

1. specific and specialised research activity in the area of physics it is offering
2. sufficient experience and productivity in that area of physics including: development of undergraduate courses, production of post-graduate theses (preferably to doctoral level) and research papers
3. a self-contained technical infrastructure for the research
4. evolved the technical infrastructure at the centre itself so that the technical infrastructure may be adapted to another developing country

without excessive cost in equipment and funding

5. a willingness (enthusiasm) to take the initiative to prepare a comprehensive program to teach, in one package, all the technology required to carry out research in the designated subject area.

Identification of Program Participants

A participant for this program must have a strong physics background, must be young and willing to, after the program, spend several years on the building and research of the selected project. The participant must come from an institution willing to build up the project. The home institution should have some minimum mechanical and electronic workshop facilities and some specified basic equipment.

Role of the Centre

The Centre should on its own initiative

1. identify a facility (modelled on its own experience) that may be built and on which research may be carried out fruitfully
2. plan a breakdown of the facility into its basic technical components
3. define the major technical requirements (related to the working principle) of each component so that its design and building may be adapted to suit local technical capabilities and individual needs
4. plan the basic theory and model needed to optimise the parameters of the facility, and on which the behaviour of the facility may be studied fruitfully and with possibility of extension
5. plan for computation and numerical modelling to be done with modest computing facilities like microcomputers
6. plan the building of the power and control systems and basic diagnostics so that these may be built in simple (preferably modular) forms in the local environment
7. plan a comprehensive series of experiments and lectures to demonstrate all the above in modular as well as in assembled working form
8. identify the basic equipment that may not profitably be home-built in the framework of the particular program, such as, for example, vacuum pumps, oscilloscopes, electronic and power components
9. select the participants (bearing in mind the suitability also of the environment of the home institution)
10. conduct a course (from 3-6 months as necessary) based on the above for a group of 2-8 participants

11. round off the course by planning with each participant how the facility may be adapted and designed to suit the environment and resources of that participant's home institution and
12. provide follow-up help in a technical and advisory capacity as well as, in the early stages, on research planning.

Role of International Agencies

When a Regional Centre for Research Transfer has prepared its program, and ready participants are identified, the question of funding will require the assistance of international agencies. Travel and living expenses need to be provided for the participants. Follow-up grants to promising participants selected at the end of the course need to be provided for those basic components not available at the home institutions Some follow-up travel expenses may need to be budgetted. The question of follow-up grants will necessarily limit the possible projects to those which require special component costing less than some pre-set limit, perhaps say US$10,000.00 .

The inter-relationship among the three parties concerned is illustrated in the Figure.

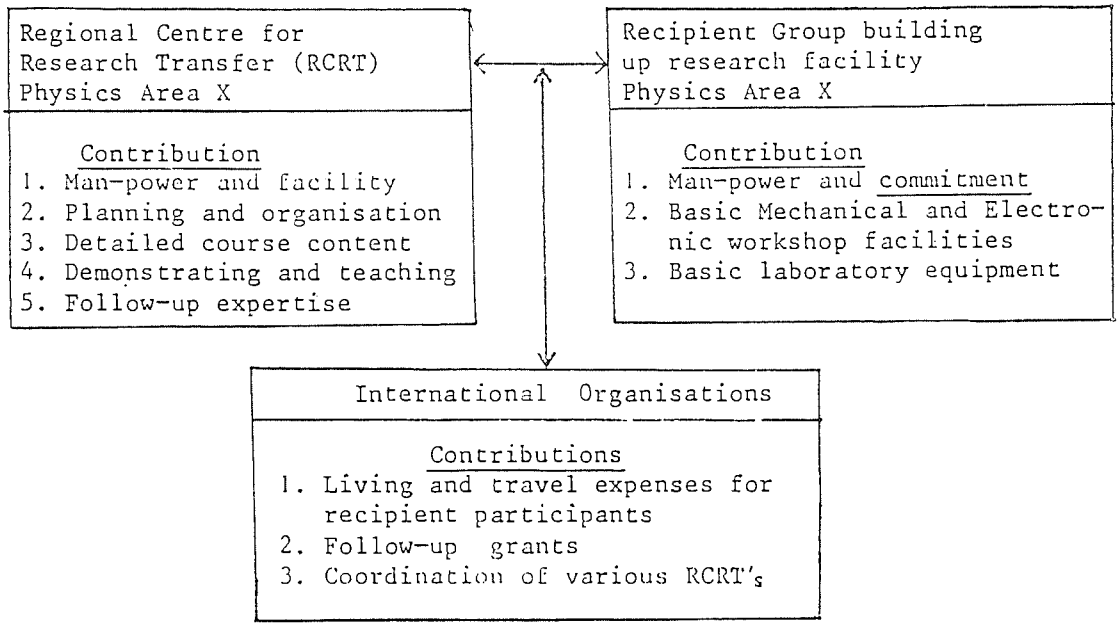

Cost and Benefit

As seen in the Figure, the implementation of this program would represent a cooperative effort between two developing countries aided by an appropriate international agency. No capital cost is required to establish the Regional Centre, since it is already in existence and only needs to be identified and designated. In terms of operating cost the Regional Centre in the developing country would bear the greatest cost in terms of man-power, facilities, planning, teaching, demonstrating and follow-up work. The international agnecy will have to bear an estimated US$20,000 (living, travel and follow-up grant) per project involving two participants from one recipient institution.

The success of a research transfer project would bring great benefit to both the existing Centre and the recipient group. To the existing Centre, the intense teaching would bring deeper understanding to the technical and research problems and the gain in confidence and self-esteem would lead to greater maturity in its continuing research effort. To the recipient group, a successful project could cut away 5-10 years of development time resulting in the early establishment of the research facility with all the attendant uplifting effects on research and teaching morale. Ten such Centres would completely alter the history of physics research in South-East Asia. Even two or three Centres would have a great impact. Some form of coordination by an international physics Centre such as the ICTP would be very useful.

Possible Areas for Research Transfer

Against the background of actual research activity in South-East Asia the following subject areas may be regarded as more likely to succeed for this plan: plasma physics, laser physics, solar and wind energy, materials and solid state physics, computer controlled instrumentation, radiation and environmental monitoring. Other possible areas are in biophysics, geophysics, crystallography, atmospheric physics, repackaging of successful computer codes for microcomputer operation, electronic, pulse and radiation techniques and application to testing and measurement.

An Example

As an example of a feasible project for research transfer we may

consider the plasma focus which has been recommended by the IAEA Consultant's Meeting on Fusion Program for developing countries as far back as 1978 as one of two devices suitable for developing countries. It is a low-cost device, yet produces a plasma extremely rich in physical phenomena including intense bursts of soft x-ray (argon operation) and fusion neutrons (deuterium operation). Even a small plasma focus facility with very basic control and disgnostics provide rich research possibilities for high temperature physics and associated technologies.

The plasma focus facility may consist of a simple vacuum system (rotary pump) with fill gas, coaxial electrodes, a capacitor bank with fast switches, power supplies, control electronics for capacitor switching and CRO synchronisation, and simple diagnostics for measuring current, voltage and magnetic field waveforms which are sufficient to interpret the dynamics and structure of the plasma phases when coupled to a plasma dynamic model. A plasma electro-dynamic model with structure and chemistry has been developed with possibility of extension to include turbulent heating, electrode losses, radiative collapse and machine characteristics; all computation may be carried out on microcomputers.

Experiments, lectures and design instructions on the complete facilities including the focus electrodes, power supplies, capacitor bank, control electronics and diagnostics, and computation and optimising packages have been designed bearing in mind the need to adapt to the individual resources of a recipient institution in a developing country. This technology package has been designed by a group at the University of Malaya and is offered for transfer to any interested institution. Several possible recipient institutions have also been identified.

The construction of this facility requires some not-so-common components namely high-power capacitors, ignitron switches and several specialised electronic components; the total cost of these components is under $10,000.00. The recipient institution is expected to have basic mechanical and electronic workshop, and basic equipment like rotary pumps and oscilloscopes.

Conclusion

This paper has very briefly outlined the crucial problems of physics research in South-East Asia. Whereas there is active progress made in the region for provision of satisfactory physics education, the

problems of physics research in a background of lack of man-power, initiative, equipment, incentive and atmosphere are much more formidable.

A proposal is made in the light of South-East Asian capabilities to attack all these problems simultaneously by means of identifying existing successful research groups for designation as Regional Centres for Research Transfer in specific experimental areas. The proposal will have an existing Centre plan a complete package for the transfer of research capability, including all technical infrastructure and expertise to a recipient group. The actual transfer is via a 3-6 months training program conducted at the Regional Centre. Aided by international funding to the extent of travel and living expenses for participants and limited follow-up component grants, the plan will have the recipient group build a complete facility and hence be in a position to begin a sustained research effort. Several such Centres for Research Transfer in South-East Asis will have a considerable impact on the development of physics research in the region.

J. Phys. D: Appl. Phys., 17 (1984) 733–741. Printed in Great Britain

A current-stepping technique to enhance pinch compression

S Lee
Plasma Research Laboratory, Physics Department, University of Malaya, Kuala Lumpur 22-11, Malaysia

Received 22 September 1983

Abstract. It has been shown that the quasi-equilibrium radius ratio κ_p of a fast compressional pinch is independent of the absolute magnitude of the driving current; it depends only on the current shape and on the length variation of the pinch during pinching. In this paper it is shown that a current step, switched on to the discharge current of a pinch as it approaches its quasi-equilibrium radius ratio κ_p as defined by a lossless energy balance theory, shifts the value of κ_p to a significantly lower value, thus enhancing pinch compression. It is proposed that this current-stepping technique may be used as a prelude to radiation cooling to eventually achieve the very small radius ratios required for a pinch fusion reactor.

1. Introduction

A pinch fusion reactor concept has been proposed that fulfils the Lawson criterion and at the same time has enhanced stability due to large ion Larmor radius effects (Haines 1982). One of the key technical features of this proposal is the requirement of a small final pinch radius of the order of 10 μm–100 μm. From the view point of fast compressional pinches the achievement of this order of pinch radius is a major difficulty as, even with the advent of new high-power electrical discharge technology, an initial radius of the order of 1 cm has to be used in order to provide sufficient running time of the pinch compression for effective energy transfer.

Thus a pinch radius ratio, that is the final radius divided by the initial radius, of 0.01 to 0.001 is required. Potter (1978), using a slug model, has shown that for a constant current pinch in deuterium the pinch ratio is fixed at 0.3. Lee (1981) has proposed a lossless energy balance theory and used it to show that the pinch ratio is reduced to 0.14 for a plasma focus treated as a pinch with a length which increases as the radius decreases (Lee 1983a). The theory has also been used to show that for a constant length deuterium pinch, the radius ratio depends only on the current shape and varies from 0.17 for a linearly rising current (Lee 1983b) to 0.4 for an energy-optimum plasma-coupled L–C discharge (Lee 1983d). The effect of specific heat ratio, γ, on the pinch ratio for argon (Lee 1983c) has also been computed.

It has therefore been demonstrated that based on a lossless theory the pinch radius ratio does not depend on the absolute magnitude of the current, but only on the time variation of the current pulse. For the various types of current functions discussed above

0022-3727/84/040733 + 09 $02.25

the pinch ratios are relatively large. Haines (1982) has suggested the small radius ratios required for the pinch fusion reactor may be attained by radiation cooling compression, by operating the pinch at the Pease–Braginskii limiting current.

It is proposed in this paper that as a prelude to radiation cooling compression a technique of current stepping may be used to reduce the pinch ratio, thus enhancing plasma compression. This technique relies on the fact that when an equilibrium pinch ratio is approached as defined by the energy balance condition it is possible to shift the equilibrium pinch ratio to a reduced value by rapidly increasing or stepping-up the driving current.

2. Theory

The energy-balance theory (Lee 1981, 1983a) applied to the fast compression radial pinch equates the work done by the magnetic piston to the plasma enthalpy. The resultant expression for temperature, T, is compared to the temperature obtained from the Bennett pressure balance to obtain the following condition governing the quasi-equilibrium pinch radius ratio:

$$I_p^2 = \frac{2(\gamma - 1)}{\gamma l_p} \int_{r_p}^{r_0} I^2 l \frac{dr}{r} \tag{1}$$

where I_p is the current flowing at the time the pinch reaches quasi-equilibrium at r_p and l_p is the length of the pinch at quasi-equilibrium. The integration is done from initial radius r_0 to final radius r_p.

For a constant length pinch we may rewrite equation (1) in the following normalised form:

$$\iota_p^2 = \frac{2(\gamma - 1)}{\gamma} \int_{\kappa_p}^{1} \frac{\iota^2 \, d\kappa}{\kappa} \tag{2}$$

where $\iota = I/I_0$, $\kappa = r/r_0$ and $I_0 = V_1/(L_1/C_1)^{1/2}$ is the characteristic peak current of the L–C discharge circuit.

The implication of this condition governing the quasi-equilibrium pinch position may be understood in terms of a radial snow-plough model coupled to a L–C discharge (Lee 1983d). The κ and ι curves as functions of normalised $\tau = t/t_0$ (where $t_0 = (L_1/C_1)^{1/2}$) have the general form as depicted in figure 1(a). From these curves may be

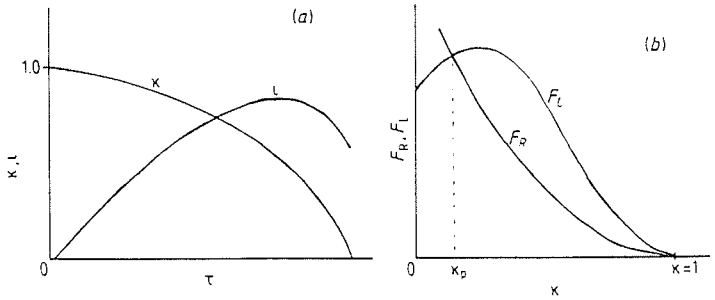

Figure 1. (a) General forms of snow-plough trajectory and circuit current as functions of time. (b) General forms of the functions F_L and F_R as derived from (a).

derived the curves of $F_L = \iota^2$ and

$$F_R = \frac{2(\gamma - 1)}{\gamma} \int_{\kappa}^{1} \frac{\iota^2 \, \mathrm{d}\kappa}{\kappa}$$

as functions of κ. The general forms of F_L and F_R are as depicted in figure 1(*b*). An analysis of F_L and F_R shows that at $\kappa < 1$, F_L is larger than F_R but that as $\kappa \rightarrow 0$, the value of F_R must exceed F_L at some point. The point where the two curves intersect is the point at which condition (2) is met and the quasi-equilibrium radius ratio κ_p is achieved. It is not energetically possible to compress beyond this point.

As the compression proceeds F_R rises to meet F_L at a value of κ corresponding to κ_p. If just before κ_p is reached the current ι is raised rapidly, or stepped up, the value of F_L will increase faster than the value of F_R because F_L is the absolute value of the current squared whereas F_R is an integral. Thus it is possible to diverge the values of F_L and F_R and move the quasi-equilibrium point to a lower value of κ_p. A simple example with a single current step added to the primary current will now be discussed.

3. The model

Consider the circuit as shown in figure 2. The switch S_1 in the primary circuit is closed so that the capacitor C_1 charged to voltage V_1 starts to discharge with current I_1 through inductance L_1 into the pinch of varying inductance L_p. The pinch is depicted in coaxial form with pinching current flowing at radius r, and the return current in the return conductor of radius r_0. The initial radius of the pinch is approximated as r_0. As the pinch approaches its equilibrium position as determined by equation (2), the switch S_2 in the current-stepping circuit is closed so that the capacitor C_2 starts discharging current I_2 through inductance L_2 into the pinch.

Applying the snow-plough model to govern the pinch dynamics we have:

$$\frac{\mathrm{d}}{\mathrm{d}t}\left(\pi\rho_0(r_0^2 - r^2)\frac{\mathrm{d}r}{\mathrm{d}t}\right) = -\frac{\mu I^2}{4\pi r} \tag{3}$$

where

$$I = I_1 + I_2. \tag{4}$$

The currents I_1 and I_2 are governed by the circuit equations:

$$\frac{\mathrm{d}}{\mathrm{d}t}(L_1 I_1) + \frac{\mathrm{d}}{\mathrm{d}t}(L_p I) = V_1 - \frac{\int I_1 \, \mathrm{d}t}{C_1} \tag{5}$$

with

$$I_2 = 0 \tag{6}$$

until switch S_2 is closed; whereupon

$$\frac{\mathrm{d}}{\mathrm{d}t}(L_2 I_2) + \frac{\mathrm{d}}{\mathrm{d}t}(L_p I) = V_2 - \frac{\int I_2 \, \mathrm{d}t}{C_2}. \tag{7}$$

The plasma inductance L_p is given by

$$L_p = \frac{\mu}{2\pi}\left(\ln\frac{r_0}{r}\right) l. \tag{8}$$

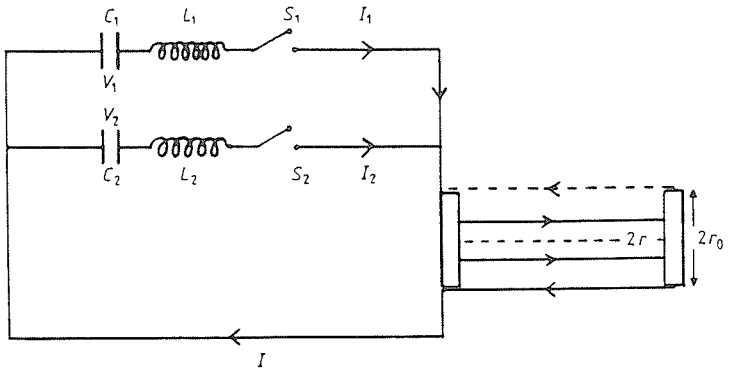

Figure 2. Schematic diagram of the arrangement for a current-stepping pinch.

The decision of when to switch on S_2 may be related to how close the condition as expressed in equation (4) is approached. For the purpose of numerical computation we may define a convergence ratio as:

$$\psi = \frac{2(\gamma - 1)}{\gamma} \int_{\kappa}^{1} \frac{\iota^2 \, \mathrm{d}\kappa}{\kappa} \iota^{-2} \tag{9}$$

and numerically we may experiment with switching on S_2 at the time when ψ attains a value such as $\psi_0 = 0.8$.

4. Normalisation

To formulate the problem in terms of relevant scaling parameters we adopt the following normalisation:

$$\tau = t/t_0 \qquad \kappa = r/r_0$$

$$\iota = I/I_0 \qquad \iota_1 = I_1/I_0 \qquad \iota_2 = I_2/I_0.$$

Then the governing equations may be written in the form:

Motion:

$$\frac{\mathrm{d}^2\kappa}{\mathrm{d}\tau^2} = \left[-\alpha_0^2 \frac{\iota^2}{\kappa} + 2\kappa \left(\frac{\mathrm{d}\kappa}{\mathrm{d}\tau} \right)^2 \right] (1 - \kappa^2)^{-1} \tag{10}$$

Primary current circuit:

$$\frac{\mathrm{d}\iota_1}{\mathrm{d}\tau} = \left(1 - \int \iota_1 \, \mathrm{d}\tau + \beta_0 \frac{\iota}{\kappa} \frac{\mathrm{d}\kappa}{\mathrm{d}\tau} - \beta_0 \ln \kappa \frac{\mathrm{d}\iota_2}{\mathrm{d}\tau} \right) (1 - \beta_0 \ln \kappa)^{-1} \tag{11}$$

Current-stepping circuit:

$$\frac{\mathrm{d}\iota_2}{\mathrm{d}\tau} = 0 \tag{12a}$$

or

$$\frac{\mathrm{d}\iota_2}{\mathrm{d}\tau} = \left(\frac{\lambda}{\beta} - \frac{1}{\beta\delta} \int \iota^2 \, \mathrm{d}\tau + \frac{\beta_0}{\beta} \frac{\iota}{\kappa} \frac{\mathrm{d}\kappa}{\mathrm{d}\tau} + \frac{\beta_0}{\beta} \ln \kappa \frac{\mathrm{d}\iota_1}{\mathrm{d}\tau} \right) \left(1 - \frac{\beta_0}{\beta} \ln \kappa \right)^{-1} \tag{12b}$$

Total current:

$$\iota = \iota_1 + \iota_2 \tag{13}$$

and the switching condition for equation (12) is specified by presetting a value for ψ in equation (9).

The three characteristic quantities in the set of equations are taken to be r_0, the initial radius of the pinch column, and t_0 and I_0 which are selected to relate to the primary current circuit:

$$t_0 = (L_1C_1)^{1/2} \qquad I_0 = V_1/(L_1/C_1)^{1/2}. \tag{14}$$

Then the scaling parameters which appear naturally in the equation are:

$$\begin{aligned} \alpha_0 &= t_0/t_p \\ \beta_0 &= \frac{\mu l}{2\pi} \Big/ L_1 \\ \beta &= L_2/L_1 \\ \delta &= C_2/C_1 \\ \lambda &= V_2/V_1 \end{aligned} \tag{15}$$

where

$$t_p = \left(\frac{4\pi^2\rho_0 r_0^4}{\mu I^2}\right)^{1/2} \tag{16}$$

appears naturally as the characteristic time for the pinching process. The length of the pinch is here denoted as l.

Thus α_0 is a scaling parameter for matching the characteristic discharge time of the primary current circuit to the characteristic pinching time of the system and β_0 is the scaling parameter for matching the characteristic pinch inductance to the primary circuit inductance L_1. The other scaling parameters β, δ, λ allow variation to be made in the ratio of the electrical parameters of the primary circuit to those of the current-stepping circuit. The preset ratio ψ_0 may also be considered as a parameter for selection of switching time for the current step.

5. Computation procedure

The scaling parameters α_0, β_0, λ, δ, β and ψ_0 are set at desired values. The numerical computation is then initiated by setting $\tau = 0$, $\kappa = 1$, $d\kappa/d\tau = 0$, $\int \iota_1 \, d\tau = 0$, $\iota_1 = 0$, $d\iota_1/d\tau = 1$ are fixed initial conditions. The initial value of the acceleration $d^2\kappa/d\tau^2$ is not defined by equation (10), but it is found that a trial initial value of -1 is suitable for the numerical integeration to converge quickly. The other initial conditions are set as $\int \iota_2 \, d\tau = 0$, $\iota_2 = 0$ and $d\iota_2/d\tau = 0$.

Equations (10), (11), (12*a*) and (13) are then integrated numerically by a linear approximation method which is found to give sufficient accuracy with a time step of 0.001; the results agree with integration by a Runge–Kutta scheme. At each step of the computation ψ_0 is computed numerically by equation (9) and compared with the preset value of ψ. When $\psi \geqslant \psi_0$ the equations for integration are changed to equations (10),

(11), (12b) and (13). The integration continues until the value of ψ attains $\psi > 1$ at which point the energy balance condition as expressed by equation (4) has been reached. The integration is then stopped. The computation is performed for a $\gamma = 5/3$ plasma.

6. Results

The results for two sets of parameters are presented here to demonstrate the capability of the technique to significantly reduce the radius ratio of the pinch. The first set of parameters, $\alpha_0 = 0.7$, $\beta_0 = 1$, $\beta = 10$, $\delta = 0.01$, $\lambda = 30$, $\psi_0 = 0.8$, is suitable for a system where the primary circuit is a capacitor bank and the current step is provided by a second capacitor bank charged to 30 times the voltage of the primary bank. This might in practice be a capacitor bank–Marx combination. The values of $\alpha_0 = 0.7$ and $\beta_0 = 1$ ensure a good energy transfer between the primary bank and the plasma has occurred (Lee 1983d) at about the time the current step is switched. Under these conditions, the value of κ_p would be about 0.4 in the absence of the current step. The effect of the current step is quite significant as is seen in figure 3(b), which shows the values of F_L and F_R converging as κ approaches 0.4 and then diverging as the current is stepped, until a final convergence at $\kappa_p = 0.24$. Figure 3(a) shows the trajectory κ versus τ and the current shape ι versus τ.

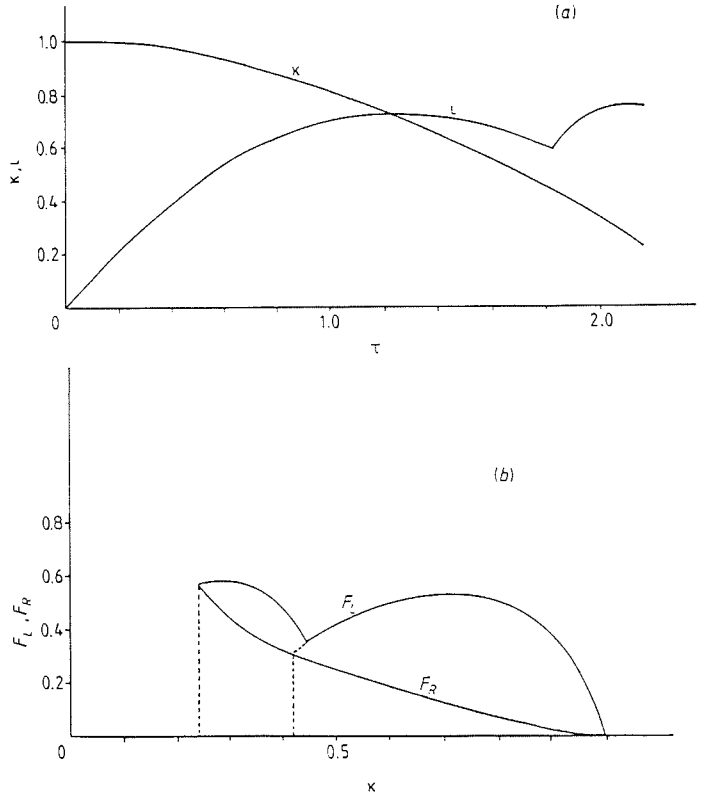

Figure 3. (a) Computed values of κ and ι versus τ for $\alpha_0 = 0.7$, $\beta_0 = 1$, $\beta = 10$, $\delta = 0.01$, $\lambda = 30$, $\psi_0 = 0.8$. (b) Computed values of F_L and F_R versus κ showing the shift in the energy balance point due to the current step for $\alpha_0 = 0.7$, $\beta_0 = 1$, $\beta = 10$, $\delta = 0.01$, $\lambda = 30$, $\psi_0 = 0.8$.

The second set of parameters, $\alpha_0 = 1, \beta_0 = 0.1, \beta = 0.25, \delta = 2, \lambda = 2, \psi_0 = 0.8$, may be more suitable for a system powered by two conventional capacitor banks, with the second bank having twice the voltage and capacitance as the first but only one quarter the inductance. With $\beta_0 = 0.1$, the energy efficiency of the first bank is relatively low (Lee 1983d). Under this condition the value of κ_p would be about 0.25 in the absence of a current step. Figure 4(*b*) shows the effect of switching on this current step. The quasi-equilibrium position is seen to have been shifted dramatically to $\kappa_p = 0.14$. Incidentally this compression already equals that of the plasma focus which typically (Lee 1983a) has a κ_p also of 0.14.

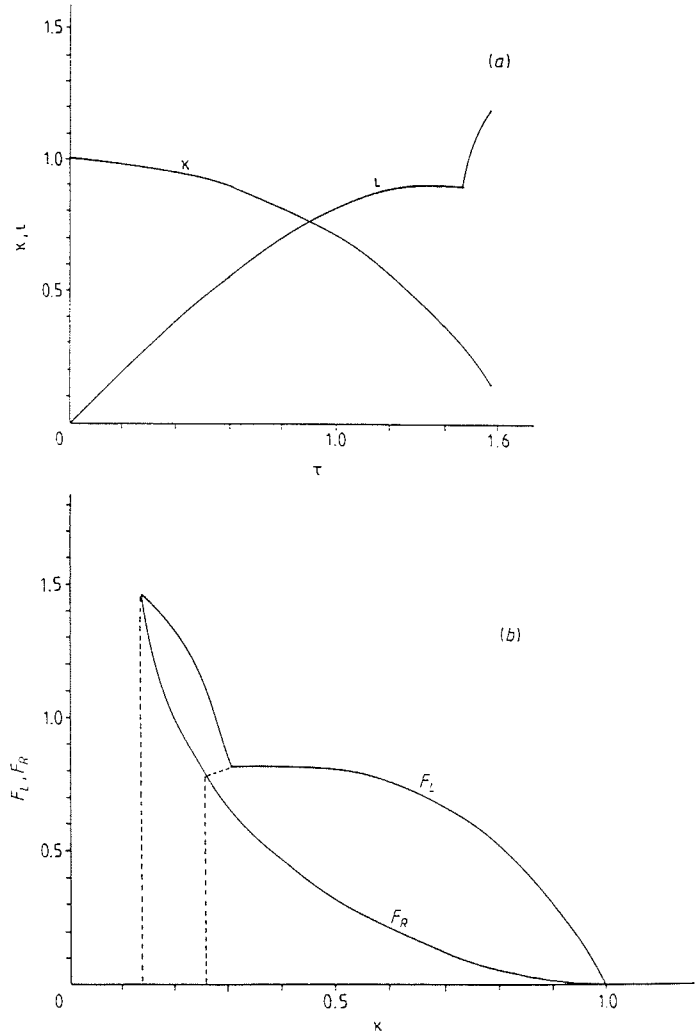

Figure 4. (*a*) Computed values of κ and ι versus τ for $\alpha_0 = 1, \beta_0 = 0.1, \beta = 0.25, \delta = 2, \lambda = 2, \psi_0 = 0.8$. (*b*) Computed values of F_L and F_R versus κ showing the shift in the energy balance point due to the current step for $\alpha_0 = 1, \beta_0 = 0.1, \beta = 0.25, \delta = 2, \lambda = 2, \psi_0 = 0.8$.

For a practical situation it is necessary to consider the possibility of excessively large voltage reversals across the first capacitor C_1. This is particularly the case in the first example considered since the second capacitor C_2, at 30 times the charging voltage of

C_1, is switched on to both the pinch as well as C_1 at a time when the voltage across C_1 is near zero and its current is dropping from its peak value. It is found that the effect on the current I_1 is to force its value down faster than it would have fallen had C_2 not been switched. However because the value of $(L_2C_2)^{1/2}$ is only 0.32 times the value of $(L_1C_1)^{1/2}$, a consequence of the parameters $\beta = 10$, $\delta = 0.01$, the voltage on C_2 has dropped through zero soon after I_1 has been forced through zero.

In order to ensure that in each case the current or voltage on C_1 do not swing past acceptable limits in a discharge, the behaviour of the currents and voltages have been followed by continuing the integration of equations (11) and (12*b*) up to $\tau = 6.3$, representing one complete cycle of the short-circuited L_1–C_1 combination. To do this beyond the time when the pinch has reached its quasi-equilibrium point, the value of κ is kept fixed at its quasi-equilibrium value and $d\kappa/d\tau$ and $d^2\kappa/d\tau^2$ are taken as 0. This integration shows that in both the examples considered above the magnitude of the voltages on the capacitors and their currents remain within reasonable limits. In the capacitor–Marx combination of the first example I_1 reaches a second peak of 0.9 of $V_1/(L_1/C_1)^{1/2}$ at $\tau = 3.35$ and the voltage on C_1 reaches a value of $-0.82V_1$ at $\tau = 4.0$. For the capacitor–capacitor combination of the second example, because of the greater initial charge on C_2, the voltage on C_1 does reach a reverse peak value of $-1.02V_1$ at $\tau = 6.1$. In an actual experiment it may be expected that stray resistance and plasma resistive effects will significantly damp these swings. These values do not represent impractical values for the safe operation of the capacitors.

7. Discussion and conclusions

The use of a snow-plough equation of motion would by itself produce a non-physical final radius of zero. In the present model the snow-plough trajectory is terminated by the use of an energy balance criterion thus giving a proper non-zero radius ratio. This procedure has certain limitations. For example if a constant current is instantaneously imposed on the pinch the initial condition would be $\tau = 0$, $\iota = 1$. It is not possible to start the integration of the snow-plough equation of motion (10) with this condition. This means that the trajectory of the compression cannot be followed even though the final radius ratio may be obtained simply by integrating equation (2). This particular situation could be improved by replacing the structureless snow-plough equation of motion with a model with structure such as the slug model (Potter 1978). It should also be stressed that the model discussed here applies only to fast (supersonic) compressions.

This current-stepping technique has been shown to be able to significantly reduce the plasma pinch ratio. From the results obtained it is evident that further enhancement of the pinch compression may be attained by using multiple steps added to the primary pinching current. It is doubtful though that radius ratios of the order of even 0.01 may be achieved by this technique with practical current generators whilst maintaining the assumption of a lossless plasma. However the pinch compression may be sufficiently enhanced for this technique to be of importance in the design of high intensity soft x-ray sources using argon or xenon plasmas.

Also, provided that the pinch is operated with the correct line density to be in the finite Larmor radius stabilised regime (Haines 1982) the current-stepping technique may be useful as a prelude to a final process of compression due to radiation cooling leading to the desired small radius ratios. In terms of the energy balance theory, radiation cooling will lead to a reduced slope in the F_R curve in figure 2(*b*). Linking the F_R curve to radiation losses will thus result in a further reduction of the final values of κ_p.

Acknowledgments

The assistance of Jalil bin Ali in part of the computation is acknowledged.

References

Haines M G 1982 *Phys. Scr.* **T2/2** 380–90
Lee S 1981 *Bul. Fiz. Malaysia* **2** 240
—— 1983a *Plasma Phys.* **25** 571
—— 1983b *J. Appl. Phys.* **54** 3603
—— 1983c *Austr. J. Phys.*
—— 1983d *J. Phys. D: Appl. Phys.* **16** 2463
Potter D E 1978 *Nucl. Fusion* **18** 813

J. Fiz. Mal. 5, 149(1984)

PRELIMINARY MEASUREMENTS ON A LINEAR PINCH PLASMA

S.M. LOW, B.C. TAN and S. LEE

Physics Department,
University of Malaya
Kuala Lumpur 22-11,
Malaysia.

Abstract

A ring-electrode linear pinch hydrogen plasma powered by a 40 μF capacitor bank was constructed. It was found that the time taken for the plasma column to pinch depends on the square root of the density of the gas as predicted by theory. Streak photographs gave an insight into the dynamics of the plasma column. The shock front and the reflected shock from the plasma axis were observed. A quasi-equilibrium plasma column was found to exist for (1.2 ± 0.2) μs, with a radius ratio of 0.4 and an estimated plasma temperature of 30,000 K.

Introduction

A Z-pinch plasma system may be represented by an equivalent circuit as shown in Fig. 1, where a current I is discharged from a capacitor bank C_o through a circuit inductance L_o. During this high current discharge, a strong azimuthal magnetic field B_θ is produced encircling the current stream. The interaction of this axial current density J, and the azimuthal magnetic field produces a strong imploding electromagnetic force, F_m, given by

$$F_m = \frac{B^2}{2\mu_o} A = \frac{\mu_o I^2}{8\pi^2 r^2} A \qquad (1)$$

where A and r are the surface area and the radius of the plasma column respectively. Basing on the snowplough model and the concept of energy balance, Lee[1] had shown that for a constant length, variable current pinch, the time taken t_p, for the plasma column to pinch was given by the expression

$$t_p = (4\pi^2 \rho_o r_o^4 / \mu_o I_o^2)^{1/2} \qquad (2)$$

where ρ_o is the density of the gas producing the plasma, r_o is the original radius of the plasma column, I_o is the peak current discharged into the system and μ_o is the permeability of free space. One can observe that the pinch time t_p is directly proportional to the square root of the density, $\sqrt{\rho_o}$.

Experimental Set-up

The plasma system was formed by two 2.5 cm diameter brass ring-electrodes separated by a distance of 10 cm, in a 6.5 litre spherical gas chamber. The chamber was evacuated to a pressure of about 10^{-5} torr. Commercial hydrogen gas was supplied to the chamber via a needle valve, which allowed the passage of the hydrogen gas to the chamber to be controlled.

Electrical energy to this system came from a 40 μF capacitor bank built from two 20 μF-10 kV capacitors connected in parallel. A GL-7703 ignitron was used as a switch, triggered by a krytron pulse generator via a 1:1 pulse transformer and a diode chain as shown in Fig. 2.

In the present set-up, the capacitor characteristic time $(L_o C_o)^{1/2}$ is considerably greater than t_p; so that the current is generally rising (except for inductive dips) during and after the pinch.

Experimental Technique

After evacuating the plasma chamber to a low pressure, the chamber was flushed several times with hydrogen. Hydrogen was then let in to the required pressure and the pump was isolated.

A Rogowski coil operated as a current transformer[2] and a magnetic probe made from ten turns of SWG 36 enamelled copper wire embedded in a glass tubing, were used to measure the current and the azimuthal magnetic field of the discharge respectively.

An Imacon streak camera was used to study the dynamics of the plasma. The camera was focussed, through a narrow slit, onto the discharge axis, at a distance of 50 cm. The sweep time of the streak camera was calibrated by using an FX-6A Xenon flash tube[3] of flash duration of (1.6 ± 0.1) μs, whose flash was delayed at some suitable time interval in correspondence with the camera sweeping speed. Fig. 3 shows a typical signal of such calibration at the present operating condition of the camera. The measured sweep speed was 1.17 μs/cm. This corresponds to a full length (7.6 cm) sweep time of about 8.85 μs as compared to the sweeping output signal from the streak camera of (12.5 ± 0.5) μs, and a value of 5 μs as given by the camera specification.

Results and Discussion

The variation of the pinch time t_p with the density of the gas was investigated. The results were plotted in Fig. 4 for a pressure range of 2 mbar to 9 mbar. From Eqn. 2, since pressure, P, is proportional to density, it is clear that

$$t_p \sim \sqrt{p}$$

It is evident from Fig. 4 that there is a square root dependence of t_p on the gas pressure (or gas density) thereby suggesting that the above dependence was obeyed. This would also mean that the plasma column was driven by an electromagnetic "piston".

Fig. 5 shows a typical streak photograph from which the trajectory of the shock

front was observed. Indeed, the shock front was observed to hit the axis at point 'a' and was reflected. This was seen by the increase in intensity in that region of the streak photograph, region 2 in the retraced picture. The reflected shock met (at point 'b') the rather diffused electromagnetic piston at a time about 2.5 μs after the start of the discharge. Then the radius of the plasma column was observed to expand, from 4 mm, at point 'b', to 6 mm, at point 'c', followed by a small contraction to 5 mm, at point 'd', and remained at that value for about (1.2 ± 0.2) μs before it diffused off at point 'e'.

From the slope of the shock front, the average shock speed, q is estimated to be about 1.7 cm/μs. However, from pinch theory, one knows that the speed of the shock increases, particularly as it approaches the plasma axis. For example, using a generalised slug model[4], one may estimate that when the shock front hits the axis, the shock speed is about twice that of the average shock speed. From shock theory[5], one knows that the temperature, T, of the plasma is proportional to the square of the shock speed, with:

$$T = 1.13 \times 10^{-5} q^2 \tag{3}$$

for fully ionised hydrogen. Thus the temperature of the plasma will be 13,000 K. Similarly, one can also estimate from shock jump theory a density ratio, ρ_r/ρ_2 (where ρ_2 is the density in the forward shock and ρ_r that in the reflected shock) of 1.5 for the plasma. The temperature of the plasma in the reflected shock, region 2 is further increased by more than 2 times to about 30,000 K. In addition, Joule heating can also occur. Consequently, the plasma pressure, after the reflected shock is:

$$P_r = nkT\zeta \tag{4}$$

(where n is the number density of unionised particles, ζ is the departure coefficient and k is the Boltzman's constant) considerably greater than P_2, the pressure of the plasma after the forward shock.

For an order of magnitude estimate of the plasma pressure, one may refer to Wright[6] for the ratio of reflected shock pressure, P_r, and incident shock pressure P_2 as

$$\frac{P_r}{P_2} = \frac{(2u+1)v - u}{uv + 1} \tag{5}$$

where $u = (\gamma - 1)/(\gamma + 1)$

$y = M^2(1+u) - u$

and γ is the specific heat ratio, M is the first (incident) shock Mach number. In the present plasma, M = 12 (for an average q = 1.7 cm/μs), and if one assumes for the fully ionized hydrogen plasma that $\gamma = 5/3$, then $P_r/P_2 = 6$.

Thus when the reflected shock meets the electromagnetic piston, it is not surprising that the magnetic pressure P_m is considerably less than the kinetic pressure P_r. This causes the slight expansion at point 'b'. Subsequently at point 'c', P_m again exceeds the kinetic pressure (because of the increased value of current and the decreased value of

the kinetic pressure due to column expansion) causing the plasma column to be compressed once more. Between points 'd' and 'e' a plasma column of almost constant radius and apparently in quasi-equilibrium is observed.

Considering that the quasi-equilibrium radius is about the same as the radius where the reflected shock meets the piston, it may be expected that the temperature of the quasi-equilibrium column is about that of the reflected shock. However one notes further that the plasma current has increased during this period of time, so that the quasi-equilibrium column could be expected to be not less than 30,000 *K*.

Conclusion

The plasma behaviour of a hydrogen linear pinch system constructed from two ring-electrodes was investigated. The plasma was driven by the electromagnetic piston from the interaction of the discharge current density and the resulting azimuthal magnetic field. A quasi-equilibrium plasma column lasting (1.2 ± 0.2) μs was observed to exist at a time (3.4 ± 0.6) μs after the start of the discharge. From the observed dynamics the plasma temperature was estimated to be not less than 30,000 *K*. Streak photographs also show that the plasma column has a diameter of about 10 mm. This could indicate a quasi-equilibrium radius ratio of 10/25 = 0.4; somewhat large from energy balance consideration[1]. This is to be expected because of the diffusive nature of the rather low speed electromagnetic piston in this experiment.

References

1. S.Lee, J.Phys D: Appl. Phys. 16, 2463 (1983).
2. R.H. Huddlestone and S.L. Leonard, Plasma Diagnostic Techniques, 12 (Academic Press, 1965).
3. S. Lee, Bull. Phys. M'sia., 1, 17 (1980).
4. S. Lee, Bull. Phys. M'sia., 3, 197 (1982).
5. S. Lee, "Electromagnetic Shock Tube" in Experiments on Laser and Plasma Technology, Procs. (Part I) First Tropical College on Applied Physics, Dec. 1983 – Jan. 1984, Kuala Lumpur, (Published by ASEANIP, 1984).
6. J.K. Wright, Shock tubes (Spottiswoode, London & Colchestec, 1961).

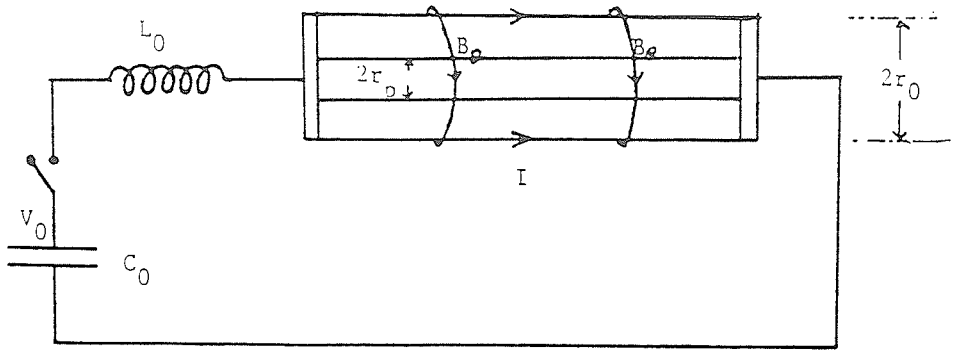

Fig. 1. Equivalent circuit of the pinch system showing also a plasma column encircled by the azimuthal magnetic field B_θ being compressed from radius r_0 to r_p.

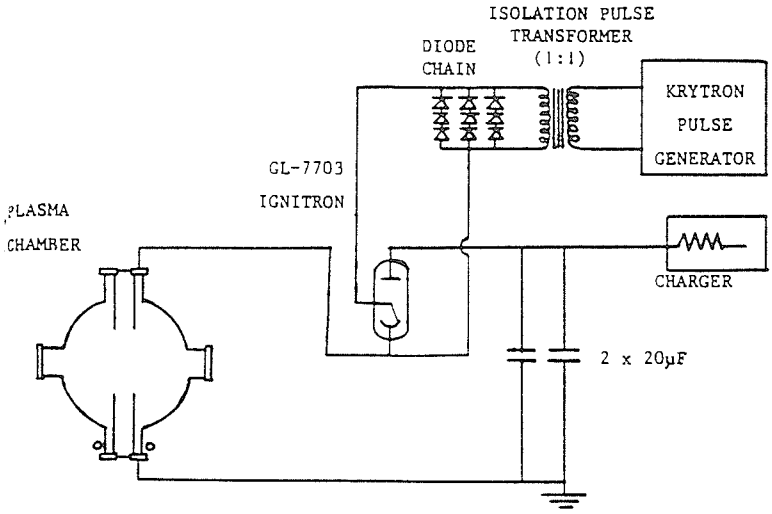

Fig. 2.

The plasma discharge system.

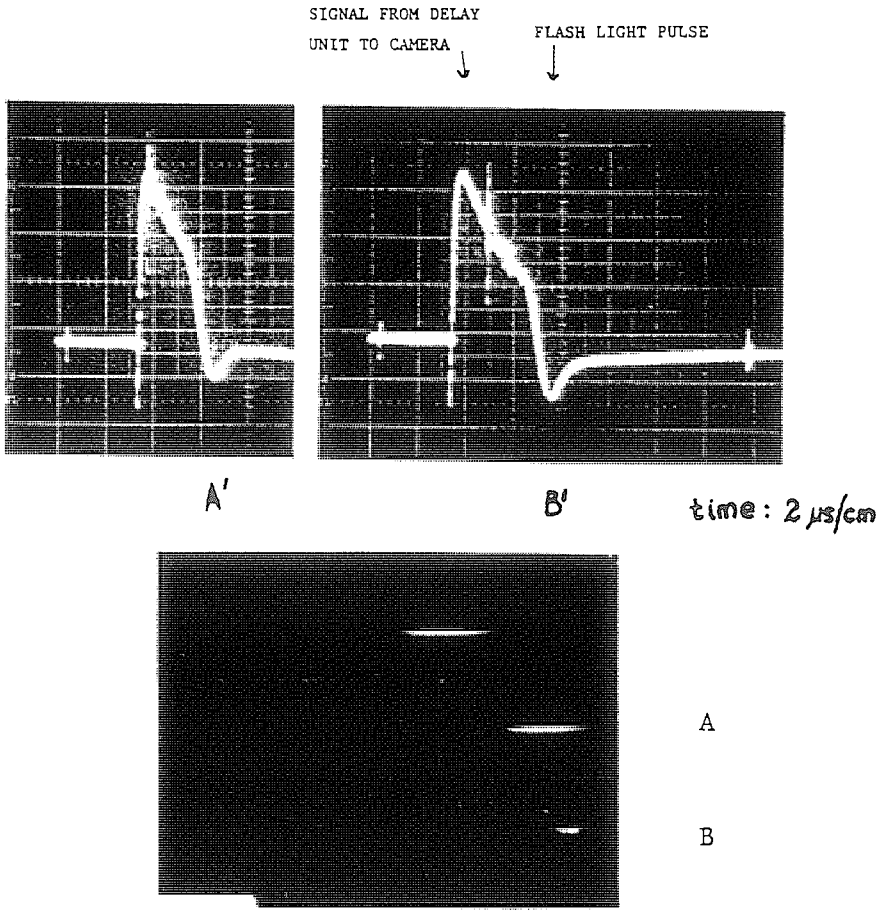

Fig. 3. Calibration of streak camera using xenon flash. A and B on streak photograph correspond to A' and B' respectively of the flash light pulses on oscillograms.

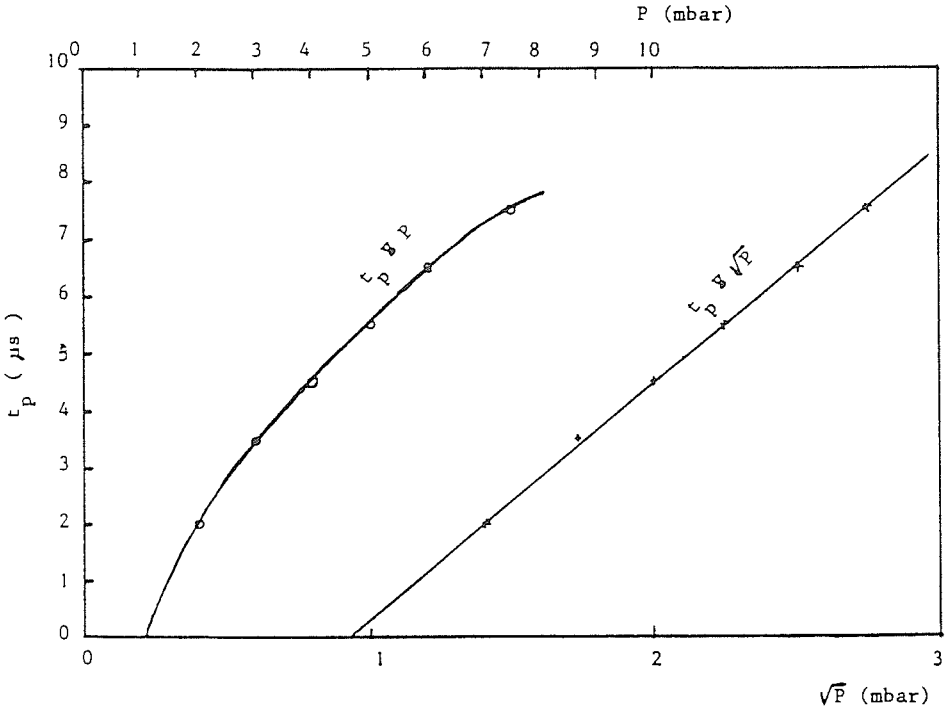

Fig. 4. Variation of pinch time, t_p, with pressure, P.

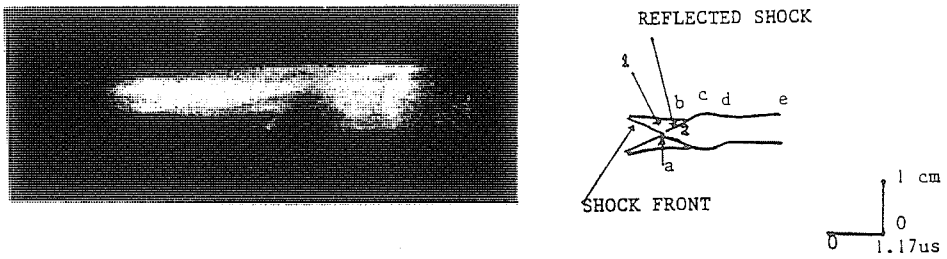

Fig. 5. Streak photograph of the plasma column, whose dynamic behaviour was observed.

J. Fiz. Mal. 5, 135(1984)

A GENERALISED SLUG MODEL FOR THE PINCH

JALIL BIN ALI, S. LEE, T. Y. TOU and Y. C. YONG*
Plasma Research Laboratory, Physics Department,
University of Malaya,
Kuala Lumpur 22-11, Malaysia.

Abstract

A generalised self-consistent slug model with coupled-current is developed for a pinch. Based on this, two regimes are described in the formation of a pinch. In the first stage a pinch is produced by a shock compression. Following this a slow compression takes place in the second stage. This model is able to provide the pinch trajectory as well as the current as a function of time. Various cases of physical interest are described.

Introduction

Although the pinch is fundamentally the simplest of fusion devices, even its gross dynamics is still not clearly understood.

The inadequacy of the common snow-plow model for pinch dynamics has been discussed by Lee[1] who has proposed a lossless energy balance theory for a variable current and a variable length pinch. Potter[2] gave one of the first detailed accounts using a slug model but applied only to a constant current and a constant length pinch. Lee[3] generalised the slug model to a plasma focus. More recently this model with the inclusion of further empirical phases[4] has been applied to an inductive plasma focus. The extension into the empirical phases was necessary for the purpose of comparison between the experimental and computed current as well as the voltage waveform.

An important quantity to characterise pinch dynamics is the quasi-equilibrium radius ratio. In the case of the snow-plow model with energy balance theory the pinch trajectory was terminated by the energy balance condition in order to obtain the final radius ratio at the quasi-equilibrium pinch radius. In the slug model for the constant current pinch[2] the final radius ratio was determined once the forward shock front has imploded on to the axis.

To apply the slug model to the general case of a circuit-coupled compression it is to be noted that the piston need not necessarily stop when the shock hits the axis. A further adiabatic phase of slow dynamics is in general necessary (Fig. 1). In this paper an attempt is made to extend the dynamics beyond the shock compression phase into a slow dynamics phase.

*Ngee Ann Polytechnic, Maths and Science Centre, Clementi Road, Singapore 2159.

Theory

Basically the pinch consists of a large electric current flowing through a gas between two electrodes as illustrated in Fig. 2. The resultant (J x B) force causes the plasma column to implode inwards. This implosion may be considered in two successive phases.

Strong Shock Compression Phase

In this regime, the shock front position, r_s, is obtained through the shock-jump equations by matching the shock kinetic pressure P_k to the magnetic pressure P_B. Thus[2]

$$\frac{dr_s}{dt} = -\left[\frac{\mu_o}{\rho_o}(\gamma+1)\right]^{1/2} \frac{I}{4\pi r_p} \tag{1}$$

where r_p is the radial piston position, r_s is the radial shock position, γ is the specific heat ratio, ρ_o is the ambient gas density, μ_o is the free space permeability, and I is the current flowing in the circuit.

The piston position is allowed to separate from the shock position by the slug mechanism[3]. For this case of the pinch the relation reduces to:

$$\frac{dr_p}{dt} = \frac{\frac{2}{(\gamma+1)}\frac{r_s}{r_p}\frac{dr_s}{dt} - \frac{r_p}{\gamma I}\left[1-\frac{r_s^2}{r_p^2}\right]\frac{dI}{dt}}{\frac{(\gamma-1)}{\gamma} + \left[\frac{1}{\gamma}\right]\left[\frac{r_s}{r_p}\right]^2} \tag{2}$$

The circuit equation is:

$$(L_o + L_p)\frac{dI}{dt} + I\frac{dL_p}{dt} = V_o - \frac{\int I dt}{C_o} \tag{3a}$$

where $L_p = \frac{\mu\ell}{2\pi}\,\ell n\left[\frac{r_o}{r_p}\right]$ is the pinch inductance at radius r_p and L_o is the external inductance of the system.

Hence the circuit equation may be written as:

$$\left[L_o + \mu\ell\ \ell n\left(\frac{r_o}{r_p}\right)/(2\pi)\right]\frac{dI}{dt} - \left[\mu\ell\frac{dr_p}{dt}\ I/(2\pi r_p)\right] = V_o - \int I dt/C_o \tag{3b}$$

Equations (1), (2) and (3b) form a closed set of 3 coupled equations with r_s, r_p and I as unknowns, which may be integrated from $t = 0$ up to the time when $r_s = 0$.

The Slow Dynamics Phase

The slow dynamics phase begins when the shock front has imploded on to the axis, i.e. $r_s = 0$.

In this phase, we may obtain the equation of motion for the piston position from pressure balance and the first law of thermodynamics.

The magnetic pressure at r_p induced by an enclosed axisymmetric current I is:

$$P_B = \mu I^2 / 8\pi^2 r_p^2 \tag{4}$$

The first law of thermodynamics is applied to our pinch in the following way[5]. We write, for a lossless system:

$$\frac{dh}{dt} = V\frac{dP_k}{dt} \tag{5}$$

where h is the enthalpy, V is the plasma volume and P_k is the plasma pressure. The enthalpy of the pinched plasma may be written in terms of γ as:

$$h = \frac{\gamma}{(\gamma - 1)} \frac{P_k}{\rho}$$

However, for the pinched plasma column, mass conservation gives:

$$\rho \pi r_p^2 = \rho_o \pi r_o^2$$

Hence we have $h = \gamma P_k r_p^2 / [(\gamma - 1)\rho_o r_o^2]$ (6)

Differentiating eq. (6) and substituting into eq. (5) gives:

$$\frac{dP_k}{dt} = -2\gamma P_k \frac{dr_p}{dt} / r_p \tag{7}$$

Differentiating eq. (4) gives:

$$\frac{dP_B}{dt} = 2\mu I \left\{ \frac{dI}{dt} - \frac{I}{r_p} \frac{dr_p}{dt} \right\} \Big/ 8\pi^2 r_p^2 \tag{8}$$

The assumption $P_B = P_k$ has been used in the strong shock compression phase. In that phase the validity of this assumption has to be carefully examined. However in the slow compression phase the piston is slowing down whilst the small disturbance speed is increasing. In this situation the assumption of $P_B = P_k$ is a very good one. Thus we may differentiate this condition to obtain

$$\frac{dP_B}{dt} = \frac{dP_k}{dt} \tag{9}$$

Hence equations (7), (8) and (9) give

$$2\mu I \left\{ \frac{dI}{dt} - I \frac{dr_p}{dt} / r_p \right\} / (8\pi^2 r_p{}^2) = -2\gamma P_k \frac{dr_p}{dt} / r_p$$

which with the help of eq. (4) and the assumption $P_B = P_k$ reduces to:

$$\frac{dr_p}{dt} = -r_p \frac{dI}{dt} / [(\gamma - 1) I] \tag{10}$$

For typical operation with strong electromagnetic drive, I is positive and large when the shock front goes on-axis. Thus for such cases Eq. (10) simply states that the piston will continue moving inwards during the slow compression provided that $\frac{dI}{dt}$ remains positive. On the other hand when $\frac{dI}{dt}$ goes negative, the slow compression leads to an expansion. Although in principle Eqs. (3b) and (10) are still valid during this expansion, we are principally interested in the dynamics immediately after the shock hits the axis. This is because in later times, reflected shocks and instability effects are observed experimentally; so that our model can at best be expected to be valid only up to a period not too long after the shock goes on-axis.

Equation (3b) together with Eq. (10) forms another closed set of 2 coupled equations describing the slow dynamics phase and may be integrated for r_p and I.

Normalisation

At this stage it is useful to introduce dimensionless variables for the equations in the two regimes. The equations are normalised by writing: $\tau = t/t_c$, $\kappa_s = r_s/r_o$, $\kappa_p = r_p/r_o$, $\iota = I/I_o$ where t_c is the capacitor characteristic time $(L_o C_o)^{\frac{1}{2}}$

I_o is defined as $V_o/(L_o/C_o)^{\frac{1}{2}}$

Thus the normalised equations are:

Shock compression phase

$$\text{Radial Shock Motion: } \frac{d\kappa_s}{d\tau} = -\frac{\alpha\iota}{\kappa_p} \tag{11}$$

$$\text{Radial Piston Motion: } \frac{d\kappa_p}{d\tau} = \frac{2\kappa_s \frac{d\kappa_s}{d\tau} / [(\gamma+1)\kappa_p] - \kappa_p \left(1 - \frac{\kappa_s^2}{\kappa_p^2}\right) \frac{d\iota}{d\tau} / (\gamma\iota)}{(\gamma-1)/\gamma + (\kappa_s/\kappa_p)^2/\gamma} \tag{12}$$

$$\text{Circuit Equation: } \frac{d\iota}{d\tau} = \frac{1 - \int \omega d\tau + \beta \iota \frac{d\kappa_p}{d\tau} / \kappa_p}{1 \quad \beta \mathcal{L} n(\kappa_p)} \tag{13}$$

Slow dynamics phase

$$\text{Radial Piston Motion: } \frac{d\kappa_p}{d\tau} = -(\kappa_p/\iota)\frac{d\iota}{d\tau}/(\gamma - 1) \tag{14}$$

Circuit Equation: This is the same as Eq. (13).

In the 2 phases $\alpha = \frac{t_c}{t_p}$ and the pinch characteristic time is:

$$t_p = [\rho_o/\mu_o(\gamma + 1)]^{1/2} \, 4\pi r_o^2/I_o$$

The parameter $\beta = \mu \ell / 2\pi L_o$ is introduced to relate the characteristic inductance of the compression with the external inductance of the system. These two scaling parameters enable one to scale the computations to various circuit and experimental conditions.

Computation procedure

The numerical integration is initialized by setting

$$\tau = 0, \kappa_s = 1, \kappa_p = 1,$$

$$\frac{d\kappa_s}{d\tau} = 0, \quad \frac{d\kappa_p}{d\tau} = 0,$$

$$\iota = 0, \frac{d\iota}{d\tau} = 1, \int \iota d\tau = 0$$

A time step of 0.001 was used. During the shock compression phase the energy matching ratio (EMR)[6] was also computed. The slow dynamics phase starts when the strong shock compression phase reaches $\kappa_s = 0$. For this phase, the last computed values of the strong shock compression phase are used to continue the integration. The integration proceeds until the value of a pre-set time is attained. In practice we allow the integration in the slow dynamics phase to proceed for a time equal to several times of the shock collapse time.

During the integration a check on the energy balance condition[6] was made at each step and from the results the radius ratio at energy balance is also noted.

Results

Figure 3 shows the κ_p, κ_s and ι profiles of different pinches. For an operating condition of $\alpha = 0.82$, $\beta = 0.01$ a radius ratio of 0.24 is obtained during the implosion

of the shock front onto the axis. When energy balance was fullfilled a radius ratio of 0.23 was observed. (This compares with a value of 0.21 from the snow-plow model). The piston converge inwards further and a maximum compression of 0.22 occurs at $\tau = 1.6$. Beyond this point radial expansion of the piston begins to take place.

For the case of $\alpha = 0.57$, $\beta = 1$ which represents a pinch with good EMR, a radius ratio of 0.37 was obtained when the shock front hits the axis. Energy balance condition was attained at $\tau = 1.97$ and a radius ratio of 0.38 was observed. This compares with a value of 0.39 from the snow-plow model. The role of a reflected shock has not been included in the present model. Taking a very approximate estimate that the reflected shock comes off the axis at 1/10 the speed of the incident shock, one may estimate in each case roughly at what point in the slow dynamics phase will the reflected shock hit the piston. The present model is valid up to this point. Following this procedure in the 2 cases presented thus far, it may be seen that the present model is valid way past the point of maximum compression. We shall now present a case (refer to Table 1) in which the model may be expected to breakdown almost as soon as the shock goes on-axis, because of the reflected shock. This is the case of a strongly driven pinch with $\alpha = 82$, $\beta = 0.01$. When the radially converging shock front hits the axis, energy balance is also fullfilled. A pinch radius ratio of 0.20 is observed which compares with Lee's value of 0.17 from the snow-plow with energy balance. The present model then indicates a slow compression leading eventually to a very small radius of 0.01. However drawing a line for the reflected shock at one-tenth of the final incident shock speed one sees that the reflected shock hits the piston at 0.13. Beyond this point the trajectory is invalid.

The two scaling parameters determine whether and how far the magnetic piston will experience an inwards convergence during the slow dynamics phase; the significance of a reflected shock from the axis which is not included in the present model, and finally the radial expansion of the piston. The results of the above discussion are summarised in Table I.

A comparison of EMR is also performed between the present model and the snow-plow model with energy balance theory. They show very good agreement in this respect.

Conclusion

A generalised self-consistent slug model with coupled-current is developed for the pinch. This model is extended into a slow dynamics phase to provide the dynamics after the shock compression phase. The results show good agreement in the pinch ratios for low values of α between the generalised slug model and the energy balance model based on a snow-plow trajectory. There is a substantial difference in the pinch ratio for very large values of α which is due to reflected shock effects not being taken into account in the slow dynamics model which is being used here.

References

1. S. Lee, Plasma Physics 25 571 (1983).
2. D. Potter, Nuclear Fusion 18,6 (1978).
3. S. Lee, A Plasma Focus Model Yielding Trajectory And Structure, Spring College on Radiation in Plasma, Trieste, May 1983 (To be published in procs.).
4. S. Lee, C.S. Wong, A.C. Chew, T.Y. Tou and Jalil B. Ali, Singapore J. Physics 1, 75 (1984)
5. C.S. Wong, Ph. D. Thesis 1983.
6. S. Lee, J. Phys. D: Appl. Phys., 16, 2463 (1983).

Table I: Theoretical values of pinch ratio r_p/r_o for constant length pinches of $\gamma = 5/3$.

CASE	ENERGY BALANCE THEORY Applied to Snowplow Model	GENERALISED SLUG MODEL		
		Shock Compression Phase at $\kappa_s = 0$	Energy Balance Theory	Slow Dynamics Phase at Maximum Compression
1. $\alpha = 0.82, \beta = 0.01$ (current waveform is approx. $I = I_o$ wt)	0.21	0.24	0.23	0 22
2. $\alpha = 0.57, \beta = 1$ (case with good energy coupling)	0.39	0.37	0.38	0 37
3. $\alpha = 81.6, \beta = 0.01$	0.17	0.20	0.20	Not valid (Refer to discussion*)

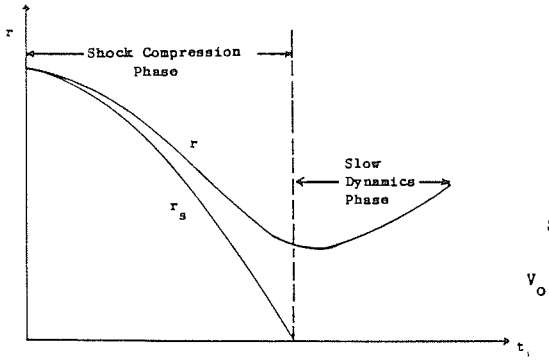

Fig. 1. Representation of the pinch based on a slug model with a shock compression phase followed by a slow dynamics phase. (Here r is the radius of a cross-section through the pinch. See Figure 2).

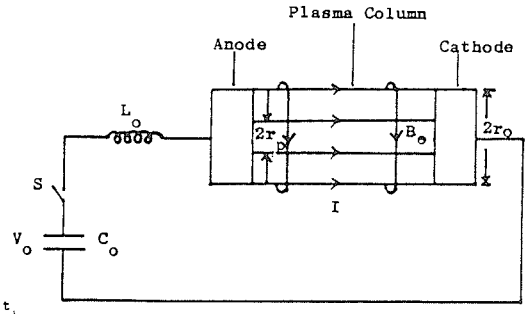

Fig. 2. Schematic diagram of a pinch circuit.

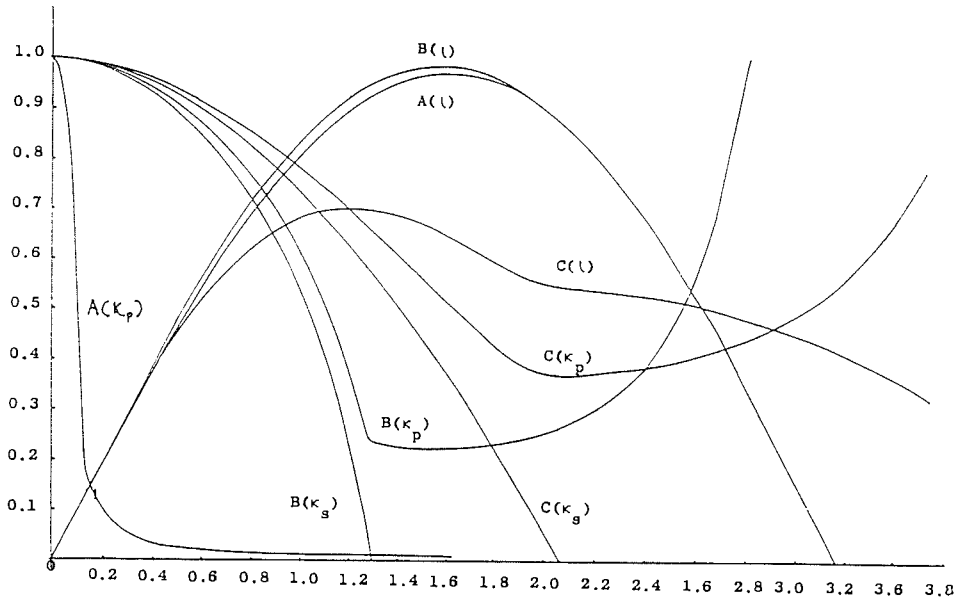

Fig. 3. Profiles of κ_p, κ_s, and ι as functions of τ for three sets of scaling parameters:
(a) $\alpha = 81.2, \beta = 0.01$; (linear current)
(b) $\alpha = 0.81, \beta = 0.01$; (sinusoidal current)
(c) $\alpha = 0.57, \beta = 1$; (good energy coupling)

J. Fiz. Mal. 5, 97(1984)

AN UNIVERSAL SOLAR-POWERED ELECTRONIC PULSER WITH VARIED APPLICATIONS – FROM ELEPHANT CONTROL TO COMMUNICATION LASERS

S. Lee, FIPM
Physics Department,
Universiti Malaya,
Kuala Lumpur 22 – 11,
Malaysia.

Abstract

A simple electronic pulser based on an SCR switched L-C-R circuit is used to provide pulses of variable pulse repetition frequency PRF (timed by an UJT) suitable for applications as varied as electrified fence for elephant control to powering a diode injection laser. Pulse width, voltage, pulse current capability and coupling to the load are discussed. Control of duty cycle enables large peak powers to be effected whilst maintaining low average power so that a regime of 'high-quality' usage may be defined in which the use of expensive solar electricity is justified. Experimental results are presented. The simple pulser is found to be sufficiently versatile for the range of applications considered. Problems of inverter efficiency at low power, and long-term reliability need to be further investigated.

Introduction

One important aspect of upgrading technology in a developing country is adaptability. Towards this end a simple modular system for versatile use of electronic pulses in several varied applications has been proposed [1-3]. This system, developed in the plasma physics laboratory[4] has since been extensively used to control and synchronise plasma, laser and high speed experiments and for ultrasonics and stroboscopic light flashes[1]. The basic module[3] consists of a capacitor and a switch. The first module is a start module. Successive modules are of increasing power until a final module, which powers a load producing the desired pulse such as an electrical, an ultrasonic pulse or a light pulse. Generally two or more modules are used for each application. By a suitable choice of pulse shape, duration and duty cycle, large pulse powers may be generated for very low average power consumption. This factor makes it suitable for solar electric panels to power this modular system; opening up an area of "high-quality" usage justifying the use of expensive solar electricity. Such "high-quality" usage of solar electricity in, for example, remotely-located repeater or communication stations or large scale electrified fences for animal control in difficult-to-access areas has the further advantage of low maintenance.

In order to stimulate more widespread use of solar powered electrical devices we consider here a simple system using commercially available solar panels, batteries and inverters, connected to a pulser and load. A simple pulser circuit with applications as varied as fence electrification and powering a diode laser is then discussed.

The System

We have set up a system with a solar panel (14 Watt peak) connected to a 40 A-hr rechargeable battery. A commonly available inverter used for night-market lighting was modified (by changing transformer turn-ratios) according to the voltage requirement of the pulser. This inverter was found to have good efficiency when operated at power levels above 10 W; but has a large standby current drain which makes it inefficient for low-power application. There is, therefore, a need to improve this aspect of the system. The system is illustrated in Fig. 1.

The Universal Pulser

The basis is an SCR circuit (see Fig. 2). The capacitor is charged from the inverter output, V, through a charging-current limiting resistor, R_c. It is then switched by the SCR through resistor R_o across which is connected the load. The discharge is an L-C-R type and in the limit of low R_o has discharge time governed by $(LC)^{1/2}$ where L = circuit inductance; and pulse impedance $(L/C)^{1/2}$. The circuit may be critically damped by putting total circuit resistance equal to $2(L/C)^{1/2}$. The pulse repetition frequency (PRF) of the pulse is easily controlled by an UJT circuit such as shown in Fig. 3. The rating of the SCR, the values of C and R_o and circuit inductance depend on the particular application, as does the method of output coupling. The cases of application to stroboscopes, ultrasonic and control of high power circuits have been discussed[1-7]. Here we discuss two interesting new applications.

Case I. Fence electrification for elephant control

An electrified fence for elephant control may consist of two stout galvanised steel wires running parallel to the ground at three feet and six feet height respectively. These wires, connected to the pulser output, are stretched taut between poles placed at regular intervals with proper insulation placed between the wires and the poles. Typically each fence runs for several km and is powered by one pulser. Considerations of pulse specifications include the need to avoid endangering the lives and safety of animals and humans. Joint tests with FELDA (Federal Land Development Authority) show that control with safety may be effected with PRF of about 0.7 per second, peak voltage of 5 kV into 1 kΩ and pulse duration of 60 μs. This gives a peak pulse power of 25 kW, output pulse energy of just over 1 J (after consideration of pulse shape), a duty cycle of 4×10^{-5} and an average output power of just over 1W.

The present pulser circuit is suitable for generating these pulses, when used with a step-up transformer. Some design consideration is discussed. We use a 1:10 step-up transformer to provide 6 kV into 1 kΩ. Thus the primary circuit would be suitably switched by an SCR of rating 600 V forward blocking, and surge current capability of 60 A. A suitable circuit with test load is as shown in Fig. 4. The output pulse is shown in Fig. 5. It is noted here that the pulse shape could be improved by a re-design of the pulse transformer to give a squarer shape.

Case II. Diode Laser for Signalling and Communication

We have chosen a fast injection diode laser to illustrate that even a simple 'slow'

pulser circuit such as described here is basically successful in powering the fast diode laser. We use the circuit as show in Fig. 6. With a capacitance of 0.015 μF and a stray inductance estimated as 1 μH the value of $\sqrt{(LC)}$ is 100 ns. We use a common MCR107 SCR which has a maxiumum current risetime of 50 A/μs. The L-C-R circuit of Fig. 6 is designed for a peak current rate of 10 A in 50 ns which exceeds the current rate capacity of the MCR107. Under these conditions the circuit risetime is slowed down by the switch and the observed current pulse shape has a risetime of 300 ns and a falltime of 500 ns with a half width of 400 ns ns (FWHM). The laser pulse width (FWHM) is 100 ns. Figure 7 shows the laser output as detected by a photodiode SD100A viewing the laser diode output through an optical fibre at 105V charging voltage and also shows the corresponding pulse current. Fig. 8 shows the photodiode outpput at various pulse currents with a current pulse waveform shown for comparison. The threshold lasing current is found to be 4.5A.

Discussion

This paper illustrates a simple SCR pulser which may be used for a wide-range of applications. The specific applications described here are in fence electrification for elephant control and in a fast injection diode laser suitable for fibre-optic and communication applications. For each application the basic pulser circuit may be used, and only the ratings of the components, the SCR, the capacitor, the resistors R and R_0 and the input voltage V together with the method of coupling to the load need to be varied. The two applications described may even be powered by a solar panel and battery combination although the inverter presently used is basically uneconomical for the low-average-power applications described here. These two pulsers deliver daily output energies of 25 W-hr (for typical elephant control) and 2½ W-hr (diode laser SG2001 operated at 200 pps at peak pulse current of 10 A) respectively, and with proper system design, particularly in the inverter section, should not require more than 75 W-hr for continuous operation. Thus a 12 V, 100 A-hr rechargeable battery will provide a 10-day no-sun reserve. Two 32-W (peak) solar panels such as the Arco M61 will provide approximately 100 W-hr[8] of charging on an average day giving a 25 W-hr excess per typical day. Use of the solar panels will eliminate replacement of batteries with freshly charged ones, a cumbersome task in distant locations.

The pulser discussed here for elephant control has the added advantage of variable PPF and voltage as the pulsing frequency may be controlled by the UJT and the voltage at the inverter output. This will have significance in the general area of animal control. The laser pulser described above could easily be improved by narrowing the current pulses to below 100 ns (FWHM). One easy way is to use a fast SCR (commercially available) with current rates of 1000A per μs. This will then enable PRF's of 100 and greater without unnecessarily overheating the diode laser.

Conclusion

The pulser described here is an attempt to adapt a simple L-C-R circuit to cope with a number of varied applications.

It appears that the simple pulser may be able to provide the pulsing capability of

the two applications discussed. In fact for elephant control this simple pulser gives the added advantage of variable PRF and voltage, though great care has to be exercised to keep the variation, especially increase in the voltage, within carefully specified limits. Several design problems remain to be solved, the most important of which is inverter efficiency at low power. Long term circuit reliability also needs to be studied.

References

1. S.Lee Bull. Phys. M'sia 2, 14 (1980)
2. S.Lee, B.C.Tan and A.C.Chew "A pulse technology laboratory-teaching of principles and applications" ASPEN Regional Conf. on Laboratory Physics Education (LAPE), Peking September 1983, to be published in Procs.
3. S.Lee, Y.H.Chen, S.P.Chow, B.C.Tan, H.H.Teh and S.P.Thong Procs. Symp. on Physics, Singapore, pg 182 (1971).
4. S. Lee, in "Fusion Energy-1981" IAEA-SMR-82 pg 289-295, published by IAEA, Vienna (1982).
5. S.Lee and Y.H.Chin, Bull. Phys.M'sia 2, 105 (1981).
6. T.Y.Tou and S.Lee, Bull. Phys. M'sia 4, 189 (1983)
7. C.S.Wong and S.Lee in "Fusion Energy-1981" IAEA-SMR-82 pg 336, published by IAEA, Vienna (1982)
8. F.T.Lee, B.C.Tan. T.Y.Goh and J.F.Tay, Bull.Phys. M'sia 2, 219 (1981)

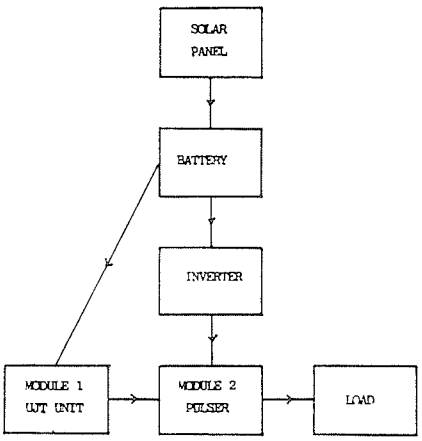

Fig. 1: Schematic of solar-powered universal pulser system.

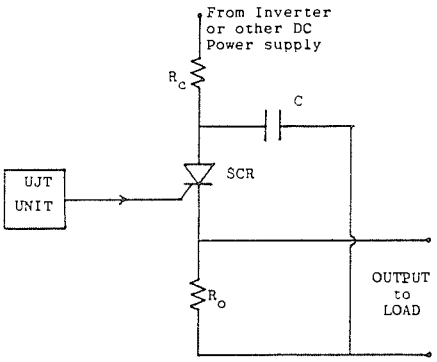

Fig. 2. The universal pulser circuit.

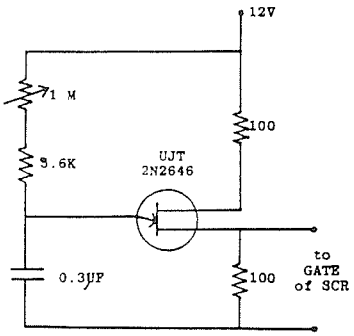

Fig. 3: The UJT circuit.

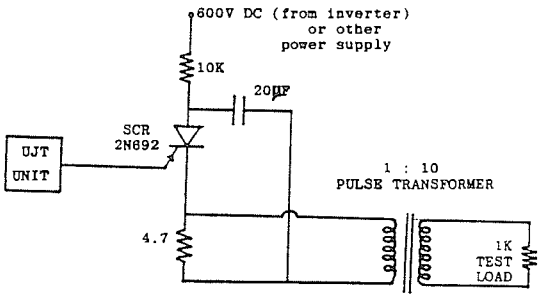

Fig. 4: Universal pulser circuit for fence electrification (with test load).

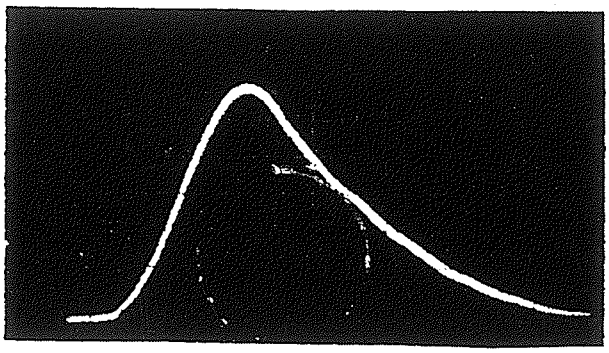

Fig. 5: Output pulse from pulser depicted in Fig. 4.

Horizontal scale: 20μs/div.,
Vertical scale: 2 kV/div.

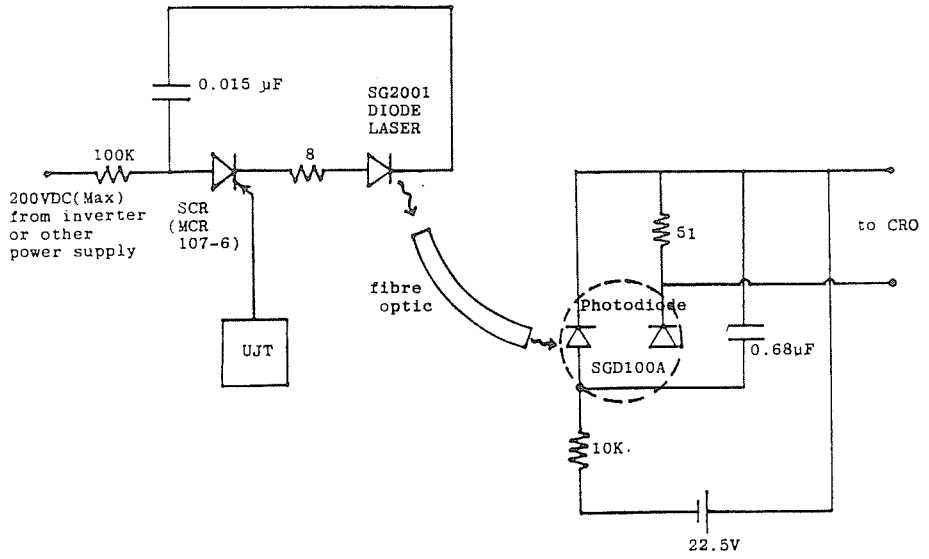

Fig. 6: Universal pulser circuit for pumping diode injection laser. Also shown is the photodiode detection circuit with fibre optic link.

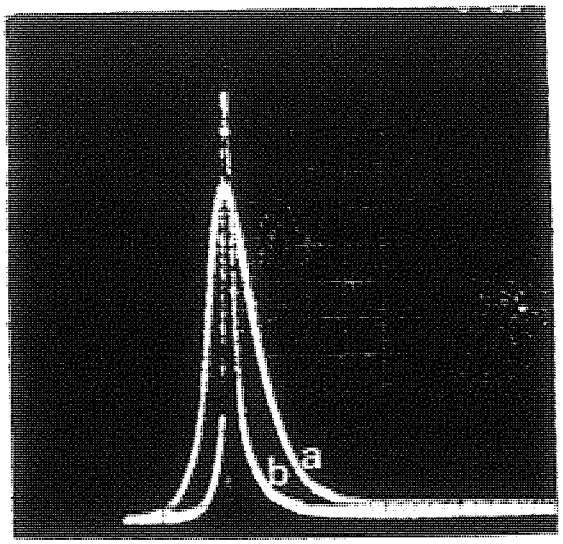

Fig. 7: Diode laser SG2001 operated at threshold current.
Trace a: current pulse (1A/div.).
Trace b: laser pulse measured with photodiode (20mV/div.).
Horizontal scale: ½ μs/div.

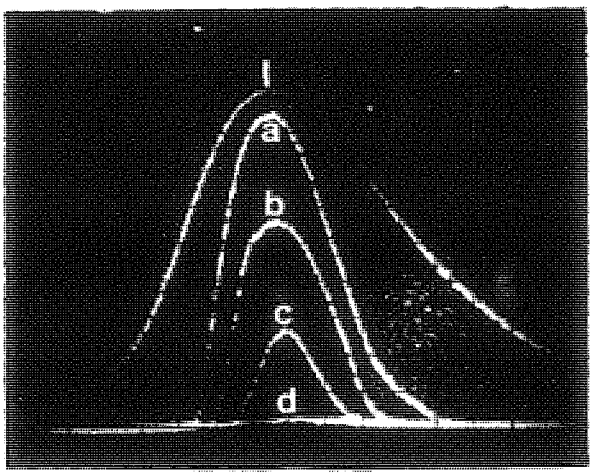

Fig. 8: Diode laser SG2001 operated at various peak currents.
Trace I. current pulse with peak current of 4.6 A.
Trace a to d. Photodiode output of laser pulses at various peak currents.
(a: 5.5A; b: 4.9A; c: 4.6A; d: 4.4A – not lasing).
Horizontal scale: 100 ns/div.

Notes: 1. All traces taken with fixed time reference;
2. Current trace I and laser pulse c (4.6A) are the corresponding traces which may be compared to find the threshold current for lasing.

J. Fiz. Mal. 5, *53*, (1984)
Research Note

ENERGY BALANCE THEORY APPLIED TO RADIATION-DRIVEN COMPRESSIONS

S. LEE, FIPM
Plasma Research Laboratory
University of Malaya, Kuala Lumpur 22-11

Abstract

An energy and pressure balance technique which has been applied to fast magnetic compressions is now applied to fast radiation-driven compressions such as are encountered in inertial fusion experiments. The results indicate, assuming a perfect transfer of radiation energy and no loss processes, that a density compression ratio of 6.2 may be expected for a constant power pulse whilst with simple pulse tailoring this ratio may be increased to 19; still two orders of magnitude below the 1000 times normal density required for laboratory inertial fusion breakeven. Further, whilst the compressed plasma temperature may be increased by increasing the radiation power, the compression ratio is independent of absolute radiation power. This indicates the necessity for tailored double or multiple compressions.

Introduction

It has been shown, by applying energy and pressure balance to a fast magnetic compression, that the plasma pinch radius ratio does not depend on the absolute magnitude of the compressing magnetic power, but only on the time variation of the current pulse producing the compressive magnetic field[1-5]. Thus, in practical cases, the large density compression ratios required to satisfy the concept of a fast pinch reactor cannot be achieved in a single magnetic compression, and to overcome this, a current-stepping technique[6] which essentially produces a carefully tailored double compression has been suggested.

Recently, shrouded in a background of security classification, it has been hinted in the literature[7] that results based on inertial confinement experiments and computer code calculations indicate that single radiation-driven compressions are also insufficient to produce the large density ratios required in order to achieve nuclear fusion energy break-even in realistic-sized laboratory fusion-fuel pellets. It is now known that for a solid target pellet of the size used in a hydrogen bomb, approximately 10 cm in diameter, radiation-driven compression of the solid target pellet to slightly above normal solid density is sufficient to produce vast quantities of fusion energy. However, even a simplified consideration of the density containment factor $n\tau$ will readily demonstrate that for a controlled fusion solid target of say 1 mm in diameter a density compression of 1000-fold above solid density is required to satisfy the Lawson $n\tau$ criterion.

In this note we will show from simple physical principles that such magnitudes of compression cannot be achieved in a single compression using radiation pressure.

Theory

Consider a solid spherical pellet irradiated uniformly by intense radiation as illustrated in Fig. 1. The radiation power $R(Js^{-1})$ has associated with it radiation intensity $I = R/4\pi r^2$ $(Js^{-1}m^{-2})$ and radiation pressure $P_R = I/c = 3.3 \times 10^{-9} R/4\pi r^2$ (Nm^{-2}) where c is the speed of light.

Assume that the radiation pressure is sufficient to rapidly (but non-relativistically) compress the target of initial radius r_o and density ρ_o to a final quasi-equilibrium plasma of radius r_m *with density* ρ_m. We compute the quasi-equilibrium plasma temperature T_m in two independent ways by equating the plasma enthalpy to the work done by the radiation pressure and by equating the plasma pressure to the radiation pressure at quasi-equilibrium.

The work done (per unit mass) by the radiation pressure on the target (assuming perfect coupling) is

$$W = \frac{1}{\frac{4}{3}\pi\rho_m r_m^3}\int_{r_m}^{r_o} F\cdot dr = \frac{1}{\frac{4}{3}\pi\rho_m r_m^3}\int_{r_m}^{r_o}\frac{3.3\times10^{-9}R}{4\pi r^2}(4\pi r^2)dr \quad \ldots.(1)$$

The plasma enthalpy per unit mass at quasi-equilibrium radius r_m is

$$h = \frac{R_0}{M} D\, T_m \frac{\gamma}{\gamma-1} \quad \ldots.(2)$$

where R_0 is the universal gas constant, M the molecular weight, D the departure coefficient and γ the specific heat ratio of the plasma at quasi-equilibrium.

Assume that all the work done by the radiation pressure is converted into the plasma enthalpy; then $W = h$ and we have:

Energy balance:

$$T_m = \frac{3.3\times10^{-9}}{\frac{4}{3}\pi\rho_m r_m^3}\frac{\gamma-1}{\gamma}\frac{1}{\frac{R_o}{M}D}\int_{r_m}^{r_\rho} R dr \quad \ldots.(3)$$

Equating the radiation pressure P_{R_m} to the plasma kinetic pressure $P_m = \frac{R_o}{M} D\,\rho_m T_m$ gives:

Pressure balance:
$$T_m = \frac{3.3\times10^{-9}R_m}{4\pi r_m^2\rho_m\frac{R_o}{M}D} \quad \ldots.(4)$$

where R_m is the radiation power at the time the radius of r_m is first reached.

Then, equations (3) and (4) give

$$R_m = \frac{3(\gamma-1)}{\gamma r_m}\int_{r_m}^{r_o} R\, dr \quad \ldots.(5)$$

Consider two cases:

Case I R = constant; constant or square pulse radiation power. Then equation (5) gives a radius ratio of

$$k_m = \frac{r_m}{r_o} = \frac{3(\gamma-1)}{4\gamma-3}$$

with $k_m = \frac{6}{11}$ for $\gamma = 5/3$.

For this case, the density compression ratio $\frac{\rho_m}{\rho_0} = \left(\frac{r_o}{r_m}\right)^3 = 6.2$

Case II $R = R_m\left(\frac{r-r_o}{r_m-r_o}\right)$; radiation power tailored to be linearly rising with decreasing r.

Then, equation (5) gives $k_m = \frac{6}{16}$ for $\gamma = 5/3$ and $\frac{\rho_m}{\rho_o} = 19$.

Conclusion

We have used a model in which intense incident radiation pressure uniformly compresses a spherical target pellet to a final high pressure high temperature plasma state. Perfect energy coupling is assumed with no loss processes. The results indicate that the density compression ratio is independent of the absolute radiation power (as long as it is sufficiently large) but that by tailoring the pulse shape the density compression ratio could be increased. A density compression ratio of 6.2 is predicted for a square pulse of radiation and this may be increased to 19 for a radiation pulse of linearly increasing power (with decreasing r). These values are two orders of magnitude below density compression requirement for pellets of mm-sizes suitable for inertial fusion experiments.

Finally, we note that although equation (5) indicates that the density compression ratio is independent of absolute radiation power, equation (4) indicates that the quasi-equilibrium temperature is dependent on the absolute radiation power. Thus, the problem of attaining the ideal ignition temperature is more a problem of brute power whilst the problem of attaining sufficient density compression ratio requires, in addition to brute power, a more subtle approach of tailored double or multiple compressions.

References

1. S. Lee, Bul. Fiz. Mal. 2, 240 (1981).
2. S. Lee, J. Appl. Phys. 54, 3603 (1983).
3. S. Lee, Plasma Phys. 25, 571 (1983).
4. S. Lee, J. Phys. D: Appl. Phys. 16, 2463 (1983).
5. S. Lee, Australian J. Phys. 36, 891 (1983).
6. S. Lee, J. Phys. D: Appl. Phys. 17, in press (1984).
7. S. Bardwell, Fusion Asia 1, 51 (1983).

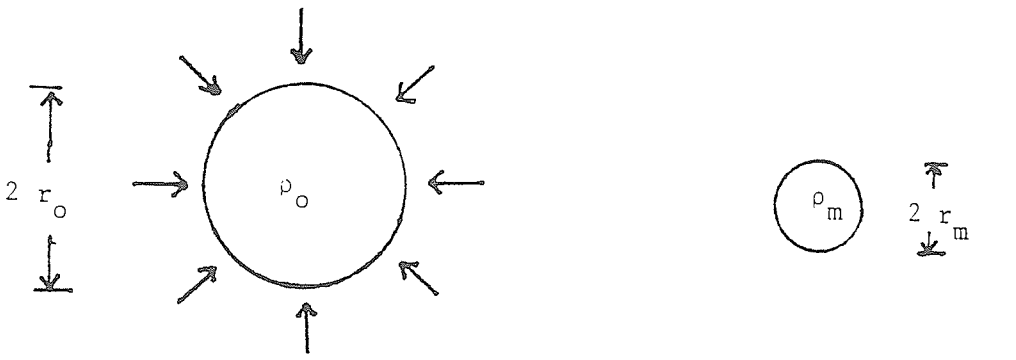

Fig. 1 Radiation-driven compression of a spherical target to a quasi-equilibrium geometry, before target disassembly.

Vacuum spark as a reproducible x-ray source

C. S. Wong and S. Lee

Plasma Research Laboratory, Physics Department, University of Malaya, Kuala Lumpur 22-11, Malaysia

(Received 4 October 1983; accepted for publication 14 March 1984)

The operational characteristics of a laser-initiated vacuum spark is studied with reference to its x-ray emission. The present system employs a fast capacitor bank (current rise time = 1 μs) with input energy of 4.4 kJ. The studies here show that for such a system, the system parameters can be adjusted for satisfactory optimum operation with respect to x-ray emission reproducibility. It is observed that intense x-ray point sources are obtained consistently by choosing the right V–d combination, where V is the discharge voltage in kilovolts and d is the electrode separation in millimeters. For the present system, this combination is found to be 20–5 and a x-ray reproducibility of better than 80% has been achieved in this system.

INTRODUCTION

The minute plasma spot produced during a vacuum spark discharge has been found to emit intense x ray which originates from highly stripped ions. The condition of the plasma has been well studied and is found to be typically as follows[1]:

$T_e \simeq 4$–10 keV;

$n_e \simeq 10^{21}$–10^{22} cm^{-3};

linear dimensions of the spot $\simeq 100$ μm or less; and x-ray emission power $\simeq$ several megawatts.

Like the laser-produced plasma, the vacuum spark is being used extensively as a pulsed x-ray point source for spectroscopic studies of ion species such as Fe-XXVI, Ni-XXVII, and Mo-XVII.[2–8] Due to the extreme conditions attainable in the plasma spot, these studies are mostly associated with the material testing of fusion reactor design.[9] Unfortunately, such application of the vacuum spark is limited by the erratic nature of its x-ray production. Despite the numerous publications on spectroscopic studies using the vacuum spark as the x-ray source, little work has been done on the systematic study of the performance characteristics of the device with reference to its x-ray production. In order to enable effective utilization of the vacuum spark as a pulsed x-ray source, however, it is necessary to optimize the performance of the device in terms of reproducibility of both the frequency of formation as well as the position of the plasma spot.

The performance of the vacuum spark is dependent on system parameters such as the discharge voltage,[10] the electrode separation and, for the present system, the laser beam irradiance and its alignment. The effects of these parameters on the x-ray reproducibility of a laser-initiated vacuum spark have been investigated and discussed in this paper. Based on the results obtained, we have been able to construct a system which produces the plasma spot consistently.

I. EXPERIMENTAL ARRANGEMENT

The configuration of the vacuum spark system used in this work is shown schematically in Fig. 1. Both the anode and the cathode are made of stainless steel and are detachable from their respective mounting so that the interelectrode separation can be varied. The electrodes are enclosed in an aluminum vacuum chamber. The base pressure of the chamber is kept below 10^{-5} Torr, which is found to be sufficient to maintain a voltage of 35 kV across an interelectrode gap of 5 mm. Although it had been reported that reproducibility had been improved with good base pressure, no noticeable effect has been observed for pressure ranging from 10^{-6} to 10^{-5} Torr in the present system. The capacitor bank[11] used to power the discharge consists of 12 Maxwell capacitors each rated at 1.85 μF, 60 kV. They are connected in parallel to two insulated circular aluminum plates via 12 parallel-plate low-inductance transmission lines; and the aluminum chamber together with the electrodes of the vacuum spark device are mounted onto the circular plates. Due to limitation in the back wall insulation, the present system can be charged to a maximum voltage of 35 kV without predischarge breakdown. The maximum energy that can be delivered by the capacitor bank to the system is thus 13.5 kJ. At a discharge voltage of 20 kV (input energy of 4.4 kJ), the current rises to its first maximum of about 600 kA in a time of approximately 1 μs. The system has an inductance of the

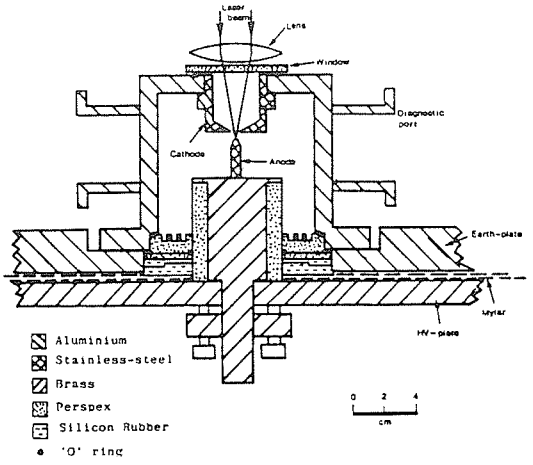

FIG. 1. The vacuum spark device shown to be mounted on top of two circular aluminum plates insulated by Mylar sheets.

 0034-6748/84/071125-04$01.30

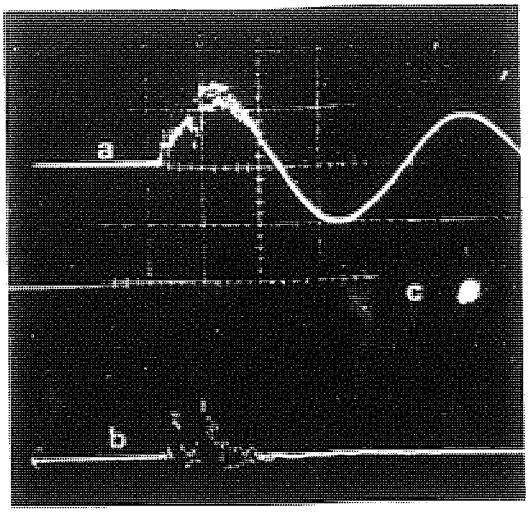

FIG. 2. Data obtained for a typcial vacuum spark discharge. (a) The discharge current waveform. (b) The corresponding x-ray pulses recorded by a PIN diode. (c) The x-ray pinhole image of the plasma spot obtained.

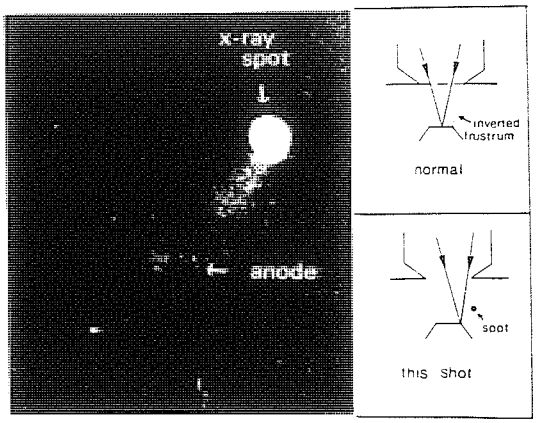

FIG. 3. The x-ray pinhole image obtained from a vacuum spark discharge where the laser beam is arranged to focus at the rim of the flattened anode tip. Also shown are the illustrations of how the laser beam is focused at the rim of the anode tip as compared to that of a "normal" arrangement where the laser is focused at the center of the anode tip.

order of 20 nH. The laser used to initiate the discharge is a 60-MW pulsed ruby laser with a nominal pulse width (FWHM) of 25 ns.

In order to monitor the performance of the vacuum spark system, the current waveform is measured by using a Rogowski coil operated as a current transformer. The x ray produced during the discharge is measured by a PIN diode (time resolved) and a pinhole camera (time integrated) simultaneously. A typical set of data obtained is shown in Fig. 2. The sharp dip in the discharge current is a common feature observed for discharges during which intense x-ray spots are obtained. The current dip is also found to correspond in time to the x-ray pulse. The regular round structure of the spot observed on the pinhole picture indicates that the size of the plasma spot is smaller than that of the pinhole (diameter = 300 μm).

II. EXPERIMENTAL RESULTS

In this work, two types of anode have been used: one with a sharp pointed tip while the other has a flattened end of 3 mm diameter. However, this difference in the anode design has been found to have no significant effect on the probability of obtaining the x-ray spot. The effects of the other system parameters on the performance of the present vacuum spark system are presented below.

A. Effect of the laser beam alignment

The lateral position of the plasma spot formation has been observed to be affected by the alignment of the laser beam to hit at the anode tip. In normal operation of the vacuum spark, the laser beam is carefully aligned to focus at the center of the flattened anode tip. In this case the plasma spots are observed to form around the axis of the electrode system and within the inverted frustrum between the 3-mm-diam anode tip and the 5-mm-diam opening of the cathode (Fig. 3). In a series of discharges, the laser beam has been intentionally aligned to hit at the rim of the anode tip. For such an arrangement, instead of being formed within the inverted frustrum, the spot is now observed outside the inverted frustrum in the direction of the position at which the focused laser beam hits the anode, as illustrated in Fig. 3. This implies that the position of the spot formation can be roughly controlled by the alignment of the laser beam.

B. Effect of the laser power

The ruby laser used to initiate the vacuum spark discharge in this work has an output power of 60 MW. The laser beam is focused down to a circular spot of diameter 740 $\pm$ 10 μm at the anode tip, corresponding to an irradiance of the order of 10^{10} W/cm^2. The fluctuation of the laser power has been observed to be less than 10% over the duration of the experiment conducted in this work. The fluctuation of the laser irradiance is believed to affect the time of occurrence of the spot formation.[12] Experimentally, the x-ray spot is observed to form within the time between 400 to 800 ns after the start of the discharge. However, the condition of the x-ray spot obtained is found to be independent on its time of occurrence.

C. Effect of the electrode separation

The chances of observing the intense x-ray spot during a vacuum spark discharge has been found to depend greatly on its electrode separation d. In a series of discharges, the separation between the electrodes has been varied over the range of 5 to 22 mm and at each separation, the discharge voltage V is varied over the range of 5 to 20 kV. For each discharge, the discharge current waveform, the time-resolved x-ray pulses as well as the x-ray pinhole image are obtained simulta-

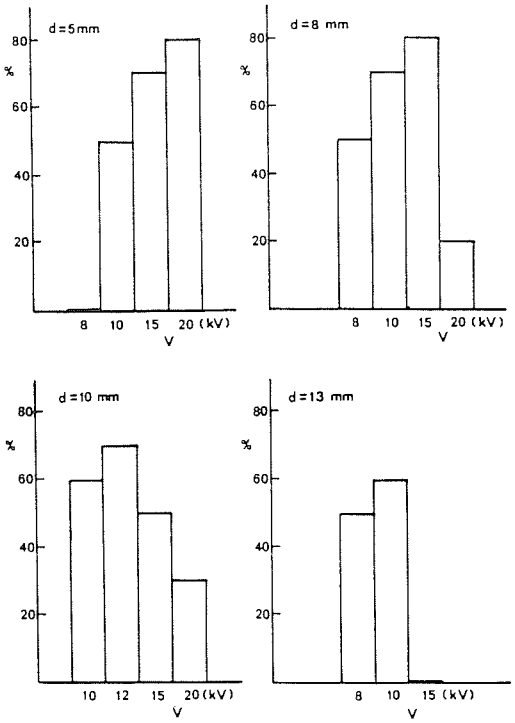

FIG. 4. Histograms of the probabilities of observing the x-ray spot at various discharge voltages at various electrode separations of the vacuum spark system. Vertical axis: percent of discharges in which x-ray spots are observed. Horizontal axis: discharge voltage V.

neously. This experiment was carried out over several days, with the electrode separation fixed at a particular value at each day. The results on the probability of observing the x-ray spot for various discharge voltages are presented in Fig. 4. It is evident that for each electrode separation, there is an optimum discharge voltage at which the x-ray spot is produced. Table I displays the probable optimum voltages for various electrode separations. Generally, it can be seen that the system seems to have higher optimum discharge voltage at narrower interelectrode gap. For example, at electrode separation of 10 mm, the optimum voltage is 15 kV while at 5 mm, it becomes 20 kV. It is, however, not possible to reduce the gap too much because of the limitation of predischarge breakdown.

On the other hand, electrode separations of larger than 20 mm have been found to be unsuitable for this setup. For

TABLE I. Optimum vacuum spark discharge voltages at various electrode separations.

Electrode separation d (mm)	Optimum discharge voltages V(kV)
5	20
8	15
10	12
13	10
22	None

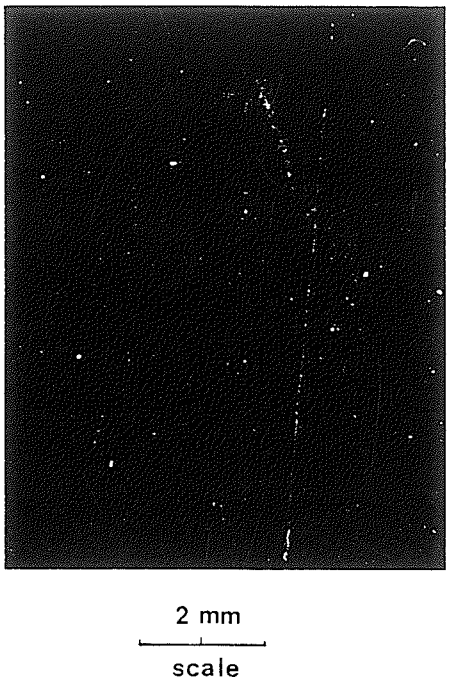

FIG. 5. The x-ray pinhole image of a vacuum spark discharge at electrode separation of 22 mm and discharge voltage of 20 kV. At these nonoptimized conditions, no plasma spot is formed. (Note: the line that appears across the anode tip is caused by an imperfection of the camera.)

example, no optimum voltage is obtained for an electrode separation of 22 mm. This may be due to the fact that the expected optimum voltage is so low that the energy input to the plasma system is not sufficient to enable the formation of the plasma spot. If the system is discharged with an electrode separation of 22 mm at a voltage of 20 kV, x ray is observed to be emitted only from the surface of the anode stem as shown in Fig. 5. This x ray may be produced by the bombardment of the anode stem by energetic electrons; and this is observed to occur near the start of the discharge.

After the above investigation, the electrode separation of the present system has been fixed at 5 mm and a series of about 100 discharges at discharge voltages of 20 kV have been performed. In this series of discharges, more than 80% of the discharges have been observed to be able to produce the bright x-ray spot. This x-ray spot reproducibility has been observed consistently during a subsequent series of experiments in which the electron temperature and density of the vacuum spark plasma are measured by the x-ray foil absorption technique.[13]

III. DISCUSSION

From the systematic investigation of the operational characteristics of a laser-initiated vacuum spark system, it has been shown that (1) the lateral position of the x-ray spot formation during a vacuum spark discharge can be controlled to be within the inverted frustrum between the electrodes (for flat-end anode) by ensuring proper alignment of

the laser beam focusing; and (2) optimum operation of the vacuum spark can be obtained by choosing the proper V–d combination. For the present system, optimum operation with more than 80% of the discharges producing the intense x-ray spot is obtained with a V–d combination of 20 kV–5 mm.

ACKNOWLEDGMENTS

The capacitor bank and the pulsed ruby laser used in this project are presented to the Physics Department, University of Malaya by the Alexander von Humboldt Foundation and Kernforschungsanlage Jülich of the Republic of West Germany. This work is supported by an F grant of the University of Malaya (F95/77).

[1]C. R. Negus and N. J. Peacock, J. Phys. D 12, 91 (1979).
[2]T. N. Lie and R. C. Elton, Phys. Rev. A 3, 865 (1971).
[3]B. S. Fraenkel and J. L. Schwob, Phys. Lett. 40, 83 (1972).
[4]W. A. Cillier, R. U. Datla, and Hans R. Griem, Phys. Rev. A 12, 1408 (1975).
[5]R. Beier and H. J. Kunze, Z. Phys. A 285, 347 (1978).
[6]Th. A. M. van Kleef and Y. N. Joshi, J. Opt. Soc. Am. 70, 895 (1980).
[7]J. Reader and A. Ryabtser, J. Opt. Soc. Am. 71, 231 (1981).
[8]S. Takagi, S. Ohtani, K. Kadota, and J. Fujita, Institute of Plasma Physics, Nagoya University, Research Report No. IPPJ-564, 1982.
[9]M. Klapisch, P. Mandelbaum, J. L. Schwob, A. Bar-Shalom, and N. Schweitzer, Phys. Lett. A 84, 177 (1981).
[10]S. Lee and H. Conrads, Phys. Lett. A 57, 233 (1976).
[11]P. Cloth and H. Conrads, Nucl. Sci. Eng. 62, 591 (1977).
[12]C. S. Wong, Ph.D. thesis, University of Malaya, 1983.
[13]C. S. Wong and S. Lee, Report No. IAEA-SMR-82, 1982, p. 337.

Sing. J. Phys., Vol. 1, No. 1, 1984, 75-84

VOLTAGE AND CURRENT COMPUTATION OF AN INDUCTIVE PLASMA FOCUS MODEL

S. LEE, C.S. WONG, A.C. CHEW, T.Y. TOU AND JALIL BIN ALI
Plasma Research Laboratory, Physics Department, University of Malaya Kuala Lumpur 22-11, Malaysia

Abstract

The slug model is applied to the radial pinch phase of the plasma focus with coupled circuit equation. This enables computations of the current and voltage waveforms to be made. Further, the computation is extended to the radial static phase and the blow-up phase by empirical model so as to produce complete current and voltage waveforms which are then compared to experimental measurements. There is generally good agreement between the computed and measured waveforms. However, there are several features on the measured current waveform which is not accounted for by the computed waveform. These features are suggestive of the occurence of resistive phenomena in the plasma for which our inductive model is not valid. On the other hand, comparison of the voltage waveforms indicates an inadequacy in the frequency response of the voltage probe employed.

Introduction

Although the plasma focus is now a well-established experimental device producing such intense plasma conditions that copious quantities of x-ray and fusion neutrons are emitted there are still considerable difficulties in the theoretical approach. We may divide the plasma dynamics in the focus device into the following phases (see Fig. 1 and 2): An axial acceleration phase lasting typically 2 μs; a radial pinch phase of typical duration 80 ns; a radial static column phase lasting typically 20 ns leading finally to a blow-up phase which results, in an exceedingly short period of time, in a large column plasma. It is well-documented that most of the fusion neutrons are produced during this large-column phase. This is also the phase for which there is no theoretical description. However, it is also known from experiment that in order to have a good reproducible neutron yield the dynamics of the pre-blow up phases have to be suitably controlled through various parameters.

Theoretically a complex 2-D code had been devised by Potter[1] for the pre-blow up phases. However only the axial phase of this code could be check against the simple 1-D snow-plow model. For the radial pinch phase until recently even the radius of the quasi-static column is still estimated[2] by methods which are completely inconsistent with energy balance[3,4].

In 1978 Potter[5] had devised a simple slug model which he used to gain a better understanding into the physics of the pinch with constant length and constant current. This model is very nearly energy-consistent and gives the essential features of the pinch as observed experimentally including the correct radius ratio at quasi-equilibrium. Lee[6] had

extended this model to a pinch of varying current and varying length and had observed that the single feature necessary to explain the greatly reduced radius ratio of the focus relative to the pinch is its length increase with time.

In this paper the slug model which is a non-resistive model based on clear physical principles is applied to the radial pinch phase of the focus. This, when coupled with a governing circuit equation, enables computations of the current and voltage to be made. Further, the solution of the circuit equation is extended to the radial static phase and the blowup phase empirically so as to produce complete current and voltage waveforms. These are compared with experimental measurements. The current and voltage waveforms are essential for a full understanding of the plasma focus discharge dynamics. However, due to limitation of the probe response, the measurement of the voltage waveform do not give satisfactory result. The voltage computation described in this paper gives a theoretical prediction of the true voltage waveform to be expected.

Theory

(a) The axial acceleration phase

In the axial phase, the normalised snow-plow equations may be written as:

Motion:
$$\frac{d^2\xi}{d\tau^2} = \frac{\alpha^2 \imath^2 - (\frac{d\xi}{d\tau})^2}{\xi} \tag{1}$$

Circuit:
$$\frac{d\imath}{d\tau} = \frac{1 - \int \imath d\tau - \beta \imath (\frac{d\xi}{d\tau})}{1 + \beta\xi} \tag{2}$$

where $\alpha = t_c/t_a$, $\xi = z/z_o$, $\tau = t/t_c$, $\imath = I/I_o$,

$$t_c = \sqrt{(L_o C_o)}$$

$$I_o = V_o \sqrt{(C_o/L_o)}$$

$$t_a = \{\frac{4\pi^2 (b^2 - a^2) \rho_o z_o^2}{\mu \ell n(b/a) I_o^2}\}^{\frac{1}{2}}$$

and
$$\beta = \frac{\frac{\mu}{2\pi} \ell n(b/a) z_o}{L_o}$$

t_c is the characteristic capacitor discharge time while t_a is the characteristic axial run-down time.

(b) The radial pinch phase

In this phase the shock front is distinguished from the magnetic piston through the shock theory. On the other hand the two positions,

namely r_s and r_p are related through an adiabatic expansion written in Lagrangian coordinates. The length of the focus is allowed to grow at the same rate as the radial collapse of the shock front because the two motions are driven by the same slug pressure. The circuit equation is also coupled to the plasma motion. The governing normalised equations for the system then become:

Radial shock motion:
$$\frac{d\kappa_s}{d\tau} = \frac{-\alpha\alpha_1 \imath}{\kappa_p} \tag{3}$$

Axial shock motion:
$$\frac{d\xi_f}{d\tau} = \frac{d\kappa_s}{d\tau} \tag{4}$$

Circuit:
$$\frac{d\imath}{d\tau} = \frac{1 - \int \imath d\tau + \frac{\beta_1}{F}\imath\{\ell n(\frac{\kappa_p}{c})\frac{d\xi_f}{d\tau} + \frac{\xi_f}{\kappa_p} + \frac{\xi_f}{\kappa_p}\frac{d\kappa_p}{d\tau}\}}{1 + \beta - \frac{\beta_1}{F}\ell n(\frac{\kappa_p}{c})\xi_f} \tag{5}$$

Voltage:
$$\upsilon = \{\beta - \frac{\beta_1}{F}\ell n(\frac{\kappa_p}{c})\xi_f\}\frac{d\imath}{d\tau} - \frac{\beta_1}{F}\ell n(\frac{\kappa_p}{c})\imath\frac{d\xi_f}{d\tau} - \frac{\beta_1}{F}\imath\frac{\xi_f}{\kappa_p}\frac{d\kappa_p}{d\tau} \tag{6}$$

where $\kappa_p = r_p/a$, $\kappa_s = r_s/a$, $\xi_f = z_f/a$, $c = b/a$, $F = z_o/a$, $\beta_1 = \beta/\ell nc$

and $\alpha_1 = F\{(\gamma + 1)(c^2 - 1)\}^{\frac{1}{2}}/(2\ell nc)$

The radial compression phase starts when the axial phase reaches $\xi = 1$.

(c) The radial static phase

In this phase the following empirical model is used:

$$\frac{d\kappa_s}{d\tau} = 0 \tag{7}$$

$$\frac{d\kappa_p}{d\tau} = 0 \tag{8}$$

$$\frac{d\xi_p}{d\tau} = 0 \tag{9}$$

so that the Eqs. (5) and (6) become:

Circuit:
$$\frac{d\imath}{d\tau} = \frac{1 - \int \imath d\tau}{1 + \beta - \frac{\beta_1}{F}\ell n(\frac{\kappa_p}{c})\xi_f} \tag{10}$$

Voltage:
$$\upsilon = \{\beta - \frac{1}{F}\ell n(\frac{\kappa_p}{c})\xi_f\}\frac{d\imath}{d\tau} \tag{11}$$

For this static phase, the values of κ_p and ξ_f are fixed at the last computed values of the radial pinch phase.

(d) The blow-up phase

In this phase ξ_f is fixed at the same values as in the static phase, but κ_p is taken as equal to 1, i.e. the original radius. Thus the same set of Eqs. (7) - (11) is used for this phase. The difference being that the column is assumed to have blown up to the original radius.

Results

We consider a plasma focus device UMDPFI[7] with the following parameters: $a = 1.54$, $b = 1.0$, $\gamma = 5/3$, $C = 3.4$, $F = 8.0$ and $M = 0.3$. A set of the results for this focus computed from the model described above is shown in Fig. 3. Fig. 3(a) shows the overall features of the current i and voltage v waveforms computed for the various phases of the plasma focus discharge. The current is seen to rise almost linearly at first after the start of the discharge and then it levels off eventually to become flattened after the time of $\tau = 1.1$. This flattening of the current signifies the effect of the axial phase of the focus dynamics on the current. At the end of the axial phase at about $\tau = 1.6$, the current sheet has reached the end of the anode and it begins to collapse radially, resulting in a sharp drop in the current. For the voltage waveform, the voltage rises initially and reaches a maximum at $\tau = 1.05$, after which it drops from a value of about 0.5 at the maximum to 0.4 just before the radial pinch takes place. At the time of the radial pinch phase, there is a sudden increase in the plasma inductance caused by both a rapid decrease in the radius and an elongation of the plasma column which is confined by the azimuthal magnetic field of the current sheet. Thus the voltage rises sharply to give a voltage spike at a time corresponding to the current dip. The rise-time of the sharpest part of the voltage spike is less than 5 ns. Following the radial pinch phase, the plasma column is assumed to be at static equilibrium for a short time and then it blows up. These postulates are in accordance with experimental observation. For these two phases, the current stays approximately constant at the value of the dip and the voltage drops sharply to low values.

The dynamics of the three radial phases - the pinch phase, the static phase and the blow-up phase can be seen clearly from the plots of κ_p, κ_s, i and v at an expanded time-scale as shown in Fig. 3(b). A departure of the shock front from the magnetic piston is clearly observed and it gives rise to a thickening of the shock-heated plasma slug between them. The computed piston speed is slowed down towards the end of the pinch phase, which is expected physically. The minimum radial position of the magnetic piston is reached when the shock front hits the axis as required by the model. At this instant, the current has dropped to its minimum while the voltage is at its maximum.

In the following radial static phase, the focussed plasma column is formed and is being sustained momentarily for about 15 ns by the azimuthal magnetic field before the blow-up phase occurs. The current stays approximately constant while the voltage drops sharply to nearly zero. The energy input to the plasma during the radial pinch and static

phases is found from the computation here to amount to about 9% of the total electrical input energy.

Comparison With Experiment

The results obtained from the computation described above are compared to experimental results as shown in Fig. 4. The main features on the current and voltage waveforms, namely the current dip and the voltage spike are observed on both experimental and computed results. However, there are several discrepancies which are to be described as follows:

(a) Current waveforms

We divide the current waveforms into that portion which corresponds to the axial run-down phase during which the current rises and then flattens out before the second portion which is a current dip corresponding to the radial pinch and subsequent phases. We note that throughout the earlier part of the axial run-down phase, the experimentally measured current has a lower value than the computed value. This agrees with the experimental observation[8] that in this portion of the run-down phase, due to mass leakage, the current sheet has a higher speed than predicted by the snow-plow model. The net effect of this higher speed is to reduce the value of the current below that computed from a snow-plow model. This effect of mass leakage is however soon compensated by a current-shedding effect[9] so that the final speed reached in the axial phase is found experimentally to be the same as the computed final speed. The average speeds also agree as indicated by the agreement between in times of the start of the radial pinch phase.

A comparison between the experimental and computed current dips shows a very important difference in features. The experimental curve shows a dip with increasing gradient (negative) followed by a current rebound. The computed curve shows a dip which levels off much more gradually and with no rebound. Based on overall computational and experimental experience we interpret the final (and sharpest) part of the dip and the corresponding rebound in the experimental current waveform as being a feature not present in our computational model. This additional feature in the measured waveform, not present in the inductive model, is hardly surprising since it is known[10] that towards the end of the pinch phase and extending into the radial static phase, the plasma column is anomalously resistive with resistivity greatly enhanced due to the strong magnetic field effect. Thus, referring to Fig. 5, we divide the experimental current waveform into a predominantly inductive phase and a predominantly resistive phase. Comparing the current dip of the predominantly inductive phase we note that this dip experimentally is significantly smaller than the computed inductive model. Again this is to be expected because there is also a current-shedding effect during this phase[2,11] that has not been included into our basic computational model. This current shedding effect would reduce the inductive portion of the dip. In the light of this interpretation it would be possible to extend the basic comparison of Fig. 5 into some quantitative account of the current-shedding effect during the pinch phase and the anomalous resistive effect.

(b) Voltage waveforms

The voltage induced across the focussed plasma computed from our model is found to be at least 10 times higher than that measured experimentally (Fig. 4(b)). This can be caused by two major factors: (i) The computed pinching speed is higher than the experimental speeds. This is an effect of the current-shedding. However, the reduction of pinching speed by a factor typically less than 2 would not explain the reduction factor of 10 in the measured voltage. (ii) The main factor causing the voltage reduction is frequency response. It is certain that the response of the resistive voltage probe is not fast enough to register the sharp rising voltage spike. The response time of the probe has been measured as 15 ns, but the greater part of the computed voltage spike occurs in a time of less than 5 ns.

Conclusion

This study has shown conclusively that our present voltage measurement of the plasma focus is inadequate. It is indeed necessary in the present state-of-the-art of plasma voltage measurements to make independent estimates, even if only a vastly simplified dynamic model is used.

References

1. D.E. Potter, Phys. Fluids, 14, 1911 (1971)

2. Petter G. Eltgroth, Phys. Fluids, 25, 2408 (1982)

3. S. Lee, Plasma Phys., 25, 571 (1983)

4. S. Lee, J. Appl. Phys., 54, 3603 (1983)

5. D.E. Potter, Nucl. Fusion, 18, 813 (1978)

6. S. Lee, Bul. Fiz. Mal., 3, 197 (1982)

7. Nucl. Fusion Special Suppl., "World Survey of Major Activities in Controlled Fusion Research", Table B1e, p. 186 (1982), IAEA, Vienna

8. S.P. Chow, S. Lee, B.C. Tan, J. Plasma Phys. 8, 21 (1972)

9. S. Lee, Y.H. Chen, S.P. Chow, B.C. Tan, H.H. Teh and S.P. Thong, Int. J. Electronics, 33, 85 (1972)

10. S. Lee and Y.H. Chen, Proc. Twelfth Int. Conf. on Phenomena in Ionized Gases, Netherland-I, p. 353 (1975)

11. T. Oppenländer, G. Pross, G. Decker and M. Trunk, Plasma Phys., 19, 1075 (1977)

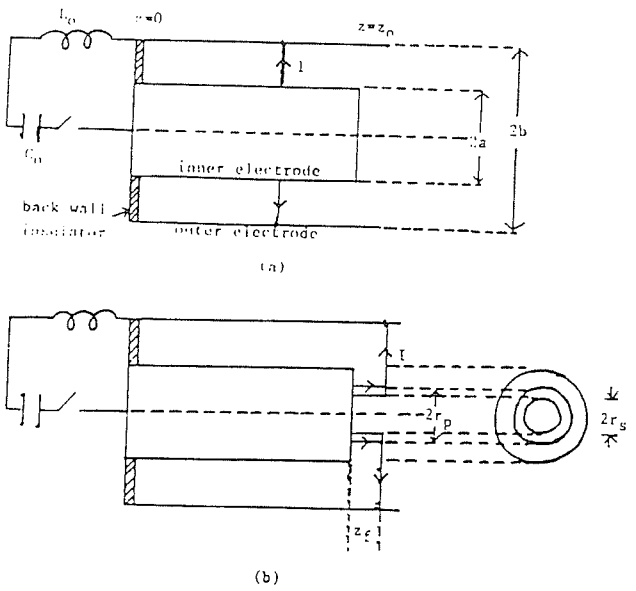

Fig. 1. Schematic diagrams of the plasma focus discharge showing (a) the axial acceleration phase; and (b) the radial pinch phase.

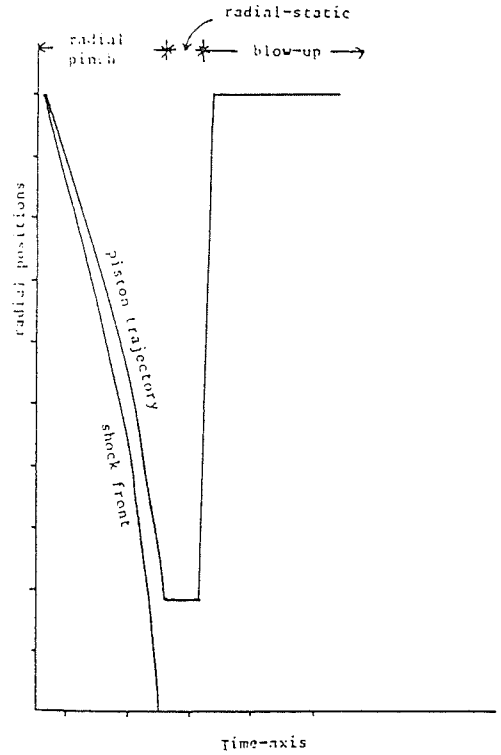

Fig. 2. Postulated radial trajectory of the plasma focus current shealth during the radial pinch phase.

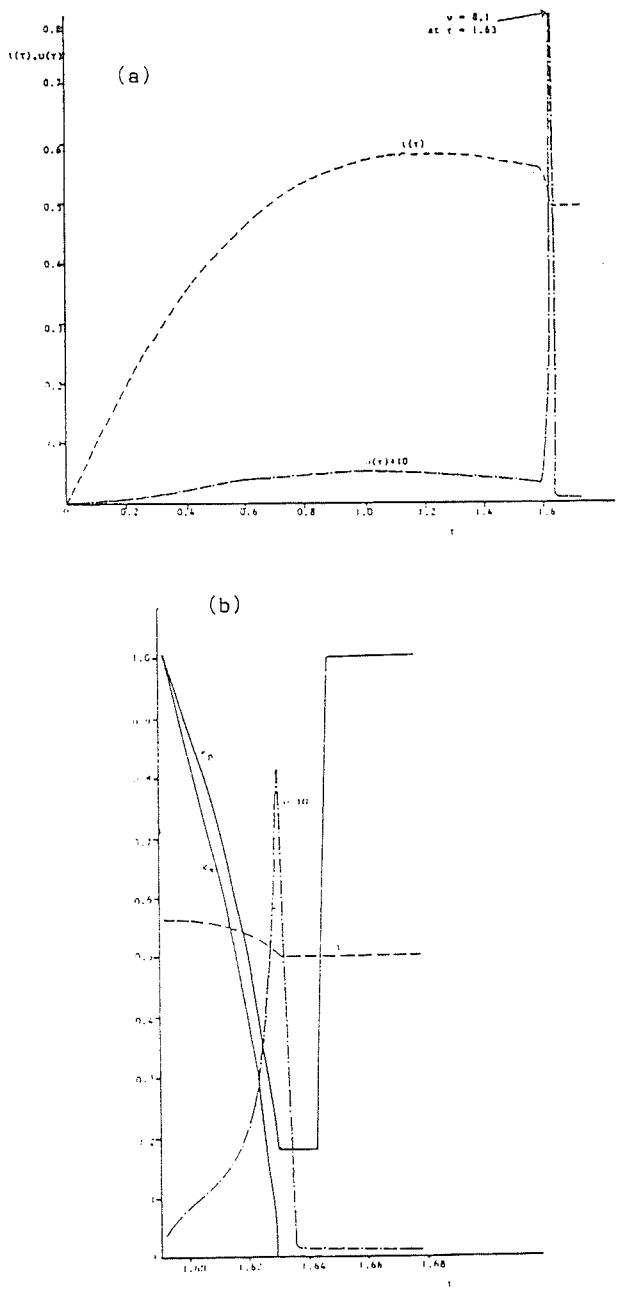

Fig. 3. (a) General features of the computed current $i(\tau)$ and voltage $U(\tau)$ waveforms. (b) Plots of current $i(\tau)$, voltage $U(\tau)$, radial trajectories of the shock front $K_s(\tau)$ and the magnetic piston $K_p(\tau)$ during the radial pinch phase computed from the model.

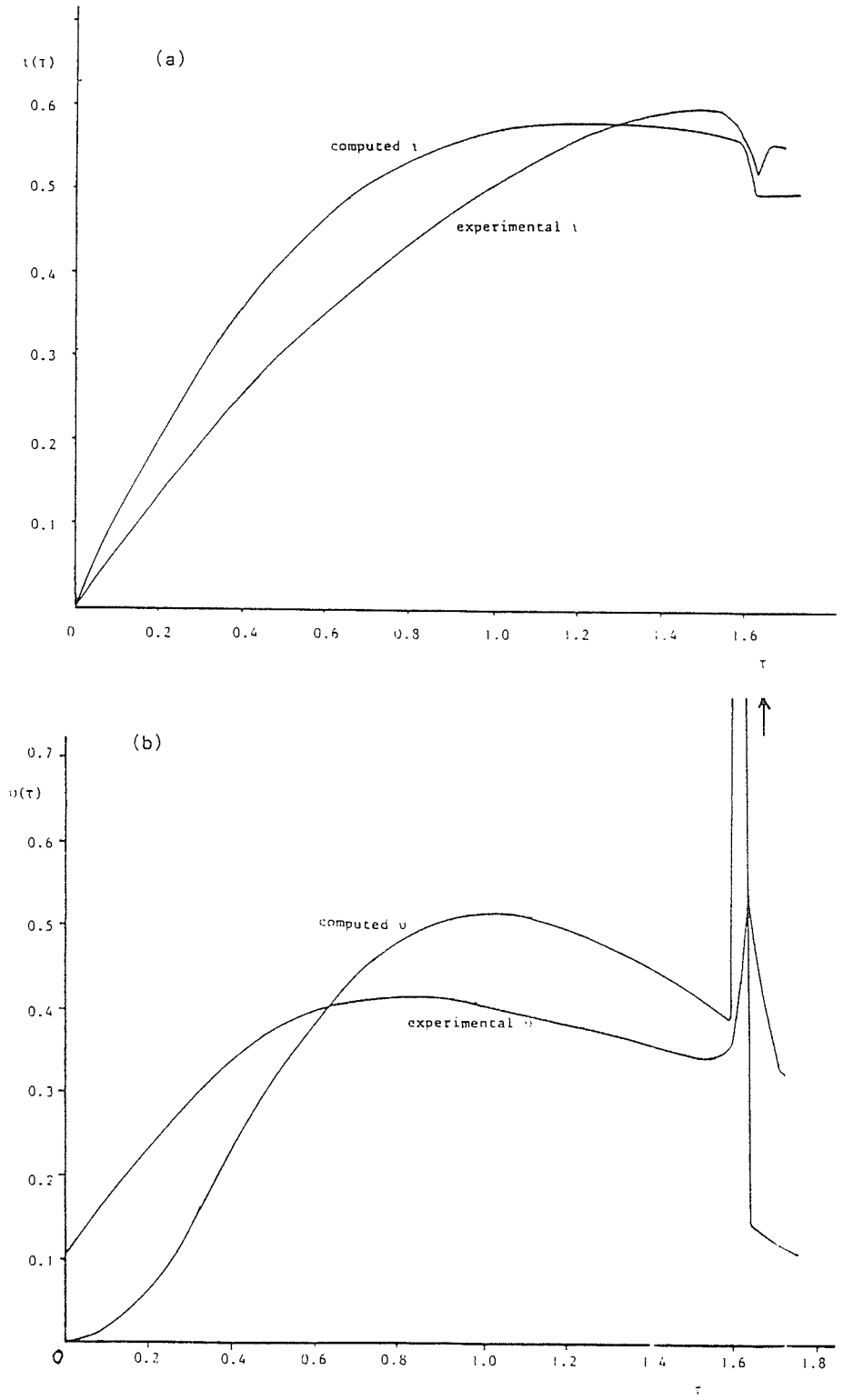

Fig. 4. Comparison of computed results with experiments: (a) current waveforms; (b) voltage waveforms.

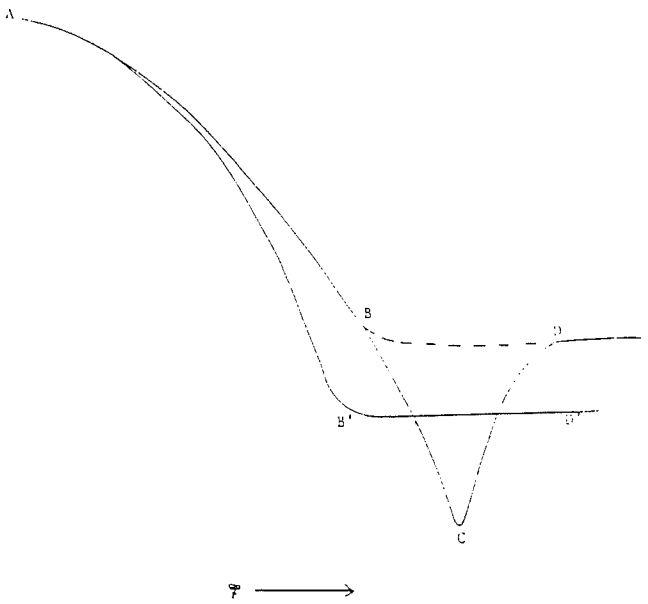

Fig. 5. Comparison of the experimental current dip(ACBD) with the current dip of the inductive model (AB'D') on an expanded scale and re-aligned. The experimental current dip is postulated to consist of an inductive section (ABD) and a resistive section (BCD). Thus we compare ABD and AB'D' and treat BCD as a feature observed experimentally but absent from the inductive model.

Sing. J. Phys., Vol. 1, 1984, 103-110 (Conference Paper)

THE DYNAMIC PINCH PROBLEM
A NEW CONCEPT AND NEW COMPUTATIONS*

S. LEE
Plasma Research Laboratory
University of Malaya
Kuala Lumpur, Malaysia

Abstract

In the theory of electromagnetic pinches one simple fundamental problem has not been clearly resolved, i.e. the determination of the quasi-equilibrium radius r_m of the pinch. In this paper recent work in Kuala Lumpur is reviewed in which a new concept based on energy balance is used to enable the value of r_m to be computed for a wide variety of pinches, including pinches with variable length, variable current and variable specific heat ratio.

Introduction

The pinch effect has been used for more than three decades as a means to generate a hot, dense, cylindrical column of plasma by means of a highly supersonic radially imploding compression. This compression is driven by a large current flowing in the plasma and interacting with its azimuthal self magnetic field as depicted in Fig. 1.

The study of the pinch is usually divided into two regimes: (1) the dynamic or rapid compression phase when the gas in the region bounded by $r = r_o$ is heated, swept up and compressed into a high temperature quasi-equilibrium column and (2) the quasi-static phase following the dynamic phase during which the stability of the column is of primary concern. Reflecting this division the standard treatment of the pinch in the literature is by two separate methods: (1) A snow-plow equation of motion which relates the rate of change of momentum in the snow-plowed sheath to the compressive magnetic force $2\pi r\ell P_B$ where the magnetic pressure $P_B = B^2/2\mu$. This equation gives a well-known trajectory which is fairly representative of the physical situation at large radii. However the snow-plow model compresses the plasma to zero radius which is physically not possible; (2) a treatment of the quasi-equilibrium column by the Bennett method. This treatment is completely divorced from the dynamics of the problem and hence is not able to give the characteristic length of the dynamic compression.

This standard treatment of the two regimes gives an unsatisfactory picture particularly to the experimentalist who would like to know first of all what the radius r_m of the quasi-equilibrium column might be expected to be. With the present revived interest in highly compressed pinches for various applications including the development of soft x-ray sources and fusion reactors[1] it appears all the more important that this fundamental problem of r_m should be resolved in a clear and simple manner.

* This paper was presented at the Asia Pacific Physics Conference held in Singapore on 12-18 June 1983

Several attempts have been made to solve this problem by introducing a kinetic retarding pressure term into the snow-plow equation resulting in a non-zero final radius. But since the snow-plow equation essentially applies to a thin structureless layer it cannot be consistent with the introduction of a kinetic force term which has to be structure- dependent. Results are therefore energy-inconsistent. In 1978 Potter[2] showed through an MHD computation using a 'slug' structure that the radius ratio r_m/r_o where r_o is the starting radius of the pinch, is dependent only on the specific heat radio γ of the pinched plasma for the specific case of a constant current, constant length pinch.

Recently Lee[3,4] has published a simple general method which shows that the radius ratio r_m/r_o is in fact uniquely determined once energy and pressure balance is applied to the compressed pinch column. With the application of this fundamental concept, the radius ratio may be computed for any situation, including plasma pinches with variable length, variable current and variable γ.

Theory

Consider the following general model for the pinch. On initiation the current I flows asisymmetrically in a thin sheath of radius r_o as shown in Fig. 1. The current acts as a magnetic piston, with field B_θ, and implodes inwards collecting all the gas encountered in a thickening sheath. This sheath collapses into a column when the front-running shock wave has imploded onto the axis. The magnetic piston continues moving inwards until the temperature of the column becomes high enough to eventually stop the piston motion. At that point we have a quasi-static column of radius r_m.

The piston exerts a magnetic pressure P_B depending on the magnetic field $B_\theta = \mu I/2\pi r$ at any radius r. The work done by the piston in moving from position r_o to r_m is:

$$W = \frac{1}{\rho_m \pi r_m^2 \ell_m} \int_{r_m}^{r_o} \frac{\mu^2 I^2}{4\pi^2 r^2 (2\mu)} \, 2\pi r \ell \, dr \qquad (1)$$

per unit mass of the final plasma column. Here in general I and pinch length ℓ are function of r (or time t) and ρ_m, r_m, and ℓ_m are the density, radius and length of the quasi-equilibrium pinch.

The enthalpy per unit mass of the quasi-equilibrium plasma may be written as:

$$h = \frac{P}{\rho_m} \frac{\gamma}{\gamma-1} = \frac{R_o}{M} T_m D \frac{\gamma}{\gamma-1} \qquad (2)$$

where $P = (R_o/M) T_m D \rho_m$ is the plasma pressure and T_m, D and Υ are the temperature, the departure coefficient and the specific heat ratio of the pinched plasma respectively; with R_o and M being the universal gas constant and the molecular weight of the ambient gas respectively.

Now in the state of quasi-equilibrium we may write independently the

pressure balance equation $P_B = P$ which on re-arrangement gives us:

$$T_m = \frac{\mu I_m^2}{8\pi^2 \rho_m r_m^2} \frac{M}{R_o D} \tag{4}$$

where I_m is the current flowing at the time r_m is reached. Combining eqs. (3) and (4) we have the expression:

$$I_m^2 = \frac{2(\gamma - 1)}{\gamma \ell_m} \int_{r_m}^{r_o} \frac{I^2 \ell dr}{r} \tag{5}$$

In general the integral in (5) which we call the energy integral may be evaluated only if I and ℓ are known functions of r. Several cases have been discussed and will be reviewed in the following.

Case I: Pinch with I = constant, ℓ = constant.

For this case[3] equation (5) immediately gives us:

$$(r_m/r_o) = \exp\{-\gamma/2(\gamma - 1)\} \tag{6}$$

where we notice that the pinch ratio is a function only of γ. For $\gamma = 5/3$ equation (6) predicts $(r_m/r_o) = 0.29$.

Case 2: Pinch with I = constant, $\ell = \{\ell_m/(r_o - r_m)\}(r_o - r)$

This case applies to the plasma focus which in its pinch phase has an approximately constant current whilst its length increases empirically as shown above[4] as its radius decreases. Substituting I and ℓ into the energy integral of eq. (5) gives:

$$\ell n(r_m/r_o) = (\frac{r_m}{r_o} - 1)\{1 + \frac{\gamma}{2(\gamma - 1)}\} \tag{7}$$

Case 3: Argon pinch with I = constant, ℓ = constant and γ varying with tempetature

The enthalpy per unit mass of an argon plasma may be computed from the following formula:

$$h = \frac{5}{2} \frac{R_o}{M} TD + \frac{1}{m} \sum_{r=1}^{r=n} \alpha_r I_r + \frac{1}{m} \sum_{r=0}^{r=n} \alpha_r \bar{E}_r \tag{8}$$

where I_r is the energy required to raise one ion from its un-ionized state to its rth-ionized state. $\bar{E}_r$ is the average excitation energy per rth-ionized ion; α_r is the rth-ionized fraction and m is the mass of the ion. The α_r's are computed from Saha equations and the $\bar{E}_r$'s from known or estimated energy levels. Once h is computed from eq. (8), γ may be computed from eq. (2). This method may be used to compute the values of γ as a function of temperature.

The result[5] is shown in Fig. 2. We note that the pinch ratio r_m/r_o goes from a low value of 0.01 at 10^5 K through two minor peaks with values of 0.04 and 0.08 respectively at 2.5×10^5 K and 2×10^6 K; before rising finally towards the ideal gas value of 0.29 at high temperatures. At 1.16×10^7 K (1 keV) we note from Fig. 2 that the value of r_m/r_o is 0.18.

Case 4: Pinch with ℓ = constant, I = circuit-coupled

To treat this general case we have used a snow-plow equation of motion coupled to the electric circuit to simultaneously compute step-by-step the current sheet position and the magnitude of the current. At each step the quantities representing respectively the left-hand-side and the right-hand-side of equ. (5) are compared with each other to check for energy balance. The computation is terminated when energy balance represented by equ. (5) is achieved; the final value of r being taken as r_m. The three equations in normalized form are:

Equation of motion:
$$\frac{d\kappa^2}{d\tau^2} = \frac{-\alpha^2 \iota^2/\kappa + 2\kappa(\frac{d\kappa}{d\tau})^2}{(1 - \kappa^2)} \tag{9}$$

Circuit equation:
$$\frac{d\iota}{d\tau} = \frac{1 - \int \iota d\tau + \beta\iota \frac{d\kappa}{d\tau}/\kappa}{(1 - \beta\, \ell n\kappa)} \tag{10}$$

Energy balance for quasi-equilibrium radius:
$$\iota_m^2 = \frac{2(\gamma - 1)}{\gamma} \int_{\kappa_m}^{1} \frac{\iota^2 d\kappa}{\kappa} \tag{11}$$

where $\kappa = r/r_o$, $\tau = t/t_c$, $\iota = I/I_o$ and

$$t_c = (L_o C_o)^{\frac{1}{2}}, \quad I_o = V_o/(L_o/C_o)^{\frac{1}{2}}$$

with the scaling factors $\alpha = t_c/t_p$ and $\beta = \frac{\mu\ell}{2\pi}/L_o$

where t_p the characteristic pinch time turns out to be:

$$t_p = \{4\pi^2 \rho_o r_o^4/(\mu I_o^2)\}^{\frac{1}{2}}$$

and ρ_o is the ambient density.

The scaling factors allow a choice of the ratio of the capacitor discharge time to the pinch characteristic time and the ratio of the pinch characteristic inductance to the fixed circuit inductance. For example, for the case of $\alpha = 1$, $\beta = 0.01$ we have a near sinusoidal discharge (i.e. the current waveform is of the type $I = I_o \sin\omega t$) and the computed value of r_m/r_o is 0.21. For the case of $\alpha = 100$, $\beta = 0.01$ we have a pinch occurring early in a sinusoidal discharge (with $I = I_o \omega t$) and the resulting value of r_m/r_o is 0.17. A parametric variation shows that at $\alpha = 0.7$, $\beta = 1.0$, good energy

efficiency is achieved with 30% of the capacitor energy transferred to the plasma column at its quasi-equilibrium radius. For this case the value of r_m/r_o is rather large at 0.39. The trajectory and current for several cases are shown in Fig. 3.

Energy-Consistent Trajectory with Structure

It can be shown that primarily the snow-plow model is not energy-consistent because of its assumed zero-thickness structure. By the above method of imposing energy-balance we can find the radius beyond which the plasma column cannot be further compressed. It would be an improvement to construct an energy-consistent model which of necessity must have structure. This may be done using a slug model[2] by linking the shock front velocity to the magnetic piston pressure and then allowing the piston to separate from the shock front by the correct application of the adiabatic expansion rule to a fixed mass of gas. We are in the process of developing this model[7] for the general case of a pinch with variable I, ℓ and γ. Some preliminary results of this model are presented in Table 1 for comparison with results of the energy balance model and experimental results.

Discussion and Conclusion

The results show good agreement between the energy balance theory and experiments over a wide range of pinch operation from the case of a constant length pinch to that of a plasma focus of variable length; from the case of a $\gamma = 5/3$ hydrogen or deuterium pinch to the case of a variable γ argon pinch and from the case of a constant current pinch to that of a circuit-coupled pinch. The simplicity of the theory makes it suitable for general application to other pinch-type devices.

References

1. M.G. Haines, Phil. Trans. Royal Soc. Lond. A300, 649 (1981)

2. D.E. Potter, Nucl. Fusion 18, 813 (1978)

3. S. Lee, Bul. Fizik Malaysia 2, 240 (1981)

4. S. Lee, "Energy Balance and the Radius of Electromagnetically Pinched Plasma Columns", Plasma Physics (in press)

5. S. Lee, Bul. Fizik Malaysia 4, 1 (1983)

6. S. Lee, "The Application of Energy Balance to compute Plasma Pinch Ratios", J. Applied Physics (in press)

7. S. Lee, Bul. Fizik Malaysia 3, 197 (1982)

8. P.F.M. Baldock, D.E. Dangor, M.B. Favre Dominguez, D. Grimsley, J.D. Hares, E. Kahan, S. Lee, "High Density High Temperature Plasma Production in Fast Z-Pinches", Ninth Ann. Conf. on Plasma Physics, Oxford (1982)

9. H.A.B. Bodin, A.A. Newton, N.J. Peacock, Nucl. Fusion 1, 54 (1960)

Case	Energy Balance Theory	Generalized Slug Model	Experiment
1. I = constant, ℓ = constant, γ = 5/3	0.29	0.31	1/3 = 0.33*
2. I = constant, ℓ = empirical (for plasma focus), γ = 5/3	0.14		0.13+
3. I = constant, ℓ = constant, $\gamma = \gamma(T)$, argon	0.18 (at 1 keV)		1/6 = 0.17** (at 1 keV)
4a. $I = I_o \omega t$, ℓ = constant, γ = 5/3	0.17		
4b. $I = I_o \omega t$ (α = 1), ℓ = constant, γ = 5/3)	0.21		0.23++
4c. I = coupled (α = 0.7, β = 1), ℓ = constant, γ = 5/3	0.39		
5. I = coupled, ℓ = coupled (plasma focus), γ = 5/3		0.16	0.13+

Table 1. Theoretical and experimental values of r_m/r_o

* Imperial College[1,8]; ** Imperial College[8];

\+ Universiti Malaya[3,4,6] ++ Culham

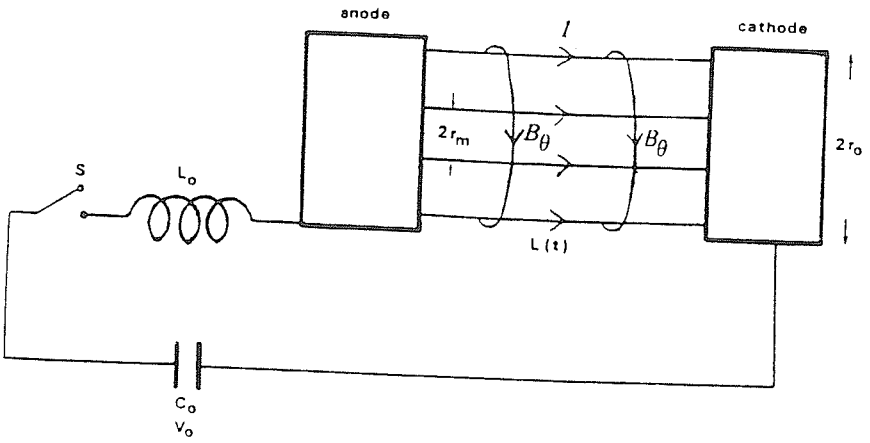

Fig. 1. Schematic drawing showing pinch dynamics and pinch circuit (Note: The pinch return current path is at radial position of r_o: this is not shown in the drawing).

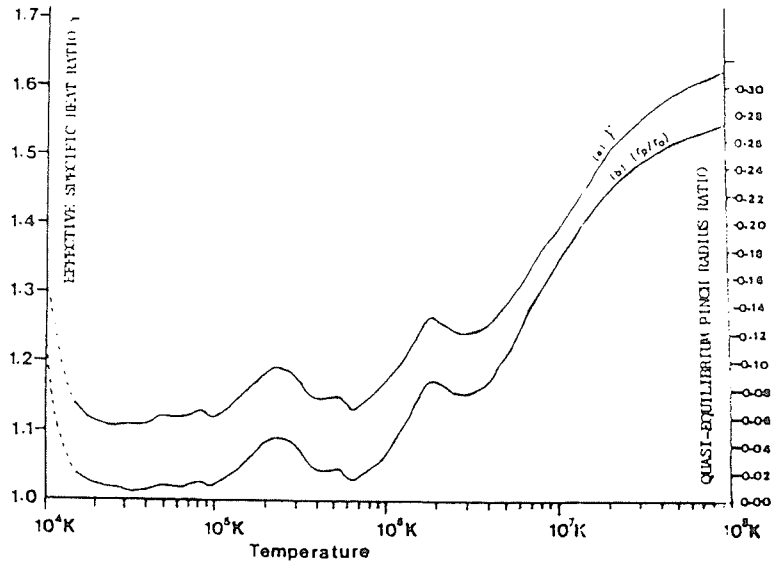

Fig. 2. (a) Specific heat ratio (b) Constant-current pinch radius ratio of argon as functions of temperature.

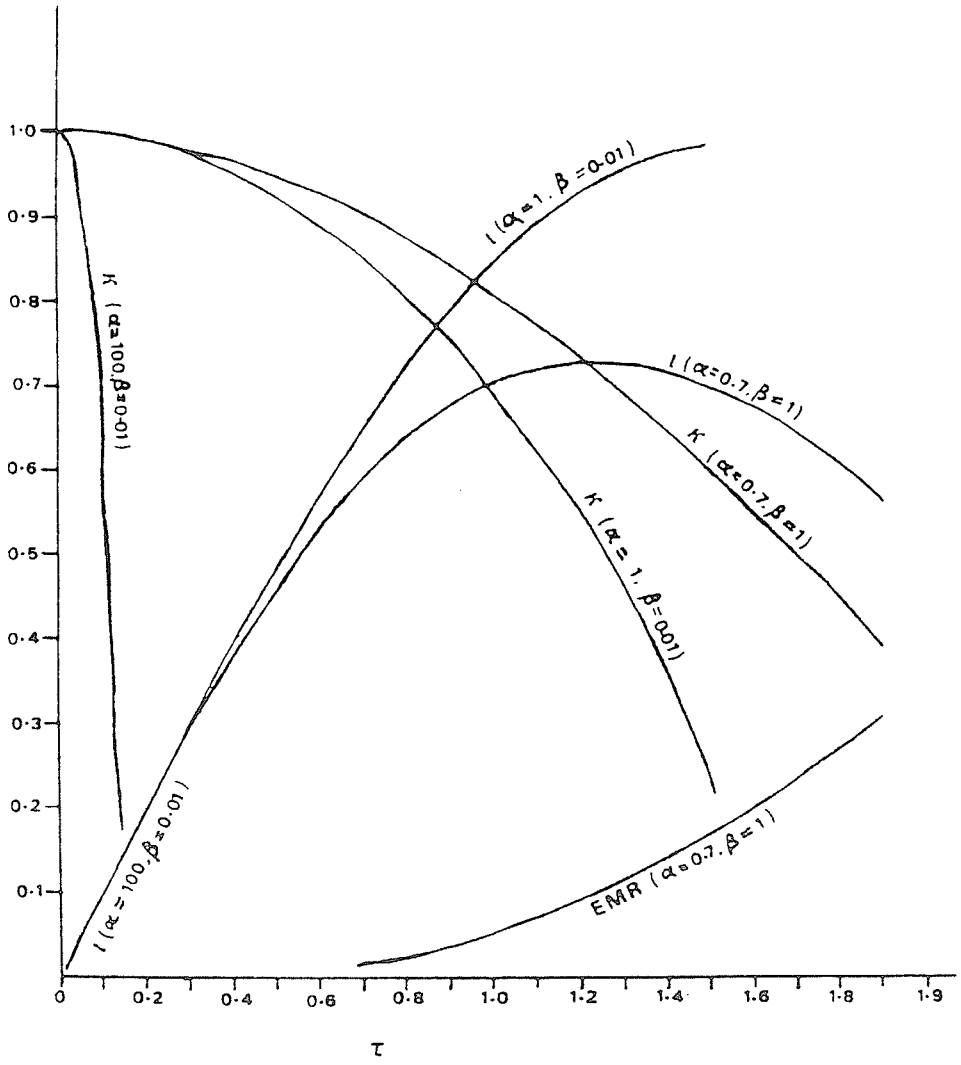

Fig. 3. Computation of κ and τ as functions of τ for three sets of scaling parameters: i) $\alpha = 100$, $\beta = 0.01$ (Linear current) ii) $\alpha = 1$, $\beta = 0.01$ (Sinusoidal current) and iii) $\alpha = 0.07$, $\beta = 1$ (Typical example with good energy coupling).

EXPERIMENTAL INFERENCE OF A PHYSICAL MODEL FOR THE VACUUM SPARK

C.S. Wong and S. Lee
Plasma Research Laboratory
Physics Department
University of Malaya
Kuala Lumpur

ABSTRACT

Experimental observations on a series of vacuum spark discharges reveal that (i) a pinch phase exists during the discharge; (ii) the final hot dense phase of the vacuum spark plasma is coincident in time with the sharp dip in the current oscillogram; and (iii) x-rays are observed to be emitted mostly from plasma spot. A physical model is thus inferred from these observations and the feasibility of the model is then checked by analysing the discharge current waveform numerically. In this analysis, the possible electromechanical interaction and its effect on the discharge current that flows through the plasma have been considered.

1. Introduction

During the operation of the vacuum spark device (Fig. 1), a high voltage of 20 kV is applied across a pair of electrodes kept at 5 mm apart. The voltage source is a 22 μF capacitor bank whose rise-time is 1 μs. The electrodes are embedded in a vacuum chamber evacuated to a pressure of lower than 10^{-5} torr so that discharge is initially prohibited. To initiate the discharge, a beam of high power ruby laser (60 MW, 25 ns) is focussed onto the tip of the anode as indicated in Fig. 1; whereby some anode materials are vaporised to form a burst of weak plasma. Discharge will then occur through this weak plasma, thus heating the plasma to extremely hot and dense conditions. This phenomenon has been investigated by numerous workers[1 - 8]. The plasma produced at the hottest and densest phase of the discharge is found to consist of minute spots at electron density of 10^{21} to 10^{22} per cm^3 and electron temperature of 4 to 10 keV[9].

The heating mechanism responsible for the formation of the dense plasma spot is yet to be determined, though several possibilities have been proposed[7]. It is generally believed that electron beam plays an important role in the plasma heating mechanism but the origin of the electron beam is not exactly known. In this paper, we consider the inference of a possible physical model for the vacuum spark mechanism

Procs. First Asia-Pacific Phys. Conference, Ed. A. Arima et al World Scientific Publishing Co. (1984)

from experimental observations based on streak and pinhole photography as well as analysis of the discharge current waveforms. The description of the model starts from the moment when the discharge is initiated and extends to the sharp current dip which corresponds to the time when the hot dense plasma spot is formed. This takes a total time of 500 to 800 nanoseconds as usually observed in the discharge current waveform of the vacuum spark discharge of our device.

2. Experimental observations

The existence of pinching plasma column has been confirmed in our device by using both pinhole and streak photography. Fig. 2 shows the pinhole image of the visible light emitted from the region between the electrodes during a vacuum spark discharge at 4 kV. It can be seen from this picture that almost all the light are emitted from the inverted frustrum between the electrodes, and at the center of the image a bright column with diameter of about 1 mm is clearly observed. This column is in fact embedded in a bright surrounding and from the fact that it can be observed clearly on a time-integrated pinhole picture indicates that it is fairly stable while it is emitting light of much stronger intensity than the surrounding. It is believed to be the pinched plasma column of the vacuum spark. However, such a stable plasma column has not been observed for discharges at higher discharge voltages(>10 kV). This is mainly due to the extremely strong light emitted from the discharge which causes poor contrast between the image of the column and its surrounding.

Time-resolved streak image of the pinching plasma column during the vacuum spark discharge has been observed using an IMACON camera, an example of which is shown in Fig. 3. The picture shows the evolution of a plasma column pinching from an initial diameter of about 5 mm to a minimum diameter of about 1 mm. The radial trajectory togather with the average brightness of the column have also been plotted against time in the same figure. The maximum brightness of the column occurs approximately coincident in time with the minumum radius. The pinching is observed to be slow, with an average speed of the order of only 10^4 m/s.

As mentioned earlier, the image of the plasma column cannot be observed on the visible pinhole picture and also the streak picture for discharges at high voltages of above 10 kV. However, under this condition, the image of the x-ray emitting region of the plasma can be observed instead by using a x-ray pinhole camera. The most intense x-ray is observed to be emitted from plasma spot as shown in Fig. 4. This spot is found to be formed at a time coincident with the sharp dip of the discharge current.

From the above experimental observations, it is probable to conclude that a pinch phase is present during the vacuum spark discharge. Since the image of the pinch column has not been observed clearly on x-ray pinhole picture, the temperature of the plasma in the column is probably

much lower than that of the plasma spot. This indicates that the main plasma heating mechanism does not occur during the pinch phase. However, the subsequent phase of the vacuum spark discharge during which the plasma is heated to its extremely hot and dense conditions is probably a consequence of the pinch phase.

3. Electromechanical analysis of the discharge current waveform

A macroscopic picture of the vacuum spark dynamics can be deduced from the analysis of the discharge current waveform, a typical one of which is displayed in Fig. 5. In this figure, it can be seen that the flow of the discharge current through the plasma begins to deviate from that of an ideal damped L-C-R discharge (indicated by the dotted line in the figure) at about 150 ns after the start of the discharge. This deviation in the discharge current is the consequence of the variation of the plasma dynamics. Hence, it will be useful to analyse this waveform by relating the mechanical behaviours of the plasma during a vacuum spark discharge to its electrical properties such as its resistance and inductance; or vice-versa.

The equivalent circuit of the vacuum spark discharge can be represented as shown in Fig. 6. In this circuit, the plasma is represented by the combination of a variable inductance $L_p(t)$ and a variable resistance $R_p(t)$ so that the total inductance and resistance of the discharge circuit can be written as

$$L(t) = L_e + L_p(t)$$

and

$$R(t) = R_e + R_p(t) \qquad (1)$$

where L_e and R_e are respectively the stray inductance and resistance of the system external to the plasma. The circuit equation is then given in the form :

$$V_o - \frac{\int I\,dt}{C} = \frac{d}{dt}(LI) + IR \qquad (2)$$

where V_o is the discharge voltage of the capacitor C, while L and R are the total inductance and resistance respectively of the circuit given by (1). The intantaneous current that flows through the circuit is $I(t)$. The rate of change of $I(t)$ can be obtained by re-arranging (2) as

$$\frac{dI}{dt} = \frac{V_o}{L} - \frac{I}{L}\frac{dL}{dt} - \frac{I\,R}{L} - \frac{\int I\,dt}{LC} \; . \qquad (3)$$

This expression can be used to calculate the instantaneous rate of change of current of the discharge circuit if the expressions for $L_p(t)$ and $R_p(t)$ are known. In our analysis here, we shall choose the functions for these quantities according to our postulate of the possible physical model of the vacuum spark discharge as inferred from experimental observations.

We shall divide the time of interest during the vacuum spark discharge (during the first quarter period of the discharge) into three regimes as indicated in Fig. 5. These time regimes can be described mathematically as follows :

Regime I : The total inductance and resistance of the circuit are assumed to be constant; i.e.

$$\left.\begin{aligned} L(t) &= L_o \simeq 20 \text{ nH} \\ R(t) &= R_o \simeq 1 \text{ m}\Omega \end{aligned}\right\} \quad (0 < t < 150 \text{ ns})$$

Regime II : The plasma column pinches during this regime causing an increase in the plasma inductance thus results in the deviation (reduction) of the discharge current from that of ideal L-C-R discharge. This occurs during the time-interval from 150 ns to about 700 ns for this particular case. In this regime, we have dL/dt positive; but R is still constant.

Regime III: At the end of the pinch phase (Regime II) of the discharge, a mechanism is induced such that the plasma resistivity increases anomalously thus causing the discharge current to drop sharply. From Fig. 5, it can be seen that this occurs at the time from 700 ns to 760 ns. The plasma column is assumed to be at its maximum compression in this regime. Thus we take dR/dt as positive while $L = L_{max}$.

With the above postulations of the possible dynamics of the vacuum spark discharge, we may then write down the functions of $L(t)$ and $R(t)$ in explicite forms and use them to solve equation (3) for $I(t)$. We have chosen the simplest forms of linear function for both $L(t)$ and $R(t)$ as shown in Fig. 7. The values of $I(t)$ thus obtained are plotted against time in Fig. 5, super-imposed onto the experimental curve. It can be seen that the agreement between the computed values and the experimental ones is indeed very good. This agreement is further demonstrated in Table I.

4. Conclusions

We have seen from the above discussion that, a physical model for the vacuum spark discharge can be inferred from experimental observations to be consisting of a pinch phase followed by a turbulent phase. During the pinch phase, the plasma has not been heated to high enough temperature but it is responsible for inducing mechanisms by which the main plasma heating occurs. These physical pictures of the plasma dynamics have been expressed in terms of plasma inductance and resistance so that the effect of the electromechanical interaction on the discharge current can be coupled into the circuit equation. The solution of the circuit equation with functions of plasma inductance and resistance postulated empirically with reference to possible model inferred from experimental observations shows that the model is a feasible one. Work is presently in progress to develop a numerical model to describe the vacuum spark mechanism base on the physical model concluded above.

Acknowledgement

The capacitor bank and the pulsed ruby laser used in this work are presented to the Physics Department, University of Malaya by the Alexander von Humboldt Foundation and Kernforschungsanlage Jülich of the Republic of Germany. The project is subsequently supported by a F-grant (F95/77) of the University of Malaya.

References

[1]L. Cohen, U. Feldman, M. Swartz and J.H. Underwood, J. Opt. Soc. Am. 58, 843(1968).

[2]R.C. Elton and T.N. Lie, Space Sci. Rev. 13, 747(1972).

[3]T.J. Welch and E.J. Clothiaux, J. Appl. Phys. 45, 3825(1974).

[4]T.J. Turechek and H.J. Kunze, Z. Physik A 273, 111(1975).

[5]T.N. Lee, Ann. N.Y. Acad. Sci. 251, 112(1975).

[6]S. Lee and H. Conrads, Phys. Lett. 57A, 233(1976).

[7]C.R. Negus and N.J. Peacock, J. Phys. D: Appl. Phys. 12, 91(1979).

[8]E. Ya. Gol'ts, I.A. Zhitnik, E. Ya. Kononov, S.L. Mandel'shtam and Yn. V. Sidel'nikov, Sov. Phys. Dokl. 20, 49(1975).

[9]C.S. Wong and S. Lee, "*Fusion Energy - 1981*", IAEA-SMR-82, p337.

Time (ns)	Experimental Current (kA)	Simulated Current (kA)
100	121	122
200	220	221
300	275	280
400	321	320
500	348	345
600	358	360
700	367	367
725	358	357
750	230	235
767	92	90

Table I

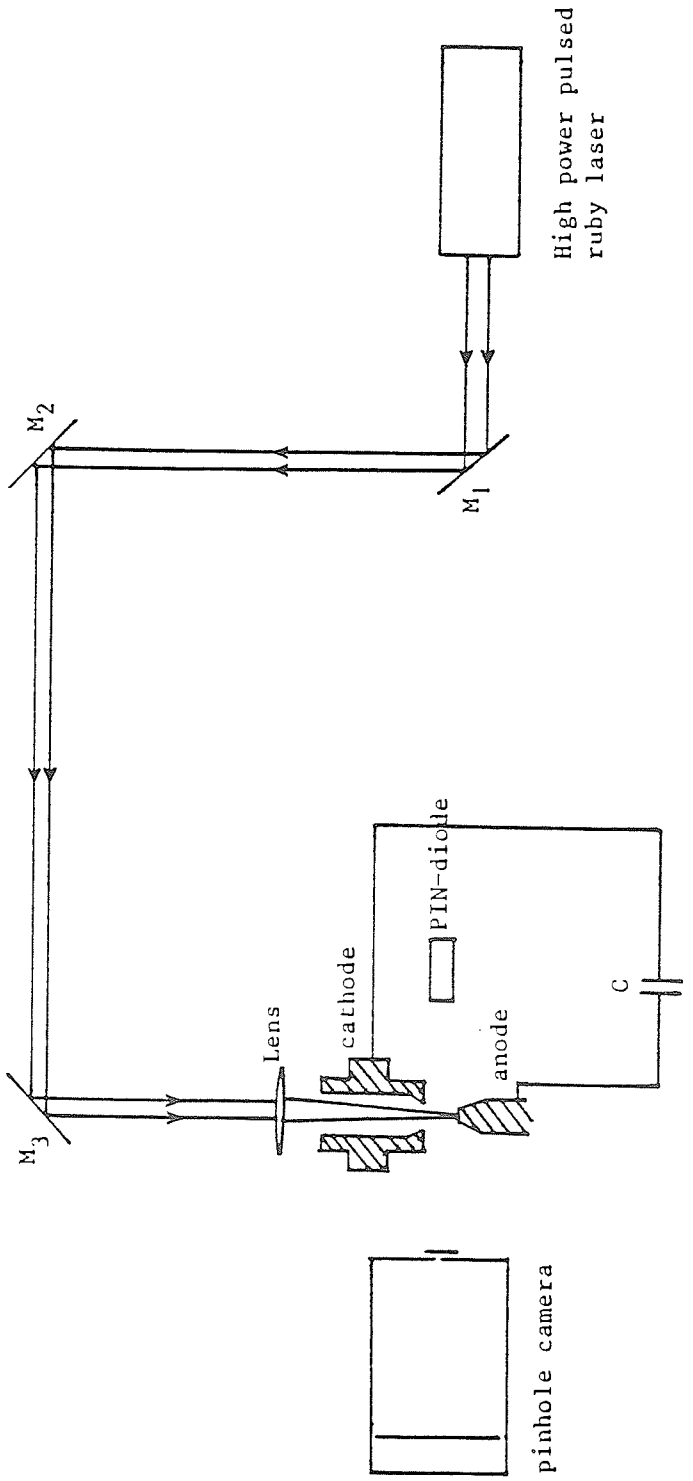

Fig. 1. Schematic of the vacuum spark experimental layout.

Fig. 2. Visible pinhole image of the vacuum spark discharge.

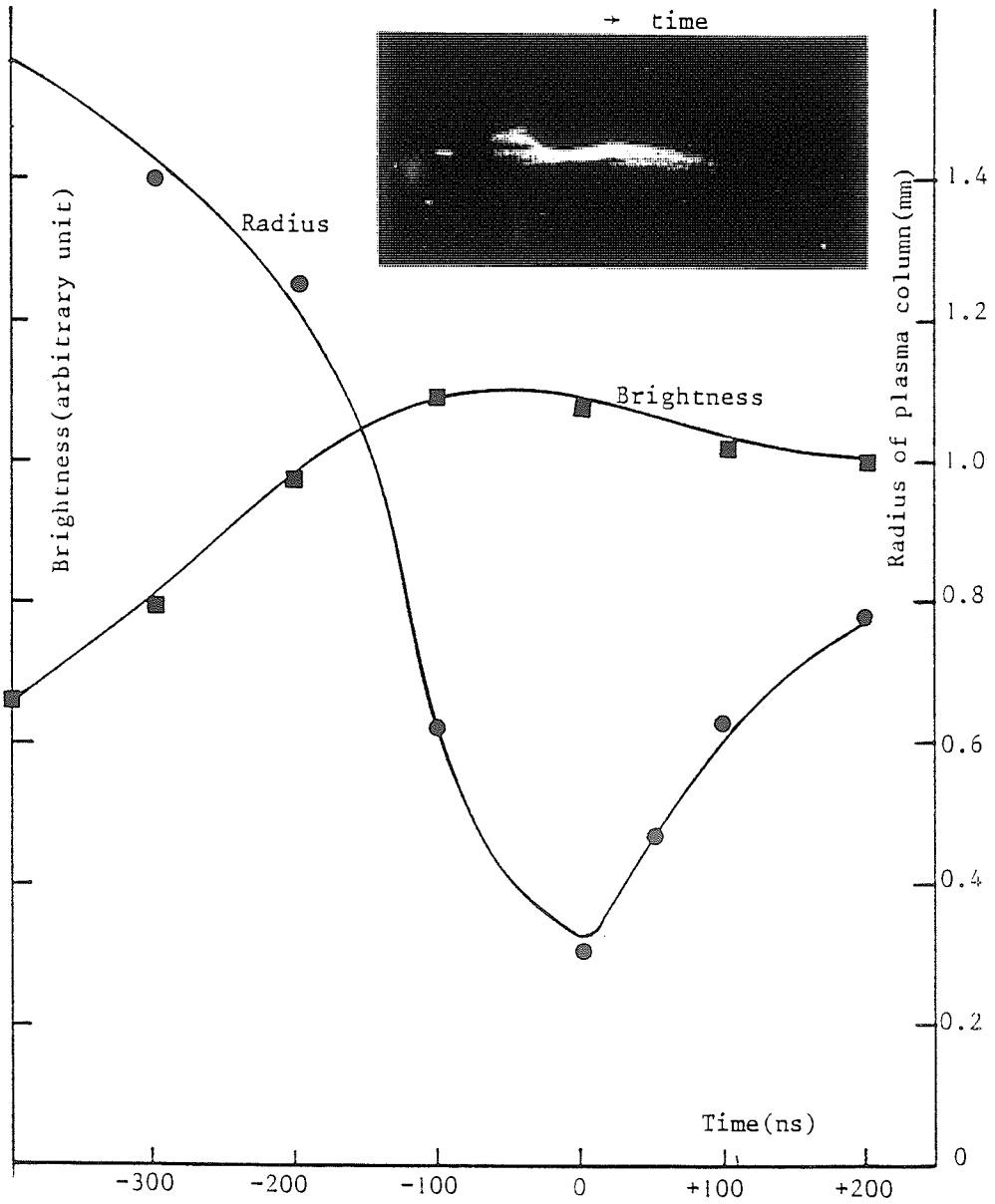

Fig. 3. Time evolution of the radius and the brightness of the pinched plasma column of vacuum spark discharge at 6 kV. Inset shows the streak picture from which these curves are deduced.

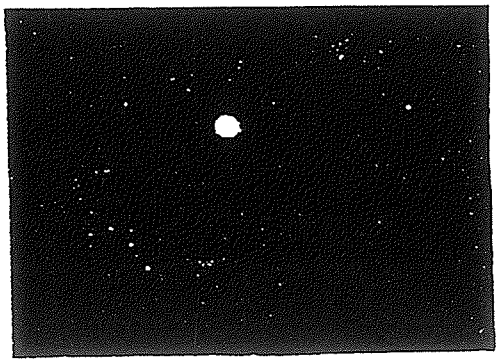

Fig. 4. X-ray pinhole image of the dense plasma spot.

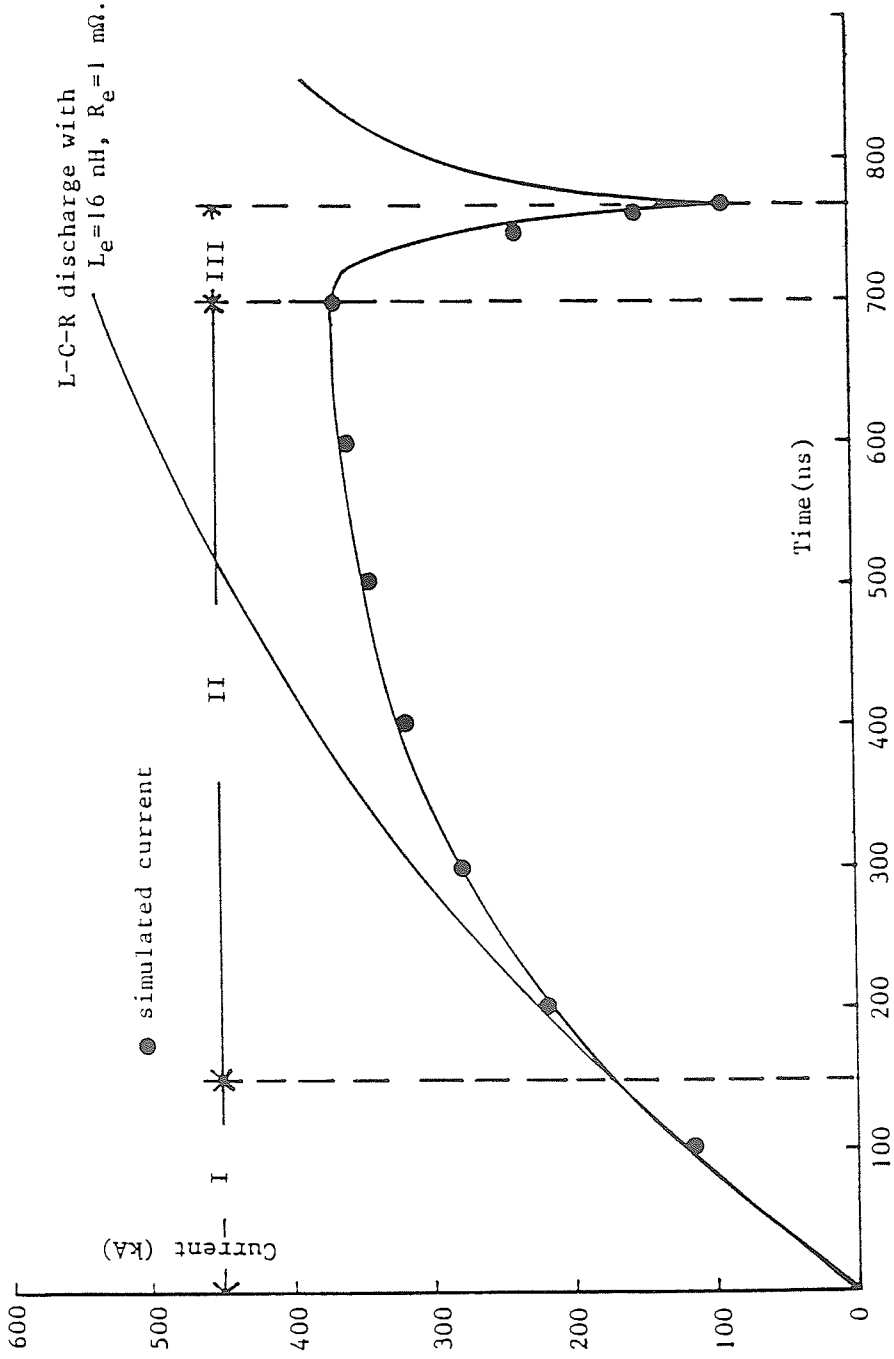

Fig. 5. Discharge current waveform of the vacuum spark traced out from the current oscillogram.

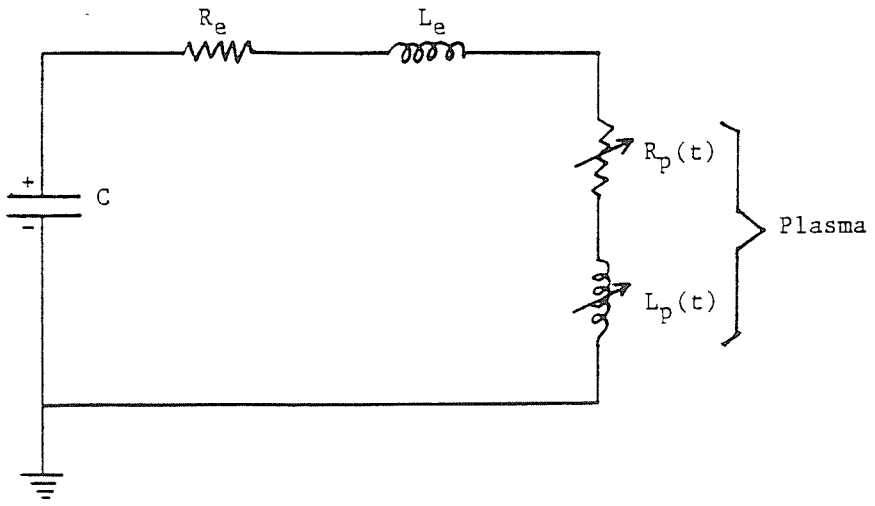

Fig. 6. Equivalent circuit of the vacuum spark discharge.

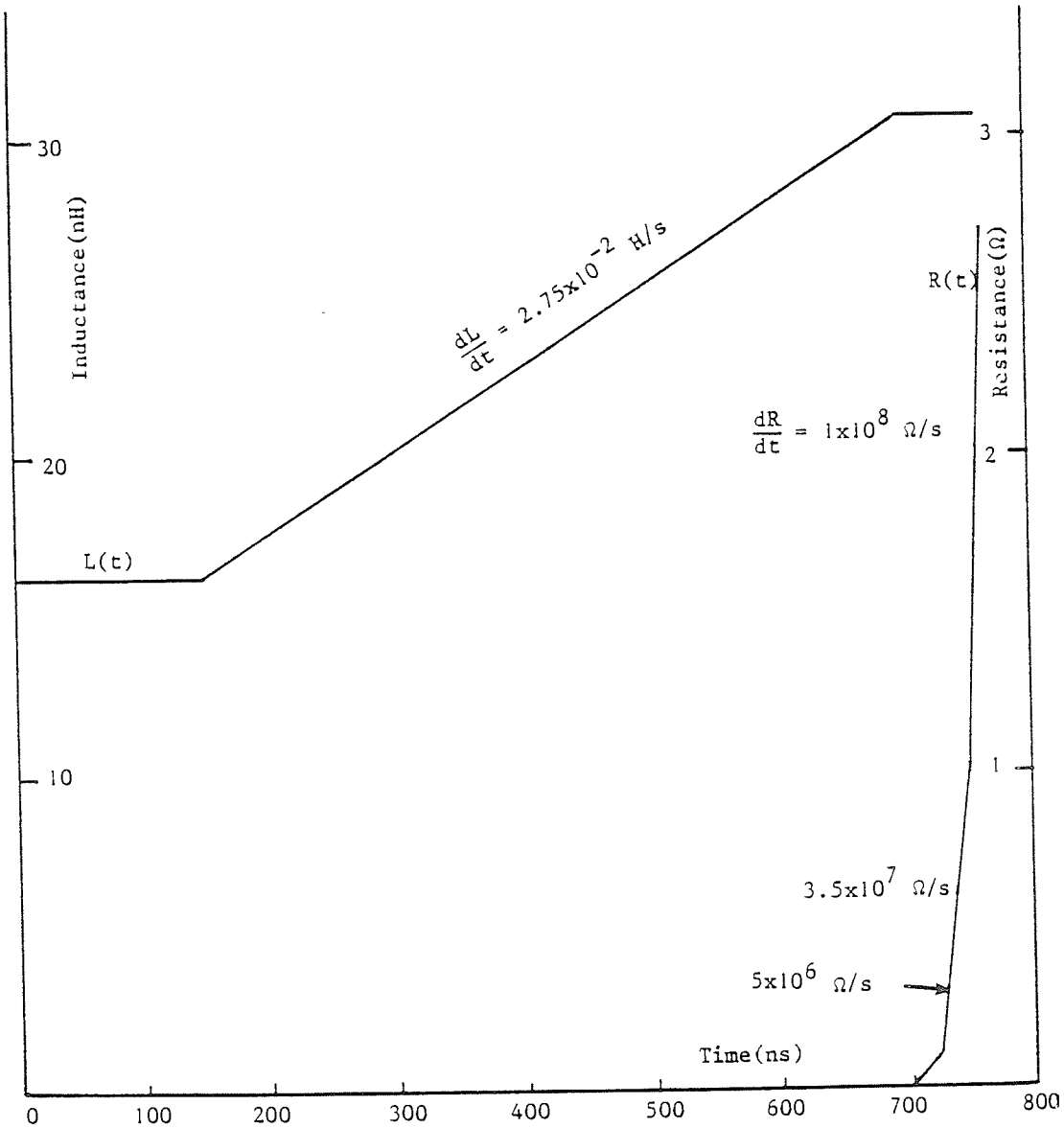

Fig. 7. Time-functions of overall inductance and resistance of the vacuum spark discharge circuit used for current simulation.

FIRST TROPICAL COLLEGE ON APPLIED PHYSICS

LASER AND PLASMA TECHNOLOGY

Kuala Lumpur

26 December 1983 - 14 January 1984

PAPER XIV

PINCH DYNAMICS OF THE PLASMA FOCUS

T.Y. Tou and S. Lee
Plasma Research Laboratory
Physics Department, University of Malaya
Kuala Lumpur 22-11, Malaysia

Abstract:

The formation of a pinch in both the deuterium and argon plasma focus was investigated by streak camera observations of the visible emission. A generalised slug model was proposed to describe the observed trajectory and structure of the pinch and to predict the final quasi-equilibrium pinch radius which is related to the anode radius. These final radii were compared with those predicted by an energy balance theory.

"Laser and Plasma Technology" Ed. S. Lee et al
World Scientific Publishing Co. (1985)

Introduction

The snowplow model[1] has been widely used to picture the radial pinch phase of the plasma focus. The plasma is assumed to tbe swept into an infinitesimally thin shell at the magnetic piston. The time history of the piston position can be resolved by solving the equation of the motion. Such a model provides no structure in space and suggests that the shell will collapse into zero radius. Several retardation mechanisms[2,3,4] have been included to the model to give non-singular infinite compressions on the axis. These models, however, have not been able to correctly predict the final pinch radius when quasi-equilibrium phase is first established. Based on the Potter's slug model[5], a generalised slug model[6,7] was proposed for the radial pinch phase of the focus which enabled the time histories of the shock, piston, current and voltage profiles to be computed. In this paper, the temporal evolution of the focus pinch obtained from streak photographs will be compared to the numerical solutions of the generalised slug model. The observed end-point of the pinch will also be compared to the predictions of the generalised slug model and the energy balance theory[8].

Generalised Slug Model for the Focus Pinch

For a coaxial system with plasma focus geometry, two phases of plasma heating are considered, namely the axial phase and the radial pinch phase.

In the axial phase, a snowplow model[6,7] is used. The equations of motion and circuit are solved to provide the time-dependent solutions of magnetic piston, current and voltage. At the end of the axial phase, a finite-thickness slug model is proposed for the radial pinch phase.

The slug model assumes collision-dominated plasma between an infinitely conducting current sheath and a shock front. The shock front is assumed to be thin compared to the anode radius so that Rankine-Hugoniot conditions for a strong shock can be used to describe the pressure, velocity and density of the plasma in terms of the filling pressure p_o, shock velocity and the specific heat ratio γ.

An equation for the shock front position, $r_s(t)$ is obtained by linking the shock pressure to the magnetic pressure. Using the adiabatic

law for the plasma and the equality of plasma pressure and the magnetic pressure, the equation of piston position, $r_p(t)$ is obtained. The length of the imploding plasma column is allowed to grow at the same rate as the radial collapse of the shock front because the two motions are driven by the same plasma pressure within the slug. The circuit equation is coupled to the plasma motion. The numerical solution for a deuterium focus during the dynamic pinch phase is shown in Fig. 1. The scaling parameters chosen for the computation are comparable to the experimental values. The figure shows a slug with finite thickness between the shock front and the magnetic piston. The slug thickness increases with radial compression. When the shock front hits the axis, the piston reaches a radius $r_p(t) \approx 0{,}17 r_o$. With the present model the computation is terminated at this quasi-equilibrium pinch.

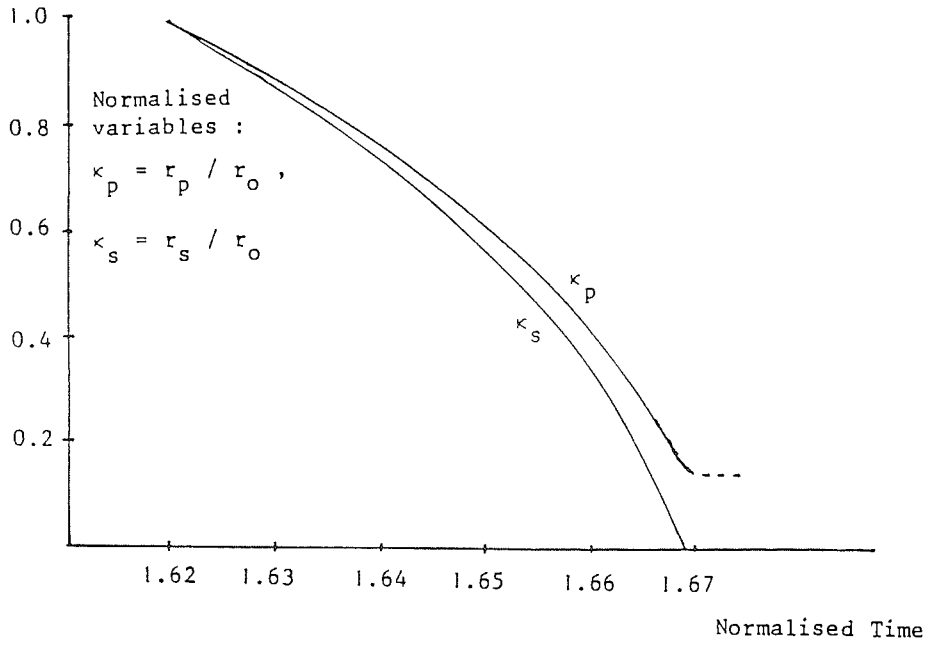

Fig. 1 Trajectories of the magnetic piston (κ_p) and the shock front (κ_s) according to the generalised slug model.

Application of Energy Balance to Focus Pinch

In the radial pinch phase, the current is assumed to flow axisymmetrically through a thin cylindrical sheath. The current sheath acts as a magnetic piston and implodes radially inwards onto the axis, doing work on the gas. Part of the energy imparted to the gas will initially be in the form of kinetic energy. But eventually when the pinch achieves a quasi-equilibrium state we may equate the work done by the magnetic piston to the plasma enthalpy. This energy equation together with the Bennett equation for the pressure balance will give an expression[8] regarding the final pinch radius:

$$I_p^2 = \frac{2(\gamma - 1)}{\gamma \ell_p} \int_{r_p}^{r_o} I^2 \ell \frac{dr}{r} \qquad (1)$$

where ℓ is the length of the plasma column,
γ is the specific heat ratio,
I is the current and
r is the radius of the pinch.

The subscript p indicates quantities at the time quasi-equilibrium is first achieved. An expression for ℓ has been obtained experimentally[9],

$$\ell = \ell_p \left(\frac{r_o - r}{r_o - r_p} \right) \qquad (2)$$

For simplicity, a constant current is assumed for the radial pinch phase, then an expression relating the final pinch radius to the initial radius r_o is then obtained:

$$\ell n(1/\kappa_p) = (1 - \kappa_p)\left(1 + \frac{\gamma}{2(\gamma - 1)}\right) \qquad (3)$$

where $\kappa_p = r_p/r_o$.

The above expression shows that the pinch radius ratio is a function of the specific heat ratio of the plasma.

Experimental Results and Comparisons

The pinch phase of a geometrically optimised plasma focus[10] was studied using a calibrated streak camera[11]. Figure 2a shows the set-up for the side-on streak photography with slit position perpendicular to the focus axis. A typical side-on streak image for a deuterium focus operating with filling pressure of 5.5 torr and 14 kV firing voltage is shown in Figure 2b. Comparable photographs were obtained over a reasonably wide range of filling pressure (4.5 torr to 12.0 torr) and firing voltage (10 kV to 20 kV). Figure 2b was magnified and traced to show the shock front $r_s(t)$, magnetic piston $r_p(t)$ and the quasi-equilibrium pinch. During the pinching, the plasma slug increases in thickness, as predicted by the generalised slug model. The compression, however, does not stop when the shock front hits the axis at $r_p(t) \simeq 0.18 r_o$ but proceeds slightly further until $r_p(t) \simeq 0.12 r_o$. A quasi-equilibrium pinch is then established. The observed pinch ratio of 0.12 may be compared to 0.14 predicted by the energy balance theory with $\gamma = 5/3$ for fully ionised deuterium.

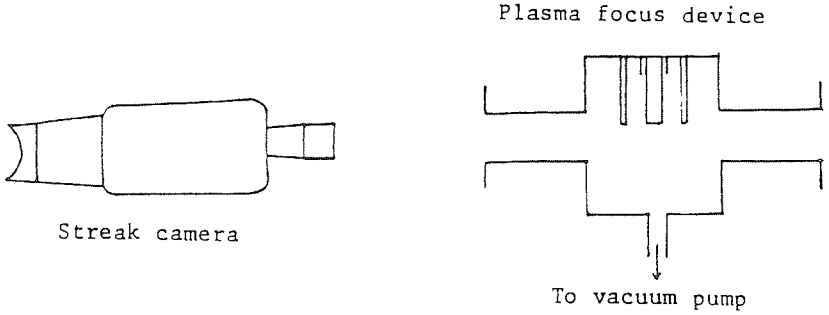

Figure 2a Side-on streak photography of the focus pinch

Figure 3 shows another side-on streak image of the argon focus for filling pressure of 1.5 torr and 18 kV firing voltage. The operating parameters of argon focus have been varied with filling pressure between 0.5 torr and 2.5 torr and firing voltage from 10 kV to 20 kV. When the shock front hits the axis, $r_p(t) \simeq 0.12 r_o$, but a final pinch radius

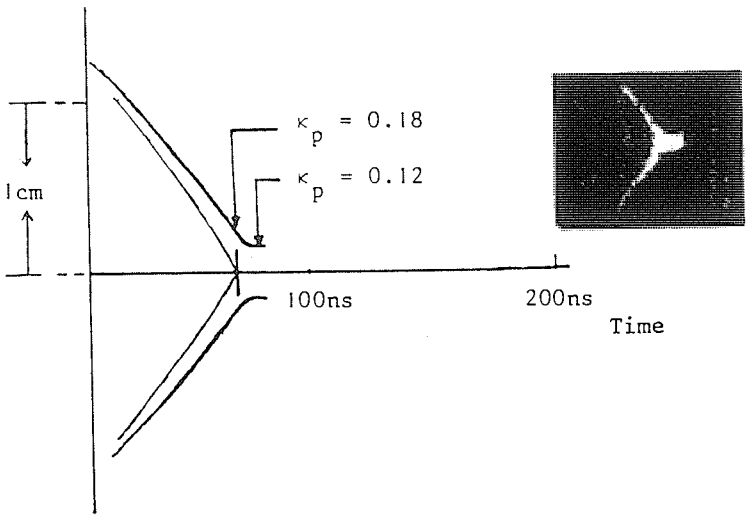

Figure 2b Side-on streak image of a deuterium focus pinch at 5.5 torr, 14 kV.

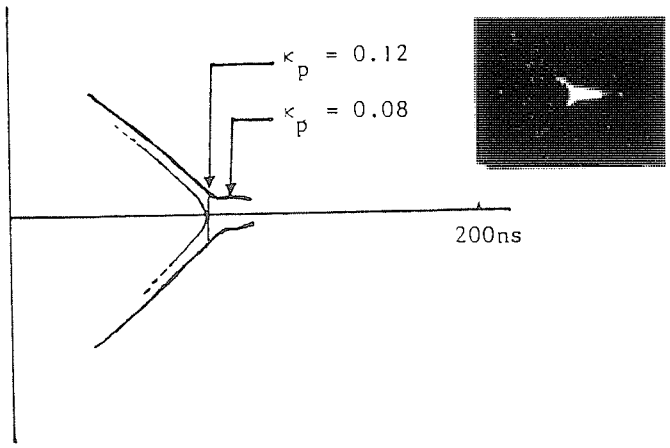

Figure 3 Side-on streak image of a argon focus pinch at 1.5 torr, 20 kV.

$r_p(t) \simeq 0.08 r_o$ is measured.

In order to predict the radius ratio of the argon focus pinch using the energy theory, the specific heat ratio of the argon plasma is estimated in the following way. The shock velocity estimated from the streak photograph (see Fig. 3) is about 30 cm/μs, which corresponds to 3×10^6 °K from the strong shock theory. The specific heat ratio γ for this temperature of argon plasma is about 1.34 and thus from the energy balance theory, $r_p(t) \simeq 0.06 r_o$ at the quasi-equilibrium pinch. The temperature dependent solution of the specific heat ratio for argon[12] is given in Fig. 4.

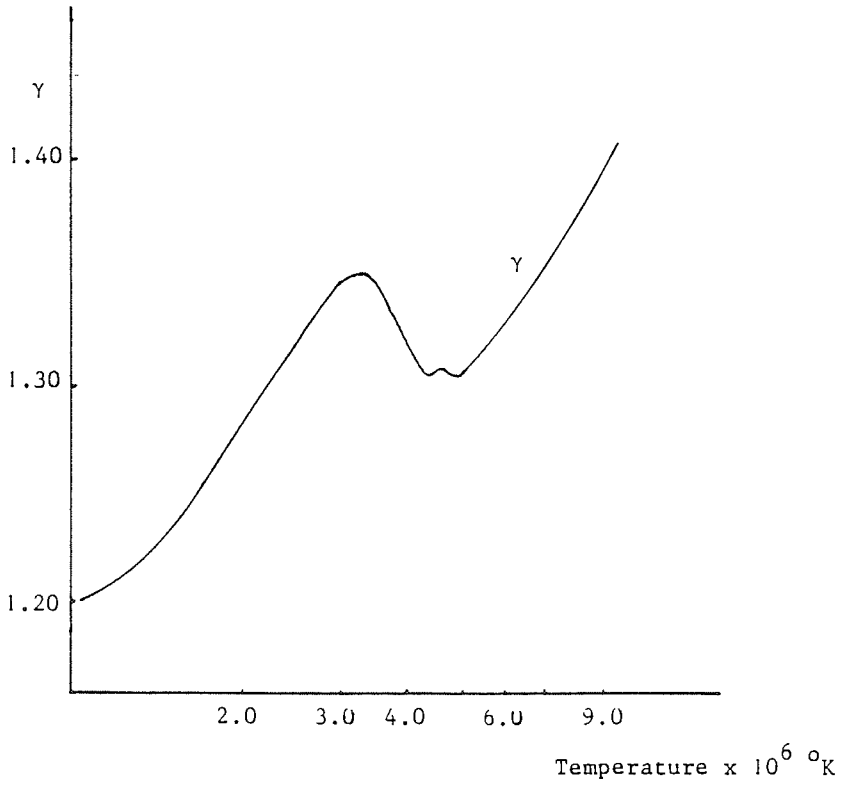

Fig. 4 Solution of γ as a function of temperature

Table I summarised these results with some earlier laser shadowgraphic results for the deuterium focus.

Gas	Experimental values of κ_p		Theoretical values of κ_p	
	when shock front $\kappa_s=0$	when piston stops, $\kappa_p=0$	generalised slug model, $\kappa_s=0$	energy balance
Deuterium	0.18	0.12	0.17	0.14
Argon	0.12	0.08	----	0.06
Shadowgraphic result[9]: $\kappa_p = 0.13$ (Deuterium)				

Table I Summary of results

Discussion and Conclusion

Several important features observed in both the deuterium and argon focus agree reasonably well with the theoretical predictions. Firstly, the increasing thickness of the slug for both the deuterium and argon focus pinches are envisaged by the generalised slug model. For deuterium focus, the measured value of $r_p(t)/r_o \approx 0.17$ may be compared to 0.18 by the generalised slug model. A further radial compression after the shock front hits the axis is observed but not predicted by the generalised slug model. The final pinch ratio of 0.12 may be compared to 0.14 predicted by the energy balance theory for a fully ionised deuterium with $\gamma = 5/3$. The authors believe that a small amount of impurity such as air which is possibly present may result in a slightly smaller effective specific heat ratio values than 5/3. The energy balance theory would then give a smaller pinch radius ratio.

A smaller pinch radius ratio is observed in the argon focus. This may be ascribed to the smaller specific heat ratio of argon[12]. The experimental measurement of pinch ratio of 0.08 may be compared to 0.06 predicted by the energy balance theory. The generalised slug model for a real gas such as argon requires γ to be computed at each step of the trajectory.

The generalised slug model, together with the energy balance theory, is able to explain satisfactorily the important features observed in streak photography of the deuterium and argon plasma focus.

Acknowledgement

The authors would like to acknowledge the experimental assistance of Mr. Jasbir Singh and Mr. Toh Teck Seng. This work is supported by an F Grant from the University of Malaya.

References

1. M. Rosenbluth, R. Garwin and A. Rosebuth, Los Alamos Report LA-1859 (1954).
2. M.A. Leontovich and S.M. Osovets, J. Nucl. Energy II, 4, 209 (1957).
3. P.C. Patou, A. Simonnent and J.P. Watteau, Le. J. De Physique, 973 (1968).
4. S. Lee and Y.H. Chen, "The Plasma Focus - A Radial Trajectory Computation", Proc. Twelfth Int. Conf. on Phenomena in Ionised Gases, Eindhoven, Netherland; I, Paper 353.
5. D.E. Potter, Nucl. Fusion, 18, 813 (1978).
6. S. Lee, "A Plasma Focus Model Yielding Trajectory and Structure", Spring College on Radiation in Plasma, Trieste, May (1983).
7. S. Lee et. al, Sing. J. Phys., 1, 75 (1984).
8. S. Lee, J. Appl. Phys., 54, 3603 (1983).
9. S. Lee and Y.H. Chin, Bul. Fiz. Mal., 2(2), 105 (1981).
10. Y.H. Chen, Ph.D. Thesis, U.M., Kuala Lumpur, Malaysia (1978).
11. C.S. Wong, Ph.D. Thesis, U.M., Kuala Lumpur, Malaysia (1983).
12. S. Lee, Australian J. Phys., 36, 891 (1983).

J. Fiz. Mal. 6, 23 (1985)

DYNAMICS OF REB–SPUTTERED COPPER PLASMA JETS

S.LEE, HARITH AHMAD, T. Y. TOU, K. H. KWEK and C. S. WONG
Plasma Research Laboratory
Physics Department
University of Malaya,
Kuala Lumpur 22-11.

Abstract

A dense copper plasma jet, blasted out of the centre electrode of a plasma focus by the action of the focus-associated relativistic electron beam (REB), is studied by shadowgraphy. The jet is found to have a distinctive structure at least in the space between 1 to 4 cm downstream of the centre electrode, and flows in the time interval from several hundred ns up to at least 1.8 μs after focus time zero at a fairly constant speed of 2.2 cm/μs. The observations are consistent with a total jetted mass of ¼ mg per shot carrying 50 J of kinetic energy, with the copper atoms having each an energy of 300 eV.

Introduction

One distinctive characteristic of the plasma focus is that during the focusing action a large axial electric field is generated due to the rapid change of magnetic flux. Measurements of the centre-of-mass energy of fusion neutrons[1], among others[2], have indicated that the electric potential difference generated is of the order of 250 kV even for a small (12 kJ) plasma focus operated at 20 kV discharge voltage. This large induced voltage is also predicted by computation based on a dynamic slug model[3]. This large downstream-pointing electric field, whilst accelerating deuterons in the axial direction away from the centre electrode, also at the same time produces a relativistic electron beam (REB) which bombards the centre of the anode producing the very characteristic hole which is observed in every seasoned well-tuned focus. A typical estimate of the amount of copper excavated after 1000 shots indicates that about ¼ mg per shot is excavated by the REB in a typical Mathers-type machine operated at 12 kJ. This copper excavation is also consistent with the observation of a greenish flash of light whenever a deuterium focus is 'properly' focusing.

The extent and dynamics of the sputtering has hardly been studied[4]. This is because all the interest is concentrated in the 100 ns or so before and after focus time zero; when all the interesting characteristics and mechanisms, from the point of view of the densely focused plasma and its nuclear fusion and soft x-ray potential, occur. The copper plasma jet dominates the region up to 5 cm downstream only in the time between a few hundred ns to a few μs after focus time zero. Recent interest in this REB-sputtered plasma jet has arisen because of the possibility of generating very pure plasma jets which may be of importance for deposition applications. In the present work some characteristics of the copper plasma jet are deduced from shadowgraphs.

Experimental set-up and observations

The experimental set-up for laser shadowgraphy used for the University of Malaya

plasma focus has already been described[4]. The main difference in the present set-up is that the laser pulse-chopper is not used as it is not required since the speed of the jet is more than 10-fold slower than the final focusing speed.

For this series of shots, the focus is operated at 15 kV, 60μF in 10 torr deuterium. The centre electrode has a slightly hollowed-out face at the focusing end.

Figure 1 shows the ruby Q-switched laser pulse (λ = 6943 Å) used in this series of experiment. The laser beam, made parallel by means of a beam expander, is directed through the plasma focus chamber onto a photographic plate fitted with a 6943 Å narrow-band pass filter placed 2 m away. To produce a composite sequence of the Sputtering, the laser pulse is delayed, by means of a variable delay unit controlling the pockels cell Q-switch. By varying the laser pulse delay relative to the focus time zero, shadowgraphs of the copper jet could be obtained at different moments of time after focus time zero.

A fast photodiode, picking up a little scattered laser light from one of the beam steering mirrors, is used to register the time of laser pulse relative to focus time zero which is defined by the characteristic plasma focus voltage spike. These two timing pulses are displayed on a carefully real-time-aligned double beam oscilloscope. The resulting oscillograms (Figure 2a) enable the time of the shadowgraph, relative to focus time zero, to be measured to an accuracy of 20 ns.

Figure 2b is a shadowgraph showing the copper plasma jet just coming into view 1 cm beyond the end of the centre electrode. The timing of this shadowgraph is indicated by the oscillogram of Figure 2a at τ_D = 0.55 μs.

A composite time sequence of shadowgraphs is shown in Figure 3. Table 1 shows a tabulation of measured positions from the centre electrode as a function of measured delay time τ_D, relative to focus time zero. This data is presented in Figure 4 which indicates that the jetting speed of the sputtered material averages 2.2 cm/μs in the space from 1 to 4 cm downstream of the anode. This agrees with earlier piezoelectric pressure measurements[5]

The speed of the distinctive features of the jet remain fairly constant over the range of positions measured. It is reasonable to assume that this jet is an undriven free flow. The uniformity of its speed is therefore consistent with the idea of a jet composed of material of much greater density than the environment it is moving through. This indicates that the jetting material is not a deuterium structure but is composed of copper plasma jetting from the anode.

At the measured speed, the copper atoms possess kinetic energy of 300 eV each and using the previously estimated mass of ¼ mg a total kinetic energy of 50 J is assigned to the jet. Considering that the electrical input into the focus during the focusing action, as measured from the voltage spike and current dip of the focus, has been estimated at 1 to 2 kJ, this indicates that the electron beam carries with it a not insubstantial proportion of the energy in the plasma focus.

Discussion and conclusion

Time sequence shadowgraphs of the REB-sputtered copper jet of a plasma focus is presented. These show the structure and evolution of the copper plasma jet in the space 1 cm to 4 cm down-stream of the centre electrode up to 1.8 μs after the focus time zero. Over this range of observation the flow speed remains uniform and constant at 2.2 cm/μs. The measurements are consistent with a total copper mass in the plasma jet of ¼ mg carrying a total of 50 J of kinetic energy, and having individual atomic kinetic energy of 300 eV.

Preliminary observations of sputtered deposits on a flat glass plate indicate the possibility of depositing areas of very clean film of copper by this method. These observations also raise the possibility of producing plasma jets of other materials by simply placing an insert of the desired material in the anode cavity so that this insert may then be bombarded by the relativistic electron beam. This technique may have useful applications.

Acknowledgement

The technical assistance of Jasbir Singh and T.S. Toh is acknowledged. This research is funded by University of Malaya Research Grants No. 232/74 and No. 95/77.

References

1. S. Lee and Y. H. Chen, Mal. J. Sci., 3 (B), 159 (1975)
2. G. Decker and R. Wienecke, Physica, 82C, 155 (1976).
3. S. Lee. C.S. Wong, A. C. Chew, T. Y. Tou and Jalil Ali, Sing. J. Phys., 1, 75 (1984).
4. S. Lee and Y. H. Chin, Bul. Fiz. Mal., 2, (1981).
5. S. Lee and T. H. Tan, Procs. Seventh Euro. Conf. on Controlled Fusion and Plasma Phys., Lausanna Vol. 1 pp 65 (1975).

Table I : Tabulation of delay time, τ_D with the position of the front of the sputtered copper plasma. (from photographs shown in Fig. 3)

Delay time, τ_D in μs	Displacement from the central electrode (cm)
0.55	1.00
0.60	1.50
0.65	1.50
0.70	1.90
1.05	2.50
1.15	2.20
1.35	2.80
1.50	3.20
1.55	3.55
1.75	4.00

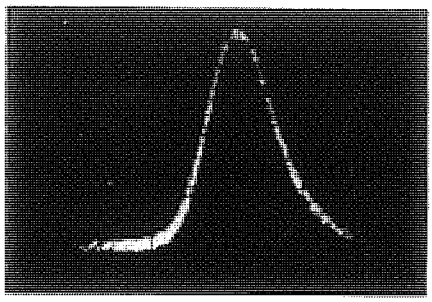

Fig. 1. Laser pulse from the JK 2000 Ruby Laser with pulsewidth of ~50 ns (FWHM).

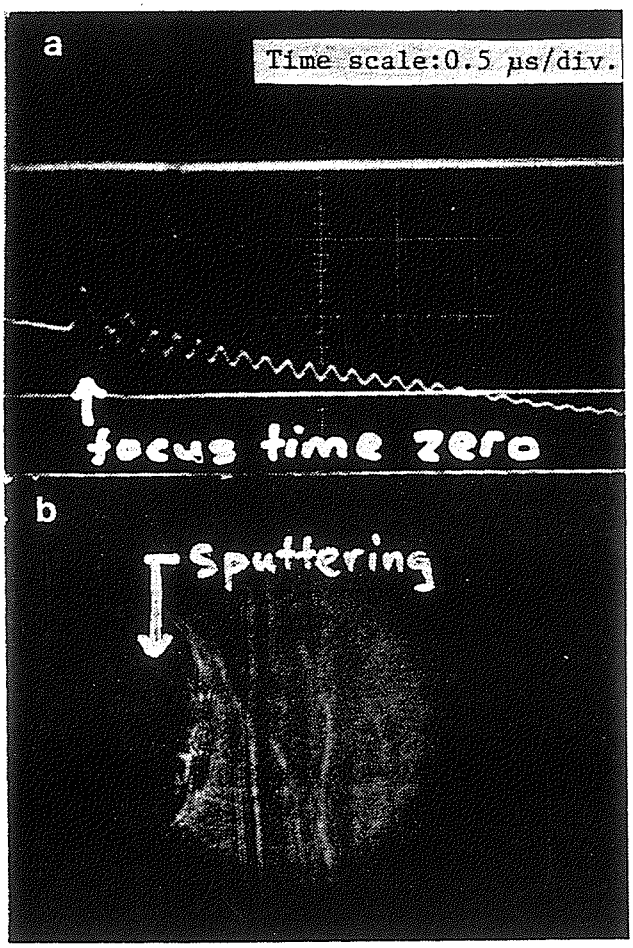

Photodiode signal.

Plasma focus voltage signal taken between the electrodes.

Fig. 2. (a) Temporal relationship between the photodiode and the plasma focus voltage signals. The delay time, τ_D, between the peaks of the two pulses is about 0.55 μs.
(b) Dark background indicates the emergence of copper sputtering from the central electrode.

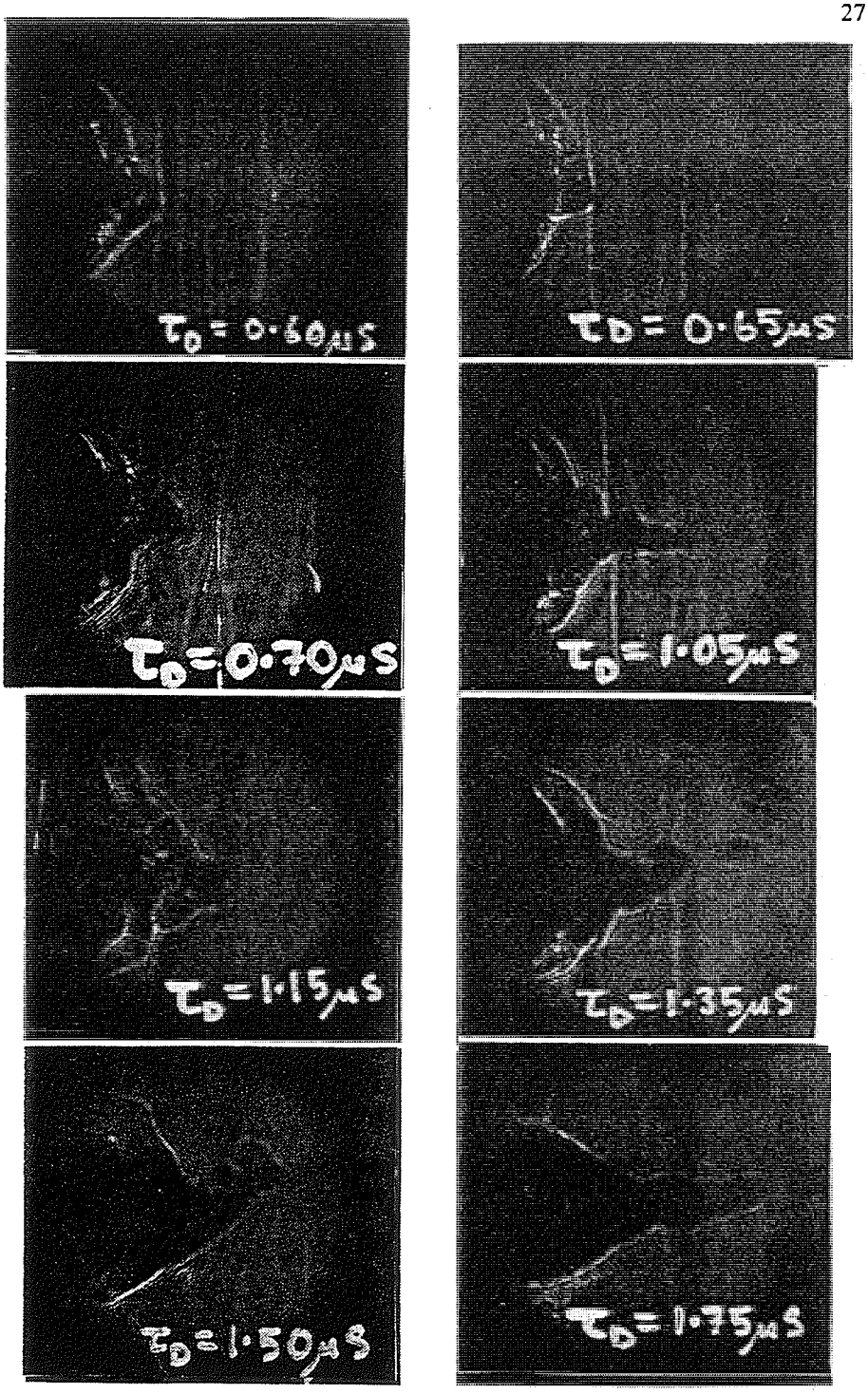

Fig. 3. Time sequence of the copper plasma jet.

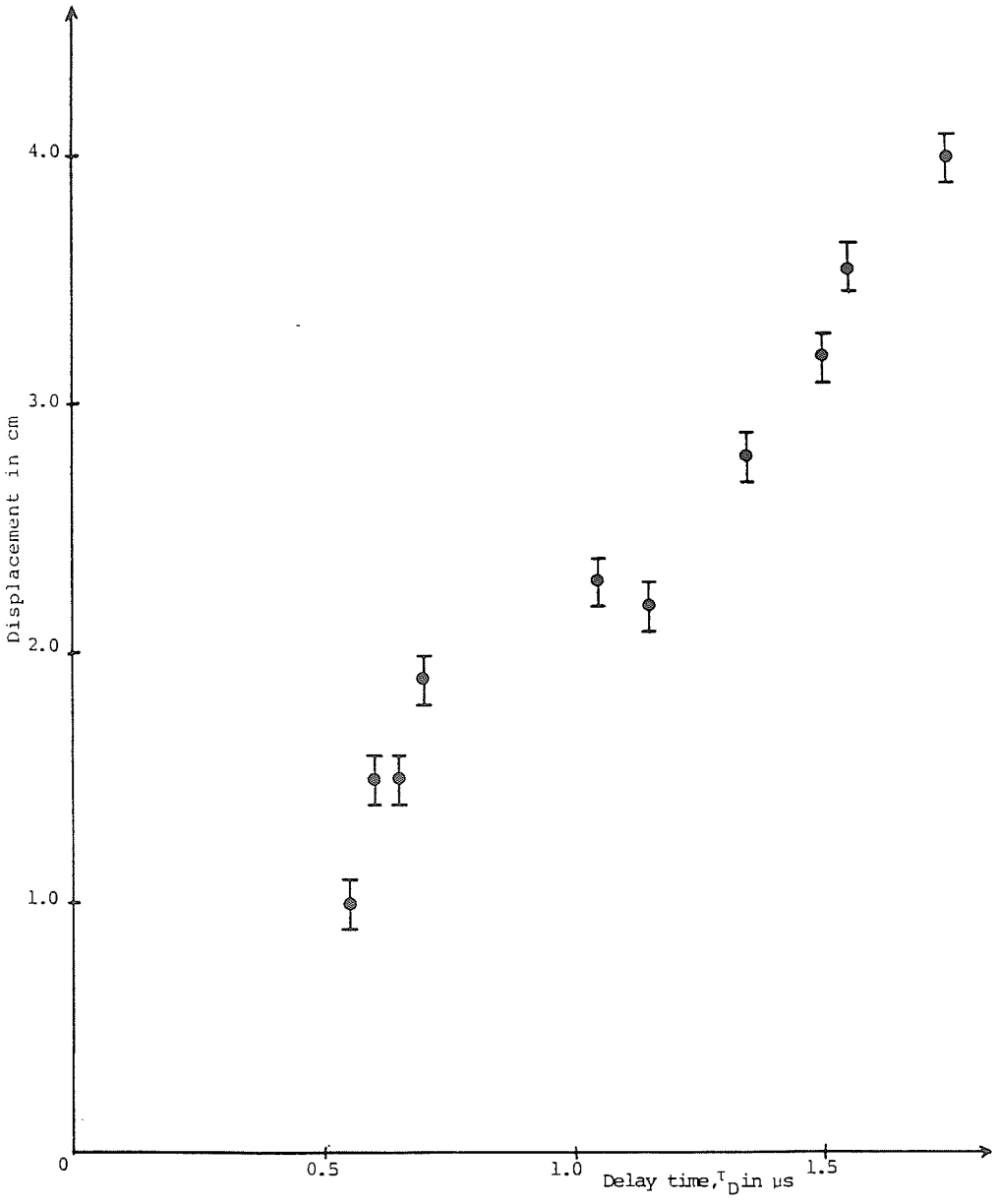

Fig. 4. Graph of plasma jet position against the delay time, τ_D.

Simple method of pulsed plasma discharge current analysis

C. S. Wong and S. Lee
Plasma Research Laboratory, Physics Department, University of Malaya, Kuala Lumpur 22-11, Malaysia

(Received 13 September 1984; accepted for publication 9 November 1984)

A simple method is proposed to analyze the current waveform of a pulsed plasma discharge from which the voltage waveform and hence the temporal evolution of the plasma inductance can be deduced. As an example, the application of the method to a typical plasma focus discharge is illustrated.

The measurements of the discharge current and the transient voltage induced across the plasma are essential in the experimental studies of pulsed plasma discharges. The discharge current can be measured conveniently by using a Rogowski coil operated as a current transformer.[1] Such a measurement is considered as the most basic diagnostic in the investigation of a pulsed plasma device. On the other hand, the measurement of the transient voltage across the plasma is often found to be more difficult than the current measurement. Recently, several designs of high-performance capacitive voltage dividers for measuring this transient voltage have been reported.[2,3] In these designs, the voltage probes are made an integral part of the plasma device. This may be difficult to implement in some situations, particularly in some existing experiments in small laboratories. In order to obtain sufficient information to enable the study of the discharge dynamics even without direct measurement of the transient voltage, we propose here a simple method to analyze the experimental discharge current waveform from which the voltage waveform can be deduced. Even in the case where the voltage waveform is being measured experimentally, this method of current analysis can be useful as a method to check the result of the voltage measurement.

Pulsed plasma devices are frequently powered by capacitor discharge, and a typical equivalent circuit of the discharge circuit is as shown in Fig. 1. In this circuit, C is the capacitance of the storage capacitor; L_e and R_e are, respectively, the inductance and resistance of the circuit external to the plasma. The effect of R_e is usually negligible as compared to the effect of L_e. The plasma is represented by a time-varying resistance $R_p(t)$ and a time-varying inductance $L_p(t)$ in the circuit.

When the capacitor is charged to a voltage V_0 and then discharged through the circuit, the instantaneous current $I(t)$ that flows through the circuit is described by the circuit equation as follows

$$V_0 - \frac{\int I(t)dt}{C} = \frac{d}{dt}[L(t)I(t)] + I(t)R_p(t), \tag{1}$$

where $L(t) = L_e + L_p(t)$ is the total inductance of the circuit. Rearranging Eq. (1) gives the voltage across the plasma at any instant as

$$V_p(t) = V_0 - \frac{\int I(t)dt}{C} - L_e\frac{dI}{dt}. \tag{2}$$

This equation can be normalized by introducing the following dimensionless parameters:

$$\tau = t/t_c,\ \iota(\tau) = I(t)/I_0,\ \upsilon_p(\tau) = V_p(t)/V_0,$$

where $t_c = \sqrt{(L_e C)}$ is the capacitor characteristic time and $I_0 = V_0\sqrt{(C/L_e)}$ is the short-circuited peak current. The normalized form of Eq. (2) is

$$\upsilon_p(\tau) = 1 - \int \iota d\tau - \frac{d\iota}{d\tau}. \tag{3}$$

Hence the instantaneous transient voltage induced across the plasma of a pulsed plasma discharge can be deduced if the explicit form of its current waveform is known. In practice, the form of $\iota(\tau)$ in Eq. (3) can be obtained by digitizing and then curve-fitting the measured current waveform. This will be illustrated in the following by analyzing the current waveform of a typical plasma focus discharge using the method outlined above.

A typical set of current and voltage waveforms obtained for the University of Malaya Dense Plasma Focus I (UMDPFI)[4] is shown in Fig. 2. The current waveform has

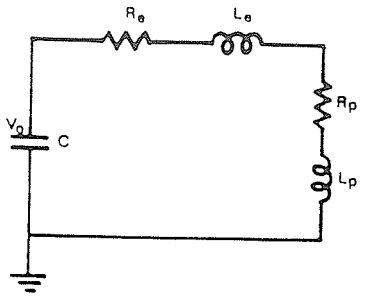

FIG. 1. Equivalent circuit of a pulsed plasma discharge.

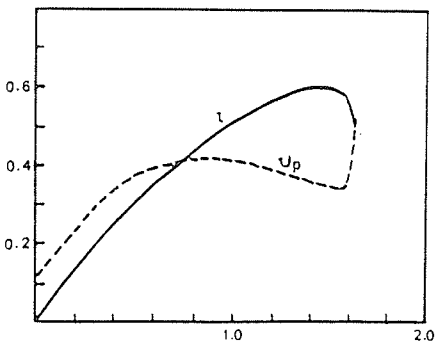

FIG. 2. Experimental current and voltage waveforms (in normalized forms) of a typical plasma focus discharge.

 0021-8979/85/115102-03$02.40

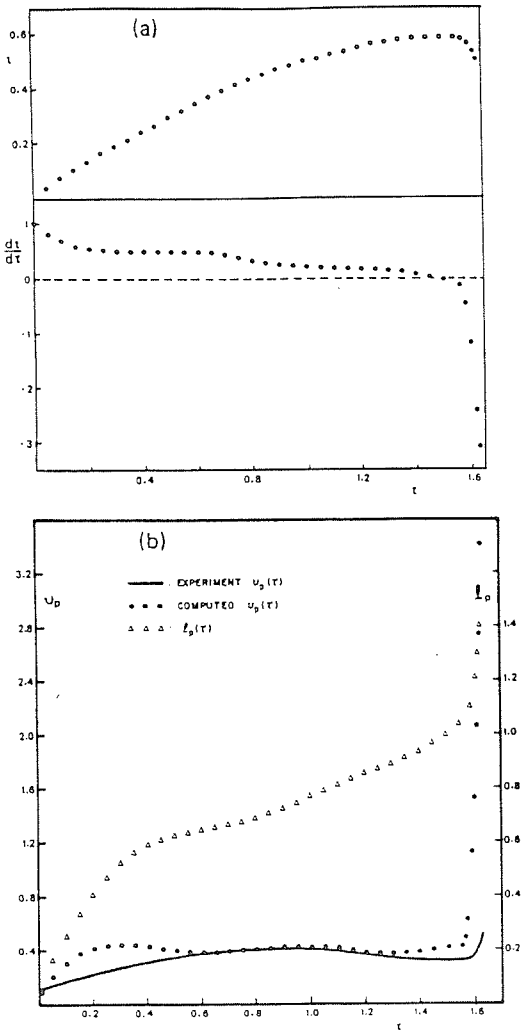

FIG. 3. Results obtained from the analysis of the plasma focus discharge current waveform in Fig. 2. (a) The curve-fitted $\iota(\tau)$ and the corresponding $d\iota/d\tau$. (b) Comparison of the experimental and the computed voltage waveforms and the temporal evolution of the focus tube inductance by assuming an inductive model for the focus discharge.

been carefully traced onto a graph paper and digitized to produce a set of points (τ, ι) to be curve-fitted into polynomial of $\iota(\tau)$. We shall confine ourselves to the interval between $\tau = 0$, to $\tau = 1.628$, where the current has reached the minimum of the dip.

Using the least-square curve-fitting technique, we obtain the following two polynomials of $\iota(\tau)$ for two time regimes:

Regime I. $\tau = 0$–1.54 (positive gradient),

$$\iota(\tau) = -2.8169\times10^{-5} + 0.9303\tau - 1.60595\tau^2 + 2.7603\tau^3 - 1.5817\tau^4 - 0.6485\tau^5 + 0.4259\tau^6 + 0.4689\tau^7 - 0.0966\tau^8 - 0.2278\tau^9 + 0.0832\tau^{10}; \quad (4)$$

Regime II. $\tau = 1.54$–1.628 (current-dip, negative gradient)

$$\iota(\tau) = -161.88 + 144.628\tau + 60.389\tau^2 - 24.935\tau^3 - 11.016\tau^4 - 41.092\tau^5 + 15.713\tau^6 + 4.649\tau^7 + 4.363\tau^8 - 2.825\tau^9. \quad (5)$$

It should be noted from these two polynomials that (i) at $\tau = 0$, $\iota \simeq 0$ which is expected experimentally; (ii) it can be deduced from Eq. (4) that $d\iota/d\tau = 0.9309$ at $\tau = 0$ which is close to unity; (iii) the value of ι at $\tau = 1.54$ is calculated to be 0.5935 from Eq. (4) and 0.6013 from Eq. (5) which are in good agreement; and (iv) similarly, the value of $d\iota/d\tau$ at $\tau = 1.54$ is calculated to be -4.3×10^{-3} from Eq. (4) and 0.064 from Eq. (5) which can both be approximated to zero. These considerations, together with point by point comparison of the computed and experimental values of ι at various τ indicates that the two polynomials (4) and (5) are accurate representation of the current waveform in the two respective time regimes.

The results obtained from the analysis of the current waveform in Fig. 2 are presented in Fig. 3. The curve-fitted current waveform, together with the corresponding $d\iota/d\tau$ are shown in Fig. 3(a); whereas the voltage waveforms, both computed and experimental, are shown in Fig. 3(b). The computed voltage waveform shows three distinctive regions: (i) the initial slow rise from $\tau = 0$ to $\tau = 0.25$, (ii) the roughly flat plateau region from $\tau = 0.25$ to $\tau = 1.54$, and (iii) the sharp spike which occurs from $\tau = 1.54$ to $\tau = 1.628$. In the measured voltage waveform, however, the voltage is seen to rise more slowly than the computed one, especially in the region of the sharp voltage spike. At the tip of the voltage spike, the measured value is only 0.53 whereas the computed value is as high as 3.4. This is believed to be due to the inadequate response of the probe used.[5] The features of the voltage waveform computed from the current analysis in fact resemble those observed by others,[6,7] although their observed voltage spikes are still low compared to our computation.

With the measured current waveform (curve-fitted into polynomials) and the voltage waveform computed as described above, the temporal evolution of the focus tube inductance can be deduced if an inductive discharge model is assumed. In terms of $v(\tau)$ and $\iota(\tau)$, the normalized form of the tube inductance is given by

$$l_p(\tau) = \frac{\int v_p(\tau)d\tau}{\iota(\tau)}. \quad (6)$$

This has been computed for the example considered here and the result obtained is shown in Fig. 3(b). The sharp rise in l_p corresponding to the current dip is a feature commonly observed for a typical plasma focus discharge. The rise in the focus tube inductance at the start of the discharge is unexpected from a consideration of the focus dynamics. This is probably due to the fact that at the start of the discharge, the tube resistance is not negligible and hence the inductive model is not valid. This tube resistance, however, will soon drop to a negligibly low level as the plasma is heated up. This is most likely to occur during the lift-off phase of the focus discharge dynamics.

We thank T. Y. Tou for providing the set of current and voltage waveforms of the UMDPFI for the above analysis.

[1]S. L. Leonard, in *Plasma Diagnostic Techniques*, edited by R. H. Huddlestone and S. L. Leonard (Academic, New York, 1965), Chap. 2.
[2]C. A. Ekdahl, Rev. Sci. Instrum. **51**, 1645 (1980).
[3]W. A. Edson and G. N. Oetzel, Rev. Sci. Instrum. **52**, 604 (1981).
[4]Parameters of the UMDPFI are listed in *World Survey of Major Activities in Controlled Fusion Research*; Nucl. Fusion Suppl. (IAEA, Vienna, 1982).
[5]S. Lee, C. S. Wong, A. C. Chew, T. Y. Tou, and Jalil Ali, Singapore J. Phys. **1**, 75 (1984).
[6]A. Bernard, A. Coudeville, A. Jolas, J. Launspach, and J. de Mascureau, Phys. Fluids **18**, 180 (1975).
[7]G. Decker, W. Kies, and G. Pross, Phys. Fluids **26**, 571 (1983).

J. Fiz. Mal. 6, 165 (1985)

PARAMETRIC STUDY OF THE NITROGEN LASER CIRCUIT

S. LEE, A.V. GHOLAP*, A.J. SMITH*, K.H. KWEK,
A. C. CHEW, T.Y. TOU, S. SAPRU*.
United Nations University Training Programme
Plasma and Laser Technology
Physics Department
University of Malaya
Kuala Lumpur, Malaysia

Abstract

A non-dimensionalised model for the pulsed nitrogen laser circuit is developed and scaling parameters are identified so as to enable a study of the laser over its range of discharge modes. Results are presented for the critically damped laser gap and for the more typical case of damping factor of 0.3. The analysis shows that in a typical nitrogen laser the rate of rise of laser gap voltage $\frac{dV_g}{dt}$ prior to laser gap breakdown is 0.5 kV/ns and experiments reported in the literature suggest that such a $\frac{dV_g}{dt}$ is required for a uniform breakdown across the laser gap as a pre-requisite for good lasing action. A laser pulse width of about 5ns is also predicted for lasing threshold at a normalised power level of 0.3.

Introduction

The transversely excited pulsed nitrogen laser depends for its operation on two important requirements: (i) a uniform discharge occurring throughout the length of the discharge channel – this uniformity depends on a sufficiently fast rate of rise of voltage dV_g/dt across the laser gap, and (ii) a sufficiently high rate of energy absorption in the laser gap plasma during the main discharge. Whilst the second requirement is generally well known since population inversion has to be achieved in a time shorter than the relevant transition life time of 40 ns the first requirement of a minimum dV_g/dt is not so well known. This requirement may be seen in the following way.

The laser channel consists of two long parallel-placed electrodes[1,2] forming a constant gap of about 1 cm along the whole length ($\sim$ 50 cm). The gap is at about 100 torr of nitrogen. Although the gap may be set at a uniform spacing, local irregularities exist and at any given time the breakdown voltage across this gap will vary, if only by small

*UNU Fellows with the following permanent addresses;
A.V. Gholap; Physics Dept., Rivers State University of Science and Technology,
Port Harcourt, Nigeria.
A.J. Smith; Physics Dept., Njala University college, Sierra Leone.
S. Sapru; Electronics Dept., Sri Pratap College, Srinagar, India.

amounts, from point to point along the gap. If such a gap is subjected to a slow rising voltage difference across it, i.e. dV_g/dt is small, then when the voltage difference becomes suficient to break down that point of the gap which happens to have the lowest breakdown voltage at that given time, the gap will break down at that point. As soon as that point breaks down, a pulse of zero voltage will traverse the length of the gap at the speed of electromagnetic waves, thus stopping any further breakdown except at the first point of breakdown.

However, if an infinitely fast rising pulse is applied i.e. $dV_g/dt \rightarrow \infty$, then after the first point breaks down and as the pulse of zero voltage traverses away from the point of breakdown, the other points will also breakdown because before the pulse of zero voltage arrives, these points have already been stressed to breakdown by the infinitely rising voltage pulse. It may be seen from this argument that for uniform breakdown the rate of rise of gap voltage dV_g/dt must be such that the point (in the gap) with the highest breakdown voltage (due to surface differences) rises to this breakdown voltage before the pulse of zero voltage arrives from the first breakdown point. Thus there is in general a minimum dV_g/dt for uniform breakdown. This value will of course depend on uniformity of gap spacing and electrode surface condition. In general again however nitrogen laser gaps will have been built to a high standard of uniformity of gap setting and gap surface condition. It then remains to be seen if a minimum dV_g/dt may be experimentally observed to be required for good uniformity. To help answer this question a lumped parameter model for the nitrogen laser circuit is set-up. Such a circuit theory has been discussed[1,2,3]. However in these earlier discussions the circuit equations are solved for specific cases. In the present work the circuit equations are written with greater details and are non-dimensionalised so that scaling parameters are identified. The scaling parameters are then varied to cover a wide range of operation of the nitrogen laser. The computations are used to determine the rate of rise of laser gap voltage dV_g/dt and the rate of energy absorption at the laser gap as functions of the scaling parameters.

Theory

A typical nitrogen laser circuit may be represented by Fig. 1. The fast parallel plate capacitors C_1 and C_2 with very low inductances L_1 and L_2 are charged to voltage V_o and connected to the laser gap represented by a resistance r_g and an inductance L_{go} as shown in the diagram. The inductances L_{g1} and L_{g2} represent the channel inductance on either side of the laser gap. The capacitor C_2 is connected to an external spark gap represented by resistance r_e in the diagram and with inductance L_e. Typically $C_1 \sim 20nF$, $C_2 \sim 10nF$, $L_1 \sim 0.4nH$, $L_2 \sim 0.2nH$, $L_{g1} \sim L_{g2} \sim 0.8nH$, $L_{go} \sim 3nH$ and $L_e \sim 30nH$. The external spark gap resistance r_e has a value such that the external circuit $L_2 - L_e - r_e - C_2$ is fairly oscillatory; whilst for good and fast energy transfer one would hope to design for r_g to have such a value that the laser discharge circuit i.e. $C_1 - L_1 - L_{g1} - r_g - L_{go} - L_{g2} - L_2 - C_2$ should be nearly critically damped. However one would expect that typically this latter circuit would be less than critically damped.

When the external spark gap switches at $t = 0$ the voltage V_2 drops from its initial value V_0, swings negative towards $-V_0$ with a time constant given by $\sim \sqrt{(L_e C_2)}$ since $L_e >> L_2$, thus providing a rate of rise of gap voltage of the order of $2V_o/\sqrt{(L_e C_2)}$ which if sufficient should cause the laser gap to not only breakdown, but to breakdown uniformly at time $t = t_s$. The main dischage between C_1 and C_2 should then occur with a

short time constant $\sim \sqrt{(L_1 + L_2 + L_g)(C_1 C_2)/(C_1 + C_2)}$, where $L_g = L_{g1} + L_{g2} + L_{go}$, modulated with a slower discharge with time constant $\sim \sqrt{\{L_e (C_1 + C_2)\}}$ which subsequently removes all the stored energy through the external spark gap r_e.

The equations describing the discharge sequence are as follows: For $0 \leqslant t < t_s$ (before laser gap breakdown):

$$I_L = 0 \tag{1}$$

$$L_2 \frac{dI_e}{dt} + L_e \frac{dI_e}{dt} + r_e I_e = V_o - \frac{\int I_e dt}{C_2} \tag{2}$$

where I_L = laser circuit current, I_e = external circuit current, with initial conditions:

$$t = 0,\ I_e = 0,\ \frac{\int I_e dt}{C_2} = 0,\ \frac{dI_e}{dt} = \frac{V_o}{L_2 + L_e} .$$

For $t_s \leqslant t$ (after laser gap breakdown) equations (1) and (2) are replaced by

$$L_2 \frac{dI_e}{dt} - L_2 \frac{dI_L}{dt} + L_e \frac{dI_e}{dt} + r_e I_e = V_o - \frac{\int I_e dt}{C_2} + \frac{\int I_L dt}{C_2} \tag{3}$$

and

$$L_1 \frac{dI_L}{dt} + (L_{g1} + L_{go} + L_{g2}) \frac{dI_L}{dt} + L_2 \frac{dI_L}{dt} - L_2 \frac{dI_e}{dt} + r_g I_L \tag{4}$$

$$= V_o - \frac{\int I_L dt}{C_1} - V_o - \frac{\int I_L dt}{C_2} + \frac{\int I_L dt}{C_2} .$$

At the moment of laser gap breakdown i.e. $t = t_s$, the values of I_e, dI_e/dt and $\int I_e\, dt$ are known from the numerical integration of Eq. (2) whilst the other values necessary to start the integration of Eqs. (3) and (4) are

$$t = t_s,\ I_L = 0,\ \int I_L dt = 0 \text{ and}$$

$$\left\{\frac{dI_L}{dt}\right\}_{t_s} = \frac{\left\{\frac{\int I_e dt}{C_2}\right\}_{t_s} + \left\{L_2 \frac{dI_e}{dt}\right\}_{t_s}}{L_1 + L_2 + L_g} .$$

Normalisation

The equations (1), (2), (3) and (4) and the conditions at $t = 0$ and $t = t_s$ are normalised by putting:

$$\tau = t/t_o, \quad i_e = I_e/I_o, \quad i_L = I_L/I_o$$

where $t_o = \sqrt{(L_2C_2)}$ and $I_o = V_o/\sqrt{(L_2/C_2)}$.

This normalisation procedure gives us the governing equations and conditions in the following form:

$$0 \leqslant \tau < \tau_s : \quad \frac{di_e}{d\tau} = (1 - \int i_e d\tau - \alpha_e i_e) / (1 + \beta_e) \tag{5}$$

with starting conditions: $\tau = 0, \; i_e = 0, \; \int i_e d\tau = 0$

$$\text{and } \frac{di_e}{d\tau} = \frac{1}{1+\beta_e}$$

where the scaling parameters $\beta_e = L_e/L_2$ and $\alpha_e = r_e/\sqrt{(L_2/C_2)}$.

and for $\tau \geqslant \tau_s$:

$$\frac{di_e}{d\tau} = \frac{1 - \int i_e d\tau + \int i_L d_\tau - \alpha_e i_e + \frac{di_L}{d\tau}}{1 + \beta_e} \tag{6}$$

$$\text{and} \quad \frac{di_L}{d\tau} = \frac{\int i_e d\tau - (1+\delta) \int i_L d\tau - \alpha_e \alpha_1 i_L + \frac{di_e}{d\tau}}{1 + \beta_1 + \beta_g} \tag{7}$$

with starting conditions for this phase given by:

$$\tau = \tau_s, \quad i_e = (i_e)_{\tau_s}, \quad \int i_e d\tau = (\int i_e d\tau)_{\tau_s}, \quad \frac{di_e}{d\tau} = (\frac{di_e}{d\tau})_{\tau_s}$$

being given by the numerical integration of Eq. (5) up to $\tau = \tau_s$ and also at $\tau = \tau_s$,

$$i_L = 0, \; \int i_L d_\tau = 0 \text{ and } (\frac{di_L}{d\tau})_{\tau_s} = \frac{(\int i_e d\tau)_{\tau_s} + (\frac{di_e}{d\tau})_{\tau_s}}{1 + \beta_1 + \beta_g}$$

where the scaling parameters are:

$$\beta_1 = \frac{L_1}{L_2}, \quad \delta = \frac{C_2}{C_1}, \quad \alpha_1 = \frac{r_g}{r_e} \text{ and } \beta_g = \frac{L_g}{L_2}$$

Besides the values of i_e and i_e other important quantities to be obtained from this exercise are:

(a) Laser gap voltage, for $\tau < \tau_s$: $\upsilon_g = \frac{d\imath_e}{d\tau} + \int \imath_e d\tau$ and (8)

for $\tau \geqslant \tau_s$: $\upsilon_g = \frac{d\imath_e}{d\tau} + \int \imath_e d\tau - \int \imath_L d\tau (1+\delta) + (1+\beta_1 + 2\gamma\beta_g) \frac{d\imath_L}{d\tau}$ (9)

where $\gamma = \frac{L_{g_1}}{L_g} = \frac{L_{g_2}}{L_g}$.

It is worthwhile to note that the measured voltage across the laser gap is usually taken between the points V_{M1} and V_{M2} (Fig. 1) and is given by

$$\upsilon_M = \upsilon_{M1} - \upsilon_{M2}$$

$$= \int \imath_e d\tau - \int \imath_L d\tau + \frac{d\imath_e}{d\tau} - \frac{d\imath_L}{d\tau} - \delta \int \imath_L d\tau - \beta_1 \frac{d\imath_L}{d\tau} \qquad (10)$$

It should be noted that before laser gap switching this voltage is equal to υ_g the spark gap voltage.

(b) Power absorbed by laser gap

The power absorbed by the laser gap $I_L^2 r_g$ may be normalised to the average power of discharge of the $C_1 - L_1 - L_g - L_2 - C_2$ circuit. This average discharge power may be written as

$$\frac{\frac{1}{2} C_1 V_0^2}{\sqrt{\{(L_1 + L_2 + L_g)\ (\frac{C_1 C_2}{C_1 + C_2})\}}}$$

(c) Effective parameters controlling discharge modes

The performance of the laser depends on the discharge modes of (a) the $C_2 - L_2 - L_e - r_e$ circuit (external circuit) and (b) the $C_1 - L_1 - L_g - r_g - L_2 - C_2$ circuit (the laser gap circuit). The mode mentioned here refers to the degree of damping in the respective circuit. Ideally from the electrical parameters one would like to have the external circuit of (a) to be nearly undamped in order to have the biggest voltage reversal thus enhancing the maximum value of V_g. On the other hand for the laser-gap circuit of (b) the biggest power developed in the gap is for the case of critical damping. The effective parameters controlling the damping of these two circuits are:

For the external circuit

$$\alpha_{eff\text{-}e} = \alpha_e \sqrt{\left(\frac{L_2}{L_2 + L_e}\right)} = \alpha_e \sqrt{\left(\frac{1}{1 + \beta_e}\right)} \qquad (11)$$

For the laser-gap circuit

$$\alpha_{eff\text{-}L} = \frac{r_L}{\left\{\frac{L_1 + L_2 + L_g}{\left(\frac{C_1 C_2}{C_1 + C_2}\right)}\right\}} = \alpha_e \alpha_1 \sqrt{\left\{\frac{1}{(1 + \beta_1 + \beta_g)(1 + \delta)}\right\}} \qquad (12)$$

Computation procedure

Computation of this model is performed by numerical integration using the Euler's linear approximation method which proves to be of sufficient accuracy if a time step of 0.001 is used.

The starting conditions are as described earlier and the laser gap is switched at the time when the voltage v_2 has reached – 0.7.

Results and discussion

To study the electrical behaviour of the circuits as a function of $\alpha_{eff\text{-}e}$ and $\alpha_{eff\text{-}L}$ we note that typically we may have the following values of circuit elements :

L_2 = 0.18 nH
L_1 = 0.4 nH
L_{g1} = 0.75 nH = L_{g2}
L_{go} = 3 nH
C_2 = 10 nF
C_1 = 20 nF
L_e = 32 nH

giving

β_1 = 2.2
β_e = 178
δ = 0.5
β_g = 10
γ = 0.42

We first choose a typical value for $\alpha_{eff\text{-}e}$ as 0.1 (external circuit lightly damped). This gives from Eq. (11), α_e = 1.34.

Case 1 : Laser gap circuit critically damped : $\alpha_{eff\text{-}L}$ = 2

Choosing the case of a critically damped laser gap circuit for good power transfer we note that for $\alpha_{eff\text{-}L}$ = 2, we require, from Eq. (12),

α_1 = 6.6

Results for this case are presented in Fig. 2. The voltage υ_2 falls from 1.0 through $\upsilon_2 = 0$ at $\tau = 21.5$ to $\upsilon_2 = -0.7$ at $\tau = 34.0$ when the laser gap is set to break down. On breakdown the voltage υ_2 rises sharply as the laser electrodes are momentarily separated only by the voltage $L_{go} \frac{dI_L}{d\tau}$. However as I_L rises quickly, the voltage drop across the electrodes is quickly dominated by the term $r_g I_L$ so that υ_2 drops once again to about $\upsilon_2 = -0.5$ before rising again in a damped oscillation with periodic time of about $70t_o$, as the capacitors C_1 and C_2 eventually discharge through the external spark gap. Between the time $\tau = 34$ to $\tau = 50$ the laser gap current I_L flows in its critically damped mode. The corresponding power goes up to a peak of 0.57 in $3t_o$ and drops back down with a FWHM value of $5t_o$.

Case 2: Laser gap with effective damping factor of $\alpha_{eff\text{-}L} = 0.3$.

Although the critically damped case may be the mode for maximum power, there are indications that the typical case reported in the literature has a damping factor that is close to $\alpha_{eff\text{-}L} = 0.3$. For this value of $\alpha_{eff\text{-}L}$ we have from Eq. (12).

$$\alpha_1 = 1.0.$$

Results for this case are computed and shown in Fig. 3. As in case 1, υ_2 drops from 1.0 to -0.7 at $\tau = 34.0$, then rises sharply on laser gap breakdown and continues with an oscillation of periodic time of $\sim 18t_o$ superimposed on the slower periodic time of $\sim 90t_o$ of the external circuit. This behaviour is also reflected in the $\imath_e$ curve.

The laser gap current $\imath_L$ rises to a peak value of 0.33 in a time of $4t_o$ and oscillates in a damped mode with a periodic time of $\sim 18t_o$ with modulation. The corresponding power developed across the laser gap resistence has a peak value of 0.42 and a FWHM value of $5.5t_o$. The voltage υ_M that may be measured across the laser electrode (i.e. outside the laser channel) is also shown in Fig. 3.

From the above results the value of $\frac{dV_g}{dt}$ for a typical nitrogen laser may be estimated. We note that a typical value of $t_o = \sqrt{(L_o C_o)}$ is 1.3 ns. Operating at a voltage of 15 kV, the average dV_g/dt is $(1.7 \times 15\ kV) / (34 \times 1.3)\ ns \sim 0.5$ kV/ns. Such a value is experimentally known to be able to initiate the uniformity of discharge which is the first requirement in the nitrogen laser mechanism. We may compare this value with experimental values reported in the literature[4,5,6].

The FWHM value for the power peak is $5t_o$ (6.7 ns) for the critically damped laser channel and $5.5t_o$ (7.4 ns) for the more typical case of the laser channel with effective damping factor of 0.3. It may be expected then that such a typical nitrogen laser will have a full width pulse of less than 7.4 ns after consideration of threshold effect. For example for the case of $\alpha_{eff\text{-}L} = 0.3$, if the lasing threshold is at a power level of 0.3 then the full width of the laser pulse would be $3.5t_o$ or 4.7 ns. This is a typically observed value.

Conclusion

A non-dimensionalised model for the nitrogen laser circuit is developed and scaling parameters are identified. It is shown that the external circuit should be little damped so as to maximise the rate of rise of laser gap voltage in order to ensure uniformity in breakdown across the laser gap. The laser gap circuit should be critically damped from the point of view of optimum laser gap power. However the typical case of an effective damping factor of 0.3 for the laser gap circuit yields a full width laser pulse of about 5 ns for lasing thresholds at a power level (normalised) of 0.3.

From the analysis a typical value of $dV_g/dt \sim 0.5$ kV/ns is suggested as being required for good uniformity of discharge in the laser gap.

Acknowledgement

We (A.V.G., A.J.S. and S.S.) acknowledge the assistance of United Nations University Fellowships without which this work could not have been completed. We also acknowledge University of Malaya Research Grant no. 95/77.

References

1. Eward T. Gerry, Applied Physics Letters **7**, 6 (1965).
2. W.A. Fitzsimmons, L.W. Anderson, L.E. Riedhauser and Jan. M. Vrtilek, IEEE J. Quantum Electronics QE-12, 624 (1976).
3. Chugusa Iwasaki and Takahisa Jitsuno, IEEE J. Quantum Electronics QE-18, 423 (1982).
4. H. Strowald and H. Salzmann, Appl. Phys. Lett. 28, 272 (1976).
5. M. Montaser Foad Sabry, A. Hassan, M. Ewaida, J. Phys. E Sci. Instrum, 17, 103 (1984).
6. I.N. Knyazev, Opt. Commun, 6, 250 (1972).

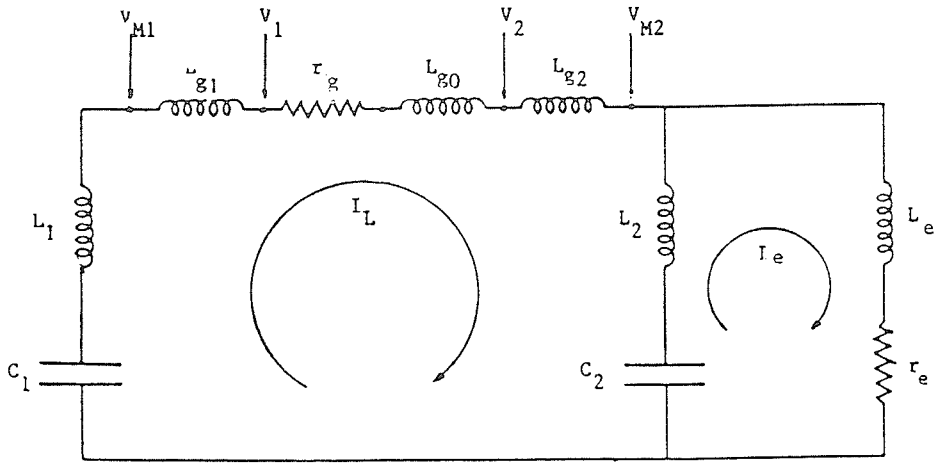

Fig. 1 Equivalent circuit for nitrogen laser.

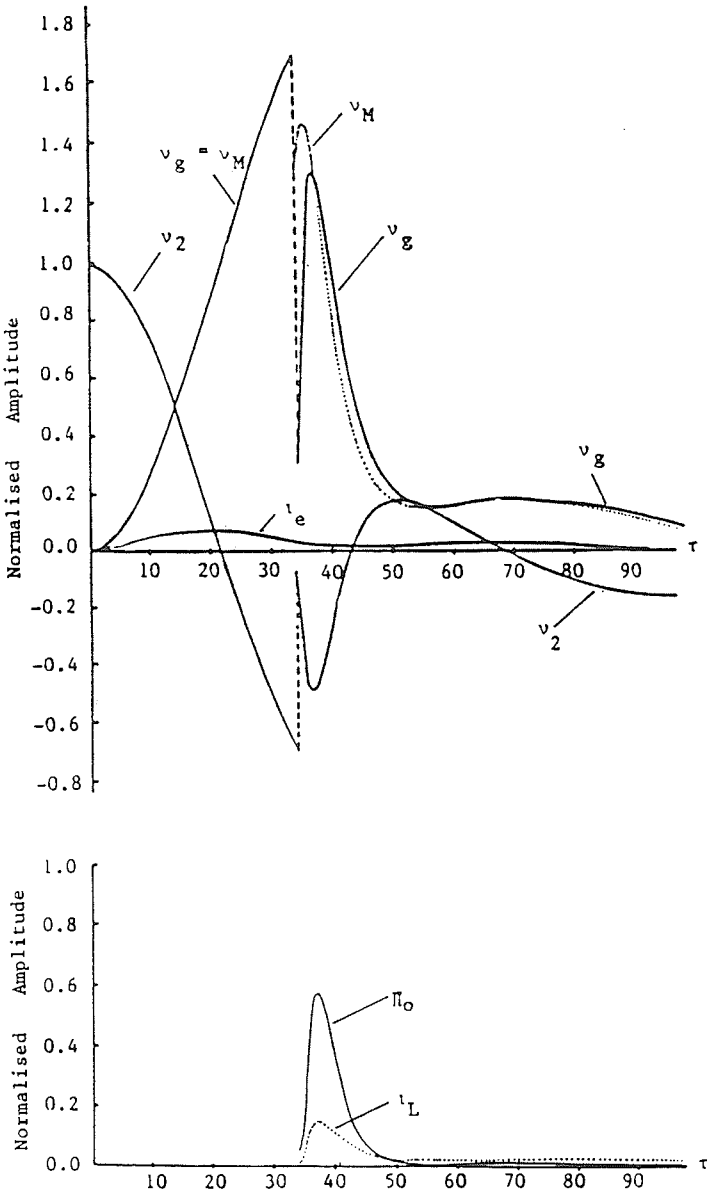

Fig. 2 Solutions of currents, voltages and laser gap power for $\alpha_{\text{eff-e}} = 0.1$ and $\alpha_{\text{eff-L}} = 2$ (laser gap critually damped)

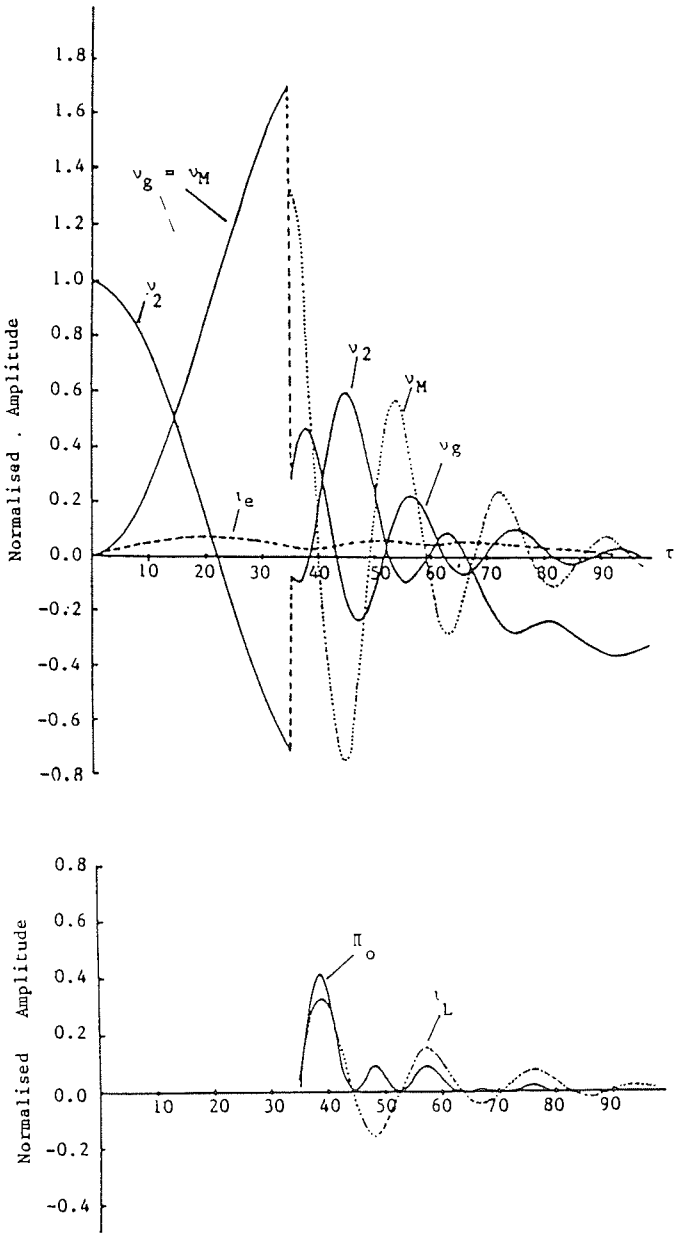

Fig. 3 Sulutions of currents, voltages and laser gap power for $\alpha_{\text{eff-e}}$ = 0.1 and $\alpha_{\text{eff-L}}$ = 0.3 (laser gap lightly damped).

ENERGETIC PLASMA-INJECTED PARTICLES FOR SPUTTERING APPLICATIONS

Harith and S. Lee
Physics Dept., University of Malaya
Kuala Lumpur 22-11, Malaysia.

INTRODUCTION

As a result of advancement in lasers, there has been a revival in optical industries, especially those which manufacture mirrors and coated lenses. A major portion of these industries can be categorized as small-scale industries. Primarily they are involved in producing laser mirrors and also provide thin-film coatings service. There has been a rapid growth in thin-film technology whereby nowadays we can get broadband laser mirrors with reflectivity of $\sim$ 100%.

There are two major techniques in coating thin-films on suitable substrates namely,

(i) vacuum evaporation and
(ii) vacuum sputter deposition

The former is a well-known technique. By increasing the temperature of the material until its vapour pressure is high enough, $P > 10^{-2}$ Torr with respect to ambient pressure which is sufficiently low, the vapour from the hot source will deposit on the substrate.

Procs. International Conference on Physics and Industry, September 1985, Jakarta - Ed. Parangtopo et al (1985)

Sputtering utilizes a different physical principle whereby it involves accelerating a gas ion and allowing it to collide with the film source material. During this collision, the gas ions transfer their momentum and energy to the atoms in the source material. As a result of this, the atoms in the source material will be ejected out and form a thin film onto the substrate.

At present, research work and experiments are focussed in improving the techniques of sputtering rather than observing the dynamical behaviour of the sputtered particles. In this paper we would like to report observations of the dynamics of sputtered particles in plasma focus machine.

EXPERIMENTAL ARRANGEMENT AND OBSERVATIONS

In the observations of the dynamic behaviour, a JK 2000 ruby laser system is used to illuminate the sputtered particles. This gives a shadow pattern as a result of different refractive indices in the plasma (1).

The plasma focus machine used in this experiment is the Mathers-type operated at 12kJ with deuterium filled pressure of 10 Torr, operating voltage, V = 15kV and capacitor bank of 60 μF. Detailed aspects of the operational procedure of this has been reported elsewhere (2). Basic experimental arrangement is shown in Fig. 1.

It comprises a JK2000 laser system, plasma focus machine with its associated capacitor bank and electronics, a delay system and

an optical beam deflector with a camera back (3). In this experimental set-up synchronization is very important. Timing must be precisely varied to coincide the illumination laser pulse with the sputtered particles which requires a delay time $\sim$ 3.03 μs (typically, depending on operating pressure and voltage) after the initiation of the axial phase in the plasma focus machine.

With both the laser and focus tube systems charged and ready, on pressing the manual start-push button on the JK laser system, a trigger pulse will trigger the flashlamp. This pulse will also trigger the delay unit DU1 with delay time set at 1.25ms. The output pulse of DU1 is then used to trigger the 2D21 thyratron unit which triggers the krytron unit. The krytron unit in turn triggers the ignitrons which act as a switch in the plasma focus machine. Output pulse from the thyratron unit also controls the triggering of the oscilloscope as well as the second delay unit DU2. The DU2 controls the delayed triggering of the Pockell cell which when triggered allows the laser pulse to go through and illuminate the sputtering process occuring in the focus tube. The shadowgrams are obtained with the help of a camera back covered with a narrow-band filter at λ = 6943 Å.

Fig. 2 shows the Ruby laser pulse with pulsewidth of $\sim$ 50ns (FWHM) which is narrow enough to resolve the time spectrum of the sputtering action. The synchronization and delaying of pulses is shown in Fig. 3 between the voltage spike taken across the electrodes of the plasma tube and the laser pulse

which is derived from the photodiode signal placed at mirror M1. By adjusting the delay units, the laser pulse can be precisely timed to coincide and resolve the dynamical process of sputtering from the centre electrode of the plasma focus tube.

When the plasma collapsed into the radial phase, a large axial electric field is generated due to the rapid change of magnetic flux. Measurements (4 & 5) have indicated that the electric potential difference generated is of the order of 250kV even for a small 12kJ plasma focus operated at 20kV discharge voltage. This large electric field produces a relativistic electron beam (REB) which bombards the centre of the anode, thus producing the sputtered copper atoms which is collected on a microscopic glass slide.

A typical estimate of the amount of copper excavated after 1000 shots indicates that about $\frac{1}{4}$mg per shot is excavated by the REB.

Fig. 3b is a shadowgraph showing the copper plasma jet just coming into view 1cm beyond the end of the centre electrode. The timing of this shadowgraph is indicated by the oscillogram of Fig. 3a with delay time, τ_D = 0.55 μs. A composite time sequence of shadowgraphs is shown in Fig. 4.

A tabulation of measured positions from the centre electrode as a function of measured delay time τ_D, relative to focus time zero is shown in Table 1. This data is presented in Fig. 5 which indicates that jetting speed of the sputtered material averages 2.2 cm/μs in the space from 1 to 4 cm downstream

of the anode. This agrees with earlier piezoelectric pressure measurements (6).

DISCUSSION AND CONCLUSION

Time sequence shadowgraphs of the REB - sputtered coppec jet of plasma focus is presented. These show the structure and evolution of the copper plasma jet in the space of 1 cm to 4 cm dowstream of the centre electrode up to 1.8 μs after the focus time zero. Over this range of observation the flow speed remains uniform and constant at 2.2 cm/μs. It is resonable to assume that this jet is an undriven free flow. The uniformity of its speed is therefore consistent with the idea of a jet composed of material of much greater density than the environment it is moving through. This indicates that the jetting material is not deuterium structure but is composed of copper plasma jetting from the anode.

At the measured speed, the copper atoms possess kinetic energy of 300 eV each and using the previously estimated mass of $\frac{1}{4}$ mg, a total kinetic energy of 50 J is assigned to the jet.

Preliminary observations of sputtered deposits on a flat glass plate indicate the possibility of depositing areas of very clean film of copper by this method. From these observations, it is possible to produce this film coatings of different materials simply by inserting the desired materials in the anode cavity.

REFERENCES

1. V. Dvorak, Ann. Phys. Lpz. 9, 502 (1880) and U. Ascoli - Bartoli, S. Martellucci, E. Mazzucato 6th Conference on Ionization Phenomena in Gases, SECTION VIII, 23 (Paris 1963)

2. "Laser and Plasma Technology", editors : S. Lee, B.C. Tan, C.S. Wong and A.C. Chew; World Scientific Publishing Co. Pte Ltd. (1985), Singapore.

3. S. Lee and Y.H. Chin, Buletin Fizik, 2, 105 (1981)

4. S. Lee and Y.H. Chen, Mal. J. Sci., 3(B) 159 (1975)

5. G. Decker and R. Wienecke, Physica, 82C, 155, (1976)

6. S. Lee and T.H. Tan, Procs. Seventh Euro. Conf. on Controlled Fusion and Plasma Physics, Lausanna Vol. 1, p65 (1975).

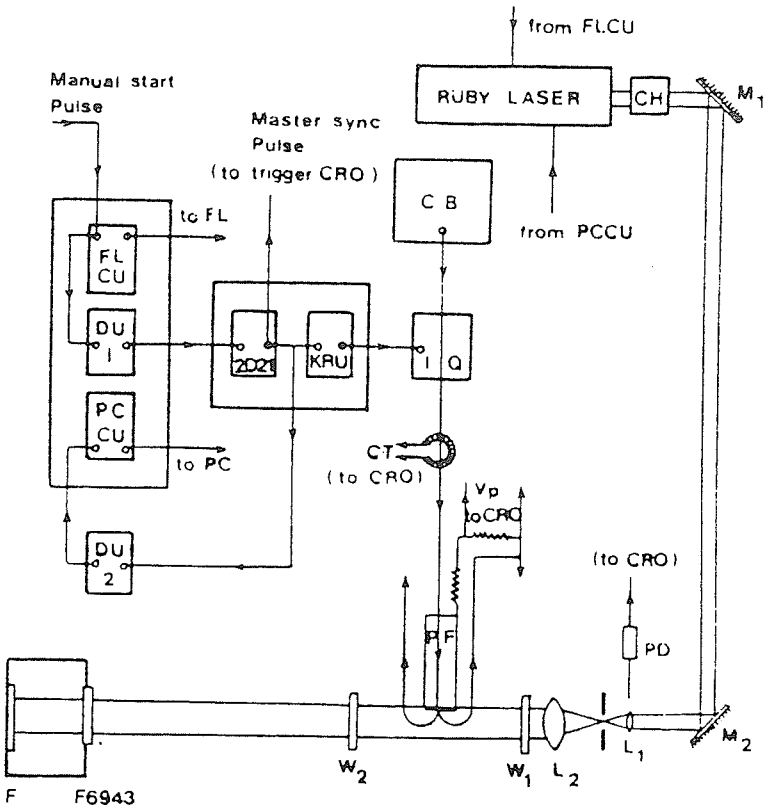

Figure 1 : Synchronising circuit and optical set - up for shadowgraphy (not to scale).

FLCU = Flash lamp control unit
CH = Pulse chopper
2D21 = Thyratron 2D21
CB = 60 F capacitor bank operated at 20 kV
L = Lens
M = Laser mirror
FP = Plasma focus tube
VP = Voltage probe
F6943 = Narrow band filter centred at 6943 Å
DU = Delay unit
PCCU = Pockel cell control unit
KRU = Krytron trigger unit
IG = ignitrons switching the capacitor bank
W = Window
F = Polaroid film
CT = Current transformer
PD = Photodiode

Table 1 : Tabulation of delay time, τ_D with the sputtered plasmoids displacement for photographs shown in Fig. 3.

Delay time, τ_D in μs	Displacement from the central electrode (cm)
0.55	1.00
0.60	1.50
0.65	1.50
0.70	1.90
1.05	2.50
1.15	2.20
1.35	2.80
1.50	3.20
1.55	3.55
1.75	4.00

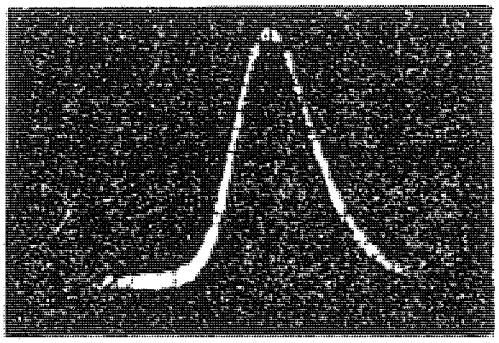

Fig. 2 : Laser pulse from the JK 2000 Ruby Laser with pulsewidth of ~50 ns (FWHM).

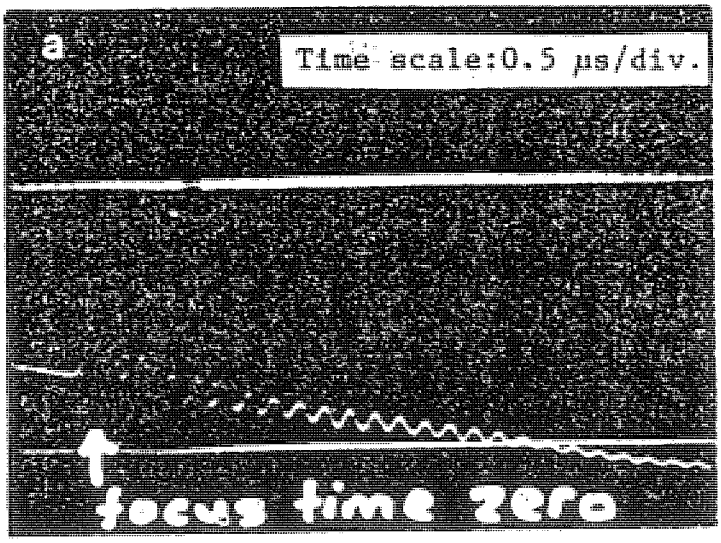

Photodiode signal

Plasma focus voltage signal taken between the electrodes.

Fig. 3a : Temporal relationship between the photodiode and the plasma focus voltage signals. The delay time, τ_D between the peaks of the two pulses is about 0,55 μs.

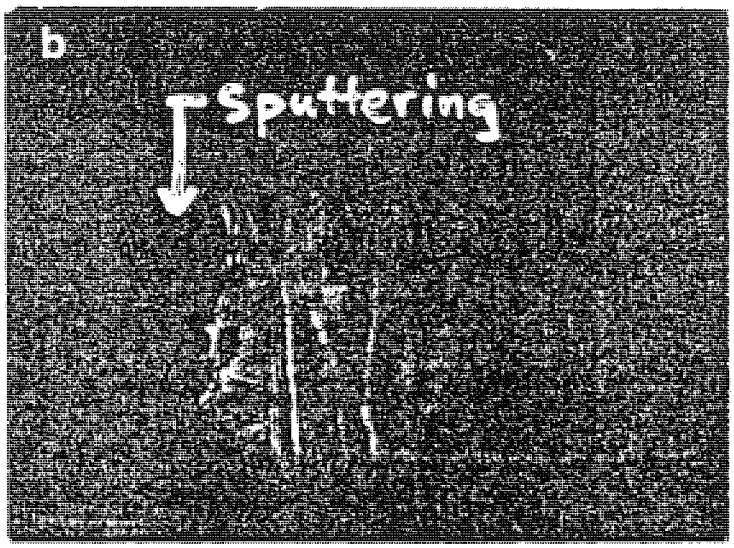

Fig. 3b : Dark background indicates the emergence of copper sputtering from the central electrode.

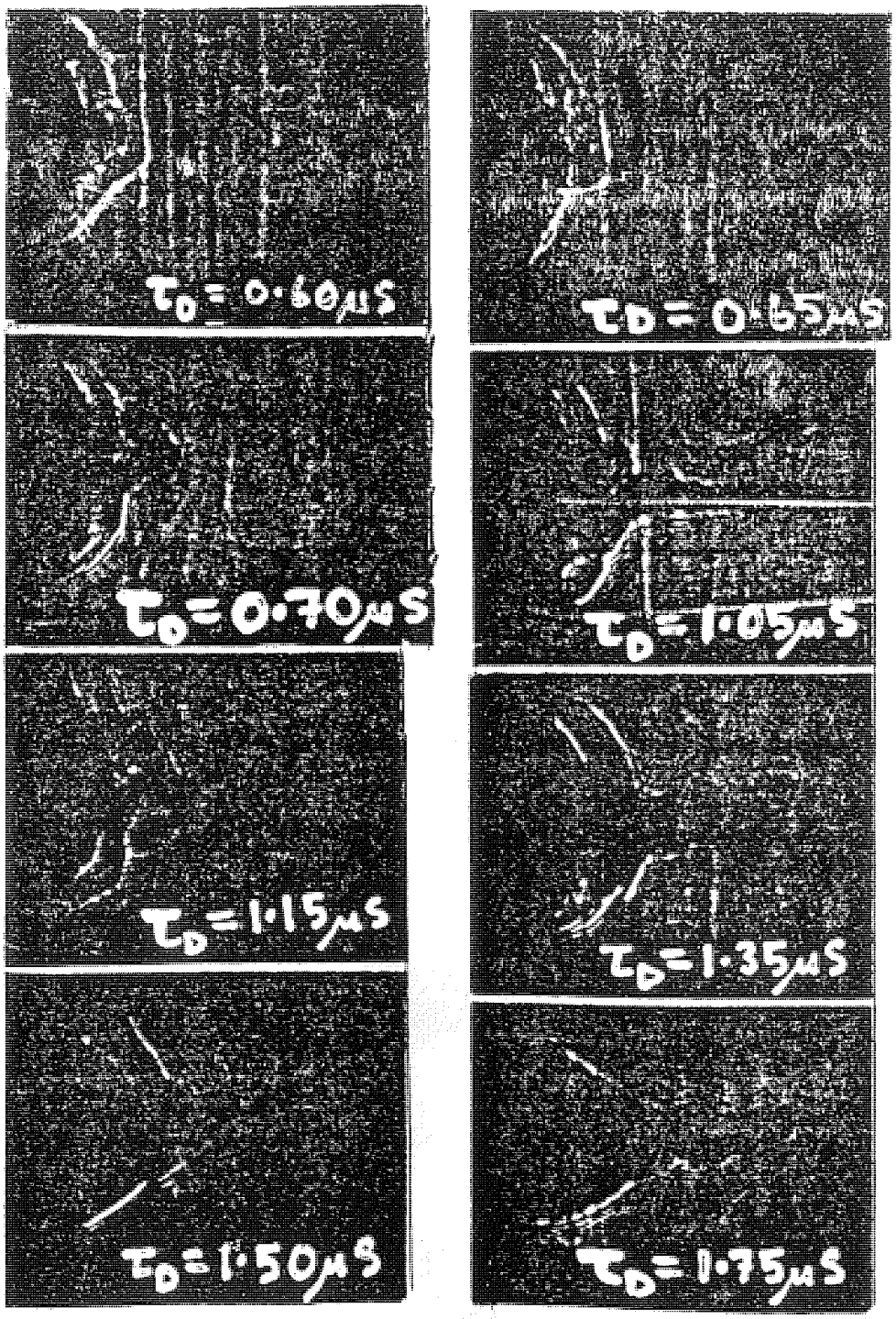

Fig 4. Time sequence of the copper plasma jet.

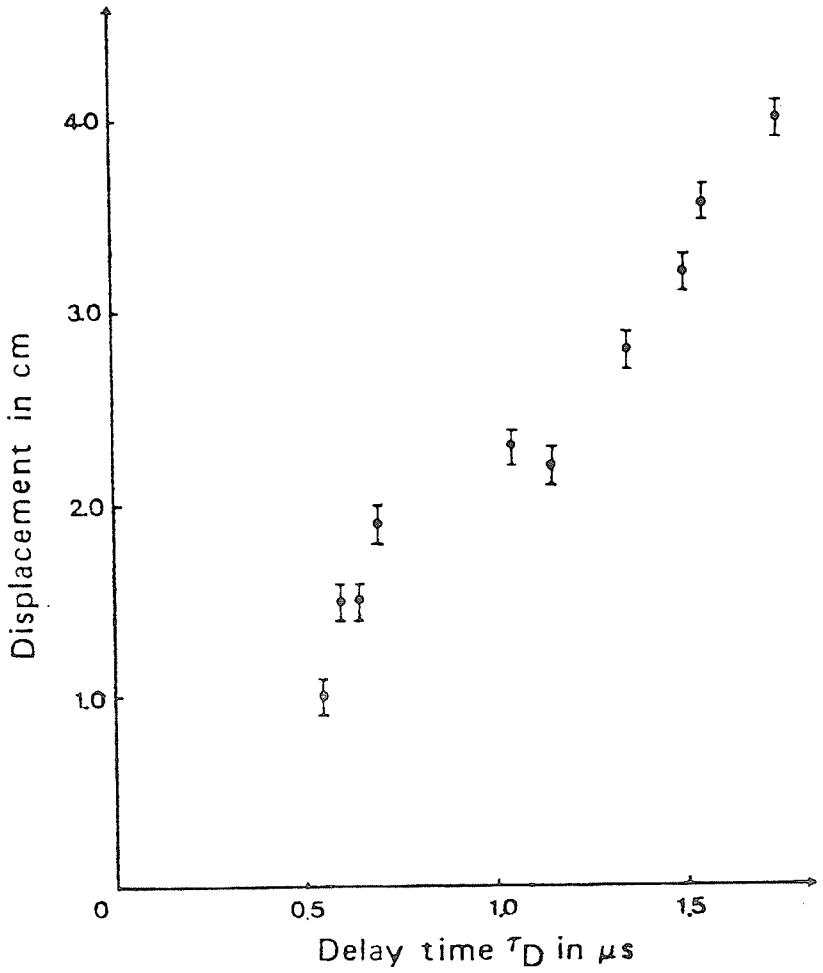

Fig .5. Graph of plasma jet position against the delay time, τ_D

sing, J. Phys., Vol. 3, No. 1, 1986. 75-82

TOROIDAL PLASMOIDS IN AN ELECTROMAGNETIC SHOCK TUBE

S. Lee, M. Eissa*, A.V. Gholap*, K.H. Kwek,
S. Mulyodrono*, S. Sapru*, A.J. Smith*, Suryadi*, T.Y. Tou
W. Usada*, C.S. Wong and Mohamad Zakaullah*

United Nations University Training Programme
Plasma and Laser Technology
Physics Department, University of Malaya
Kuala Lumpur, Malaysia

A toroidal plasmoid enclosed by poloidal current loops is identified in an electromagnetic shock tube. At current reversal the plasmoid becomes completely decoupled from the capacitor bank. The plasmoid is estimated to have an energy content (magnetic and kinetic) of 95J, being 6% of the initial capacitor energy, and is stable at least from t = 8.5 μs to t = 14 μs as evidenced from the measurement of the remnant magnetic flux. It is proposed that this energy content could be increased by operating the shock tube in a more efficient regime and also by means of enhancing the current of the second half cycle so as to provide additional drive for the plasmoid.

Introduction

Current loops in compressed plasmas have been studied in a Z-pinch and the relevance of these loops to other important plasma configurations such as the plasma focus and tokamaks have been inferred[1].

In this present study it is shown that current loops also feature prominently in a coaxial electromagnetic shock tube. The study of such loops in a shock tube besides having the advantage of simplicity and ease of interpretation has also a feature of special interest. The closed loops surround and define toroidal plasmoids and it is well known that the toroidal geometry may possess properties of stability of interest to fusion technology. Using a magnetic field mapping technique[2] parameters

* M.A.A. Eissa, Physics Department, Al-Azhar University, Cairo, Egypt
A.V. Gholap, Physics Department, Rivers State University of Science and Technology, Port Harcourt, Nigeria
S. Mulyodrono, Indonesian National Institute of Aeronautics and Space, (LAPAN) Jakarta, Indonesia
S. Sapru, Physics Department, Sri Pratap College, Kashmir, India
A.J. Smith, Physics Department, Njala University College, Sierra Leone
Suryadi, PPBMI, BATAN, National Atomic Energy Agency, Yogyakarta, Indonesia
W. Usada, PPBMI, BATAN, National Atomic Energy Agency, Yogyakarta, Indonesia
M. Zakaullah, Physics Department, Quaid-I-Azam University, Islamabad, Pakistan

of these plasmoids are measured including speed, volume, energy content and time history.

Experimental

This study is performed in an electromagnetic shock tube which has previously been described[3]. As illustrated in Fig. 1 the shock tube has an inner radius of a = 2 cm, an outer radius of b = 3.8 cm and a length of z_o = 20 cm. The breakdown occurs over a glass insulator at the back-wall which has a ring knife-edge attached to the cathode to promote a uniform axisymmetric breakdown. The outer electrode consists of a ring of 8 equally spaced rods forming a coaxial cylindrical structure.

The magnetic probe consists of a small coil of 30 turns SWG44 enamelled copper wire wound on a plastic former 1 mm in diameter. The assembly is placed in a glass tubing (see Fig. 1). The output of the coil is taken out by a pair of wires tightly twisted around each other and connected by coaxial cable to a 50 MHz double beam oscilloscope. The glass tubing is movable without breaking the vacuum so that the axial position, Z, of the probe coil may be moved from Z = nearly zero to Z = 20 cm.

The capacitor system driving the shock tube has capacitance C_o = 60 μF, inductance L_o = 115 nH (inclusive of inductances of capacitor, ignitron switch, connecting plates, connecting coaxial cables and shock tube flange). Operated at 7 kV (i.e. 1.5 kJ) it attains a peak current of 145 kA at t = 4.2 μs. With an argon pressure of 1 torr the shock tube operates with the scaling parameters $\alpha \sim 0.25$ and $\beta \sim 0.2$ where $\alpha = t_o/t_a$ is the ratio of the capacitor bank characteristic time of $\sqrt{(L_o C_o)}$ to the shock tube characteristic transit time[3] and β is the ratio of the shock tube inductance to the external inductance. With these values of α and β the shock tube operates in a mode of rather low energy transfer from the capacitor bank. The shock wave trajectory and current waveform have been computed according to a circuit coupled slug model[3].

Results

Figure 2 shows a series of oscillograms each displaying magnetic probe and current coil signals obtained from the same shot. Time sychronisation is carefully observed. From the magnetic signals, composite profiles of the azimuthal magnetic field $B_\theta(Z)$ as a function of Z are obtained at different times t using the method of Burkhardt and Lovberg[2]. These are displayed in Fig. 3.

These $B_\theta(Z)$ profiles show a magnetic structure that moves with time down the shock tube. The increase in magnetic field B_θ in the front of the magnetic field profile represents the current sheet. In the time between 3-5 μs when the shorck wave system is well formed and strongly driven by the current sheet the width of the current sheet structure is

1 cm. Since the magnetic probe is calibrated the absolute rise of B_θ is measured and the data indicates that between 3-5 μs nearly the full capacitor current flow through this current sheet.

At 4.5 μs i.e. just after peak current also corresponding to capacitor voltage reversal, the profiles show that there is a tendency for a closed current loop to be formed, with axial dimension of 2 cm. Because of the axisymmetry of the system, this current loop represents a toroidal system, like a doughnut around the inner electrode, with the current flowing in the poloidal direction of the torus. From the B_θ profile it is seen that the minor section of this torus has expanded in axial dimension to 6 cm by t = 6 μs. This current loop carries the full capacitor current across the front edge, with about half this value of current, reversed, flowing in the backward moving edge of this loop. Behind this loop a second current sheet is evident carrying sufficient current to bring the value of the current flowing out of the shock tube back to the capacitor current flowing at that time.

By t = 8.5 μs, the front of the loop is at Z = 15 cm and the rear of this loop has moved back to Z = 5 cm. At this time the capacitor current has dropped to zero and the magnetic field distribution shows that the current distribution in the shock tube has formed a completely closed loop with the value of B_θ rising from zero at Z = 15 cm to a maximum value of 0.28T at Z = 10 cm, dropping in a partial current loop to value of 0.12T at Z = 5 cm, then rising to 0.2T at Z = 4 cm and finally dropping to zero at the backwall Z = 0 to form the completely closed current loop, decoupled from the capacitor bank.

After t = 9 μs as the capacitor current reverses, a second current sheet carrying reversed flux moves down the shock tube pushing the closed current loop with its remnant flux ahead of it. This closed current loop surrounds and defines a toroidal plasmoid as shown in Fig. 4. The remnant flux is evident up to t = 14 μs corresponding to the time of peak negative current. The decay of the magnetic flux corresponds to a power release of 2 MW into the plasmoid.

From the magnetic field distribution of trajectory and speed of the current sheet have been plotted in Fig. 5. These results agree with theoretical computation based on a circuit coupled snow-plow model[3]. Moreover the speed of 2 cm/μs in argon from t = 2 to 5 μs gives a magnetic Reynolds number[3] of 4. Thus the shock tube may be considered as operating in a typically reproducible electromagnetic mode.

Estimates of the magnetic and kinetic energies in the shock tube are obtained from the magnetic field distribution and assuming a reasonable snow-plow action. These estimates are shown in Fig. 6. The magnetic energy in the shock tube peaks at 66 J at t = 5 μs just after peak current, then drops rapidly until at t = 8.5 μs it has a value of 10 J as the current loop decouples from the capacitor bank. The kinetic

energy also rises in the early stages, but remains below the value of magnetic energy until about 5 = 5.5 μs. This is consistent below the fact that dI/dt is positive during the quarter cycle so that the magnetic component of the input power into the shock tube exceeds that going into 'mechanical' energy of the plasma. After the current peak, dI/dt goes negative making it possible for the kinetic energy to exceed the magnetic energy attaining a peak value of 90 J at about t = 8 μs. It is estimated that the closed loop toroidal plasmoid starts off with a kinetic energy of 85 J and a magnetic of 10 J. This energy content represents 6% of the initial capacitor energy. The internal energy of the plasmoid may also be estimated to be around 85 J at this time since shock theory predicts an equipartition between the kinetic and the internal energy modes.

Discussion and Conclusion

Mapping of the azimuthal magnetic field in a coaxial shock tube enables the identification of the formation of a partial current loop just after peak current and a completely capacitor decoupled current loop. This completely decoupled loop enclosing a toroidal plasmoid is formed just as the capacitor current goes negative at t = 8.5 μs. This second, negative, current sheet then drives the toroidal plasmoid and its remnant magnetic flux which remains evident, although of decreasing amplitude, up to t = 14 μs.

The energy content, magnetic plus kinetic, of the toroidal plasmoid totals 95 J or 6% of the original stored capacitor energy. This compares with an estimated peak energy in the shock tube of 130 J just after peak current. The present shock tube study is made in the low energy efficiency regime of $\alpha = 0.2$ and $\beta = 0.23$. It is expected that a considerable increase in percentage energy storage in the toroidal plasmoid can be attained by operating at the more efficient regime of $\alpha = 1$ and $\beta = 1$.

The stability of the moving toroidal plasmoid extending from t = 8.5 μs to t = 14 μs may prove of some interest; particularly as the plasmoid may be compressed and its energy further increased by enhancing the magnitude of the current of the second half cycle. This could be done by suitably switching on another capacitor bank. These plasmoids may then be extracted from the shock tube for plasma injection purposes or as a toroidal plasma in its own rights.

Acknowledgement

The authors (M. Eissa, A.V. Gholap, S. Mulyodrono, S. Sapru, A.J. Smith, Suryadi, W. Usada and M. Zakaullah) thank the United Nations University for UNU Fellowships which make their participation in this work possible. We also acknowledge the support of Universiti Malaya

research grant F232/74.

References

1. I. Ya. Butov and Yu. V. Matveev, Sov. Phys. JETP 54(2), 299 (1981).
2. L.C. Burkhardt and R.H. Lovberg, Phys. Fluids 5(3), 341 (1962).
3. S. Lee in Laser and Plasma Technology, ed. by S. Lee, B.C. Tan, C.S. Wong and A.C. Chew pp. 3 - pp. 35, World Scientific Pub. Co. (1985).

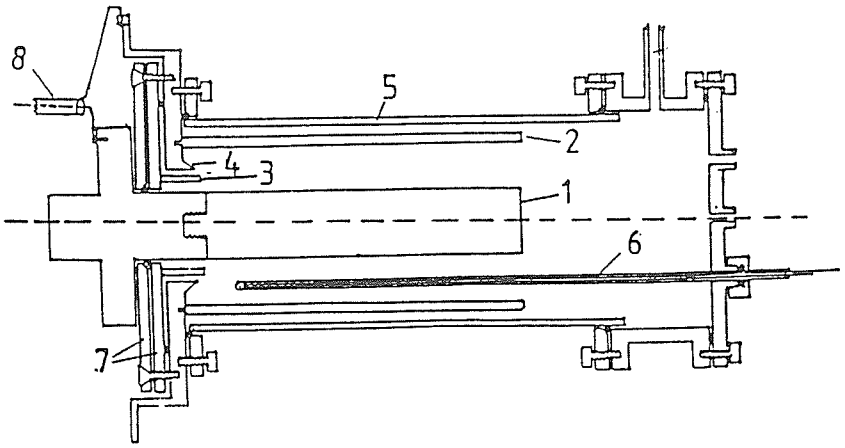

Fig.1 Schematic of the electromagnetic shock tube
1=anode 2=cathode consisting of a ring of rods
3=background glass insulator 4=cathode knife-edge
5=glass cylinder 6=magnetic coil in movable glass jacket
7=perspex insulator 8=coaxial cables from ignitron switch

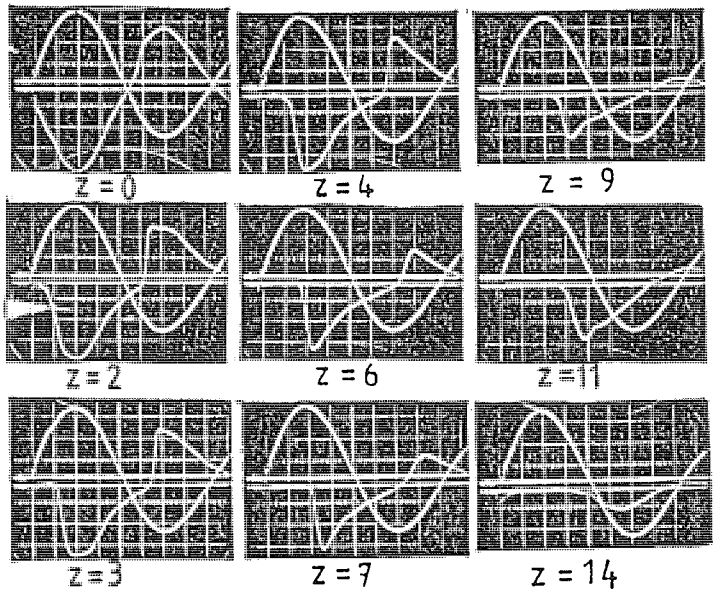

Fig.2 Oscillograms of discharge current (top trace) and magnetic probe (bottom trace) signals. The position of the magnetic probe is shown (in cm) below each oscillogram; horizontal scale: 2μsec/cm (1 big division =1cm)
vertical scale: 39kA/cm for current coil;
0.23T/cm for magnetic coil (z=0 to 9 cm)
0.12T/cm for magnetic coil (11 & 14 cm)

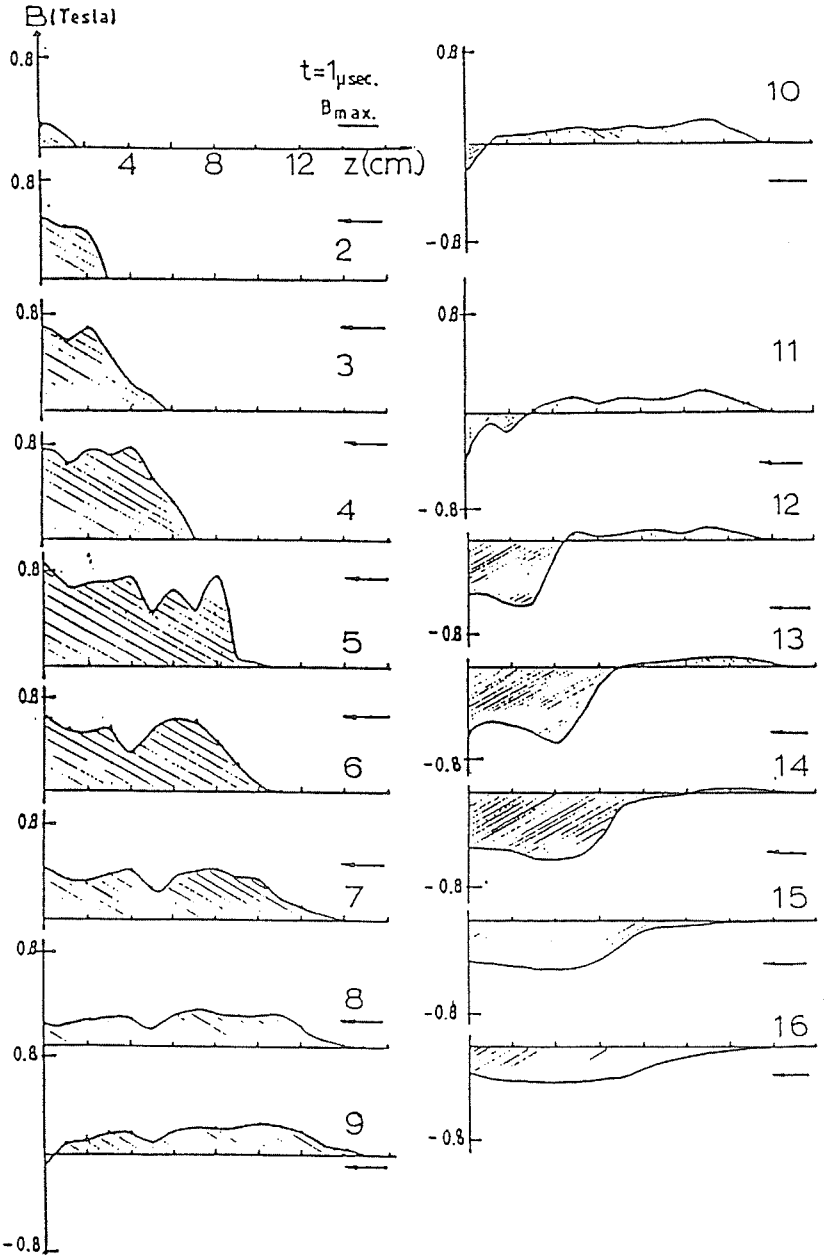

Fig.3 Distribution of azimuthal magnetic field B_θ in the shock tube for different times t=1 μsec to t=16 μsec obtained from the B_θ signals of Fig.2. The arrow on the right of each profile is $B_{\theta max}$ corresponding to the magnetic field at the probe positioned at radial position 3.1 cm if all the capacitor current at that time t were to flow past the probe.

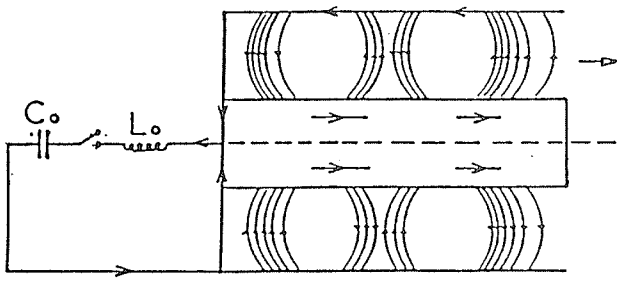

Fig.4 Schematic reconstruction of current loops defining a moving toroidal plasmoid at t=9μsec (compare with Fig.3 t=9μsec)

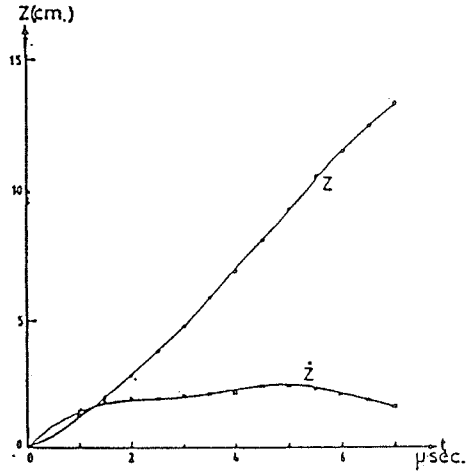

Fig.5 Experimentally obtained trajectory; z is position and $\dot{z}$ is speed. Maximum $\dot{z}$ occurs at t=5μsec and has a value of 2 cm/μsec

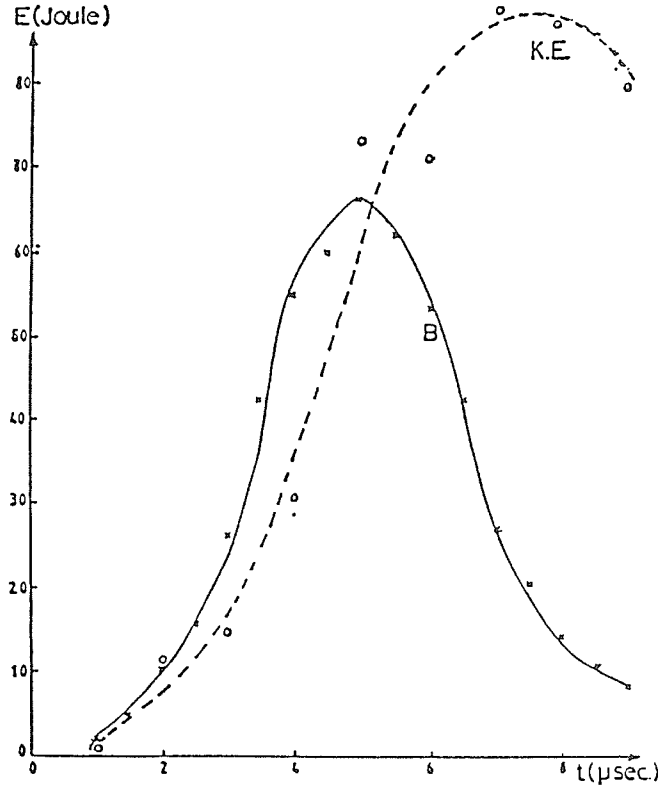

Fig.6 Magnetic (B) and kinetic (K.E.) energies estimated from the profiles of Fig.3 and from Fig.5 using a simple snow-plow model

Initiating Physics Research in Developing Countries

Since October 1985, the United Nations University (UNU)/International Centre for Theoretical Physics (ICTP) Training Programme on Plasma and Laser Technology has been conducted at the University of Malaya. The 6-month programme is attended by 8 specially selected UNU Fellows.

The aim of the Training Programme is to help developing countries initiate experimental research in plasma/laser physics by the transfer of a comprehensive technology package, sufficient to enable a UNU Fellow to build a plasma/laser device, complete with basic measurement and computational capabilities, back at his home institution.

This Training Programme is part of a wider concept of regional cooperation for research initiation to facilitate technology sharing/transfer among developing countries. There exist in many developing countries research groups which have built up, over the last one or two decades, a self-contained environment for research, incorporating all the technical and physics elements required for a sustained research effort. Some of these group have the capacity and willingness to take the initiative in research initiation and transfer. Our proposal is to use the facilities and resources of such a group to prepare a programme to transfer its total research technology to another group in the region having an interest in and a commitment to the subject area offered.

The concept of such a research initiation had been submitted in the form of a specific proposal for a Training Programme in Plasma Physics at the University of Malaya to various international bodies in 1983. Following communication with Mr. Soedjatmoto, the Rector of the United Nations University, and a site visit by Dr. Walter Shearer, Senior Programme Officer of UNU, in May 1984, the UNU responded by establishing an exploratory training course on plasma and laser physics at the University of Malaya with the cooperation of the University of Malaya and the Malaysian Institute of Physics.

In accordance with the UNU's rigorous selection procedure, site visits were conducted between December 1984 to May 1985 in countries geographically stretching between Indonesia in South-East Asia to Sierra Leone in West Africa resulting in the selection of the following UNU Fellows: Dr. A.J. Smith (Sierra Leone), Dr. A.V. Gholap (Nigeria), Dr. Mahmoud Ali Eissa (Egypt), Dr. Mohamad Zakaullah (Pakistan), Dr. S. Sapru (India), Mr. Susetyo Mulyodrono (Indonesia), Mr. Suryadi (Indonesia) and Mr. Widdi Usada (Indonesia).

Dr. Smith briefing Professor Abdus Salam about the UNU/ICTP Plasma Fusion Facility during the latter's visit to the Plasma Research Laboratory on 20 Jan 1986

The Programme started in October 1985 and was divided into 2 parts, each for a 3-month duration. The first part consisted of equal proportions of lectures and experiments. Some lectures covered the fundamentals of plasma and laser theory required for the construction of working facilities whilst other lectures covered specially designed courses on electronics for control of high power pulsed devices and computation on pulsed circuits and plasma dynamics. The lectures were complemented by plasma and laser experiments and further experiments on the development of complete systems of pulse control modules and plasma dynamic computation packages. At the same time intensive discussions were carried out to determine the requirements of each Fellow and the compatibility of these requirements with the resources of his home institution and of the Training Programme.

The second part of the course, the project part, has progressed at a rate faster than planned. The systems to be individually assembled include six sets of electromagnetic shock tube/plasma focus and four nitrogen lasers complete with triggering spark gaps and control electronics, power supplies and basic measuring probes for pulsed voltage, current and magnetic field measurements. A glow discharge system and a high speed flow simulation system are also planned. These are all designed and are being tested in the Plasma Research Laboratory.

By the third week of the project part of the course, one of the nitrogen lasers has been finally assembled and tested successfully and one of the electromagnetic shock tube has been fully assembled and fired and has been tuned for operation both as a shock tube as well as a plasma focus operating in argon and deuterium. Fusion neutrons from a deuterium plasma, the first in a UNU training device, was recorded (10^7 neutrons per discharge) on January 11, 1986. The other laser and plasma systems are being assembled all over the Plasma Research Laboratory. Another nitrogen laser is being assembled in the Laser Research Laboratory by one of the Fellows.

Some of the experimental work of the group has been written up as two research papers which have been submitted for

publication. More are expected to follow. The computational model developed for the plasma focus project has been used to guide the development of the small plasma focus which is table-top sized, economical and is probably the lowest voltage device to achieve nuclear fusion: at 11 kV, 40 μF. In the development of this plasma focus, a very simple cost effective parallel plate switch was designed and tested, triggered by an SCR pulse stepped up to 20 kV by a standard TV transformer. The switching system, costing less than US$100.00 compared to a commercially available system priced above US$5000.00, is performing with 100% reliability and low jitter after more than 60 discharges of 200 kiloamp each. Several other remarkable innovative designs could also be listed.

The International Centre for Theoretical Physics through its External Activities Committee headed by Prof. Jan Nilsson and with the approval of its Director, Prof. Abdus Salam also supports the concept of research initiation with a grant for some critically needed follow-up equipment to some of the Fellows. Because the targets for this Programme have been progressively raised by the performance of the Fellows, the material requirements have also gone beyond expectation and original budget. The ICTP grant fills a crucial gap in providing storage capacitors for four Fellows, who otherwise would have no means to power their electromagnetic shock tube/plasma focus.

At the moment of writing, 3.5 months into the Programme, the plan is for the construction, testing, disassembly and transporting of 6 almost complete electromagnetic shock tube/plasma focus systems and 4 nitrogen laser systems. Each Fellow has taken part in the design and construction of every detail of 10-20 sybsystems. Technically he can design, maintain, operate and improve on the system and train his technicians for the system. The experience in experiments and modelling that he has conducted on the electromagnetic shock tube, plasma focus and glow discharge will enable him to carry out research on the facility after he has built it up in his home institute. Each UNU Fellow has agreed on a time frame of 1 year to report on the operational facilities and initial results.

The financial cost of the materials for construction and for components? Besides US$15,000.00 provided by the ICTP for the bigger single components, storage capacitors and oscilloscopes, another US$10,000.00 has been allocated by the Programme Coordinator from UNU Programme resources for the construction and transport costs of the 10 facilities. There is little doubt that these expenditures have been most cost-effective. Of course the cost of maintaining and training the UNU Fellows, borne by the UNU, is higher than the above mentioned figures.

Can developing countries effectively exchange and share efforts in order to initiate new research in experimental plasma physics? Will this programme succeed? This question will be answered by mid-1987, a year after the Fellows have returned to their home institutes when their first postprogramme reports to UNU are expected. In the meantime this Programme—a bold new experiment—continues.

Lee Sing
Coordinator
UNU Programme on Plasma & Laser Physics
Physics Department
Universiti Malaya
Kuala Lumpur, Malaysia

UNU Fellows in action

M.A. Eissa (Egypt) adjusting connection on 15 kV, 30μF capacitor

Mohammad Zakaullah (Pakistan) testing HF high voltage probe

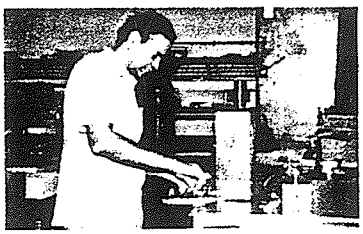

A.V. Gholap (Nigeria) testing Nitrogen laser

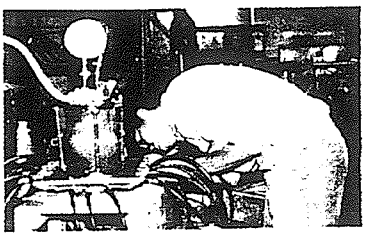

W. Usada (Indonesia) assembling UNU/ICTP Plasma Fusion Facility

Collaboration in Laser Physics Research

A link arrangement between the Laser and Optics Section of Peking University, Beijing and the Laser Research Laboratory of University of Malaya, Kuala Lumpur, has in principle been agreed to by the two parties. It is expected that the Unesco will provide funding for the link which involves an interchange of research staff from the two laboratories. Dr. Hong-du Liu and Professor B.C. Tan are the coordinators of the Chinese and Malaysian sides respectively.

The Laser and Optics Section and the Modern Optics Research Laboratory of Peking University will hold a series of international schools on lasers and applications. The first school will be on Laser Applications in Industry and in Medicine, which is expected to be held in late 1986 or early 1987 in Beijing. It will be funded by the Unesco and the Laser Research Laboratory of University of Malaya is expected to be involved in the organisation of the school.

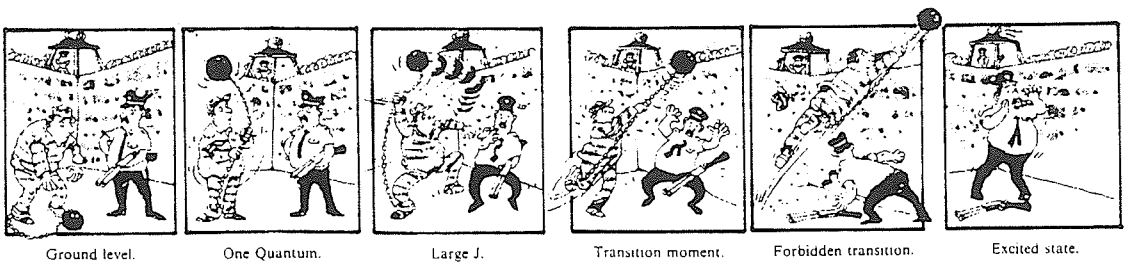

Ground level. One Quantum. Large J. Transition moment. Forbidden transition. Excited state.

SECOND TROPICAL COLLEGE ON APPLIED PHYSICS

LASER AND PLASMA TECHNOLOGY

Kuala Lumpur

17 March - 5 April 1986

PLASMA RESEARCH AT THE UNIVERSITY OF MALAYA

S. Lee
Plasma Research Laboratory
Physics Department, University of Malaya
59100 Kuala Lumpur, Malaysia

Abstract:

The work in the Laboratory is briefly reviewed with some attention to historical perspective and to the academic continuity from undergraduate through to doctoral programmes. The research in the areas of glow-discharge, small tokamak, pinch, current-stepped pinch, vacuum spark pinch and the plasma focus is then reviewed. The central research theme threading all this research is then identified as a study of the limits and enhancement of compressions. Our work shows that in general density compressions are limited and independent of the absolute magnitude of the compressive force. Enhancement of compression may be achieved through time variation of the force field, e.g. specifically using a force-stepping technique, through a reduction in specific heat ratio and in the case of the pinch through an elongation of pinch length during the compression. These ideas are applicable to magnetic field compressions as well as to radiation-driven compressions and should prove useful to aid in understanding e.g. the plasma focus scaling laws.

This review also reports the experience of the research group in its attempt to share fusion related technology among developing countries by the development of specific training packages. One such package the UNU/ICTP Plasma Fusion Facility has already been developed and 5 sets will be sent back to the home institutes of the UNU Fellow trainees.

"Laser and Plasma Technology" Ed. S. Lee et al
World Scientific Publishing Co. (1988)

REVIEW PAPER

Introduction

The Plasma Research Laboratory was started in the early 1960s' by Prof. Thong Saw Pak who at that time was associated in glow discharge work in collaboration with Prof. K.G. Emeleus of Belfast. Aware of the work already on-going at that time in Britain on controlled fusion research Prof. Thong had the foresight to acquire from the British Government through the Colombo Plan 100 pieces of 40 kV 0.6 μF fast discharge capacitors.

In 1970 the technical problems of installing these capacitors were solved with a design dividing the 100 capacitors into 4 modules each switched by 2 ignitrons with the help of a voltage division technique. In 1972 1.9 MA was measured in a full test[1]. This capacitor bank has been continuously operating since then. A plasma focus was designed and in October 1973, nuclear fusion neutrons (D-D) were measured from the focus by TOF method giving an energy of 2.2 ± 0.1 MeV in a 'backward' direction[2].

During this period of development and since then we have planned our research mainly on academic basis, resulting in the production of 11 M.Sc. and 4 Ph.D. theses[3-17]. Academic continuity between undergraduate and postgraduate work is maintained by 3 undergraduate courses in basic plasma physics augmented by undergraduate experiments in glow discharge, electromagnetic shock tube[35,3,4,39,40] and pulsed electronics.

Experimental research is currently carried out on the following devices: glow discharge, small tokamak, Z-pinch, vacuum spark pinch and the plasma focus; also on various lasers for diagnostic development work.

Glow Discharge

Measurements on glow discharge[7] have been continued. Recent developments include pulsed Langmuir double probe studies[18] in various gases and a computer based data acquisition system[19].

Small Tokamak

A small Tokamak was planned[20] and plasma obtained in June 1983 with the following parameters:

major radius R	0.25 m
minor radius a	0.05 m
R/a	5
toroidal field B_ϕ	0.5 T
plasma current	10 kA
safety factor q	2.5
lifetime (optically observed)	200 μs
operational pressure	10^{-3} torr
T_e	10 eV

Stabilization bank

Capacitance	60 μF
Charging voltage	26 kV
Coil inductance	63 μH
No. of turns	100
Coil current	25 kA
risetime	100 μs

Heating bank

Capacitance	100 μF
Charging voltage	4 kV
Coil inductance	360 μH
No. of turns	20
Coil current	2 kA
risetime	300 μs

The toroidal stabilization field, planned at 2T is severely reduced by induced current effects in the stainless steel wall of the plasma chamber.

Pinch

A low performance linear Z-pinch with $\alpha = 15$, where α = electrical characteristic time/pinch characteristic time, has been built for laser scattering diagnostics in a joint project with the Laser Group[21,16]. This pinch produces a plasma with $T_e \sim 30{,}000$ K estimated from observed converging shock waves.

Another pinch with $\alpha = 0.8$, $\beta = 0.9$ has been designed to give a hotter plasma with the aim of connecting to two sequenced capacitor banks for testing the current-stepped pinch compression enhancement effect[22].

Modelling of the pinch has been carried out using circuit coupled snow-plow model with energy balance limit[23-25]. A generalised slug model was also developed for general pinch computation including radiation cooling effects[26,13].

Vacuum Spark Pinch

In this experiment[27,15,28] a plasma is injected into a vacuum gap by irradiating a pointed cathode with a 60 MW ruby laser pulse. This plasma is then compressed using the current from a 22 μF fast capacitor bank charged to 20 kV. From X-ray emission measurements[15] hot spots with electron temperatures up to 10 keV have been measured.

Plasma Focus

A Mather's type plasma focus, the UMDPF1[29] has been operated in this laboratory for a number of years[35]. The following are the typical

operating conditions:

inner electrode radius	1.3 cm (hollow copper tube)
outer electrode radius	4.3 cm (six copper rods)
length	16 cm
Capacitance	60 μF (ignitron switched)
current	550 kA at 20 kV
current risetime	3½ μs
pressure (D_2)	8 torr
neutron yield	10^9 per discharge

The device has also been operated in argon.

Measurements made on this device include device characterisation[30,31,5,6,41], soft X-ray pinhole photography[32] and temperature measurement[32], shadowgraphs[33,34], holographic interferometry[12], neutron time of flight[2,14], neutron counting[9,36], neutron half-life measurements[37] and dynamic modelling[38,35,17].

The objectives of the plasma focus research are shifting more and more to the following:

development of diagnostics and modelling of dynamcis
development of applications e.g. as neutron or soft X-ray sources
development of scaling laws
development as a cost-effective training packages for international cooperation[36,45].

Research Theme

Much of the work in the plasma laboratory may be connected by the central research theme of study of compression limits and compression enhancement for fast compressions. Using an energy balance principle it may be shown that for a general compression driven by a piston force field F, energy and pressure balance gives for the final compressed position r_m an expression

$$F_m = \frac{f(\gamma)}{f_{rs}} \int_{r_m}^{r_o} F \frac{dr}{r}$$

where $f(\gamma)$ is a function of the specific heat ratio γ and f_{rs} is related to the reflected shock over-pressure as the reflected shock hits the incoming piston force field.

This relationship determines the radius ratio r_m/r_o and shows that in principle the radius ratio may always be computed and that:

i) the radius ratio (i.e. density compression) is independent of the absolute peak magnitude of the force F,

ii) the density compression depends only on the space- or time-variation of the force field,

iii) it depends on the specific heat ratio, and

iv) it depends on the reflected shock over-pressure factor f_{rs}.

For an elongating pinch, such as the plasma focus, the energy balance equation becomes:

$$\iota_m^2 = \frac{2(\gamma-)}{f_{rs}\ell_m} \int_{\kappa_m}^{1} \iota^2 \ell \frac{d\kappa}{r} \qquad \text{where } \kappa_m = r/r_o$$

From this several methods of compression enhancement may be proposed:

1. pinch elongation[35], as in a plasma focus.
2. reduction of γ[42], e.g. as $\gamma \to 1$, $\kappa_m \to 0$, this applies particularly to gases which remains freely ionizing even at high temperatures e.g. argon[10] or xenon.
3. current-stepping[22] method.

Effect of radiation cooling[13] may also be included.

For a radiation-driven compression in a spherical geometry[43,44] the corresponding energy balance equation is:

$$R_m = \frac{3(\gamma-1)}{f_{rs} r_m} \int_{r_m}^{r_o} R dr$$

where R is the radiation power.

This expression may be used to show that a square pulse radiation power will produce a density compression of only 27 for a $\gamma = 5/3$ fully ionised plasma whereas a sequenced double pulse[44] each with linearly rising power may increase the compression to 1750, greatly increasing the energy gain factor for a given absorped energy.

These ideas will be applied further to our future experiments and to our attempts to identify and improve plasma focus scaling laws.

Development of Fusion-related Technology in Developing Countries

In view of our relatively extensive experience in experimental plasma physics the Plasma Research Group has pioneered the concept of sharing of fusion-related technology in developing countries. We have

developed the concept of packaging cost effectively an integrated facility consisting of well defined sub-systems which together make up a complete facility for research and training.

For example we have identified that the following sub-systems are necessary to start experimental research in a developing country on the plasma focus:

simple vacuum system
focus electrode system with vacuum feed-through and proper insulation
small capacitor bank (3 kJ) and switch
control and triggering electronics
power supplies
simple diagnostics for current, voltage, magnetic field, X-ray, neutron and laser shadowgraphy
plasma dynamic model with structure and chemistry suitable for use on a microcomputer.

These ideas expounded at the ICTP in Trieste[45] have been further developed with the help of the First Tropical College[35] and has just received its first full test in the 6-months UNU Training Programme in Plasma and Laser Technology. For this Training Programme eight UNU Fellows (from Indonesia, India, Pakistan, Egypt, Nigeria and Sierra Leone) have worked together with us to develop research packages for the plasma focus, glow discharge and nitrogen laser. The work has produced a number of research reports and papers[36, 37, 39, 46-57].

During this Training Programme was developed a complete Fusion Facility now designated as the UNU/ICTP PFF (plasma fusion facility).

Five complete sets of the device were tested over a period of two months, and each was found to work reliably producing well-defined dynamics and reproducible fusion neutron bursts. On 20th January recently ICTP director Prof. Abdus Salam honoured us with a visit to the training programme when he witnessed a fusion discharge.

The follow-up equipment going with the Fellows back to their institutes is being paid for mainly from a Grant by ICTP.

Time will tell whether this concept of training will succeed in raising the level of competence in experimental plasma research in developing countries.

Acknowledgement

The Plasma Research Group acknowledges the contributions of equipment from the British Government under the Colombo Plan (40 kV, 60 μF capacitors) and the Kernforchungsanlage Juelich and the Alexander von Humboldt Foundation under a post AVH grant scheme (60 kV, 22 μF capacitor bank and ruby laser system 2000). We acknowledge the help from UNESCO for the two Tropical Colleges and the generous support from the United Nations University and the International Centre for Theoretical Physics for our Training Programmes and follow-up help for the UNU Fellows. We acknowledge the continuing support of our Vice-Chancellor Royal Professor Ungku A. Aziz and the University of Malaya through its research Grants F232/74 and F95/77.

Reference

1. S.P. Thong and S. Lee, Malaysian J. of Science 2(B), 157 (1973).
2. S. Lee and Y.H. Chen, Malaysian J. of Science 3(B), 159 (1975).
3. S. Lee, Some shock wave phenomena in a ring-electrode system, (M.Sc. Thesis UM 1966, Supervisor: H.H. Teh).
4. C.K. Pang, Shock wave studies in a ring-electrode shock tube, (M.Sc. Thesis UM 1969, Supervisor: H.H. Teh).
5. Y.H. Chen, Study of coaxial plasma gun in mode 1 operation, (M.Sc. Thesis UM 1972, Supervisor: S. Lee).
6. S.P. Chow, Current sheath studies in a coaxial plasma focus gun, (M.Sc. Thesis UM 1972, Supervisors: S. Lee and B.C. Tan).
7. K.W. Lee, Current oscillations in glow discharge, (M.Sc. Thesis UM 1972, Supervisor: H.H. Teh).
8. A.C. Chew, Plasma focus in an axial magnetic field, (M.Sc. Thesis UM 1974, Supervisors: S. Lee and B.C. Tan).
9. C.S. Wong, Some neutron measurements of the plasma focus, (M.Sc. Thesis UM 1978, Supervisors: S.P. Moo and S.A. Husain).
10. Y.C. Yong, Multiple ionization in an argon plasma focus, (M.Sc. Thesis UM 1978, Supervisor: S. Lee).
11. Y.H. Chin, Shadowgraphic studies of a plasma focus, (M.Sc. Thesis UM 1981, Supervisor: S. Lee).
12. K.H. Kwek, Holographic interferometric measurements of electron densities in a dense plasma focus, (M.Sc. Thesis UM 1982, Supervisor: Y.H. Chen).
13. Jalil B. Ali, The enhancement of pinch compression - A numerical study, (M.Sc. Thesis UM 1986, Supervisor: S. Lee).
14. Y.H. Chen, Parametric study of focus optimization, (Ph.D. Thesis UM 1978, Supervisor: S. Lee).
15. C.S. Wong, Experimental and numerical studies of a Laser-initiated vacuum spark, (Ph.D. Thesis UM 1983, Supervisor: S. Lee).

16. S.M. Low, An investigation of a linear hydrogen plasma pinch using a low power dye laser, (Ph.D. Thesis UM 1986, Supervisor: B.C. Tan).

17. T.Y. Tou, Pinch radius ratio of the plasma focus, (Ph.D. Thesis UM 1987, Supervisor: S. Lee).

18. C.S. Wong, J. Fiz. Mal. 5, 115 (1984).

19. C.S. Wong, S.H. Saw and O.H. Chin, J. Fiz. Mal. 6, 115 (1985).

20. S. Lee, Fusion Energy-1981. IAEA-SMR-82, p.289-295, Procs. Symposium on plasma research, theory and experiment, ICTP, Trieste, Italy, June 1981.

21. S.M. Low, B.C. Tan and S. Lee, J. Fiz. Mal. 5, 149 (1984).

22. S. Lee, J. Phys. D: Applied Physics 17, 733 (1984).

23. S. Lee, J. Appl. Phys. 54, 3603 (1983).

24. S. Lee, Plasma Physics 25, 571 (1983).

25. S. Lee, J. Phys. D: Applied Physics 16, 2463 (1983).

26. Jalil B. Ali, S. Lee, T.Y. Tou and Y.C. Yong, J. Fiz. Mal. 5, 153 (1984).

27. S. Lee and H. Conrads, Phys. Lett. 57A, 233 (1976).

28. C.S. Wong and S. Lee, Rev. Sci. Instru. 55(7), 1125 (1984).

29. S. Lee and Y.H. Chen, Fusion Energy - 1981, IAEA-SMR-82, p.296-303, Proc. Symposium on plasma research, theory and experiment, ICTP, Trieste, Italy, June 1981.

30. S.P. Chow, S. Lee and B.C. Tan, J. of Plasma Physics 8, 21 (1972).

31. S. Lee, Y.H. Chen, S.P. Chow, B.C. Tan, H.H. Teh and S.P. Thong, Int. J. Electronics 33, 85 (1972).

32. Y.H. Chen and S. Lee, Int. J. Electronics 35, 341 (1973).

33. S. Lee and Y.H. Chin, Bull. Phys. M'sia 2, 105 (1981).

34. S. Lee, Harith Ahmad, T.Y. Tou, K.H. Kwek and C.S. Wong, J. Fiz. Mal. 6, 23 (1985).

35. S. Lee in Laser and Plasma Technology Ed. S. Lee et. al. (World Scientific Co. 1985) Experiment II, Chapter VIII and Paper XIV.

36. S. Lee, T.Y. Tou, S.P. Moo, M.A. Eissam A.V. Gholap, K.H. Kwek, S. Mulyodono, A.J. Smith, Suryadi, W. Usada and M. Zakaullah, A simple facility for the teaching of plasma dynamics and plasma nuclear fusion, American J. Physics 56, 62 (1988)

37. S.P. Moo and S. Lee, Singapore J. Phys. 4, 131 (1987).

38. S. Lee, A plasma focus model yielding trajectory and structure, Spring College on radiation in plasma, Trieste, May 1983; Published in "Radiation in Plasmas", p.978-987, World Scientific Pub. Co. (1984).

39. S. Lee, M. Eissa, A.V. Gholap, K.H. Kwek, S. Mulyodrono, S. Sapru, A.J. Smith, Suryadi, T.Y. Tou, W. Usada, C.S. Wong and M. Zakaullah, Singapore J. Physics 3, 75 (1986).

40. S. Lee, Malaysian J. Science (B), 165 (1975).

41. S. Lee and T.H. Tan, Dependence of focus intensity on mass and field distribution, Procs. Seventh European Conf. on Controlled Fusion and Plasma Physics, Lausanne, Switzerland (1975).

42. S. Lee, Australian J. Physics 36, 891 (1983).

43. S. Lee, J. Fiz. Mal. 5, 53 (1984).

44. S. Lee, Density ratios in compressions driven by radiation pressure, accepted by Laser and Particle Beams.

45. S. Lee, Regional Centres for research transfer within South-east Asia Countries - Invited paper presented at the International Conf. 1984, ICTP, Trieste, Italy:

46. A.J. Smith, K.H. Kwek, T.Y. Tou, A.V. Gholap and S. Lee, IEEE J. Quantum Electronics QE-23, 283 (1987)

47. K.H. Kwek, A.J. Smith, T.Y. Tou, A.V. Gholap and S. Lee, J. Fiz. Mal. 7, 125 (1986).

48. S. Lee, A.V. Gholap, A.J. Smith, K.H. Kwek, A.C. Chew, T.Y. Tou and S. Sapru, J. Fiz. Mal. 6 165 (1985).

49. C.S. Wong, O.H. Chin, M.A. Eissa, A.V. Gholap, S. Mulyodrono, C.X. Ong, S. Sapru, S.H. Saw, A.J. Smith, Suryadi and W. Usada, J. Fiz. Mal. 7, 45 (1986).

50. A.J. Smith, A.V. Gholap and K.H. Kwek, Plasma focus operation in different gases, Paper presented at the Second Tropical College on Applied Physics: Laser and Plasma Technology, Mar/April 1986, Kuala Lumpur, to appear in Proceedings.

51. M.A. Eissa, M. Zakaullah and S. Lee, Circuit effects on the operation of a plasma focus, Paper presented at Second Tropical College on Applied Physics: Laser and Plasma Technology, to appear in Proceedings.

52. W. Usada and Suryadi, Design of BATAN plasma focus facility, Paper presented at Second Tropical College on Applied Physics: Laser and Plasma Technology, to appear in Proceedings.

53. S. Sapru, C.K. Lee and K.S. Low, A high power double Blumlein nitrogen laser, Paper presented at Second Tropical College on Applied Physics: Laser and Plasma Technology, to appear in Proceedings.

54. A.V. Gholap, M. Zakaullah and M.A. Eissa, Mangetic field measurements in coaxial electromagnetic shock tube, Paper presented at Second Tropical College on Applied Physics: Laser and Plasma Technology, to appear in Proceedings.

55. Suryadi, W. Usada and T.Y. Tou, Neutron production from the UNU/ICTP Plasma Focus Facility, Paper presented at the Second Tropical College on Applied Physics: Laser and Plasma Technology, to appear in Proceedings.

56. A.J. Smith, Suryadi, Jasbir Singh and S. Lee, A simple high current switch, Paper presented at Second Tropical College on Applied Physics: Laser and Plasma Technology, to appear in Proceedings.

57. S. Mulodrono, C.S. Wong and S. Lee, High speed flow simulation in an electromagnetic shock tube, Paper presented at Second Tropical College on Applied Physics: Laser and Plasma Technology, to appear in Proceedings.

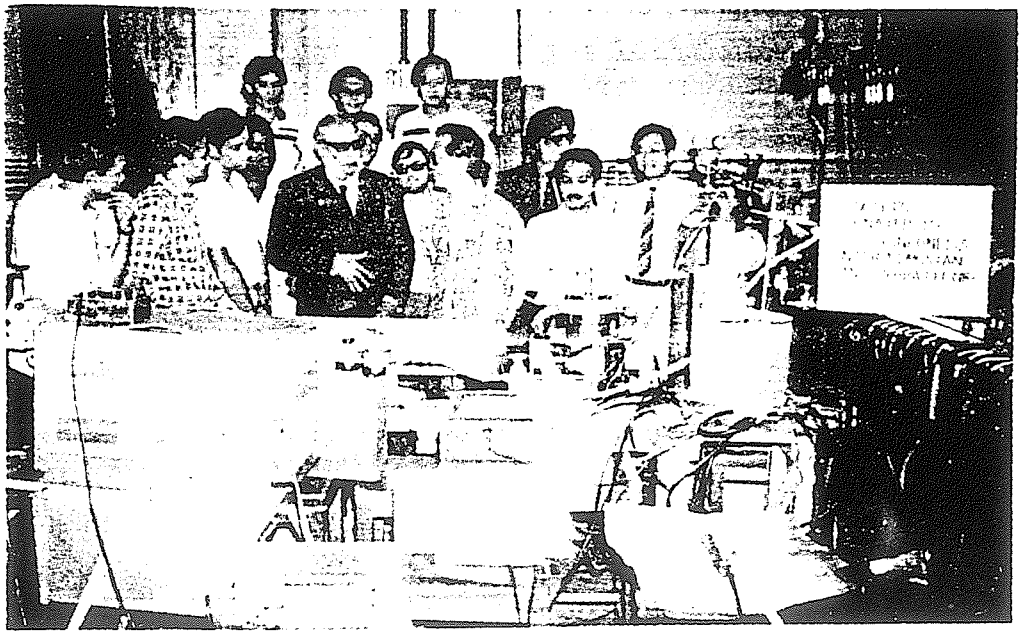

Professor Abdus Salam visiting the Plasma Research Laboratory
and inspecting the UNU/ICTP Plasma Fusion Facility - 20th January 1986.

SECOND TROPICAL COLLEGE ON APPLIED PHYSICS

LASER AND PLASMA TECHNOLOGY

Kuala Lumpur

17 March - 5 April 1986

ANALYSIS OF VOLTAGE AND CURRENT MEASUREMENTS IN DPF

T.Y. Tou and S. Lee
Plasma Research Laboratory
Physics Department, University of Malaya
59100 Kuala Lumpur, Malaysia

Abstract:

This paper presents an analysis of voltage and current measurements in a dense plasma focus (DPF). A multi-slit streak photograph is necessary in this analysis to provide the axial rundown trajectory Z of the current sheath. This enables the plasma current I_p, current sheath resistance R_p, leak current I_L and the leak resistance R_L to be determined for the axial rundown phase. A deuterium plasma focus is analysed in this paper.

"Laser and Plasma Technology" Ed. S. Lee et al
World Scientific Publishing Co. (1988)

PAPER

Analysis of voltage and current measurements in DPF

T.Y.Tou and S.Lee
Plasma Research Laboratory
Physics Department
University of Malaya
59100 Kuala Lumpur
Malaysia

Abstract

This paper presents an analysis of voltage and current measurements in a dense plasma focus(DPF). A multi-slit streak photograph is necessary in this analysis to provide the axial rundown trajectory Z of the current sheath. This enables the plasma current I_p, current sheath resistance R_p, leak current I_L and the leak resistance R_L to be determined for the axial rundown phase. A deuterium plasma focus is analysed in this paper.

Introduction

The measurements of the discharge current I and the transient voltage V often form the most basic diagnostic in the dense plasma focus experiment. These electric signals (I and V) are message-coded, so a proper decoding may extract useful information about the plasma focus discharge. Attempts[1,2,3] have been made to determine the dynamic behaviour of the plasma current sheath from an analysis of V and I signals. From these attempts, some parameters including the plasma sheath resistance R_p and inductance L_p (introduced by the current sheath into the circuit) may have been determined without considering the current-shedding factor.

During the plasma focus discharge, it is well-known that current shedding happens in the focus tube[4,5,6]. In the following reference (6), V,I,I_p and V_z (the axial velocity of the current sheath) were measured so that the plasma sheath resistance R_p and the leak resistance R_L could be determined. The measurements of I_p and V_z were done using a magnetic probe.

In this paper, a similar analysis is proposed to determine I_p,

R_p, I_L and R_L from the measurements of V and I. Instead of measuring the average axial vslocity V_z by using a magnetic probe, a mutli-slit streak photograph[7] is taken simultaneously with the measurements of V and I so that the time-dependent axial rundown trajectory Z of the current sheath (adjacent to the anode) is obtained. Knowing the trajectory Z, the inductance L_p may be calculated at any time t and hence it enables the plasma current. I_p to be determined. Subsequently, R_p, I_L and R_L are determined. For this analysis, the circuit current I is measured by a Rogowski coil operated as a current transformer[8] and the voltage V by a high-voltage resistive probe[8].

Some circuit equations

Figure 1 shows the schematic of the plasma focus facility UMDPF1 (Universiti Malaya Dense Plasma Focus 1). The input flanges (consisting of a positive and a negative flange) form an interface between the capacitor bank (L_{oe}-C_o-R_{oe}) and the focus tube. The electrical representation of this interface are the inductance L_{oi} and resistance R_{oi} as shown in Figure 2. Values of L_{oi}≈25nH and R_{oi}≈1mΩ have been determined experimentally[7].

During the plasma focus discharge, there is current partition(or shedding) inside the focus tube where the circuit I is divided into two components I_p and I_L (see Figure 1). The current I_p drives the current sheath down the annulus of the focus whereas the leak current I_L is here assumed to remain at the glass insulator. With reference to Figure 2, some useful circuit equations may be written:

(a) Voltage V_p

The voltage V is always measured across the junction CD (or across the input flanges) so that

$$V = V_p + L_{oi}\frac{dI}{dt} + R_{oi}I \qquad (1)$$

Here V_p is often called the plasma voltage across the junction AB (see Figure 1). V_p is in fact the induced back emf of the current sheath. It may be written as follow :

$$V_p = \frac{d}{dt}(L_p I_p) + R_p I_p \qquad (2)$$

(b) Currents I_p and I_L

From equation (2), the plasma current I_p may be obtained:

$$I_p = \frac{\int_{a'}^{b'} V_p\,dt - \int_{a'}^{b'} V_R\,dt}{L_p} \tag{3}$$

where $a' = t_1$, $b' = t_a$ and

$$V_R = I_p R_p \tag{4}$$

For simplicity, a planar geometry is assumed for the current sheath (see Fig.1) so that:

$$L_p = \frac{\mu}{2\pi} \ell n\left(\frac{b}{a}\right) Z \tag{5}$$

and Z is given in Figure 4. The leak current is simply given as

$$I_L = I - I_p \tag{6}$$

(c) Resistances R_p and R_L

From equation (4), the plasma current sheath resistance R_p is given as :

$$R_p = \frac{V_R}{I_p} \tag{7}$$

The plasma resistive voltage V_R is measured by connecting a high-voltage resistive probe across the electrodes at the downstream of the focus tube. This measurement is carried out in a separate discharge so that the V and I signals are not disturbed in the previous experiment. Assuming that the magnetic field behind the current sheath does not penetrate through it, then V_R is largely noninductive before the current sheath arrives at the probe. Figure 3 shows the V_R waveform as a function of time. The plasma voltage V_p across the junction AB may also be written as follow :

$$V_p = I_L R_L \tag{8}$$

So the leak resistance R_L is given by

$$R_L = \frac{V_p}{I_L} \tag{9}$$

The plasma voltage V_p is by no means easy to measure because the point A is technically difficult to access (see Figure 2). However, V_p may be determined from V using the equation (1).

Presentation of results

This section presents the results of V_p, I_p, I_L, R_p and R_L by analysing the measured V and I signals using the circuit equations derived in the previous section.

(a) Voltage

The measured signals V and I are shown in Figures 5 and 6 respectively. Using equation (1) and obtaining $\frac{dI}{dt}$ and I from Figure 6, the plasma voltage V_p is calculated; shown also in Figure 5. V_p has been defined in the previous section as the induced back emf generated by the travelling current sheath. Before the time t_1, V_p is always near zero indicating that there may be no current sheath lift-off from the glass insulator. It rises steadily during the axial rundown phase ($t_1 < t < t_a$). For time $t > 1.71\mu s$ V_p appears to saturate at about 5.3kV. And for $t > 2.38\mu s$, the plasma focus discharge enters the more transient radial phase during which V_p rises sharply.

(b) Current

Next, the plasma current I_p is calculated using equation (3) , with values of V_p from the previous calculation, V_R from Figure 3 and Z from Figure 4. Figure 6 shows the plasma current I_p, the leak current I_L (Eq. 6) in addition to the circuit current I. I_p rises with respect to I until the time $t \approx 1.71\mu s$ it then also appears to saturate irrespective of the continuous rise in I.

For $t < 0.9\mu s$, the leak current I_L is about the same as I_p in absolute magnitude. It then decreases because of increased ionization due to the kinetic heating at the plasma current sheath. This mode of heating may reduce the sheath resistance R_p and hence allows more current to flow as I_p. For $t > 1.71\mu s$, I_L rises again. It is proposed in this paper that there is further breakdown at the glass insulator when V_p tries to exceed 5.3kV. The further breakdown enables more current to flow along the glass insulator as I_L. I_p is thus maintained at a constant value (see Figure 6) and if the axial velocity V_z is also maintained constant, then one would expect V_p to be maintained at 5.3kV. From Figure 4, the gradient of the graph (Z versus t) is constant for the period $2.0\mu s < t < 2.38\mu s$, giving $V_z = 10 cm/\mu s$. So, the glass insulator may be regarded to have behaved like a voltage regulator.

(c) Resistances R_p and R_L

Figure 7 shows the resistances R_p (Eq. 7) and R_L (Eq. 9) as functions of time. The plasma sheath resistance R_p is about 10mΩ at t = 0.4μs and it drops to about 1mΩ at t = 1μs. For this period 0.4μs < t < 1.0μs, the drop in R_p may be due to the increased kinetic heating of the current sheath. For the period 1.5μs < t < 2.3μs, R_p appears to have reached a constant value of about 0.4mΩ.

The leak resistance R_L characterises the leak current path along the glass insulator. Initially, it acts as the only discharge path to introduce the circuit current I into the focus tube. After that one may want it to be a good insulator so that it does not break down under the increasing induced back emf (or V_p). A further breakdown is proposed at the time t = 1.71 μs under these operating conditions : 14kV and 10mbar for deuterium focus. So the leak current I_L increases whereas the plasma current I_p remains constant for t > 1.71μs. Thus R_L appears to decrease (see Eq. 9) from its maximum value of 100mΩ.

The range of values of R_p between 0.4mΩ and 10mΩ determined in this paper agrees with the earlier report[6] using a similar analysis. And for R_L (between 25mΩ and 100mΩ in this paper), it agrees with the reported: 25mΩ < R_L < 200mΩ for the Frascati Plasma Focus Experiment[9].

Dicussion and conclusion

A method of analysing the voltage and current measurements has been proposed. From the measured voltage V and circuit current I, the plasma voltage V_p is first determined so that the plasma current I_p, current sheath resistance R_p, leak current I_L and the leak resistance R_L are calculated. The analysis is made possible with the axial trajectory Z measured from the multi-slit streak photograph.

From the apparent saturation of V_p and I_p, a hypothesis is proposed for a further breakdown at the glass insulator. This may explain a further rise in I_L and a drop in R_L for t > 1.71μs. So, the glass insulator may be regarded to have behaved as a voltage regulator under these operating conditions : 14kV and 10mbar in deuterium focus.

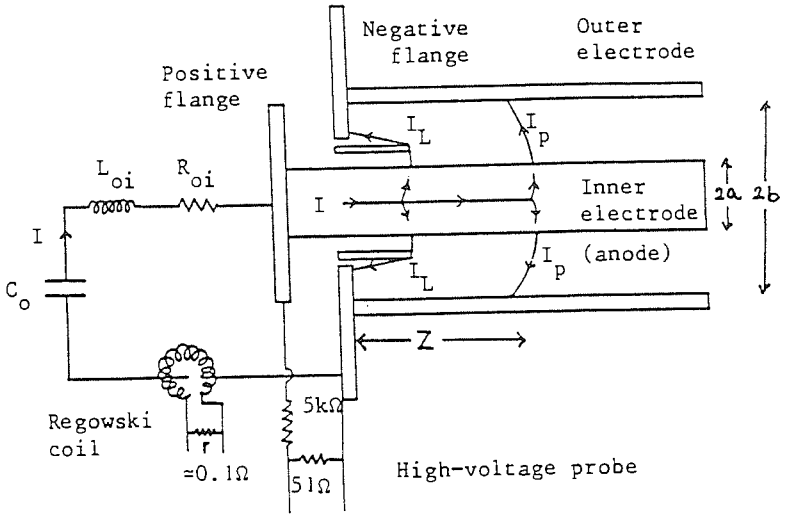

Figure 1. The schematic of the plasma focus facility UNDPF1.

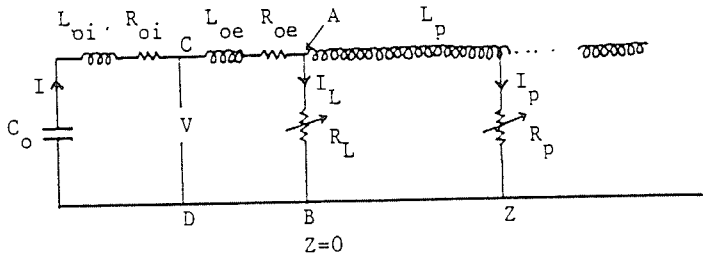

Figure 2. The equivalent discharge circuit of UMDPF1.

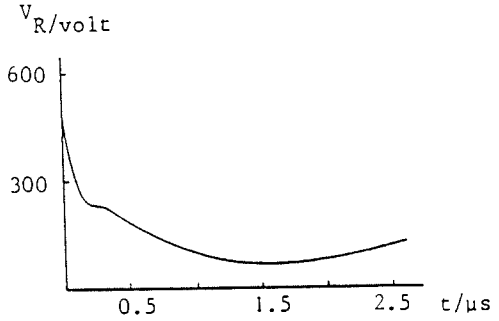

Figure 3. The plasma resistive voltage V_R as a function of time.

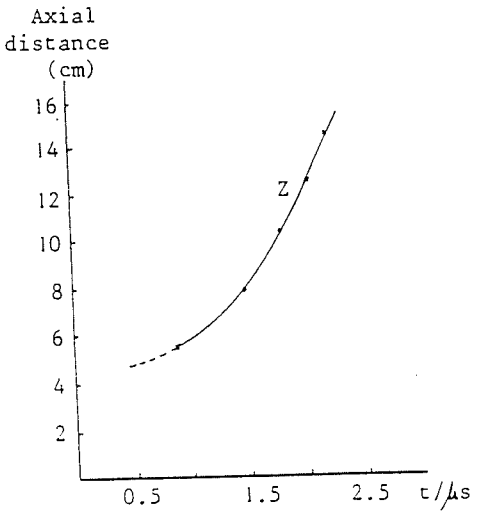

Figure 4. The axial trajectory Z as a function of time.

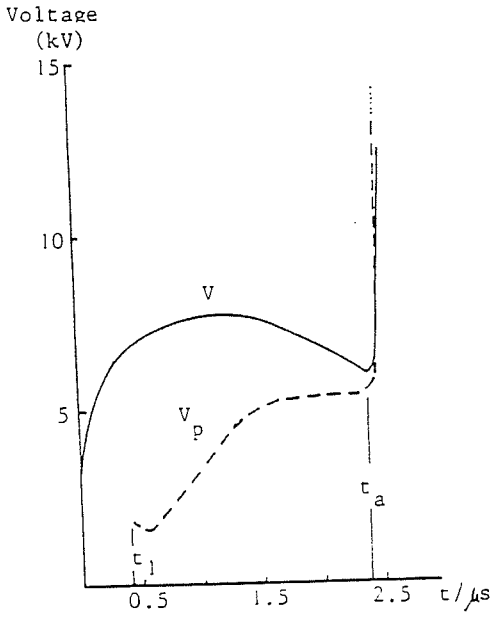

Figure 5. Voltages V and V_p as functions of time.

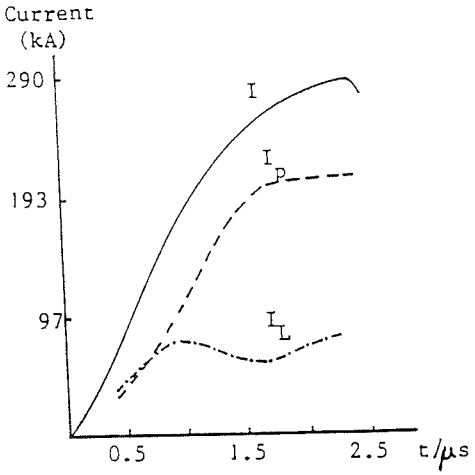

Figure 6. Currents I, I_p, I_L as functions of time.

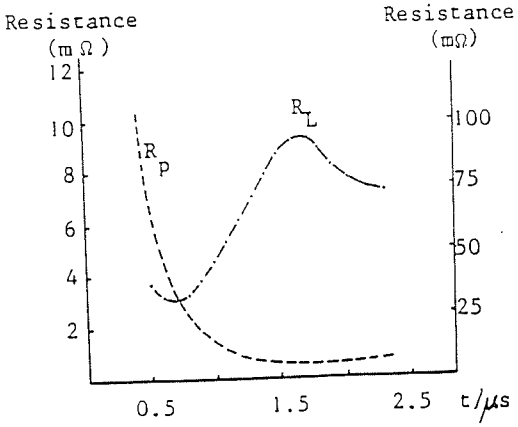

Figure 7. Resistances R_p and as functions of time.

Reference

1. J.W.Mather and P.J.Bottom, Phys. Fluids, 11, 611(1968).
2. G.Patou, A.Simonett and P.J.Watteau, Proc. APS Topical Conf. Pulsed High Density Plasma, September 1967, Los Alamos Sci. Lab. Rep., LA-3770, p.C2-1.
3. C.S.Wong and S.Lee, J. Appl. Phys., 57, 5102(1985).
4. T.Oppenländer, G.Pross, G.Decker and M.Trunk, Plasma Phys., 19, 1075(1975).
5. S.P.Chow, S.Lee and B.C.Tan, J. Plasma Phys., 8, 21(1972).
6. T.Oppenländer, IPF-81-2, Universität Sttugart, 1981.
7. T.Y.Tou, PhD thesis in preparation, Universiti Malaya, Malaysia.
8. S.L.Leonard, in Plasma Diagnostic Techniques, edited by R.H. Huddlestone and S.L.Leonard (Academic, New York, 1965).
9. P.G.Eltgroth, Phys. Fluids, 25, 2408(1982).

SECOND TROPICAL COLLEGE ON APPLIED PHYSICS

LASER AND PLASMA TECHNOLOGY

Kuala Lumpur

17 March - 5 April 1986

CIRCUIT EFFECTS ON THE OPERATION OF A PLASMA FOCUS

M.A. Eissa*, M. Zakaullah+ and S. Lee
United Nations University Training Programme
on Plasma and Laser Technology
Physics Department, University of Malaya
59100 Kuala Lumpur, Malaysia

Abstract:

The operation of high temperature plasma devices e.g. plasma focus strongly depends on external inductance of the circuit L_o, rise time of the switch and as a result the current flowing in the circuit. Here, attempts to reduce the inductance of the circuit using a single 30 μF capacitor and the effects of the change of switch and ignitron to swinging cascade spark gap are presented.

*M.A. Eissa, Physics Department, Al-Azhar University, Cairo, Egypt.

+M. Zakaullah, Physics Department, Quaid-i-Azam University, Islamabad, Pakistan.

"Laser and Plasma Technology" Ed. S. Lee et al
World Scientific Publishing Co. (1988)

PAPER

CIRCUIT EFFECTS ON THE OPERATION OF A PLASMA FOCUS

M.A. Eissa*, M. Zakaullah* and S. Lee

United Nations University Training Programme
on Plasma and Laser Technology
Physics Department, University of Malaya
59100 Kuala Lumpur, Malaysia

Abstract:

The operation of high temperature plasma devices e.g. plasma focus strongly depends on external inductance of the circuit L_o, rise time of the switch and as a result the current flowing in the circuit. Here, attempts to reduce the inductance of the circuit using a single 30 μF capacitor and the effects of the change of switch and ignitron to swinging cascade spark gap are presented.

I. Introduction

The dense plasma focus is a device in which initially the energy stored in the capacitor bank is converted into magnetic energy behind a moving current sheath. This is followed by a rapid conversion of this energy into plasma energy during the collapse of current sheath beyond the end of the centre electrode. In the focus phase, intense burst of neutrons, X-rays and charged particles are emitted. Moreover, recent developments in plasma focus seem to suggest the possibility of a break even reactor[1]. However, the origin of neutrons in the plasma focus is yet controversial.

In the United Nations University Training Programme on Plasma and Laser Technology, it was aimed to develop a plasma focus using a single 15 kV, 30 μF capacitor. Thus the selection of a switch and other techniques for reduction of external inductance L_e were very crucial, as division of

---

*M.A. Eissa, Physics Department, Al-Azhar University, Cairo, Egypt.

*M. Zakaullah, Physics Department, Quaid-i-Azam University, Islamabad, Pakistan.

capacitor bank into parallel modules for reduction ofparasitic inductance was not possible. Different connecting plate dimensions for carrying current from the condenser; and ignitron and swinging cascade air gap as a switch were tried, ultimately reducing the inductance to 95 nH.

II. Design

The design of this plasma focus is based on a simple dynamic model[2] which considers the focus dynamics in two phases - the axial run-down phase, similar in operation to a coaxial accelerator; and focus phase which resembles a z-pinch operation, but with variable plasma column length. However, there is a crucial difference between the operation of the two devices. In the z-pinch, the energy is transferred to the plasma from a condensor, which occurs in 1 to 3 μs. In the plasma focus, firstly the energy is transferred from capacitor bank to electromagnetic storage behind the current sheath and then to the pinched plasma in a much smaller time, typically a few tens of nanoseconds. The rapid transfer of energy to the plasma pinch is the key principle of plasma focus operation which produces the plasma dense and hot enough that intense bursts of neutrons and X-rays are emitted. Although neutron emission has been observed in different linear and toroidal pinch configurations, since the fifties, the yield of plasma focus is by far the highest among all. Thus it may be used as an intense pulsed neutron source.

It is obviously required that the focus phase should start when electromagnetic energy stored behind the current sheath, $\frac{1}{2}LI^2$, is maximum, that is, just after the peak current, i.e.

$$t_a = \frac{2\pi}{4}\sqrt{(L_o C_o)} \qquad (1)$$

where t_a is the time required for the axial run down phase and $2\pi\sqrt{(L_o C_o)}$ is the period of the L_o-C_o circuit, L_o being the inductance of the capacitor C_o together with all the connections up to the plasma section of the tube. The maximum current flowing in the circuit is just below the value of

$$I_o = \frac{V_o}{Z_o} \qquad (2)$$

with $Z_o = \left(\frac{L_o}{C_o}\right)^{\frac{1}{2}}$ (3)

where V_o is the initial voltage on the capacitor C_o and Z_o is the surge impedance of the L_o-C_o circuit. Thus a reasonably low value of L_o is required.

III. Experimental arrangement

The schematic drawing of connections with the capacitor is shown in Fig. 1. To keep the inductance low, parallel connecting plate connections were used to the capacitor. In order to measure the inductance of the system, the capacitor was discharged at reasonably high pressure $\sim$ 25 torr inside the vacuum chamber. If the pressure is too high, the breakdown may not occur, if it is too low, the damped sinusoidal oscillations of L_o-C_o circuit may not be sufficiently sinusoidal but may be rather deformed in shape due to plasma dynamics. Once the periodic time T of the circuit is recorded, the inductance may readily be calculated by using the formula

$$L = \frac{T^2}{4\pi^2 C} \quad (4)$$

Initially, the earth plate had a hole of five inches diameter surrounding the anode stud for insulation. But it was found that with an ignitron switch, the inductance of the system was $\sim$ 220 nH. Then the earth plate was extended nearly up to the anode and the insulation was provided by a nylon cap around the anode stud, which dips into a pool of oil. To prevent the oil from splashing out, an O-ring was placed around. Mylar sheets sandwiched by polythelene sheets, two inches wider all round the conducting plates, were placed between the HV and earth plates for insulation.

The capacitor was tested with an ignitron type 7703. However, it was found that the ignitron resistance dominated the discharge behaviour lengthening the rise time to more than 4 μs with an average periodic time of only 13 μs. Then a simple parallel plate spark gap with a swinging cascade configuration was developed. After a series of tests, it was found

that to operate between 13-15 kV, the suitable ratio of gaps is 4.5 mm to 3 mm (3:2). The gap was triggered via an isolating capacitor from a 1.5 kV kryton unit via a TV transformer which was found to have a step up ratio of 17 times and a rise time of 1 μs. The isolating capacitor is a one meter long of UR67 cable. The parallel plate spark gap was made from 0.5 inch thick copper plate and proved maintenance free for 200 discharges between 13-15 kV before it was cleaned. The triggering jitter was found to be ± 50 nanosecond.

IV. Results

The inductance of the system with different configuration was calculated. Initially, two 10 kV capacitors, 20 μF each, were used as the energy source for the plasma focus. However, the measured inductance of the system was ∿ 220 nH, a weak focussing defined in terms of voltage spike was observed and no neutrons were detected. Then the system used a 15 kV, 30 μF single capacitor. The capacitor was connected to the earth plate, with a hole of diameter ∿ 5 inch around the anode stud for insulation. The recorded inductance of the system was ∿ 180 nH. Then the earth plate was changed with one just reaching the anode stud and a nylon cap was placed for electrical insulation. A drastic decrease in inductance of 30 nH was observed. An oscillogram representing current and voltage is displayed in Fig. 2. In both the cases, neutrons were recorded from a plasma focus in 3 torr deuterium, seeded with ∿ 1 % argon by weight. However, with the reduction of inductance, the neutron flux was increased by almost a factor of two. In this configuration, the ignitron was being used as a switch.

As a next attempt, the ignitron was replaced with a swinging cascade type air gap. In this configuration, the measured inductance of the system was ∿ 120 nH. Finally, legnth of the cables was reduced and the number of cables was increased to sixteen. The inductance of the system was reduced to ∿ 95 nH. With circuit arrangement described, peak current ∿ 180 kA was recorded using a single 15 kV, 30 μF capacitor. The system worked as a reproducible and reliable neutron source (10^8 neutrons per discharge in deuterium) as well as a reliable source of focussed plasmas of air, argon, hydrogen, helium and carbon dioxide. Figure 3 illustrates the oscillograms of current and voltage spike of focus discharge using

deuterium as the feed gas. The detailed results are presented elsewhere[3].

V. Conclusions

A simple cost-effective plasma focus device based on a single 3.3 kJ capacitor using a maintenance-free parallel-plate spark gap became possible to develop using a single 15 kV, 30 F capacitor with careful attention to circuit connections. Some more attention to the system may further reduce the inductance to ∿ 90 nH, which will result in a further enhancement of the system performance.

ACKNOWLEDGEMENT

The authors (M.A. Eissa and M. Zakaullah) thank the United Nations University for UNU Fellowships which make their participation in this work possible. They also thank the members of the Plasma Physics Group and the other UNU Fellows for support, cooperation and for freely supplying research data for this paper.

REFERENCES

1. Herold, H., Hayd, A., in Plasma Focus Research (Proc. 3rd Int. Workshop, Stuttgard, 1983), IPF, 83-6 (1983) 131.
2. S. Lee in "Laser and Plasma Technology" edited by S. Lee, B.C. Tan, C.S. Wong and A.C. Chew, World Scientific, Singapore, p. 37, 64 and 387 (1985).
3. Preliminary results of the UNU/ICTP Plasma Focus, S. Lee, T.Y. Tou, M. Eissa, A.V. Gholap, K.H. Kwek, S.P. Moo, S. Mulyodrono, A.J. Smith, Suryadi, W. Usada, M. Zakaullah, J. Fiz. Mal. 7 (1986) (accepted).

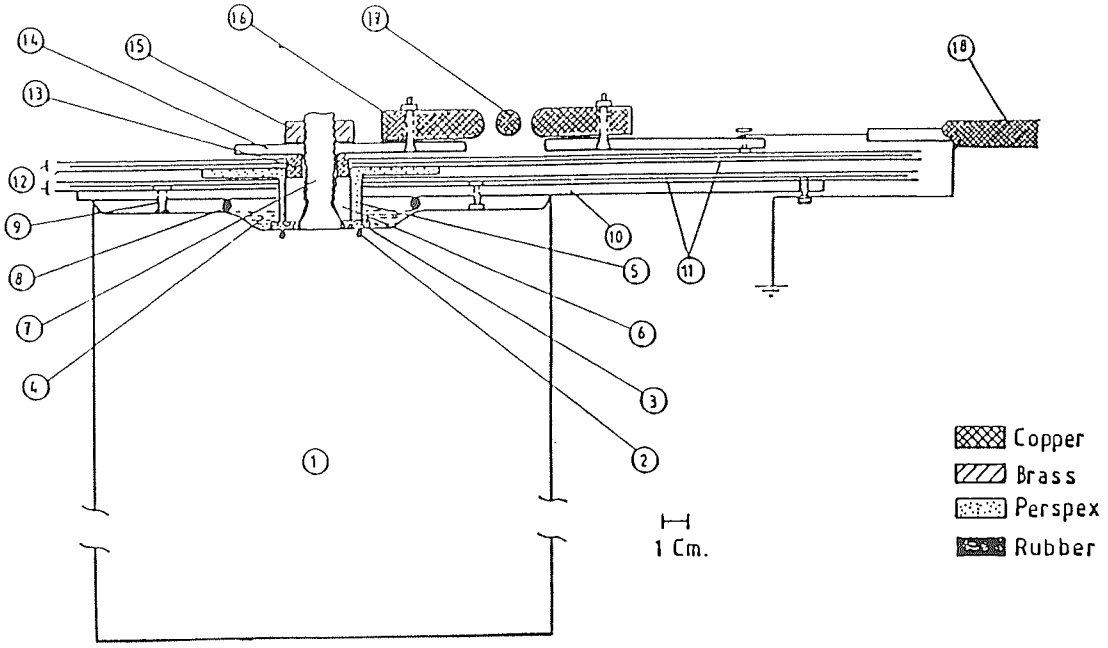

Fig. 1 The capacitor connecting plates, the spark gap and output coaxial cables. 1 = 15 kV, 30 μF capacitor; 2 = capacitor O-ring seal; 3 = washer; 4 = oil; 5 = nylon cap; 6 = steel nut; 7 = capacitor output seal; 8 = O-ring seal; 9 = earth stud; 10 = earth plate; 11 = 5-mil mylar film; 12 = polyethelene film; 13 = copper ring HV connector; 14 = capacitor high voltage (HV) output plates; 15 = lock nut for HV plate; 16 = HV electrode for swinging cascade spark gap; 17 = trigger electrode; and 18 = output coaxial cables (16 in parallel).

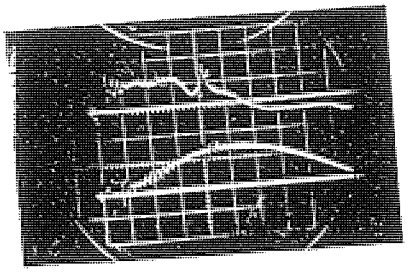

Fig. 2 Voltage and current oscillograms; ignitron as switch
Time base: 1 us/cm
Upper trace: voltage across focus tube
Lower trace: current into focus tube
Circuit inductance: L_o=180nH (V_o=15kV, C_o=30uF)
Neutron yield: $5x10^6$

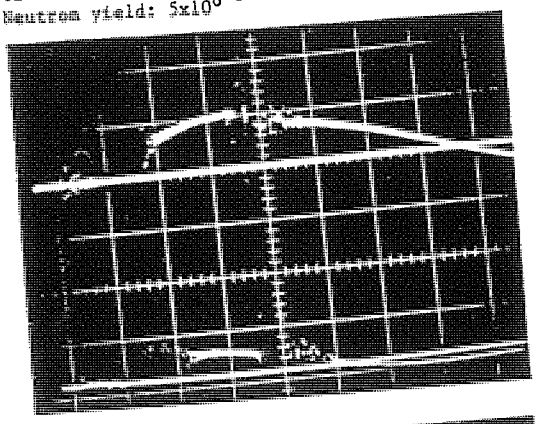

(a)

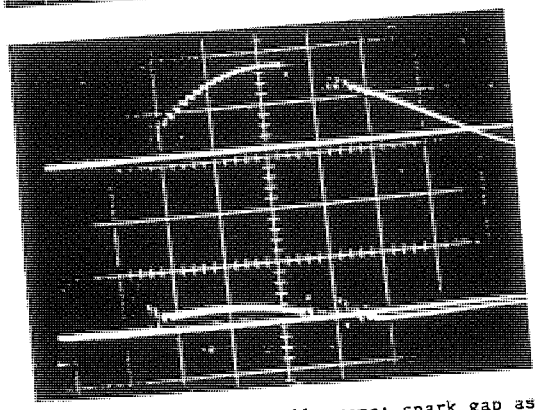

(b)

Fig.3 Voltage and current oscillograms; spark gap as switch
Time base (both photos) : 1 us/cm
Top photo (a): L_o=120 nH (V_o=15 kV, C_o=30 uF)
neutron yield: $5x10^7$
Upper trace: current into focus tube
Upper trace: voltage across focus tube

Bottom photo (b): L_o=95 nH (V_o= 15 kV, C_o=30 uF)
neutron yield: 10^8
Upper trace: current into focus tube
(peak value=180 kA)
Lower trace: voltage across focus tube

A SIMPLE HIGH CURRENT SWITCH

A.J. Smith*, Suryadi*, Jasbir Singh and S. Lee

United Nations University Training Programme
on Plasma and Laser Technology
Physics Department, University of Malaya
59100 Kuala Lumpur, Malaysia

Abstract

A simple swinging cascade spark gap capable of switching 280 kA with jitter within 50 ns was developed. The performance of the switch during testing where high currents were switched is described. The results of tests to determine the range of voltages for good operation at each gap setting are also presented.

INTRODUCTION

The production of shock heated plasmas in fusion research often begins with the discharge of a capacitor bank. Such discharge is initiated by a switch which must be able to repeatedly transmit high currents with little jitter and it must have low inductance. Studies[1,2] have shown that at switching times of 10^{-7} seconds or less the spark gap is the best alternative. In the course of developing a simple, reliable and cost effective plasma fusion device, the United Nations University/International Centre for Theoretical Physics Plasma Fusion Facility (UNU/ICTP PFF)[4], it was necessary to develop a simple, reliable and cost effective switch. The swinging cascade spark gap described in this paper has been selected not only because of its reliability during operation but also because of its fast switching times ($< 10^{-7}$ s) and ease of construction.

*A.J. Smith, Physics Department, Njala University College,
PMB Freetown, Sierra Leone.

Suryadi, PPBMI, BATAN, National Atomic Energy Agency,
Yogjakarta, Indonesia.

"Laser and Plasma Technology" Ed. S. Lee et. al.
World Scientific Publishing Co. (1988)

THE SWINGING CASCADE SPARK GAP (SCSG)

A) Operation

The Swinging Cascade Spark Gap (SCSG) is essentially a three electrode device forming two gaps in series. The common (or trigger) electrode is positioned asymmetrically between the main electrodes. Gap ratios of 3:2, with the gap toward the high voltage main electrode being larger, are used. The common electrode is held at a proportion of the gap voltage corresponding to the physical spacing. The total gap length is such that before triggering the gaps are safe at the operating voltage.

Fast operation is achieved by applying a large negative voltage pulse with a small rise time to the trigger electrode and thus swinging its potential negative until the HV (larger) gap breaks down. This connects the HV to the trigger electrode whose potential swings positive past its initial value thus applying a high voltage across the second (smaller) gap which in most cases breaks sown because of a very large overvoltage. Figure 1 shows schematic circuit diagram of the SCSG and in Figure 2 the variations in gap voltages during operation are shown.

In Figure 2, we have assumed a gap setting of 3 mm and 2 mm and an operating voltage of 10 kV. With this gap setting which was used for most of our tests (see below) the range of operation of the swinging cascade is 8.5 kV to 13 kV. In dry air and with well rounded electrodes, each mm of air gap requires about 3 kV to break down (this reduces to about 2.5 kV if the humidity is higher). As the trigger electrode potential swings from +4 kV to -4 kV say, the voltage across the smaller gap Vg_2 also changes from +4 kV to -4 kV and this gap remains within its safe region. During this same period, the voltage across the larger (HV) gap goes from +6 kV to +14 kV, this large overvoltage causes the gap to breakdown. The trigger electrode potential then immediately swings upwards towards the working voltage and it may over shoot the working voltage. In the process the voltage across the smaller gap swings from -4 kV through its original value of +4 kV and then increases towards +10 kV. The smaller gap will breakdown sometime after $Vg_1 > 6$ kV (at the same time Vg_2 will drop back to 6 kV and then

swing towards 0 kV).

B) Experimental

a) Design considerations

In selecting components for a swinging cascade spark gap the following design criteria must be net:

i) $R_c << R_1 + R_2$ to avoid voltage loss across R_c, where R_c is the charging resistor and R_1 and R_2 are the bias resistors.

ii) R_1 and $R_2 \lesssim 100$ M to give good voltage division.

iii) $R_c > V_o$/cut-off current of

iv) $R_1/R_2 = G_1/G_2$ where G_1 and G_2 are the lengths of smaller and larger gaps respectively.

v) G_2 is set to hold $V_o\{R_2/(R_1+R_2)\}$ safely. G_1 is set to hold $\{V_o R_1/(R_1+R_2)\}$ safely. Note that air break down voltage is about 2-3 kV per mm.

b) Tests

Several sets of preliminary tests to determine the current capabilities of the spark gap and the voltage ranges for various gap setting were performed. The circuit diagram for these tests is as shown in Figure 1. The spark gap used in these tests was made from ½-inch copper plates. The main electrodes were laid on top of the capacitor connector plates and between them the trigger pin made from ½-inch copper pipe was fixed in position by perspex holders. The main electrodes could be adjusted by means of slots.

The gap is triggered via an isolating capacitor ($\sim$ 100 pF, 1m length of UR67 cable) from a 600 V SCR pulse stepped up by a 1:20 pulse transformer (EG&G TR69). The pulse rise time was < 1 µs. In later tests the triggering system was changed to a krytron unit giving a 1.5 kV pulse which was then stepped up 17 times by a TV transformer.

For one of the preliminary test shots, a 60 µF capacitor was charged to 9.3 kV and then discharged through a load consisting of a strip of Aluminium. The voltage waveform obtained by a Rogowski coil with an integration time constant of 200 µs placed around the short

circuit, shows a periodic time T = 10 μs and a reversal ratio (the ratio of successive voltage peaks) f = 0.597. The peak current passed is then given by[3]

$$\hat{I} = \frac{\pi C V_o (1 + f)}{T} = 280 \text{ kA}.$$

The total inductance of the system is given by

$$L = \frac{T^2}{4\pi^2 C} = 42.2 \text{ nH}.$$

By substracting the calculated inductance of 29 nH for the rest of the system, the inductance of the gap was obtained as 13.2 nH.

To determine the range of operation, the operating voltage V_o was increased in steps of 1 kV from 0 until the gaps breaks down spontaneously . The system was triggered 10 to 20 times, the minimum voltage at which both the gaps consistently break down and the voltage just before the gaps start to spontaneously break down are recorded as the range for that particular setting. Table 1 shows a typical set of result for the 3mm:2mm gap setting. The operating range for this setting was measured as 8.5 - 13 kV. Note V_2 is the actual operating voltage since the charging resistor has such a high value. To get higher or lower voltage ranges one need only to change the gap lengths keeping the same ratio. The 4.5mm:3mm gap ratio has an operating range of ∿ 12 - 16 kV.

In these tests two HV probes connected across the smaller gap (V_1) and across both the gaps (V_2) showed that the gaps fired consistently at 1.42 μs for Gap 2 and 1.46 μs for Gap 1, after the trigger pulse, with a measured jitter less than 50 ns. The break down time (from the synchronized pulse) may be written as 1.43 ± 0.03 μs.

DISCUSSIONS

The break down time and jitter may be reduced by a faster trigger pulse using the schematic shown in Figure 3. On charging, C_2 has 9 kV across it with the trigger pin at +6 kV and the other side of C_1 (point P) at 15 kV. C_1 has 15 kV across it with point P at 15 kV. On triggering SCG1 (with a negative pulse for the trigger pin)

Table 1

Determination of Operating Voltage of a 3mm:2mm Gap

Voltage across the spark gap (kV)	% break down times			
	Gap 1	Gap 2	Cascade	
0	100			
0.61	100			
1.21	100			
1.82	100			
2.43	80	20		
3.04	100			
3.64	60	40		
4.25	90	10		
4.86	100			
5.46	100			
6.10	100			
6.71	100			
7.29	40		60	
7.89	60		40	
8.50			100	
9.11			100	
9.76			100	8.5 - 13 kV
...			...	
...			...	
...			...	
13.42			100	
14.03	continuous breakdown			

point P drops down towards −15 kV with a time constant of $\sqrt{(L_{SG1}C_1)} \sim 1.4$ ns (where $L_{SG1} \sim 20$ nH and $C_1 = 200$ pF). This fast voltage drop at P ($\lesssim 4$ kV/ns) is transmitted to the trigger pin of SCG_2 causing breakdown of SCG2 in the order of several ns The capacitor C_1 and C_2 may be made of aluminium plates sandwiching mylar. Alternatively, C_1 and C_2 may be coaxial cables or strip line in which case the system would resemble a Blumlein.

In such a system to take advantage of the low jitter of the gap the pulse for synchronising equipment should be taken either from the trigger pin of the main gap (with adequate precaution) or from the I of the main discharge using a pick up coil.

CONCLUSION

A simple swinging cascade spark gap has been constructed and tested and found to give consistent and reliable operation over a wide range of voltages. The spark gaps have been used to switch a 30 μF, 15 kV capacitor at currents up to 180 kA per shot and is found to remain maintenance-free even after 200 shots.

ACKNOWLEDGEMENT

We (A.J.S. and S.) acknowledge UNU Fellowships without which this work could not have been possible. A grant from ICTP and from the University of Malaya (F232/74) are also acknowledged. Likewise the contribution and cooperation of all staff members of the Plasma Laboratory and other UNU Fellows in the Programme are gratefully acknowledged.

REFERENCES

1. R.A. Fitch and N.R. McCormick, Procs. Inst. Elect. Eng. 106, 117-130 (1959).
2. P.M. Barnes, J. E. Graber and T.E. James, Rev. Sci. Instrum, 44, 599 (1967).
3. S.Lee in Laser and Plasma Technology Ed. by S.Lee et al, World Scientific Pub Co, Singapore, 1985, p 16.
4 S.Lee et al J.Fiz. Mal. 7, 1 (1986); also submitted to Rev. Sci. Instrum.

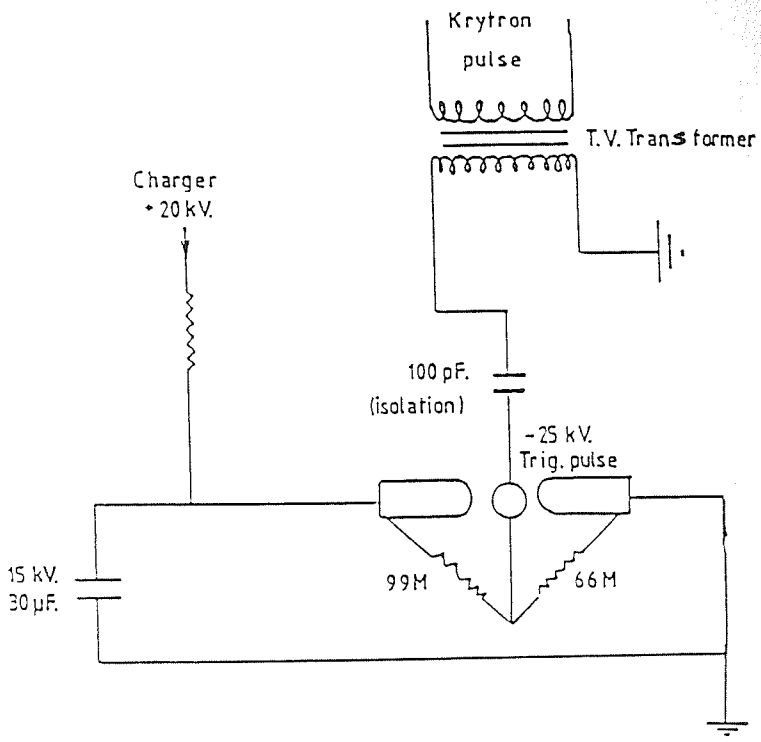

Fig. 1: Circuit diagram of a swinging cascade spark gap.

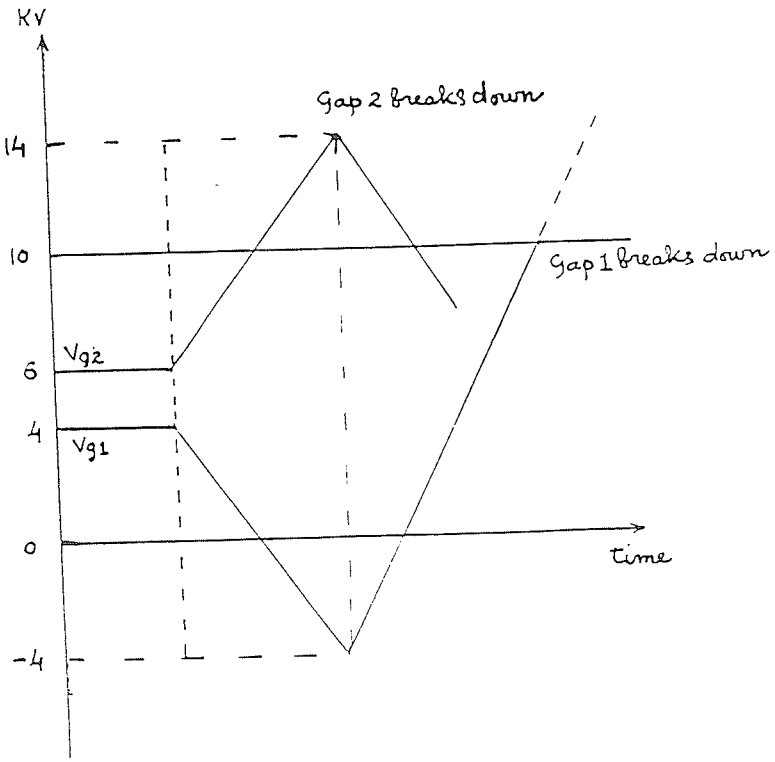

Fig. 2: Voltage waveform for a swinging cascade spark gap charged to 10 kV, gap setting and bias ratio 3:2 and triggered by a negative pulse.

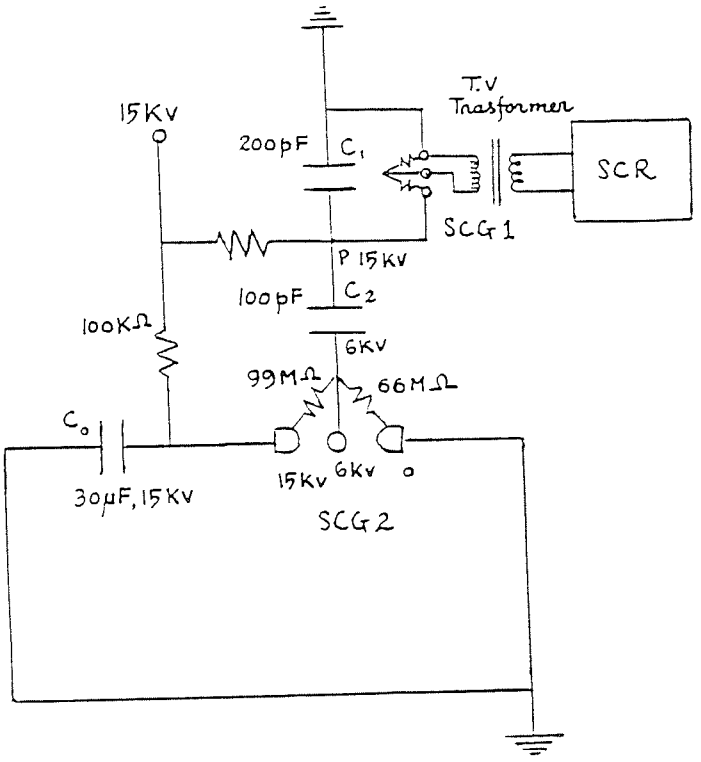

Fig. 3: Circuit diagram for a swinging cascade spark gap with very small breakdown time.

SECOND TROPICAL COLLEGE ON APPLIED PHYSICS

LASER AND PLASMA TECHNOLOGY

Kuala Lumpur

17 March - 5 April 1986

NUMERICAL DESIGN OF THE UNU/ICTP PLASMA FOCUS

K.H. Kwek, T.Y. Tou, Y.C. Yong*, Jalil Ali** and S. Lee

Plasma Research Laboratory

Physics Department, University of Malaya

59100 Kuala Lumpur, Malaysia

Abstract:

A model with two phases, an axial phase and a radial collapse phase is used to optimise numerically the design of a low-cost plasma focus. This has been applied in particular to the design of a 3.3 kJ plasma focus.

*Ngee Ann Polytechnic, Singapore.

**Universiti Teknologi Malaysia, Kuala Lumpur.

"Laser and Plasma Technology" Ed. S. Lee et.al
World Scientific Publishing Co. (1988)

PAPER

NUMERICAL DESIGN OF THE UNU/ICTP PLASMA FOCUS

INTRODUCTION

The plasma focus is a device by which a hot dense plasma may be produced with a generation of fusion neutrons in intense bursts of above 10^8 D-D neutrons per burst at the rate of 10^{16} neutrons per second in a period of tens of a nanosecond. A plasma focus system called the UNU/ICTP PFF (United Nations University/International Centre for Theoretical Physics Plasma Fusion Facility) is designed based on a dynamic model. The outcome of this design is a 3.3 kJ Mather-type plasma focus system powered by a single 15 kV, 30 μF capacitor. The design procedure is discussed below.

THEORY AND DESIGN

The focus design is based on a dynamic model[1] which considers the plasma focus as a device which operates in two distinct phases (Fig. 1) - an axial acceleration phase (in which the characteristic is very much similar to the electromagnetic shock tube) which crucially delays the radial compression phase until the plasma current reaches its peak value. The axial trajectory is computed using a snow-plow model while the radial dynamics is treated using a generalised slug model which considers a pinching plasma of increasing length with the plasma layer lying in between a shock front at position r and magnetic piston at position r. This model gives a realistic final pinch radius ratio. According to this model, the scaling parameters for the dynamics of the focus are:

The ratio of the characteristic times

$$\alpha = t_o/t_a \tag{1}$$

$$\alpha_1 = t_a/t_p \tag{2}$$

and the ratio of inductance

$$\beta = \frac{\frac{\mu_o Z_o}{2\pi} \ln \frac{b}{a}}{L_o} = \frac{L_a}{L_o} \tag{3}$$

$$\beta_1 = \frac{\beta}{\ln C} \tag{4}$$

where L_a = maximum inductance of axial phase

$C = \frac{b}{a}$

The characteristic times are given by:

$$t_o = \sqrt{(L_o C_o)} \tag{5}$$

$$t_a = \left[\frac{4\pi^2(b^2-a^2)}{\mu \ell n C}\right]^{\frac{1}{2}} \frac{Z_o \rho_o^{\frac{1}{2}}}{I_o} \tag{6}$$

$$t_p = \frac{4\pi}{\mu^{\frac{1}{2}}(\gamma+1)^{\frac{1}{2}}} \frac{a^2 \rho_o^{\frac{1}{2}}}{I_o} \tag{7}$$

where a = radius of inner electrode

b = radius of outer electrode

C = b/a

Z_o = length of focus tube

ρ_o = ambient gas density

μ = permeability of the plasma

γ = specific heat ratio of the plasma

Here t_o is the characteristic time of the L_o-C_o circuit where L_o being the inductance of the capacitor C_o together with all connections up to the plasma section of the focus tube. t_a is the characteristic time of the transit of the snowplowed plasma layer from the start of the discharge to the end of the axial phase. t_p is the characteristic 'pinching' time. The surge impedence of the L_o-C_o circuit is given by:

$$Z = \sqrt{(L_o/C_o)} \tag{8}$$

and

$$I_o = V_o/Z_o \tag{9}$$

where V_o is the initial voltage on the capacitor C_o.

Suitable combinations of the scaling parameters can be found to give design parameters that will give good efficiency in the radial collapse phase. However, adjustments of these parameters alone is not enough. In designing the plasma focus, a few design prinicples will have to be observed as a guideline to ensure proper symmetry and good snow-plow sweeping action.

In the design, one would like the axial transit time, $t_{a\,exp}$, to be matched to t_r, the rise time of the electric current I, i.e.

$$t_{a\,exp} \sim t_r \tag{10}$$

where

$$t_r = (\frac{2\pi}{4})\ t_o \tag{11}$$

Considering the effective reduction of the near sinusoidal driving current due to inductance matching in practical plasma focus system and also noting that t_a in Eq. (6) is the transit time for a constant driving driving current,

$$t_{a\,exp} \sim 2t_a \tag{12}$$

The ratio of the characteristic axial transit time to the characteristic 'pinching' time is

$$\frac{t_a}{t_p} = \frac{(\gamma+1)^{\frac{1}{2}}}{2} \frac{(C^2-1)^{\frac{1}{2}} Z_o}{(\ell nC)^{\frac{1}{2}} a} \tag{13}$$

For a Mather type focus with $C = \frac{b}{a} \sim 3$ and with γ between $\frac{5}{3}$ (for fully ionised plasma such as hydrogen or deuterium in the plasma focus) and 1.14 (for freely ionising[2] gas such as argon in the plasma focus), Eq. (12) may be approximated to:

$$\frac{t_a}{t_p} \sim CF \tag{14}$$

where F is the aspect ratio Z_o/a.

In the operation of the Mather plasma focus, the pinch phase occurs over a relative short period t_p after a relatively long period ($t_{a\,exp}$) of axial phase in which the capacitor current builds up. During the pinch phase, about 10-20 % of the initially stored energy is transferred to the plasma in approximately 2% of the current rise time. The resulting power enhancement during the pinch phase is crucial to the proper operation of the plasma focus. It is important then that the ratio t_a/t_p be of the order of 30-50 for the Mather focus.

For good snow-plow action in the axial phase, the minimum speed requirement is in the vicinity of 6 cm/μs. On the other hand, speeds greater than 10 cm/μs would result in the formation of a radial 'spoke' discharge or restriking[1,3] of the discharge at the backwall. This has the effect of introducing an asymmetry in the magnetic field pattern whilst at the same time shunting away part of the current. In the operation of the focus in deuterium, for good focussing and consistent neutron yield, the acceptable axial speeds is between the limits of 6-10 cm/μs. The corresponding test gas pressure appears to be between 0.5 to 20 torr.

The design of the plasma focus facility hinges on the choice of the capacitor bank and its characteristics such as capacitance, voltage rating and internal inductance. For the UNU/ICTP plasma focus device, a single Maxwell capacitor rated at C_o = 30 μF, V_o = 15 kV with an equivalent series inductance of less than 40 nH is used. This capacitor is chosen for reasons of economy and cost-effectiveness. A value of L_o at 110 nH is estimated from the system using a parallel-plate geometry for capacitor connections and the switch, with coaxial cables being used to connect to the plasma focus input flanges. From the above values of L_o and C_o, the following quantities are obtained:

t_o = 1.82 μs
$t_{a\,exp} = t_r$ = 2.86 μs
I_o = 248 kA

To obtain an average speed of 5.5 cm/μs (or a peak axial speed of ∿9 cm/μs[1] just before the focus phase) a value of Z_o = 16 cm will be required. The radii a and b are designed to take the values of 9.5 mm and 32 mm respectively in order to maintain the axial speed to within the limits indicated earlier. The value of b/a is of the order of 3.4 which is near optimum[4]. The above values determine the value of the ambient gas density ρ_o to be 0.21 x 10^{-3} Kgm^{-1}. This is an equivalent of 0.9 torr of deuterium which is within the operational limits indicated earlier for deuterium focus.

COMPUTATION

From the above figures, the values of the scaling parameters as

defined by Eqs. (1), (2), (3) and (4) can be calculated and be used in the dynamic model computation. Thus:

$$\alpha = \frac{t_o}{t_a} = 1.26 \qquad \beta = \frac{L_a}{L_o} = 0.36$$

$$\alpha_1 = \frac{t_a}{t_p} = 40.4 \qquad \beta_1 = \frac{\beta}{\ell nC} = 0.29$$

The computation is done for several values of the parameter α (each corresponding to a certain value of ambient gas pressure). Figure 2 shows a set of computed current waveforms (in normalised values) for various gas pressure. The computation results show good focussing action over the range of values of α from 1.5 to 0.7 corresponding to a pressure range of 0.5 torr to 2.0 torr. The computation results add confidence to the design of the plasma focus.

DISCUSSION

It must be pointed out that in the considerations mentioned above, the actual current rise time may be affected by plasma dynamic effects as well as switch characteristics, thus affecting the time matching of $t_{a\,exp}$ and t_r. Also, machine effects such as current shedding and current re-strike[1] are not included in the dynamic model. These may affect the actual performance of the plasma focus operation. Ultimately, to obtain optimum parameters for actual focus operation, fine tuning by variation of V_o, ρ_o, Z_o, a and b may be needed. However, if the above design parameters are close to optimum, then only a variation of ρ_o may be sufficient to established a regime of good plasma focus operation.

The value of β at 0.36 achieved in this design procedure appears to be quite low. For typical operations of the plasma focus, one would like to have $\beta \sim 1$. However, even at $\beta = 0.36$, the UNU/ICTP Plasma Focus performed very well when the system was tested between 13-15 kV in various gases including air, argon, hydrogen and deuterium[5]. In deuterium, strong focus is observed in 1-5 torr with the best focussing at 2.5 to 3 torr. A neutron yield of the order of 10^8 per shot is obtainable when operated at 3 torr deuterium and 15 kV. The system also shows consistency and reproducibility in operation.

CONCLUSION

A simple cost-effective plasma focus device based on a 3.3 kJ single capacitor has been designed using a dynamic model guided by a few design principles. Numerical computation indicates that good focussing actions are obtainable from the design parameters. The practicability of such design procedure is further confirmed by the consistency and reproducibility in the performance of the actual plasma focus device constructed from this design.

REFERENCES

1. S. Lee in 'Laser and Plasma Technology' edited by S. Lee, B.C. Tan, C.S. Wong and A.C. Chew, World Scientific, Singapore, p. 37, 64 and 387 (1985).
2. S. Lee, Australian J. Phys. 36, 891 (1983).
3. J.W. Mather, P.J. Bottoms, J.P. Carpenter, K.D. Ware and A.H. Williams, Report No. IAEA-CN-28/D-5, 561 (1972).
4. S. Lee and Y.H. Chen, Fusion Energy - 1981 (ICTP, Trieste) IAEA-SMR-82, Vienna p. 297.
5. S. Lee, T.Y. Tou, S.P. Moo, M.A. Eissa, A.V. Gholap, K.H. Kwek, S. Mulyodrono, S.J. Smith, W. Usada, M. Zakaullah, American J. Phys. 56, 62 (1988).

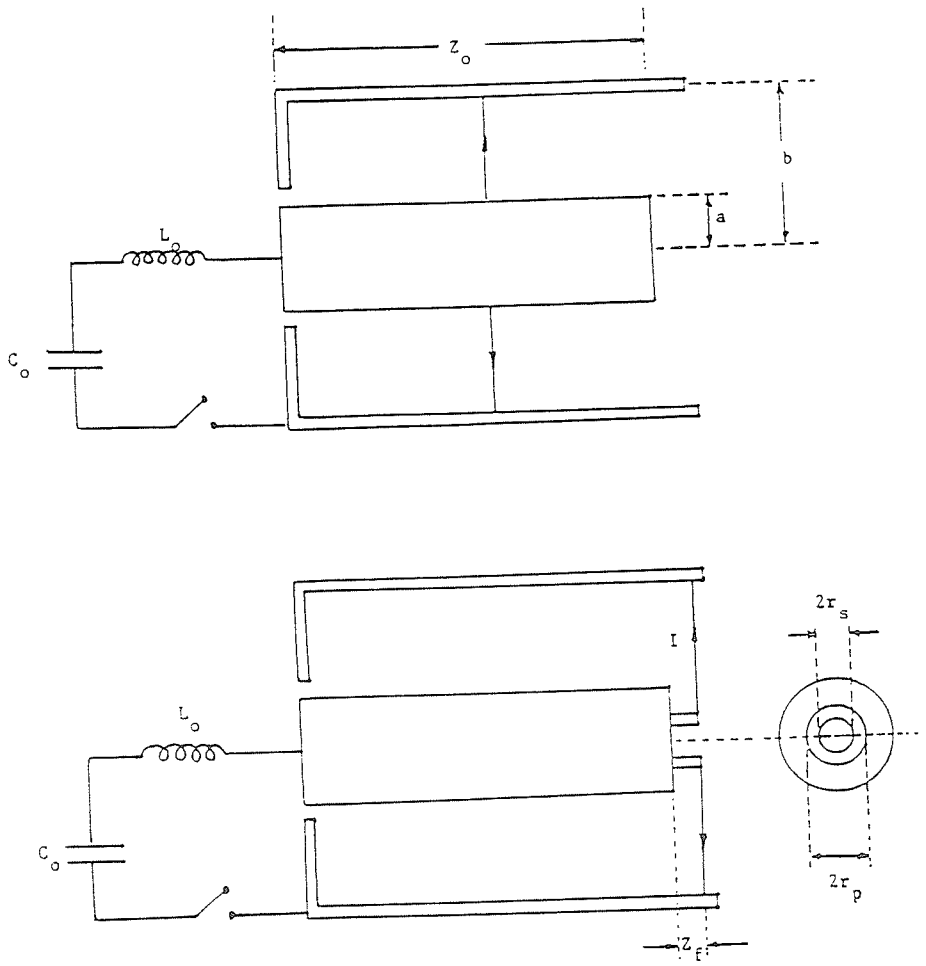

Figure 1. (a) The axial run-down (shock tube) phase of the plasma focus.

(b) The radial focus(pinch) phase of the plasma focus.

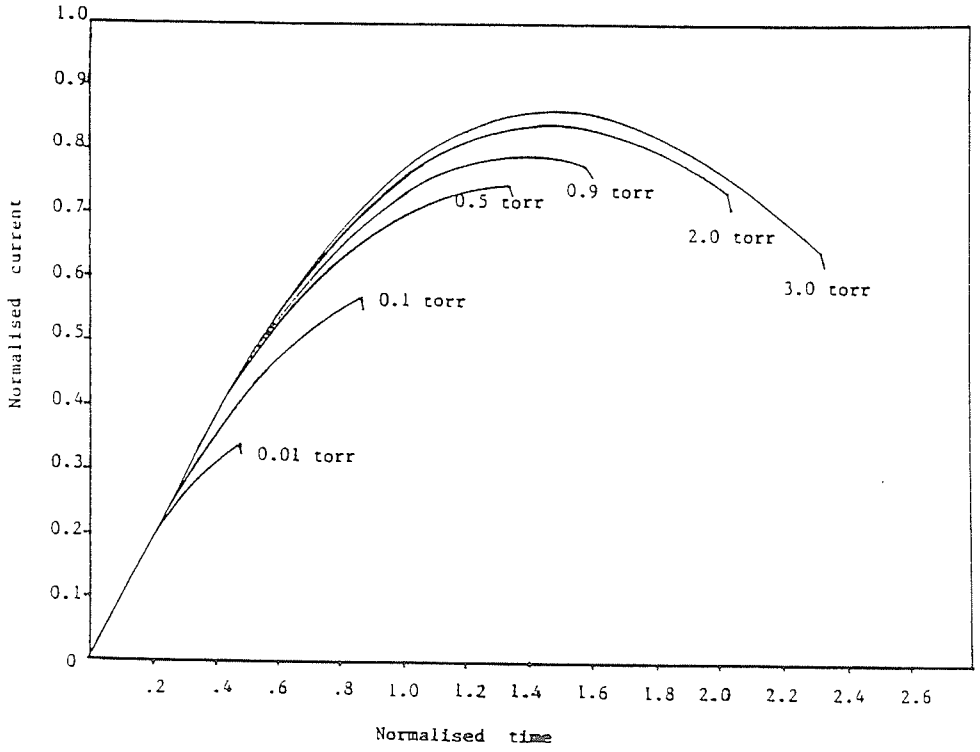

Figure 2. Computed current waveforms for various gas filling pressures.

J. Fiz. Mal. 7; 125 (1986)
Research Note

DETERMINING NITROGEN LASER CHANNEL PARAMETERS

K.H. KWEK, A.J. SMITH*, T.Y. TOU, A.V. GHOLAP* and S. LEE
United Nations University Training Programme
on Plasma and Laser Technology
Physics Department, University of Malaya
59100 Kuala Lumpur, Malaysia

Received 22 April 1986

Abstract

This paper reports the measurement of the nitrogen laser channel current using a magnetic probe. For a 46 cm laser channel of gap 16 mm operated at 10 kV, 60 torr with foil capacitors of 58 and 28 nF, the channel current, inductance and resistance are found to be 42 kA, 1.6 nH and 0.1Ω respectively.

Two critical quantities for determining nitrogen laser performance are the laser channel inductance and resistance (L_{go}, r_g). These quantities determine the laser channel discharge current as well as the electrical power absorbed by the laser channel. The quantities L_{go} and r_g have been described[1] as 'unmeasurable' so that they are either taken as parameters or computed using a gas discharge model or deduced by matching theoretical and experimental voltage waveforms[1-4]. A more direct method of measuring these quantities appears desirable. In this study the laser discharge current in a Blumlein-type nitrogen laser is measured using a magnetic probe, and from the laser channel current waveform the values of L_{go} and r_g are directly measured.

The circuit theory of the nitrogen laser has been discussed earlier[2]. Essentially the laser consists of a laser channel represented by L_{go} and r_g, two parallel plate capacitors C_1 and C_2 with very low inductances L_1 and L_2, charged to Vo. The arrangement is as shown in the circuit of Fig. 1. L_{g1} and L_{g2} are the inductances of the plates connecting C_1 and C_2 to the laser channel. The capacitor C_2 is connected to a parallel-plate swinging cascade spark gap represented by L_e and r_e in the diagram. For these measurements the values of the parameters are $C_1 \sim 58$ nF, $C_2 \sim 28$ nF, $L_1 \sim 0.13$ nH, $L_2 \sim 0.07$ nH, $L_{g1} = L_{g2} \sim 0.8$ nH and $L_3 \sim 13$ nH. The quantities L_{go} and R_g are to be measured. The triggering of the external gap switch produces a rate of rise of laser channel voltage of the order of $2V_o/\sqrt{(L_eC_2)}$ which is usually sufficient to cause a uniform break-down all along the laser channel when the voltage across the channel attains a sufficient value. The main discharge between C_1 and C_2 occurs with a periodic time given by

$$T = 2\pi\sqrt{[(L_1+L_2+L_g)\,(C_1 \cdot C_2)/(C_1+C_2)]} \qquad (1)$$

where $L_g = L_{g1}+L_{g2}+L_{go}$. This is modulated by a slower discharge with a time constant of $\sqrt{[L_e\,(C_1+C_2)]}$ which eventually removes the remnant stored energy through the external spark gap r_e. The effective damping parameter of the laser gap discharge is given by

$$\alpha = r_g/Z_L \qquad (2)$$

(2)

where the surge impedance of the laser channel circuit is:

$$Z_L = \sqrt{[(L_1+L_2+L_g)\,(C_1+C_2)/C_1C_2]} \qquad (3)$$

The laser channel (Fig. 2) consists of two horizontally placed brass rods (as electrodes), 46 cm long, soft-soldered onto thick brass strips (50 cm x 5 cm) which provide external contact for the electrodes. The gap between the electrodes is 16 mm. The laser light is brought out through two 2 – cm quartz covered holes in the perspex end pieces.

* UNU Fellows

The capacitors C_1 and C_2 are formed by 4 sheets of mylar in between strips of aluminium kitchen foil. The dimensions of C_1 and C_2 are 45 cm X 45 cm and 45 cm X 23 cm giving measured capacitances of 58 nF and 28 nF respectively. The laser channel is connected to the capacitors by pressure contact and the whole assembly is supported by a flat aluminium plate which also provides electrical contact. The capacitor C_2 is connected to a swinging cascade spark gap. For these experiments the laser peak power is maintained above 200 kW.

The magnetic probe consists of a 10-turn coil of SWG 40 wire on a 1mm former enclosed in a 3mm glass tube inserted with its axis parallel to the laser channel axis into a specially arranged space (Fig. 2). In this position the probe lies directly underneath the channel discharge current and over that portion of the earth plate which connects C_1 and C_2 and carries the return discharge current. The probe, passively integrated with a 12 μs RC time constant, has a calibration factor of 1.04 volt/tesla. The laser pulse is measured using a fast photodiode (FND 100) and a 100 MHz storage oscilloscope inside a screened cage.

The results of the measurements are summarised by oscillograms in Fig. 3. Figure 3a shows the magnetic probe signal with the channel at atmospheric presusre and the value of V_o = 10 kV so that only the spark gap breaks down. The high frequency oscillations in the signal are identified as electrostatic pick-up resulting from reflections in the transmission line C_2 as this capacitor discharges through the spark gap inductance. Figure 3b shows the typical probe signal with the laser channel at 60 torr nitrogen so that the laser channel discharges after the spark gap is triggered. The new feature of the probe signal i.e. the lower frequency damped oscillations which commences 100 ns after the spark gap break-down is due to the laser gap current. This is shown by adding the magnetic probe signal and the photodiode signal using the add mode of the oscilloscope as in Fig. 3d. The photodiode signal alone is shown in Fig. 3c. Cables are matched to 0.5 ns.

From the current signal of Fig. 3b the periodic time of the damped oscillations of the channel current is measured to be T = 50 ns. Applying Eq. (1) a value of L_{go} = 1.6 nH is obtained. Eq. (3) then gives Z_L = 0.42 Ω.

The current reversal ratio f is measured as 0.69 (Fig. 3b) and from this $\alpha = (2/\pi)\ell nf = 0.24$; so that Eq. (2) yields $r_g = \alpha Z_L = 0.1\ \Omega$ which is the time-averaged laser channel resistance.

The magnetic probe placed in this position (Fig. 2) measures a magnetic field which is related to the laser loop current I_L by the equation:

$$B = \mu I_L/\ell \qquad (4)$$

where ℓ = 0.46 m is the length of the laser channel. From the oscillogram of Fig. 3b and the probe calibration factor, I_L = 42.1 kA.

From the measured peak current and the surge impedance of the laser channel circuit the voltage across the laser channel V_g when the laser channel breaks down is obtained as 17.7 kV.

A comparison between the measured laser channel current or magnetic field waveform of Fig. 3b for measured α = 0.24 and the computed laser channel current waveform (normalised) of Fig. 4 for α = 0.3 shows good agreement between the two waveforms except that the measured current waveform shows a squaring-out effect in the first two cycles, probably due to the transmission line effects. More details will be reported.[5]

References

1. C. Iwasaki and T. Jitsuno, IEEE J. Quantum Electronics, QE-18, 423 (1982).
2. S. Lee, A.V. Gholap, A.J. Smith, K.H. Kwek, A.C. Chew, T.Y. Tou and S. Sapru, J. Fiz. Mal. 6, 165 (1986).
3. T. Mitani, J. Appl. Phys. 52, 3159 (1981).
4. W.A. Fitzsimmons, L.W. Anderson, L.E. Riedhauser and Jan M. Vrtilek, IEEE J. Quantum Electronics, QE-12, 624 (1976).
5. A.J. Smith, K.H. Kwek, T.Y. Tou, A.V. Gholap and S.Lee, accepted by IEEE J. Quantum Electronics.

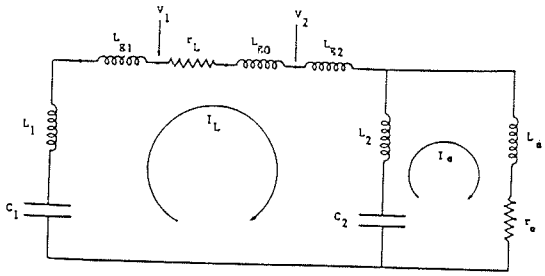

Fig.1 Equivalent circuit for the N_2 laser. I_L is the current flowing through the laser channel. I_e flows through the external gap switch.

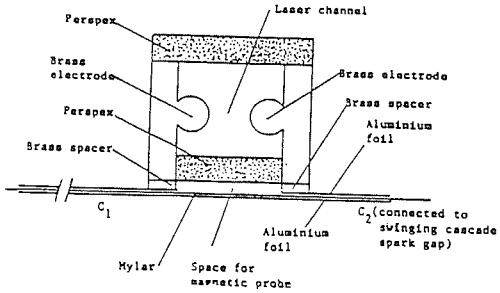

Fig.2 Cross-sectional view or the N_2 laser showing the locations of the laser channel and the space provided for magnetic probe insertion, relative to the aluminium foil capacitors.

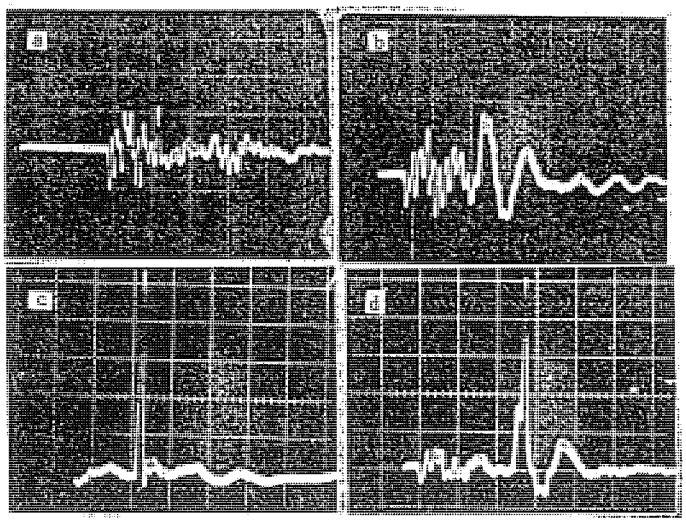

Fig.3 Oscillograms of magnetic and photodiode signals.Time-base is 50ns/div.

a) Magnetic probe signal. Laser at atmospheric pressure.No laser channel discharge.

b) Magnetic probe signal.Laser at 60 torr nitrogen.Discharge with lasing action.(0.1volt/div.).

c) Photodiode signal of laser pulse. Laser operated under same condition as in (b).

d) Photodiode signal superimposed onto magnetic probe signal.Laser operated under same condition as in (b).

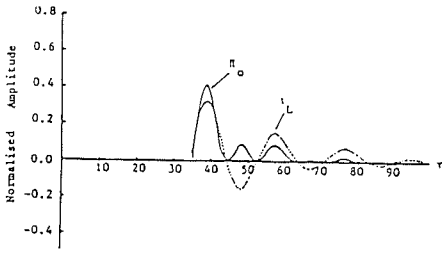

Fig.4 Computed laser channel current waveform i_L (normalised) for $\alpha = 0.3$. Also shown is the normalised power absorbed by the laser channel.

Malaysian J. Sci. 8: 135–139

MALAYSIAN
JOURNAL OF SCIENCE

Design and operation of a hard-pumped Ruby laser system

Harith bin Ahmad and S. Lee
Physics Dept., University of Malaya, 59100 Kuala Lumpur, Malaysia.

Abstract. In this paper we report the lasing observations of a home-made hard-pumped ruby laser system. The system comprises of a power supply for the flashlamps, a trigger circuit and an optical cavity. The optical cavity is constructed from brass in a closed-coupled configuration. The inside surface of the cavity is chrome-plated and is held in place by stainless-steel mountings. The trigger circuit is the UJT-SCR-krytron type which delivers ~ 1kV positive pulses into an EG&G series injection trigger transformer. This produces ~ +22 kV pulses which trigger the flashlamps, which is followed by a main current discharge. Lasing action can be observed from the deep burn mark on an exposed dark polaroid photographic paper.

IKHTISAR. *Di sini kami laporkan pemerhatian-pemerhatian melase sistem laser delima buatan sendiri. Sistem ini terdiri daripada satu pembekal kuasa bagi lampu kilat, satu litar picu dan satu rongga optik. Bahagian rongga optik diperbuat daripada loyang dalam bentuk yang tertutup. Permukaan dalam rongga ini disadur dengan kromium dan diletakkan di atas pemegang keluli nirkarat. Litar picu yang digunakan adalah dari jenis UJT-SCR-kritron yang menghasilkan ~ 1kV denyutan positif ke dalam transformer injeksi picu jenis EG&G. Ini menghasilkan denyutan bernilai ~ 22kV yang memicu lampu kilat yang diikuti dengan discas arus utama. Tindakan melase dapat diperhatikan daripada tanda terbakar pada kertas gambar polaroid gelap yang terdedah.*

INTRODUCTION

Since the first operation of the ruby laser (Maiman 1960), it has come a long way with various modifications and improvements. In this paper we report the design and construction of a simple yet powerful ruby laser which can be easily constructed using modest laboratory facilities. This design features a single shot facility and thus does not require any cooling system. It has been operated for more than 100 shots with no distortion in the structure of the ruby rod being observed. Lasing in ruby occurs in the Cr^{3+} ions which is doped into the crystal structures of $A1_2 0_3$ at 0.05%. This corresponds to ion density of $1.58x10^{19}$ ions cm\$^3$. The system is pumped by two straight linear flashlamps in closed-coupled configuration with a ruby rod in the centre. Excitation occurs between the ground state $^4A_2$ to $^4F_2$ and $^4F_1$ which corresponds to the green and blue bands of the Cr^{3+} ions. Dominant lasing action

occurs between the E and the ground state $^4A_2$ (6943 A). Although we can obtain lasing action between 2A and $^4A_2$ (6929A), this line is being inhibited by selective action of the front and back mirrors which peaks at 6943A (Koechner 1976).

In the following section the optical cavity design is considered in detail. It is machined locally in this department, which greatly reduces the overall cost of our laser.

OPTICAL CAVITY

The optical cavity comprises of the pump cavity, the back and the front mirrors. Reflectivities of the front mirror and that of the back mirror are 65% and 100% respectively and they are placed 50 cm apart. They are mounted in precision gimbal mirror mounts. The pump cavity is constructed from a solid brass block which is cut into two halves of dimension 92 mm x 79.5 mm x 20 mm (see Fig. 1.), having two hollow slots. When combined the two halves create a cavity of dimension 92 mm x 40 mm x 14 mm. The internal surfaces are chrome-plated thick enough to provide good reflectivity of the pump light from xenon flashlamps. The excitation source used in this system is a noblelight xenon flashlamp (Noblelight Ltd) operated at 450 torr with an explosion energy of 2880J at 1ms pulsewith. The flashlamps are placed on both sides of the ruby rod which is positioned at the centre of the pump cavity. The cavity is mounted into position by two mounting heads which are made of stainless steel (JK Laser system). Four mounting pins are used to hold them into position and the pump cavity is placed onto an inverted 'T' optical bench.

The ruby rod is side-pumped in a closed-coupled configuration. This geometry is generally more efficient and easier to fabricate compared to the elliptical cavity. In the closed-coupled cavity, the lamps and rods are placed as close together as possible. With the lamps placed on both sides of the ruby rod a reasonably uniform pumping could be attained. The transfer of stored capacitor energy to the xenon lamps is controlled by the UJT-SCR-krytron circuit (Lee 1985) as shown in Fig. 2.

ELECTRICAL SYSTEM

The electrical system comprises of two circuits: (i) the control or trigger circuit, and (ii) the flashlamps circuit. As given in Fig. 2, the inclusion of UJT is to generate repetitive pulses with the pulse repetition rate being controlled by the variable resistor R_1 and capacitor C_1. At present our ruby system is being operated on a single-shot basis with pulses produced by a single-shot push to make contact switch S. On pressing this switch, the current begins to flow from the +20 V power supply to charge up the capacitor C_2, thereby producing a + 20 V positive going pulse across the primary terminals of the 1:1 pulse transformer. This low voltage pulse is used to trigger the gate of the SCR with input gate current upto I_{GT} = 200 mA. At this instant, the capacitor C_3 which is charged to + 200 V via R_2 discharges through the SCR and produces a + 200 V positive pulse across the 440 Ω resistor (R_3). This pulse is then transmitted to the grid of the EG&G KN-6B krytron (EG&G 1984) via an isolating 1:1 pulse transformer to cause preionization between the grid mesh wire and the cathode. The + 1 kV charged capacitor will begin to discharge

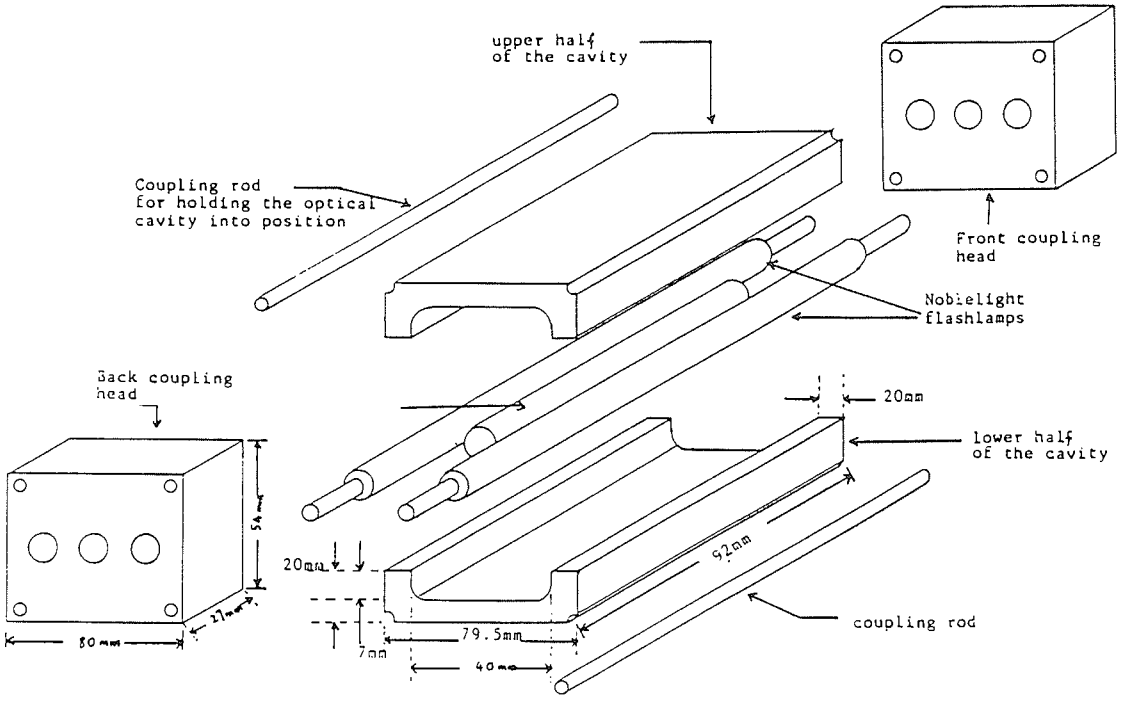

Figure 1. Exploded view of the optical cavity.

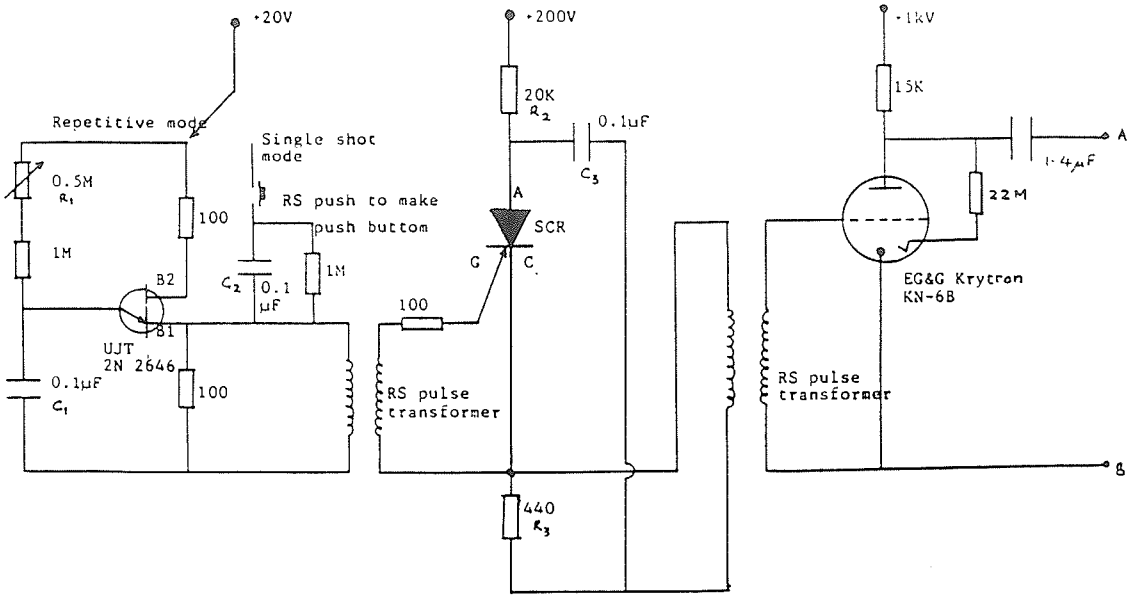

Figure 2. Trigger circuit for triggering the flashlamps.

through the krytron and at the same time produce a negative voltage swing pulse of ~ 1 kV at the output terminal AB.

This negative-going ~ 1 kV pulse is stepped up to ~ 22 kV with the aid of the EG&G TS-146A series injection trigger transformer (EG&G 1983) as shown in Fig. 3. The 480 μF capacitor bank is charged to 2 kV by a home-made power supply

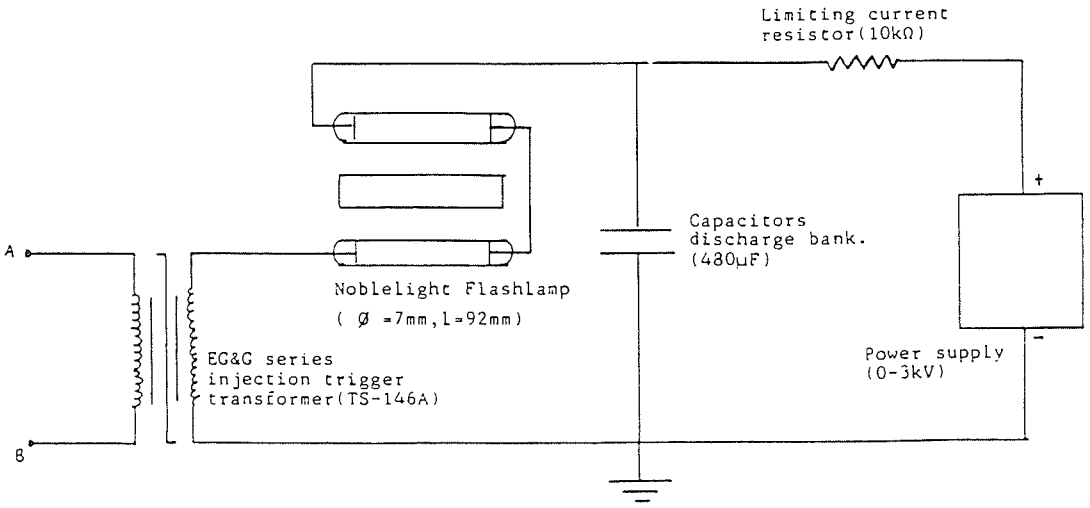

Figure 3. Flashlamps electrical circuit.

capable of producing voltages from 0-3 kV. The ~ 22 kV negative pulse applied to the cathode will swing the cathode down to ~ 24 kV which will cause preionization in the flashlamps. At this instant, the charges that are stored in the capacitor will begin to flow to initiate the main discharge. During the main discharge the series injection transformer core saturates and the circuit inductance drops to 100 μH. Powerful flashes of high intensity light are observed, with risetime of the order of 0.2 ms. This is shown in Fig. 4. The bottom trace is the optical signal from the

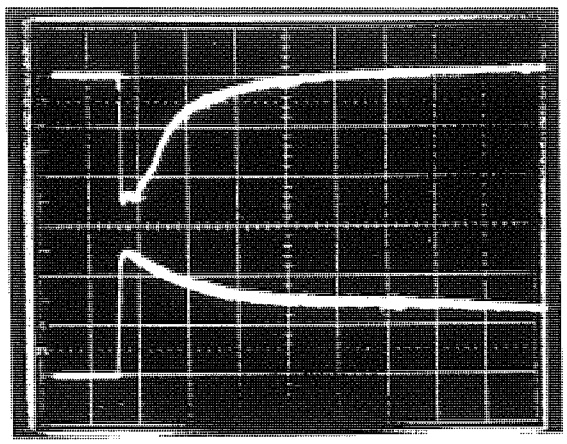

time scale: 2ms/div

Figure 4. Oscilloscope traces of the spontaneous emission and optical output from the flashlamps. (Upper trace : spontaneous emission of the ruby rod; Bottom trace : optical output from the flashlamps. Taken at 1 kV changing voltage).

flashlamp measured using the EG&G SGD-100A wide area photodiode (EG&G 1985). The long tail is due to the saturation of the photodiode. The upper trace indicates the optical output of the spontaneous emission of the ruby rod. This is taken at 1 kV charging voltage. In this system the pulse forming inductor is being omitted thereby reducing the risetime resulting in hard-pumping of the Cr^{3+} ions.

This will pump the Cr^{3+} ions into upper lasing level (^{2}E) in a much shorter time compared to the lifetime which is in the region of 1 ms. As a result this population inversion can be easily achieved at lower charging voltages. Threshold lasing action can be observed at 2 kV in our home-made laser system. At this operating voltage, a very intense burst of pinkish light is observed at the output. The lasing action is confirmed by a deep burn mark on an exposed dark polaroid photographic paper. This burn mark is reproducible which indicates a small divergence angle at the laser beam.

Further investigations and experiments are in progress to calibrate, to measure the output power, to characterize and to optimize the system. This will then act as an amplifier for the JK 2000 ruby laser oscillator to produce a very intense pulse for laser-plasma interaction studies.

Acknowledgement. We would like to thank University of Malaya for its financial assistance (F195/85) and also Mr. Toh for his technical assistance.

REFERENCES

EG&G DATA SHEET T4000D-1 (1983).

EG&G DATA SHEET K5500C-2 (1984).

EG&G DATA SHEET D3003D-2 (1985).

JK Laser System, Lumonics, Inc, 105 Schneider Road, Kanata (Ottawa) Ontario, Canada K2K 1Y3.

Koechner, W. (1976). *Solid- state Laser Engineering.* Springer-Verlag, New York.

Lee, S. (1985). In: *Laser and Plasma Technology* (edited by Lee, S., Tan, B.C., Wong, C.S & A.C. Chew). World Scientific Publishing Co., Singapore (1985).

Maiman, T.H. (1960). *Nature* 187 : 493.

Noblelight Ltd., Cambridge Science Park, Milton Road, Cambridge CB4 4BH, England.

J. Fiz. Mal. 7, 1 (1986)

PRELIMINARY RESULTS OF THE UNU/ICTP PLASMA FOCUS

S. LEE, T. Y. TOU, M. A. EISSA*, A. V. GHOLAP*, K. H. KWEK, S. P. MOO
S. MULYODRONO*, A. J. SMITH*, SURYADI*, W. USADA*, M. ZAKAULLAH*
United Nations University Training Programme
on Plasma and Laser Technology
Physics Department
University of Malaya
Kuala Lumpur.
Malaysia

Abstract

The theory of a small Mathers-type focus is summarised to obtain a simple, reliable and low-cost design. From this design is constructed the UNU/ICTP Plasma Focus. Preliminary tests on six sets of the device indicate remarkable reliability and reproducibility over a total of 1000 discharges with excellent focussing characteristics in air, argon, hydrogen and deuterium. In deuterium at 3 torr a consistent neutron yield of $0.5 - 1.0 \times 10^8$ neutrons per discharge is obtained.

Introduction

A simple plasma device is designed that produces 10^8 D-D fusion neutrons per burst during the burst which lasts for tens of nanosecond. This design is so simple that several sets have been easily duplicated for transfer to various countries. The device called the UNU/ICTP PFF (United Nations University/International Centre for Theoretical Physics Plasma Fusion Facility) is a 3.3 kJ plasma focus system powered by a single 15 kV, 30 μF capacitor switched by a simple parallel-plate swinging cascade air-gap.

The system produces remarkably consistent focussing action in several gasses including air, argon, hydrogen, and deuterium. A consistent neutron yield of $0.5 - 1 \times 10^8$ neutrons per discharge is obtained at 3 torr deuterium operating the focus at 15 kV and 180 kA current.

Theory

The focus design is based on a dynamic model[1, 6] (see Fig. 1) which considers the focus dynamics in two separate phases – the axial run-down (shock tube) phase which crucially delays the radial focus, or pinch phase until the plasma current has reached its

*M.A. Eissa, Physics Department, Al-Azhar University, Cairo, Egypt.
A. V. Gholap, Physics Department, Rivers State University of Science and Technology, Port Harcourt Nigeria.
S. Mulyodrono, Indonesia National Institute of Aeronautics and Space, (LAPAN), Jakarta, Indonesia.
A. J. Smith, Physics Department, Njala University College, Sierra Leone.
Suryadi and W. Usada, PPBMI, BATAN, National Atomic Energy Agency, Yogyakarta, Indonesia.
M. Zakaullah, Physics Department, Quaid-I-Azam University, Islamabad, Pakistan.

peak value. The first design point is therefore to have:

$$t_r = t_{a\,exp} \tag{1}$$

where $$t_r = \frac{2\pi}{4} t_o \tag{2}$$

with $$t_o = \sqrt{L_o C_o} \tag{3}$$

and $$t_{a\,exp} \sim 2t_a \tag{4}$$

where $$t_a = \left[\frac{4\pi^2 (b^2 - a^2)}{\mu \ell n \frac{b}{a}} \right]^{\frac{1}{2}} \frac{z_o \rho_o^{\frac{1}{2}}}{I_o} \tag{5}$$

Here t_r is the current rise time and $t_{a\,exp}$ is the transit time of the plasma layer for the axial phase. The quantities t_o and t_a are characteristic times of the axial phase according to the model[1]. Here L_o is the inductance of the capacitor C_o together with all connections up to the plasma section of the focus tube, 'a' and 'b' are respectively the inner and outer radii of the focus tube, z_o its length, ρ_o the ambient gas density, μ the permeability of the plasma (same as the permeability of free space) and

$$I_o = V_o/(L_o/C_o)^{\frac{1}{2}} \tag{6}$$

where V_o is the initial voltage on the capacitor.

The second design point involves the characteristic 'pinching' time of the plasma focus phase. This may be shown to be[1]

$$t_p = \frac{4\pi}{\mu^{\frac{1}{2}} (\gamma + 1)^{\frac{1}{2}}} a^2 \frac{\rho_o^{\frac{1}{2}}}{I_o} \tag{7}$$

where γ is the specific heat ratio of the plasma. From this expression of t_p it is noted that the ratio of the characteristic axial transit time to characteristic focus time is

$$\frac{t_a}{t_p} = \frac{(\gamma + 1)^{\frac{1}{2}}}{2} \frac{(c^2 - 1)^{\frac{1}{2}}}{(\ell nc)^{\frac{1}{2}}} \frac{z_o}{a} \tag{8}$$

For a Mathers type focus with $c = \frac{b}{a} \sim 3$ and with γ between $\frac{5}{3}$ (for fully ionized plasma such as hydrogen or deuterium in the plasma focus) and 1.14 (for a freely ionizing[2] gas such as argon in the plasma focus), Eq. (8) may be approximated to

$$\frac{t_a}{t_p} \cong cF \tag{9}$$

where F is the aspect ratio z_o/a.

A crucial factor in the operation of the Mathers plasma focus is that the axial phase occurs over a relatively long period $t_{a\ exp}$ enabling the build up of capacitor current. The pinch phase then occurs over a relatively short period t_p. During this time t_p approximately 10 – 20% of the initially stored energy is transferred to the pinch plasma in approximately 2% of the current rise time. This results in a power enhancement factor during the pinching phase which is crucial to the proper operation of the plasma focus. It is important then that the ratio t_a/t_p be of the order of 30 – 50 for the Mathers focus.

The third point to be considered in the design is that there are limits[1] of speed and pressure in the operation of the plasma focus. In deuterium for good focussing and consistent neutron yield, the axial speed just before focussing should be between the limits 6 – 10 cm/μs; the lower limit being the minimum speed required for a good snow-plowing action in the axial phase and the higher limit being imposed by restriking[1, 3] of the discharge at the backwall or in the shock tube section. The limits of test gas pressure appears to be between 0.5 torr to 20 torr for deuterium; the lower limit apparently governed by re-striking; the upper limit by current filamentation[4].

The design of a plasma focus may take as a starting point the availability, or choice, of a capacitor bank. For the present exercise from the point of view of economy and cost-effectiveness a single Maxwell capacitor rated at C_o = 30 μF, V_o = 15 kV with an equivalent series inductance, ESL, of less than 40 nH was selected. A parallel-plate geometry was selected for the capacitor connections and the switch, with coaxial cables being used to connect to the plasma focus input flanges. The value of L_o was estimated at 110 nH. Having fixed C_o and L_o Eqs. (3) and (2) give a value of t_r of 2.9 μs. Eq. (6) yields I_o = 248 kA. The time matching condition of Eq. (1) fixes $t_{a\ exp}$ at 2.9 μs. The value of z_o was then chosen at 16 cm to give an average axial speed of 5.5 cm/μs or a peak axial speed[1] of ~ 9 cm/μs just before the focus phase. This axial speed is expected to be suitable for a good focussing action in deuterium.

The value of I_o is considerably smaller than most operational plasma focus machines which typically have I_o of the order of 500 kA or more. Observing from Eq. (5) that the axial speed is $\sim I_o/\left[(b^2 - a^2)\rho_o\right]^{\frac{1}{2}}$ and from Eq. (7) that the radial speed is $\sim I_o/(a^2\rho_o^{\frac{1}{2}})$ it is noted that a reduction in I_o may be compensated in the first instance by a reduction in a^2 and $(b^2 - a^2)^{\frac{1}{2}}$ in order to maintain the axial speed within the speed limit indicated earlier. Thus we design for a = 9.5 mm and b = 32 mm which are smaller than typical values of most operational plasma focus devices. Moreover the value of $\frac{b}{a} \sim$ 3.4, in this case, is near optimum.[5] It is also noted that the value $t_a/t_p \sim 40$ for this design.

Having fixed the values of I_o, z_o, b and a and t_r it remains to fix the value of ρ_o from Eq. (5). This gives $\rho_o = 0.21 \times 10^{-3}$ kgm^{-3}. This is the density of deuterium at

0.9 torr, which is within the pressure limits for deuterium focus operation as mentioned earlier.

Summarizing the design parameters we have:

$C_o = 30 \times 10^{-6}$ F
$L_o = 110 \times 10^{-9}$ H
$V_o = 15 \times 10^{3}$ V
$a = 0.95 \times 10^{-2}$ m
$b = 3.2 \times 10^{-2}$ m
$z_o = 0.16$ m
$\rho_o = 0.21 \times 10^{-3}$ kgm^{-3} (0.9 torr D_2)

giving: $I_o = 2.48 \times 10^{5}$ A
$c = 3.37$
$F = 16.84$
$t_o = 1.82 \times 10^{-6}$ s
$t_r = 2.86 \times 10^{-6}$ s
$t_a = 1.45 \times 10^{-6}$ s
$t_{a\,exp} = 2.9 \times 10^{-6}$ s
$t_p = 35.8 \times 10^{-9}$ s
and $t_a/t_p = 40.4$

The above design parameters have been subjected to a computation using a dynamic model[1, 6] in which the axial trajectory is computed using a snow-plow model and the radial dynamics is traced using a generalized slug-model which considers a pinching plasma of increasing length with the plasma layer lying between a shock front at position r_s and magnetic piston at position r_p (see Fig. 1). This model has the advantage of giving a realistic final pinch radius ratio. Using the design parameters for the present device, the scaling parameters for the generalised slug model are:

$$\alpha = \frac{t_o}{t_a} = 1.26, \quad \text{and} \quad \beta = \frac{L_a}{L_o} = 0.36,$$

where L_a = maximum inductance of axial phase = $z_o(\mu/2\pi)\ell nc$. Also

$$\alpha_1 = \frac{t_a}{t_p} = 40.4, \quad \text{and} \quad \beta_1 = \frac{\beta}{\ell nc} = 0.294$$

The other parameters used for the model are $c = 3.37$, $F = 16.84$ and $\gamma = \frac{5}{3}$ (for fully ionised deuterium).

The computation indicates a strong focus with a large focussing voltage spike. The parameter α was varied between 0.7 to 1.5 (corresponding to pressure range of 0.5 torr to 2 torr) and the computation repeated at each α. Good focussing was indicated over this range of pressure. These computation results add confidence to the design of the plasma focus. However it has been found that machine effects such as current and mass shedding[1], reduced channel size due to boundary effects and current re-strike[3] which are not included in the dynamic model may alter the actual performance of the plasma focus. It is therefore to be expected that in actual operation the focus may need to be tuned[5] by a variation of the five parameters V_o, ρ_o, z_o, a and b. If the design is not too far from optimum, operation over a range of ρ_o may be sufficient to establish a regime of good focus. This is the procedure adopted in the present experiment.

Experimental Arrangement

The capacitor was first tested with an ignitron GE 7703. It was found that the ignitron resistance dominated the discharge behaviour lengthening the rise time to more than 4 μs with an average periodic time of only 12 μs. A simple parallel-plate spark gap with a swinging cascade configuration (see Fig. 2) was then developed. The ratio of the gap is 3 : 2 ($4\frac{1}{2}$ mm to 3 mm). The gap is triggered via an isolating capacitor from a 1.5 kV krytron unit via a TV transformer which was found to have a step-up ratio of 17 times and a rise time of 1 μs. The isolating capacitor is a 1m length of UR67 coaxial cable. The parallel-plate spark gap is made from ½-inch thick copper plates and proved maintenance-free for 200 discharges between 13–15 kV before it was cleaned. The triggering jitter was found to be within ± 50 ns. The circuit is shown in Fig. 2.

The arrangement for the capacitor, the connecting plates, the spark gap and the output coaxial cables is shown in Fig. 3a. To keep the inductance low the earth plate of the capacitor (labelled no. 10) is extended nearly up to the anode and insulation is provided by a nylon cap (no. 5) around the anode stud. The cap dips into a pool of oil (no. 4) which is prevented from splashing out by means of an 'O' ring (no. 8). Mylar sheets (no. 11), two inches wider all round than the conducting plates, sandwiched by polyethelene sheets (no. 12) complete the insulation between the HV plate (no. 14) and the earth plate as shown in Fig. 3a. The earth plate (no. 10) runs unbroken to the output position where the earths of the coaxial cables connect. On top of the insulating sheets the HV plate is connected to the spark gap. Between the spark gap electrodes and all along it is placed a ½"-diameter copper tubing (no. 17) which acts as the trigger electrode. The output plate of the spark gap is connected to the focus tube by means of 16 coaxial cables (no. 18) used in parallel.

Essential to the structure of the focus tube is the backwall (see Fig. 3b) insulator. The glass insulator (no. 30) plays an important role in the symmetrical formation of the current sheet and has to be properly mounted to avoid being broken by vibrations. In the present design this glass insulator is mounted in a rubber holder (no. 24) which when compressed tightly and symmetrically by the brass flange (no. 28) grips the glass insulator. The rubber holder also acts as a vacuum and high voltage seal. Figure 3b also shows the anode collector plate (no. 20) and the cathode collector plates (no. 25) onto which the coaxial cables connect.

The plasma chamber (no. 32) consists of a 30 cm length of 6½ inch diameter mild steel tubing which is chromed. Vacuum is provided by a single stage rotary pump reaching an ultimate base pressure ~ 0.01 torr. The system was adjusted for a leakage rate of less than 2 micron per minutes and pressure is read with a mechanical diaphragm gauge. Operating at a test pressure of 1 torr and with a delay of less than 5 minutes between gas filling and focus operation, the air impurity in the system is about 2%. This level of vacuum proved to be sufficient for operating with good focus in various gases and good neutron yield when operated in deuterium.

To measure the relative strength of the plasma focus action, a Rogowski coil (no. 22) with an integration time constant of 200 μs is used to measure the current flowing into the anode. A resistive voltage divider (not shown in Fig.) with 15 ns response time is strapped across the anode collector plate (no. 20) and the cathode collector plate (no. 25) to measure the voltage across the focus tube. In a plasma focus device, the axial drive phase is characterised by a smooth near-sinusoidal rising current and a corresponding smooth voltage waveform with a voltage value[1] which is proportional to the axial drive speed as the rate of change of current reduces to zero at peak current. As the focus occurs, the strong electro-mechanical action draws energy from the magnetic field pumping the energy into the compressing plasma. This mechanism is indicated in the distinctive current dip and voltage spike[1] displayed by the current and voltage waveforms. In general the stronger the focus, the more severely the plasma is compressed and the bigger the current dip and voltage spike.

To measure the magnetic field a 10-turn 1 mm coil jacketted in a 3 mm glass tubing (no. 33) is inserted into the focus tube and orientated to measure the azimuthal magnetic field. The passage of the current sheath driving the plasma layer may be measured as a sharp rise in magnetic field as the sheath sweeps past the probe. This measurement[7, 8] may be used to confirm the dynamics required to ensure a good focus

An indium foil activation system[9] is used to count fusion neutrons from the plasma. This system consists of an indium foil covering a NE 102 scintillator sitting on the photo-cathode of a 2-inch photomultiplier tube. The assembly is placed in a paraffin wax enclosure so as to thermalise the fusion neutrons. The detector is placed on the end flange of the plasma focus tube (no. 39). The PM tube is connected to a counter via a discriminator and a pre-amplifier. Operated at 900 V with a discriminator setting adjusted to give a background count of 90 counts in 30 seconds the detector has been calibrated[10] and in its present geometry has a calibration constant of approximately 5×10^4 neutrons per count, the counts being taken for a 30-second period immediately after the focus is fired.

Results

The system was tested between 13–15 kV in various gases including air, argon, hydrogen and deuterium. The strength of the focussing action is gauged from the current dip and voltage spike. Figure 4a shows an oscillogram of the current and voltage waveforms of the plasma focus in 0.5 torr of air, with focussing action about 1 μs after peak

current. Figure 4b shows a deuterium focus, at 13 kV, 2.5 torr with focussing action occuring at peak current. The deuterium focus shows signs of a secondary focus occuring some 0.4 μs after the first voltage spike. The occurrence of definite clean dynamics in the axial region preceding the focus region is confirmed by magnetic probe measurements. Figure 4c shows the output of magnetic probe (lower trace) placed at z = 10.2 cm (i.e. in the axial drive region 10.2 cm from the backwall) in a discharge of 15 kV, 3.5 torr of deuterium. From this oscillogram and in comparison with the current oscillogram (upper trace) it is found that the current sheath arrives 0.6 μs before focussing occurs off the end of the anode at z = 16 cm giving a speed of 9.7 cm/μs over this section (z = 10.2 cm to z = 16 cm) of the axial drive region. From the rise time (10% to 90%) of the magnetic signal and the speed this gives a current sheath thickness of 2 cm. The thickness and speed of this current sheath is typical of that in a good plasma focus system. The current dip during focussing is also seen as a dip in the magnetic probe out-out which shows two other current dips occuring at 0.2 and 0.6 μs after the first dip. These confirm the occurrence of multiple focussing in deuterium in the device.

In air good focus was obtained at 13 and 15 kV in a narrow pressure range of 0.5 – 1.1 torr. In argon the pressure range for good focussing is greater at 0.3 to 2 torr. At 15 kV very strong focussing action was obtained at 0.8 torr. In helium the range of focussing is from 0.7 to 3.5 torr whilst in carbon dioxide focussing is observed below 1 torr. In hydrogen the pressure range for focussing is 1.1 torr to 6 torr. However it is noticed that the focussing action, though definite, is not as intense, in terms of focussing voltage spike, as in argon. The strongest focus in hydrogen occurs at 3.3 torr to 4.3 torr. In deuterium strong focus is observed in 1 – 5 torr with best focussing at 2.5 to 3 torr.

In deuterium when operated at 15 kV and optimum pressure conditions of 3 torr consistent counts of 1000 – 2000 are obtained using the PM-scintillator counter. This corresponds to $0.5 - 1 \times 10^8$ neutrons per shot.

The system shows remarkably consistent and reproducible operation. Six systems were assembled one after the other and tested over a period of two months. Each system was assembled and tested over a period of 1 week averaging between 100 – 200 shots in the various gases. Once a system has been established to be operating normally, that is without undue leakage and after an initial period of out-gassing involving some three to five discharges, proper focussing is achieved for better than 95% of the discharges, apart from those discharges deliberately operated outside the established suitable pressure range for the gas used.

Conclusion

A simple cost-effective plasma focus device based on a 3.3 kJ single capacitor and a low maintenance parallel-plate spark-gap has been designed and operated as a reproducible and reliable neutron source (10^8 neutrons per discharge in deuterium) as well as a reliable source of focussed plasmas of air, argon, helium, carbon dioxide and hydrogen. Six sets of the equipment were constructed and tested in the course of an UNU Training Programme. The remarkably reproducible results suggest that this device may be readily built as a plasma neutron source, as well as a source of pulsed dense plasmas.

Acknowledgement

We (MAE, AVG, SM, AJS, S, WU, MZ) acknowledge UNU Fellowships without which this work could not have been completed. A grant from the I.C.T.P. and a research grant F232/74 from the University of Malaya are also acknowledged likewise the technical help of Jasbir Singh and T. S. Toh.

References:

1. S. Lee in *Laser and Plasma Technology* edited by S. Lee, B. C. Tan, C. S. Wong and A. C. Chew, World Scientific, Singapore, p. 37, 64 and 387 (1985).
2. S. Lee, Australian J. Phys. **36**, 891 (1983).
3. J. W. Mather, P. J. Bottoms, J. P. Carpenter, K. D. Ware and A. H. Williams, Report No. IAEA-CN 28/D-5, 561 (1972).
4. J. P. Rager, L. E. Bilbao, H. A. Bruzzone, V. Gourlan, U. Guidoni, H. Kroeglar, S Podda, B. V. Robouch, K. Steinmetz, *Experiments on the neutron production phase of the Frascati 1 MJ Plasma Focus,* Eighth Int. Conf. on Plasma Physics and Controlled Nuclear Fusion Research, Brussels, June 1980.
5. S. Lee and Y. H. Chen, *Fusion Energy – 1981* (ICTP, Trieste) IAEA-SMR-82, Vienna p. 297.
6. S. Lee in *Radiation in Plasma,* edited by B. McNamara, World Scientific, Singapore 1984, Vol. II, p. 978;
   S. Lee, Bul. Fiz. Mal. **3**, 197 (1982).
7. S. P. Chow, S. Lee, B. C. Tan, J. Plasma Phys. **8**, 21 (1972).
8. S. Lee, T. H. Tan, *Prqcs. Seventh European Conf. on Controlled Fusion and Plasma Phys.*, Lausanne, Switzerland, I, Paper 65 (1975).
9 C. S. Wong, S. Lee and S. P. Moo, Mal. J. Sc. 6 (B), 167 (1980).
10. C. S. Wong, *Some neutron measurements of the plasma focus,* M. Sc. Thesis, Universiti Malaya (1978).

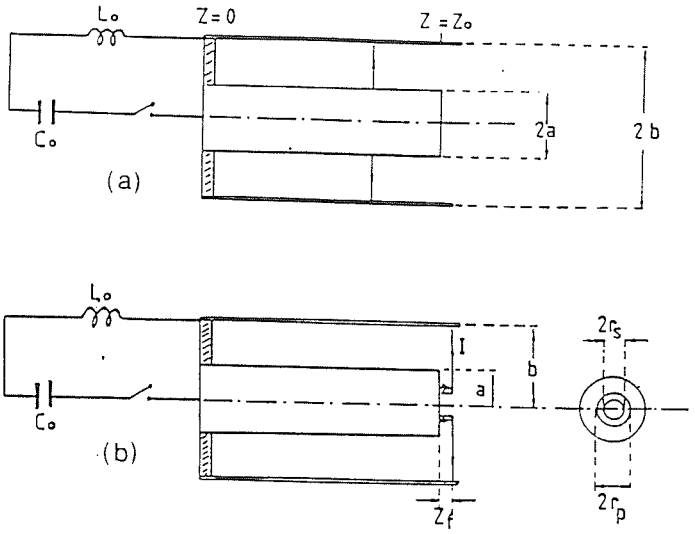

(a) The axial run-down (shock tube) phase of the plasma focus.
(b) The radial focus (pinch) phase of the plasma focus.

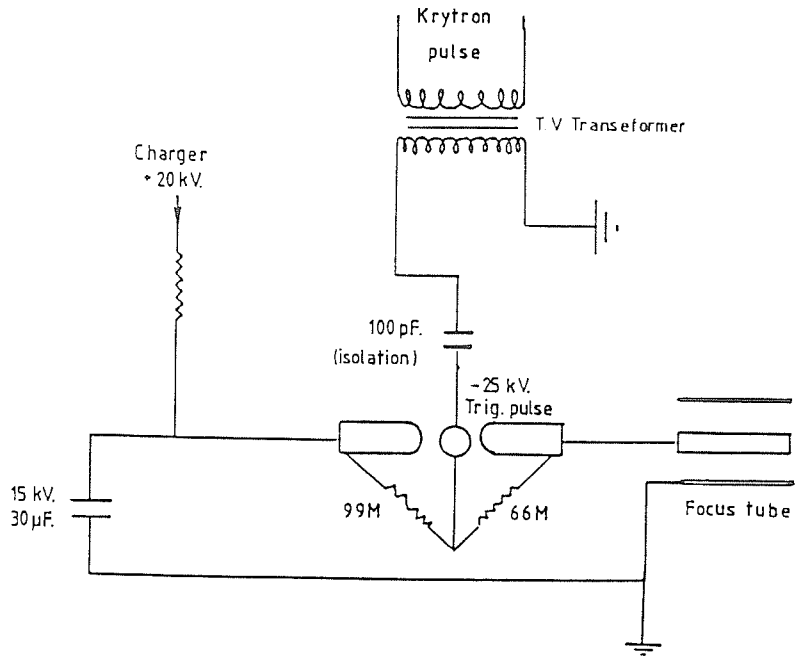

Fig. 2 Circuit for the swinging-cascade spark gap and focus tube.

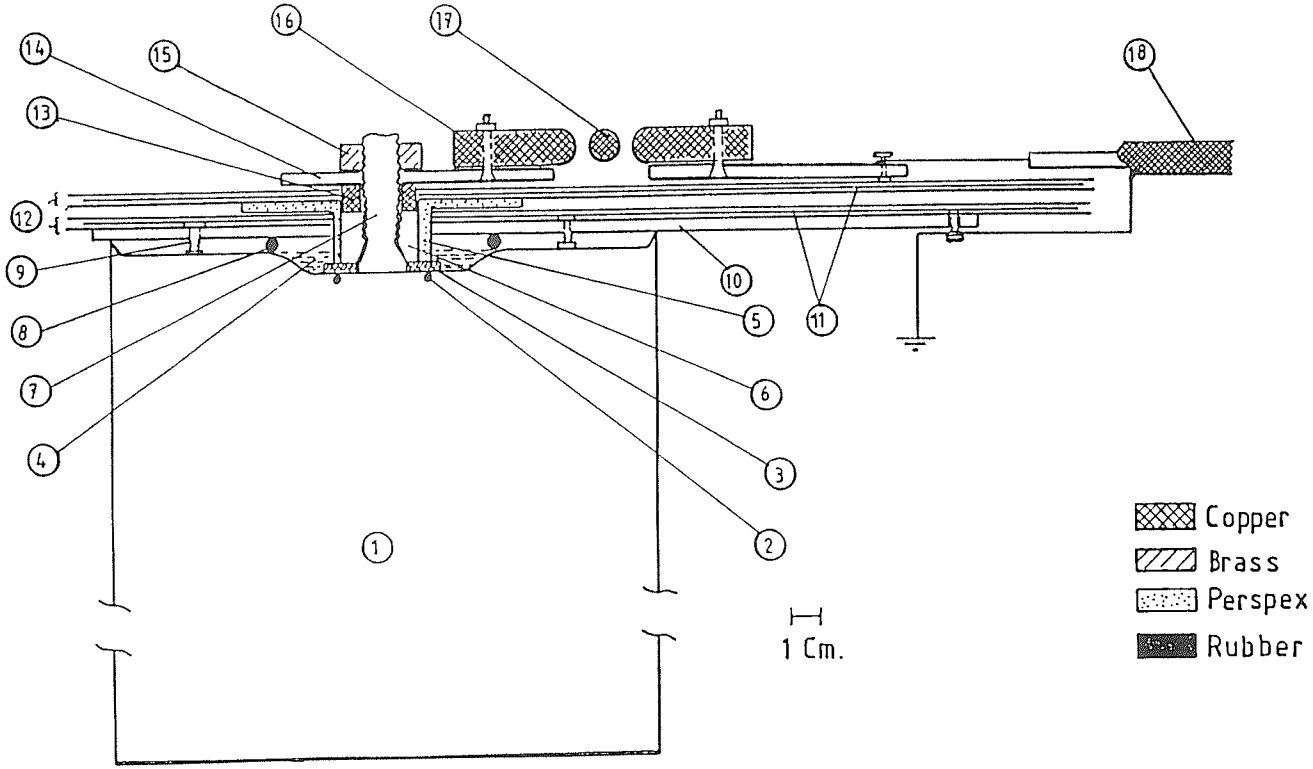

Fig. 3a The capacitor connecting plates, the spark gap and output coaxial cables. 1 = 15 kV, 30 μF capacitor; 2 = capacitor O-ring seal; 3 = washer; 4 = oil; 5 = nylon cap; 6 = steel nut; 7 = capacitor output seal; 8 = O-ring seal; 9 = earth stud; 10 = earth plate; 11 = 5-mil mylar film; 12 = polyethelene film; 13 = copper ring HV connector; 14 = capacitor high voltage (HV) output plates; 15 = lock nut for HV plate; 16 = HV electrode for swinging cascade spark gap; 17 = trigger electrode; and 18 = output coaxial cables (16 in parallel).

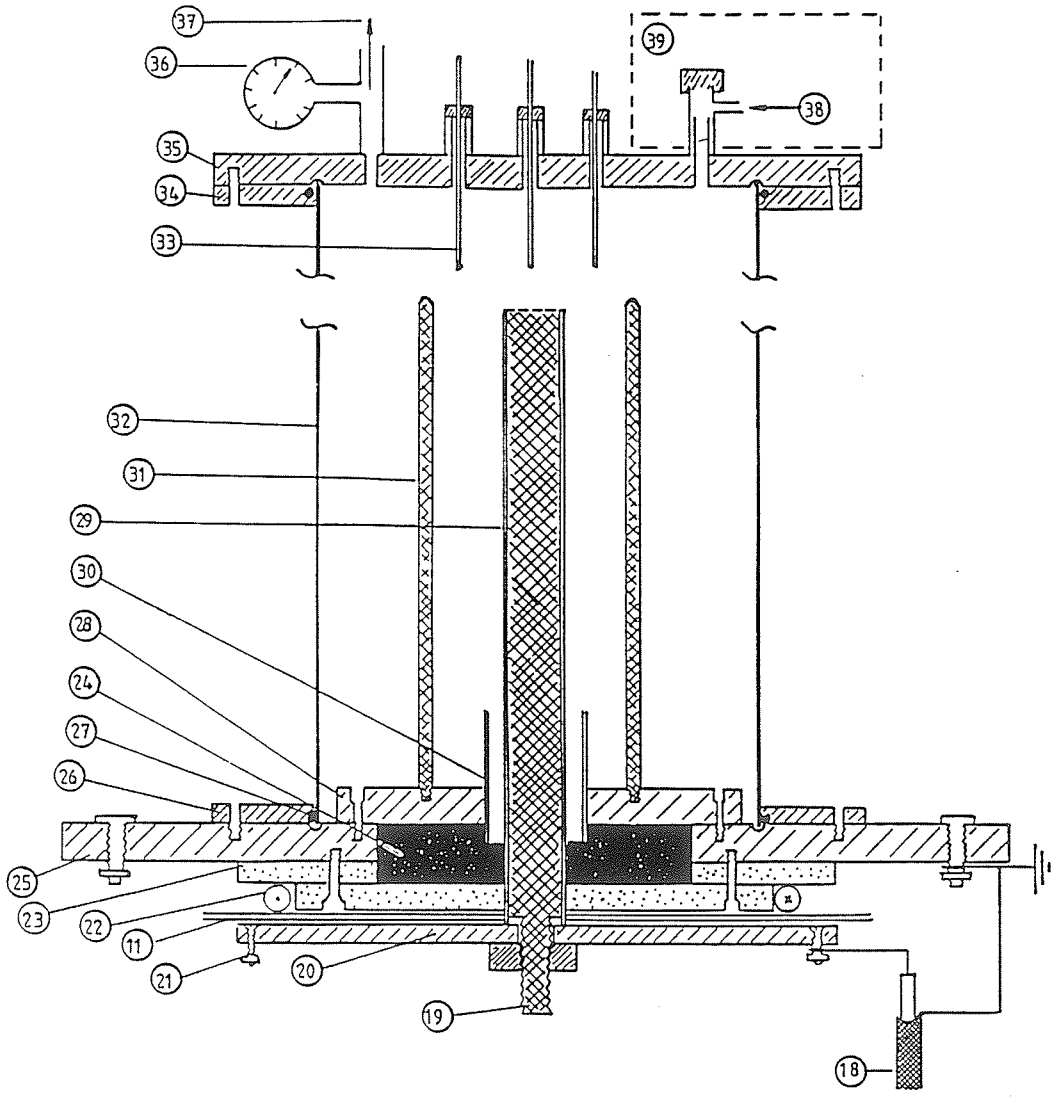

Fig. 3b The plasma focus tube
18 = input coaxial cables (16 in parallel); 19 = stud of anode; 20 = anode collector plate; 21 = connecting points for coaxial cable HV lead; 22 = Rogowski coil; 23 = perspex spacer; 24 = rubber holder; 25 = cathode collector plate; 26 = mild steel flange; 27 = O-ring seal; 28 = focus cathode support plates; 29 = focus anode; 30 = glass insulator; 31 = focus cathode (6 rods); 32 = mild steel focus chamber; 33 = movable magnetic probe in glass jacket; 34 = flange; 35 = back flange; 36 = diaphragm gauge; 37 = outlet to vacuum pump; 38 = inlet for test gas; 39 = wax container with indium foil and PM-scintillator activation counter.

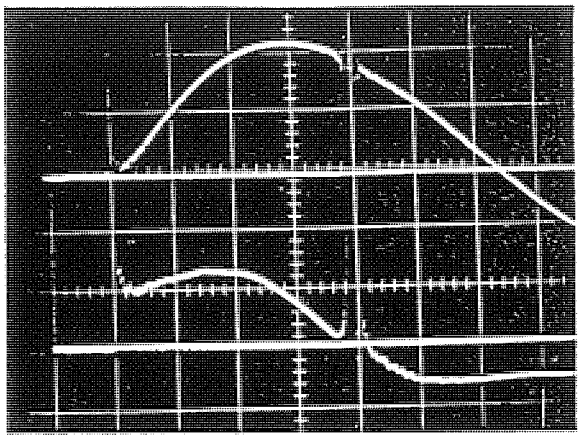

Fig. 4a Current (upper trace) and voltage (lower trace) of plasma focus in air.

13 kV, 0.5 torr
Top trace: 73 kA/cm
Bottom trace: 2kV/cm
Time scale (horizontal); 1 μs/cm

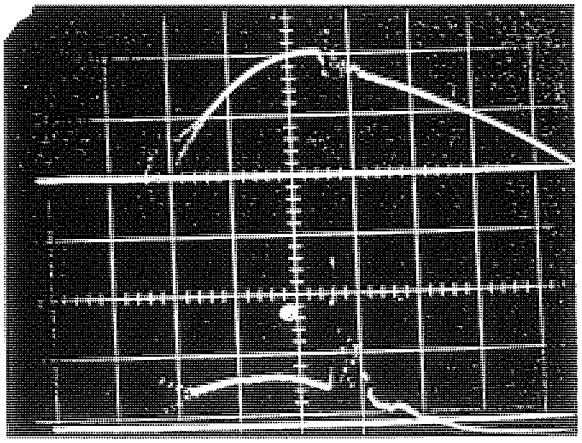

Fig. 4b Current and voltage trace of plasma focus in deuterium.

13 kV, 2.5 torr
Top trace: 75 kA/cm
Bottom trace: 4 kV/cm
Time scale (horizontal): 1 μs/cm

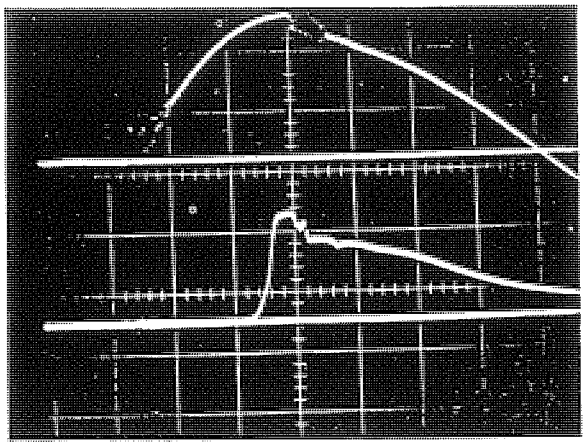

Fig. 4c Current and magnetic trace of plasma focus in deuterium

15 kV, 3.5 torr
Magnetic probe placed at z = 10.2 cm
Top trace: 73 kA/cm
Bottom trace: 0.6 T/cm